JOURNAL OF THE AERONAUTICAL SCIENCES

VOLUME 11 JANUARY, 1944 NUMBER 1

THE JOHN CRERAR LIBRARY JAN 29 1944

CONTENTS

Notes on Columns . . . . . PAUL E. SANDORFF 1

Study of Exhaust-Valve Design from Gas Flow Standpoint . . . . SENG-CHIU HU 13

Medical Activities in Military Aviation . . . . . OTIS O. BENSON, JR., DAVID B. DILL, AND W. RANDOLPH LOVELACE, II 21

Strain Energy Analysis of Incomplete Tension Field Web-Stiffener Combinations . . PAUL H. DENKE 25

Loss in Aileron Effectiveness Because of Wing Twist and Considerations Regarding the Internal-Pressure Balanced Aileron . . . . . REINHARDT ROSENBERG 41

Graphical Analysis of Response Characteristics of Rate-of-Climb Indicators . . . . KALMAN J. DEJUHASZ 48

Take-Off Distance of a Glider Train . . . . . WIESLAW Z. STEPNIEWSKI 55

Medical Activities in Naval Aviation . . . . . J. C. ADAMS, B. GROESBECK, JR., AND E. F. DUBOIS 63

Column with Equal-Spaced Elastic Supports . . . . . SHOU-NGO TU 67

Design of Elbows in Potential Motion . . . . . BOLESLAW SZCZENIOWSKI 73

Stress Problems in the Design of Wooden Airplanes . . ZBIGNIEW KRZYWOBLOCKI 76

Blade Section Variation on Small-Scale Rotors . . . . . KENNETH RAZAK 83

Vibration Frequencies of Continuous Beams . . . . . EDWARD SAIBEL 88

Letters to the Editor 91, 92

Published Quarterly by the

INSTITUTE OF THE AERONAUTICAL SCIENCES INC.

JOURNAL OF THE AERONAUTICAL SCIENCES

VOL. 11 JANUARY, 1944 NO. 1

PUBLISHED QUARTERLY BY THE INSTITUTE OF THE AERONAUTICAL SCIENCES INC.

Chairman of the Editorial Board: HUGH L. DRYDEN, *Chief of Mechanics and Sound Division, National Bureau of Standards*

Editor: ROBERT R. DEXTER *Manager:* JOSEPH J. MAITAN

The Institute of the Aeronautical Sciences publishes the JOURNAL OF THE AERONAUTICAL SCIENCES quarterly, in January, April, July, and October, and the AERONAUTICAL ENGINEERING REVIEW monthly.

The JOURNAL OF THE AERONAUTICAL SCIENCES prints papers of scientific and technical interest to Institute members and subscribers. In general, it provides an opportunity for specialists to publish articles disclosing new knowledge and new applications in the field of the aeronautical sciences. The JOURNAL restricts itself to the aeronautical aspects of advances in science and engineering, and papers printed have either been submitted directly to the JOURNAL or have been previously presented at a meeting of the Institute.

The AERONAUTICAL ENGINEERING REVIEW keeps members and subscribers informed regarding the contents of new books and current periodicals in the field of aeronautics. It reviews new developments in the aircraft industry and reports on progress from house organs and catalogues published by aircraft and engine manufacturers and other companies engaged in aeronautical activities. It publishes papers on applied engineering and aircraft production. News of Institute activities is published in the REVIEW.

Statements and opinions expressed in the JOURNAL are to be understood as individual expressions of the authors and not those of the Institute.

SUBSCRIPTION RATES

Journal of the Aeronautical Sciences
Published Quarterly

United States and Possessions		Foreign Countries Including Canada (American Currency Rates)	
1 Year	$7.00	1 Year	$9.00
Single Copies	2.00	Single Copies	2.50

Aeronautical Engineering Review
Published Monthly

United States and Possessions		Foreign Countries Including Canada (American Currency Rates)	
1 Year	$3.00	1 Year	$3.50
Single Copies	0.30	Single Copies	0.35

Notices of change of address should be sent to the Institute at least 30 days prior to actual change of address.

Manuscripts for publication, proofs, and all correspondence should be addressed to the Editorial Office of the JOURNAL.

Correspondence regarding subscriptions may be addressed to Publication Office, 20th and Northampton Sts., Easton, Pa., or to the Editorial Office of the JOURNAL OF THE AERONAUTICAL SCIENCES, 1505 RCA Building West, 30 Rockefeller Plaza, New York 20, New York.

Entered as Second-Class Matter at the Post Office, Easton, Pa., May 1, 1937. Acceptance for mailing at a special rate of Postage provided for in the Act of August 24, 1912. Authorized April 29, 1937.

JOURNAL OF THE AERONAUTICAL SCIENCES

VOLUME 11 JANUARY, 1944 NUMBER 1

Notes on Columns

PAUL E. SANDORFF*

Lockheed Aircraft Corporation

SUMMARY

Methods are presented for the determination of the failure loads of continuous columns that are elastically restrained at the supports. By means of accompanying charts, the effect of elastic restraint can be obtained as a simple multiplying factor to be applied to the Euler load. The variations in column rigidity due to plasticity and skin-buckling are discussed, and note is made of effects of eccentricity of loading which are always present to some extent in practical structure.

Certain assumptions that are usually made in the design and in the testing of aircraft column structure are shown to be precise only to within 10 or 15 per cent. A method of testing is described by which column effects may be investigated more thoroughly. The calculation of the compressive strength of aircraft panel structure from the design characteristics is suggested in the place of the usual assumption of an effective end-fixity coefficient of 1.5.

INTRODUCTION

IN AIRCRAFT DESIGN the structural engineer deals repeatedly with columns that are elastically restrained against rotation at the supports, which develop full strength only after the stresses exceed the point of skin-buckling and the elastic limit and which inevitably are, to some extent, eccentrically loaded. Problems concerning the strength of such members are usually met with an assumption of the effective end-fixity coefficient, which expresses the ratio of the column strength to the critical load of a similar pin-ended member. In many cases this method is inadequate.

The end-fixity coefficient has been determined accurately for only a few special cases. Many aircraft structural analyses, in which the weight and marginal safety would have justified better accuracy, have been based on assumptions of questionable precision. The investigations outlined below were made to obtain more generalized mathematical equipment for the solution of column problems and to promote greater accuracy in the design of aircraft column structure.

Received June 14, 1943. Based on Lockheed Report No. 4012, "Notes on Columns with Elastically Restraining Supports," January, 1943.

* Senior Research Engineer.

CRITICAL LOADS OF ELASTICALLY RESTRAINED COLUMNS

The critical load of a column is the load at which instability would occur provided the member were initially straight and centrally loaded. In this case failure takes place by sudden large lateral deflections. In contrast, when initial eccentricity of loading is present, each increment of axial load produces increased secondary bending moment and consequent bowing, so that the lateral deflection increases gradually with the load. The column then has no "critical" load but merely a maximum strength at which instability occurs.

If the column could be constructed of a material completely elastic and of infinite strength, the instability load would be unchanged by eccentricities. In the practical case, plasticity and skin-buckling effects are accentuated by the secondary bending moments, so that the strength usually differs from the critical load.

The determination of the critical load is nevertheless important in column analysis. The solutions for the critical loads of several types of elastically restrained columns are therefore developed in the following paragraphs, it being assumed for the time being that eccentricities and initial bowing are negligible. The methods employed are described by Timoshenko[1] (Chapters I and II).

Single-Span Column

In Fig. 1, the coefficients of end-restraint may be defined as:

$$\alpha_1 = -M_1'/\theta_1' \tag{1}$$

$$\alpha_2 = -M_2/\theta_2 \tag{2}$$

where M_1' and M_2 are the end-moments applied to the column and θ_1' and θ_2 are the angular deflections of the column at the supports. Downward deflection is considered positive, and positive moments are those tending to produce positive deflections. The following relations may be written:[1]

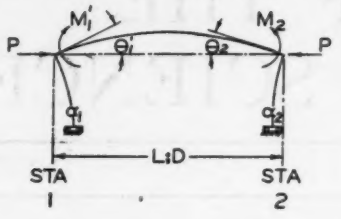

FIG. 1. Single-span beam, elastically restrained.

$$\theta_1' = \frac{L}{6D}\left[2\psi(u)M_1' + \phi(u)M_2\right] \quad (3)$$

$$\theta_2 = \frac{L}{6D}\left[2\psi(u)M_2 + \phi(u)M_1'\right] \quad (4)$$

where:

L = length of column
D = rigidity, or moment per unit curvature
P = axial load
$u = L/2\sqrt{P/D}$

$$\psi(u) = \frac{3}{2u}\left[\frac{1}{2u} - \frac{1}{\tan 2u}\right]$$

$$\phi(u) = \frac{3}{u}\left[\frac{1}{\sin 2u} - \frac{1}{2u}\right]$$

The functions $\phi(u)$ and $\psi(u)$ are tabulated against u on page 499, et seq., of reference 1. The quantity D may be further defined as:

$D = dM/dC$
$C = \dfrac{d^2w}{dx^2}$ = curvature
w = lateral deflection
x = longitudinal coordinate

In Eqs. (3) and (4), D is assumed constant over the length of the span, and, except for special cases such as plates in bending,

$D = \overline{E}\overline{I}$
$\overline{E}$ = effective modulus of elasticity of material in bending
$\overline{I}$ = effective moment of inertia of column cross section in bending

Combining Eqs. (1) and (2) with Eqs. (3) and (4),

$$\left[\frac{6D}{\alpha_1 L} + 2\psi(u)\right]M_1' + \phi(u)M_2 = 0 \quad (5)$$

$$\phi(u)M_1' + \left[\frac{6D}{\alpha_2 L} + 2\psi(u)\right]M_2 = 0 \quad (6)$$

At the critical load, the end-moments as expressed in the simultaneous Eqs. (5) and (6) become infinite, and the denominator determinant may be placed equal to zero. The resulting relation between the parameters is therefore true when P is equal to the critical load:

$$\left[\frac{6D}{\alpha_1 L} + 2\psi(u)\right]\left[\frac{6D}{\alpha_2 L} + 2\psi(u)\right] - \phi^2(u) = 0 \quad (7)$$

The critical load is therefore the smallest value of P which will satisfy Eq. (7). In the special case where the end-restraints are equal, Eq. (7) reduces to:

$$\left[\frac{6D}{\alpha L} + 2\psi(u) + \phi(u)\right]\left[\frac{6D}{\alpha L} + 2\psi(u) - \phi(u)\right] = 0 \quad (8)$$

Two solutions appear to be possible; one, however, represents an impracticable mode of buckling and the true solution is:

$$(6D/\alpha L) + 2\psi(u) + \phi(u) = 0 \quad (9)$$

Eq. (9) may also be written in the following manner:

$$(6D/\alpha L) + (3/u)\tan u = 0 \quad (10)$$

or

$$(kD/\alpha L) + \tan(kL/2) = 0 \quad (11)$$

where

$$k = \sqrt{P/D}.$$

Two-Bay Column

Dealing with an intermediate elastic support, Timoshenko[1] suggests establishing the conditions of equilibrium about the junction using the notation of Fig. 2. In such a case the following equations may be written:

$$\theta_n = -\theta_n' \quad (12)$$

$$M_n'' = -(M_n - M_n') = \alpha\theta_n \quad (13)$$

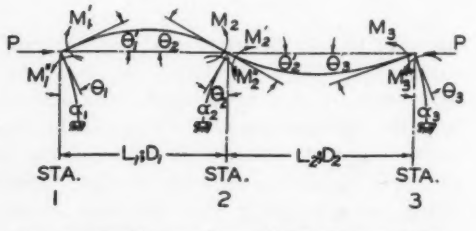

FIG. 2. Double-span beam, elastically restrained.

Proceeding as in Eqs. (3) and (4), the relations existing in the two-span column are:

$$M_1' = -\alpha_1\theta_1' = -\frac{\alpha_1 L_1}{6D_1}\left[2\psi(u_1)M_1' + \phi(u_1)M_2\right] \quad (14)$$

$$M_2 - M_2' = -\alpha_2\theta_2 = -\frac{\alpha_2 L_1}{6D_1}\left[2\psi(u_1)M_2 + \phi(u_1)M_1'\right] \quad (15)$$

$$M_2' - M_2 = -\alpha_2\theta_2' = -\frac{\alpha_2 L_2}{6D_2}\left[2\psi(u_2)M_2' + \phi(u_2)M_3\right] \quad (16)$$

$$M_3 = -\alpha_3\theta_3 = -\frac{\alpha_3 L_3}{6D_2}\left[2\psi(u_2)M_3 + \phi(u_2)M_2'\right] \quad (17)$$

Then, from Eqs. (12), (15), and (16), the continuity equation is:

$$\frac{L_1D_2}{L_2D_1}\phi(u_1)M_1' + \frac{L_1D_2}{L_2D_1}2\psi(u_1)M_2 + 2\psi(u_2)M_2' + \phi(u_2)M_3 = 0 \quad (18)$$

The equation expressing central fixity devolves from Eq. (16), while the end-fixity relations are expressed from Eqs. (14) and (17):

$$0 - \frac{6D_2}{\alpha_2L_2}M_2 + \left[\frac{6D_2}{\alpha_2L_2} + 2\psi(u_2)\right]M_2' + \phi(u_2)M_3 = 0 \quad (19)$$

$$\left[\frac{6D_1}{\alpha_1L_1} + 2\psi(u_1)\right]M_1' + \phi(u_1)M_2 + 0 + 0 = 0 \quad (20)$$

$$0 + 0 + \phi(u_2)M_2' + \left[\frac{6D_2}{\alpha_3L_2} + 2\psi(u_2)\right]M_3 = 0 \quad (21)$$

In cases where the methods of symmetry and antisymmetry can be applied, the solution of Eqs. (18) to (20) may be made fairly simple. The substitution of the conditions for the special case in the basic equations, followed by solution of the determinant, is usually less tedious than using the reverse procedure. For instance, in the special case where both spans are identical in character and length and the end-restraints are the same, M_2' may be substituted for $-M_2$, M_1' for $-M_3$, and θ_1' for $-\theta_3$, reducing the equations to the determinant in M_1' and M_2':

$$\left.\begin{matrix} -\phi(u) + 2[(6D/\alpha_2L) + \psi(u)] \\ [(6D/\alpha_1L) + 2\psi(u)] - \phi(u) \end{matrix} = 0\right\} \quad (22)$$

The critical load is then implicit in the relation:

$$2\left[\frac{6D}{\alpha_1L} + 2\psi(u)\right]\left[\frac{6D}{\alpha_2L} + \psi(u)\right] - \phi^2(u) = 0 \quad (23)$$

In the case where $M_1' = M_2$ and $M_2' = M_3$ and the central support is pinned ($\alpha_2 = 0$), then it must also be true that $M_2 = M_2'$. For these conditions to exist, the end-restraint must be a function only of the character of the column, as may be seen from Eqs. (20) and (21). The properties of the two bays are interrelated, according to Eq. (18):

$$\frac{L_1D_2}{L_2D_1}\left[2\psi(u_1) + \phi(u_1)\right] + \left[2\psi(u_2) + \phi(u_2)\right] = 0 \quad (24)$$

This equation holds true at all values of the load. It can be reduced to the simpler form:

$$\tan u_2/\tan u_1 = -(L_1D_2u_2/L_2D_1u_1) = -(L_2u_1/L_1u_2) = -\sqrt{D_2/D_1} \quad (25)$$

Stewart Way[2] presented an alternate method for the solution of column problems. Some interesting data concerning the variation of critical load with span lengths of a two-bay pin-supported column are given in that reference. However, reference 2 is concerned only with a few special-case column problems and should not be used as a basis for generalized conclusions.

Symmetric Three-Bay Column

Proceeding as in the previous section, the case of the three-bay column of Fig. 3 can readily be set up as a series of equations in terms of the end-moments. The solution of the general case, however, is too tedious to be of practical value, and it is better to make substitutions immediately.

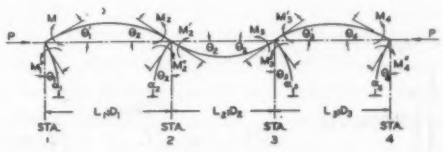

FIG. 3. Beam of three spans, elastically restrained.

In the special case of a symmetric three-bay column, in which, in Fig. 3: $L_1 = L_3$, $D_1 = D_3$, $\alpha_1 = \alpha_4$, $\alpha_2 = \alpha_3$; the solution for the critical load is obtained from the determinant in M_1', M_2, and M_2':

$$\left.\begin{matrix} \frac{L_1D_2}{L_2D_1}\phi(u_1) + \frac{L_1D_2}{L_2D_1}2\psi(u_1) + \left[2\psi(u_2) + \phi(u_2)\right] \\ + \left[\frac{6D_1}{\alpha_1L_1} + 2\psi(u_1)\right] + \phi(u_1) + 0 = 0 \\ 0 - \frac{6D_2}{\alpha_2L_2} + \left[\frac{6D_2}{\alpha_2L_2} + 2\psi(u_2) + \phi(u_2)\right] \end{matrix}\right\} \quad (26)$$

If the central supports are pinned, $\alpha_2 = \alpha_3 = 0$, and Eq. (26) becomes:

$$\frac{L_1D_2}{L_2D_1}\left[2\psi(u_1) - \frac{\phi^2(u_1)}{\frac{6D_1}{\alpha_1L_1} + 2\psi(u_1)}\right] + [2\psi(u_2) + \phi(u_2)] = 0 \quad (27)$$

This equation parallels Eq. (9) for the single-bay column, and it becomes evident that the end-restraint of the central bay of the three-bay pin-supported column is determined by the adjacent spans and may be expressed as an equivalent end-restraint coefficient:

$$\alpha_2' = \frac{6D_1}{L_1}\left\{\frac{1}{\left[2\psi(u_1) - \frac{\phi^2(u_1)}{(6D_1/\alpha_1L_1 + 2\psi(u_1)}\right]}\right\} \quad (28)$$

Columns Continuous over Several Supports

Eq. (28) suggests a method for determining the maximum load of the general case column which is continuous over any given number of supports with any given restraint conditions. It may be seen that that portion of the end-restraint on any particular bay

which is due to the effect of an adjacent bay is given by Eq. (28). The total end-restraint is the sum of this quantity and that furnished by the support. Using the nomenclature of Fig. 4, the following equations may therefore be written to express the total equivalent end-restraint on any span n of a continuous column:

$$\alpha_n' = \alpha_n + \frac{6D_{n-1}}{L_{n-1}} \left\{ \frac{1}{\left[2\psi(u_{n-1}) - \frac{\phi^2(u_{n-1})}{(6D_{n-1}/\alpha_{n-1}'L_{n-1}) + 2\psi(u_{n-1})} \right]} \right\} \tag{29}$$

$$\alpha_{n+1}' = \alpha_{n+1} + \frac{6D_{n+1}}{L_{n+1}} \left\{ \frac{1}{\left[2\psi(u_{n+1}) - \frac{\phi^2(u_{n+1})}{(6D_{n+1}/\alpha_{n+2}'L_{n+1}) + 2\psi(u_{n+1})} \right]} \right\} \tag{30}$$

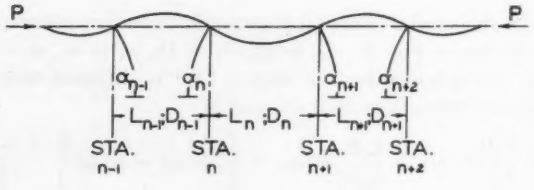

FIG. 4. Continuous beam elastically restrained.

The span in question may then be treated as a single-bay column with the end-restraints α_n' and α_{n+1}'. Because these quantities involve the restraint at the far support of the adjacent bay, it is necessary to apply the relations first to the end bays and work successively inward to the span n. The value of α' is affected by the column load through the functions $\psi(u)$ and $\phi(u)$, and for this reason α' in some cases may actually be negative. The failure load of the particular bay under consideration is given by Eq. (7), which may be rewritten for convenience as follows:

$$\left[\frac{6D_n}{\alpha_n'L_n} + 2\psi(u_n) \right] \left[\frac{6D_n}{\alpha_{n+1}'L_n} + 2\psi(u_n) \right] - \phi^2(u_n) = 0 \tag{31}$$

Column End-Fixity Related to End-Restraint

The application of the relations developed in the foregoing section is usually too tedious for practical stress analysis. In order to reduce the amount of labor, the concept of an effective pin-end length, L_e, has often been used. The critical load is then computed by a modification of the basic Euler relation for pin-ended columns, as follows:

$$P_{\text{pin-end}} = \pi^2 D/L^2 \tag{32}$$

$$P_{cr} = \pi^2 D/L_e^2 \tag{33}$$

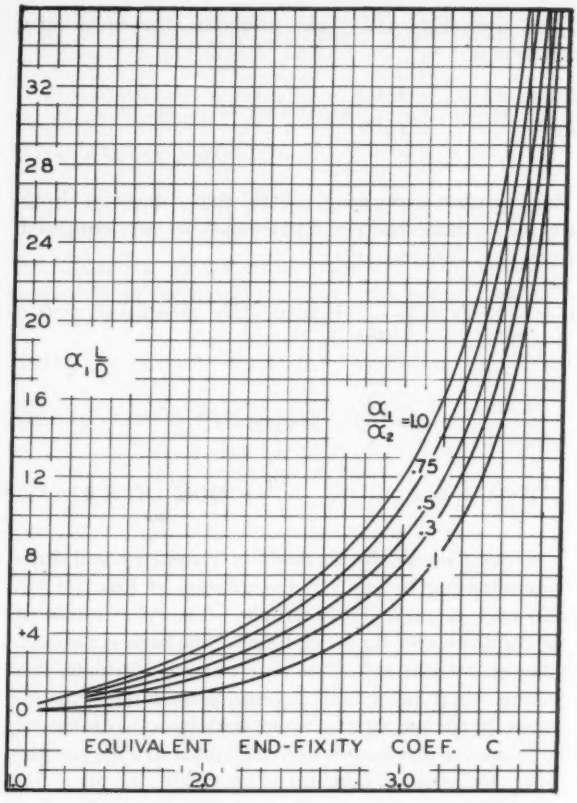

FIG. 5. Relation between end-restraint and equivalent end-fixity coefficient.

Osgood[3] presented charts by which L_e may be determined from the known end-restraints and the column characteristics. The method is not so simple, however, as that which follows by relating the end-restraint coefficients of Eqs. (1) and (2) to the end-fixity coefficient, c, defined as follows:

$$P_{cr} = cP_{\text{pin-end}} = c(\pi^2 D/L^2) \tag{34}$$

Some methods for converting from end-restraint to end-fixity have been suggested.[4] However, by using Eq. (7) and the relation

$$c = (2u/\pi)^2 \tag{35}$$

which follows from Eq. (34), the end-fixity can be obtained directly as a function of $\alpha_1(L/D)$ and $\alpha_2(L/D)$. The results are presented graphically in Figs. 5 and 6.

These figures provide a rapid and easy determination of the critical load of any single-bay column. Depending on the nature of the problem, one of the two charts will probably be more convenient to use. The application of this method to any bay of a continuous column on several supports is possible if the equivalent end-restraints, as computed by Eqs. (29) and (30), are used in place of α_1 and α_2.

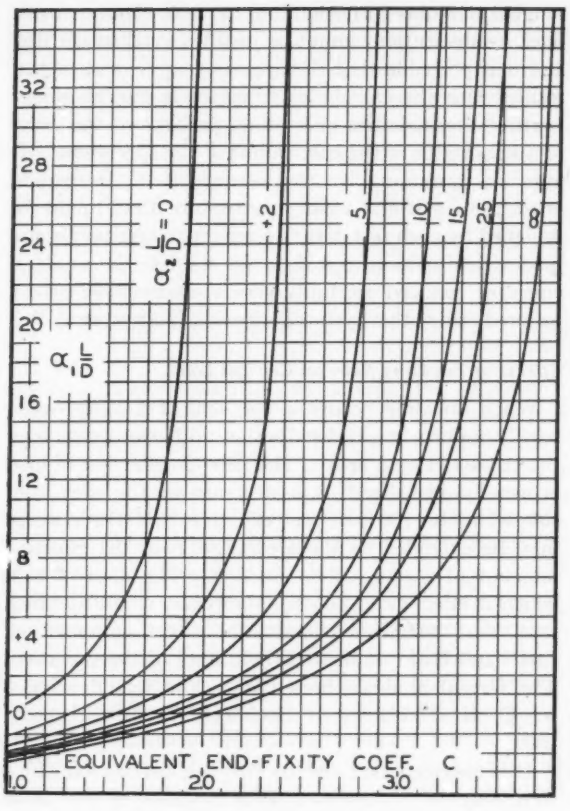

FIG. 6. Relation between end-restraint and equivalent end-fixity coefficient.

THE PRACTICAL COLUMN

Nature of the Variations in Column Rigidity

For the usual aircraft column structure, the column or bending rigidity, D, is constant if the compressive stresses remain below the skin-buckling stress and below the elastic limit of the material. When one or the other of these limits is exceeded, the rigidity becomes a function of the applied stress, because, as the stress varies, skin-buckling affects the moment of inertia (I) and plasticity changes the modulus (E).

A so-called "long column" is one that fails by instability before the compressive stress exceeds the limits of elasticity and skin-buckling and is therefore a perfectly elastic or true Euler column. A "short column" is usually considered as one of such length and design that instability occurs only *after* the stress exceeds the elastic limit.

However, as was indicated by Howland,[5] short-column effects that occur in aircraft structure are often due also to changes in the value of I caused by skin-buckling. In general, the short-column range includes any column the rigidity of which, at failure, is related to the stress. Most aircraft column structure would be classified in this range.

It has been found that the calculation of the critical load of a short column is unchanged if the original value of D, the rigidity, is modified to conform to the modulus and the moment of inertia which are effective under the critical conditions.[1, 5, 6, 7, 8, 9] The notation used in developing the formulas and relations of the preceding sections makes provision for this substitution. The determination of the effective value of D to be substituted, however, presents a problem that in most cases has led to "circular logic"; i.e., from test data, it is possible to back-figure and obtain a value of D suitable for the particular test specimen. The value of D so obtained cannot be applied with accuracy to any other column. The determination of the variation of D with column stress for a specific column shape is implicit in the current method of aircraft panel tests, the results of which are plotted as allowable stress against slenderness ratio. As noted in a later section, this method takes no accurate account of the effect of secondary or superposed bending moments on the value of D, which makes the actual column strength differ from the computed critical load.

In a short column, the column rigidity is dependent not only on the mean compressive stress but also on the stress distribution. If bending exists in the column, the value of E varies over the cross section, as determined by the local stress, in relation to the stress-strain curve for the material.[6, 10] Similarly, the extent of the skin-buckling effect is determined by the stress in the skin and not by the mean column stress. Consequently, when curvature exists in the column, the strength may differ considerably from the critical load.

All practical column structure has been found to exhibit some curvature effects. These may arise because of initial bowing, eccentricity of loading, or lateral beam loads. As a result, the central portions of the column are removed from the line of action of the axial load, and secondary moments and lateral deflections occur to an extent determined by the value of D. In the special case when the curvature is such as to increase the effectiveness of the buckled skin, the effect may actually increase the column strength. The plasticity effect, however, acts always to decrease the effective rigidity, and each increment of loading then causes increased deflections and decreased rigidity. The maximum load thus attained may fall far short of the critical or sudden-collapse load that would be reached in the absence of curvature.

By application of the same reasoning previously used to account for plasticity in the straight column, the expression for the critical load is still of practical value if D can be corrected for the column curvature at failure. The curvature effects may also be handled by combining them with the end-fixity coefficient, so that, in the basic column relation,

$$P_{max.} = c'(\pi^2 D/L^2) \qquad (36)$$

The quantity c' then includes the eccentricity, form-factor, and end-restraint effects and may be termed the "effective end-fixity coefficient."

Effects of Plasticity

As early as 1909, von Kármán presented test data to verify a precise mathematical treatment of the effects of plasticity on eccentrically loaded columns. The method, which is presented with slight modification in readily available references,[1, 10] is tedious but accurate. Plane sections are assumed to remain plane, so that for selected values of curvature and neutral axis location the stress distribution is determined from consideration of the material stress-strain curve. By processes of integration over the sectional area, the stress distribution defines the axial loads and the moments of resistance corresponding to the chosen values of curvature. These relations are simultaneously defined by the initial eccentricity and the deflection curve of the column, which may for practical purposes be assumed sinusoidal.[10] Solution for the maximum load is therefore possible by combining the two simultaneous sets of relations; the strength, however, is severely dependent on the initial eccentricity.

When only centrally loaded, straight columns are considered, as is frequently done in discussion of the effects of plasticity, the effective modulus may be expressed as:

$$\bar{E} = (E_0 I_t + E_\sigma I_c)/I' \tag{37}$$

Here the section is assumed to undergo an infinitesimal bending deformation, so that the area carrying the increment of tension acts with the Young's modulus E_0, while that area carrying the increment of compression behaves according to E_σ, the tangent modulus of the material stress-strain curve at the mean column stress. The neutral axis shifts because of the change in effectiveness of these areas, and in the above expression,

I_t = moment of inertia of the tension area about the neutral axis
I_c = similar moment of inertia of the compression area
I' = total effective moment of inertia

In Eq. (37), $\bar{E}$ is often termed the "reduced modulus,"[1] the "double modulus,"[7, 11] or the "Considere-Engesser" relation.[8] The expression can be applied only to the perfectly loaded column to obtain the theoretic critical load, since, if any bowing exists prior to failure, the extreme fibers are more highly strained than the central fibers and act at a modulus value less than that corresponding to the mean stress. von Kármán[6] emphasized the great reduction in strength due to minute eccentricities of loading.

Some recent test results[8, 11] indicate that the effective modulus, $\bar{E}$, may be placed directly equal to E_σ, the tangent modulus corresponding to mean column stress. Such a substitution cannot be justified mathematically, and it is probable that the apparent agreement of test results with the calculated strengths is due to imperceptible eccentricities of loading, perhaps of the order of a hundredth of the core radius of the specimens. It appears questionable to assume that equivalent eccentricities would exist in structure that might be designed by such test data. Such an assumption is also made when column test data are used to determine a curve of reduced modulus versus compressive stress, for predicting other types of crippling failures, etc.[9, 24]

Effects of Buckling Skin on Critical Load

When buckling occurs in the skin of a compression panel, uniform stress distribution no longer exists over the cross-sectional area. The new distribution of load is usually visualized as a decrease in the area considered to be 100 per cent effective, and the concept may be extended to the computation of the effective moment of inertia of the section. The area of skin which is effective in bending, however, is not identical with that which is effective in direct compression. Cox[12] and Hoff[13] indicated the nature of the variation. The formal analysis presented below was developed by C. H. Heilbron, of Lockheed Aircraft Corporation.

It is assumed that the buckled skin carries some load that may be represented as a function of the mean stiffener stress, σ_0, and that the total load of the panel is unchanged by the addition of a small amount of curvature. The total effective area per unit width may be defined as:

$$\Sigma A_e = P/\sigma_0 \tag{38}$$

where P is the total load carried per unit width. If a small amount of spanwise bending is added without changing the value of P, the following relations may be written:

$$P = \Sigma A_e \sigma \tag{39}$$

$$M = \Sigma (A_e \sigma) z \tag{40}$$

where σ is the fiber stress at a distance z from the neutral axis. The fiber stress is related to the curvature ($C_x = d^2w/dx^2$) by:

$$\sigma = \sigma_0 + \bar{E} z C_x \tag{41}$$

and the rigidity, as previously defined, is:

$$D_x = \bar{E} I_x = dM_x/dC_x \tag{42}$$

Using the initial assumption of unchanging P,

$$\left.\begin{aligned} dP/dC_x = 0 &= \sum [d(A_e\sigma)/dC_x] \\ 0 &= \sum (d\sigma/dC_x)\,[d(A_e\sigma)/d\sigma] \end{aligned}\right\} \tag{43}$$

By combining Eqs. (41) and (43), the variation of fiber stress with curvature is found to be:

$$\frac{d\sigma}{dC_x} = \bar{E}\left[z - \frac{\sum z[d(A_e\sigma)/d\sigma]}{\sum[d(A_e\sigma)/d\sigma]}\right] \quad (44)$$

Then, combining Eqs. (40) and (42) and substituting for $d\sigma/dC_x$ according to Eq. (44),

$$D_x = \bar{E}\left\{\sum z^2\,[d(A_e\sigma)/d\sigma] - \frac{\sum z[d(A_e\sigma)/d\sigma]^2}{\sum[d(A_e\sigma)/d\sigma]}\right\} \quad (45)$$

By representing $\bar{A}_e$ as the "effective area, per unit width, in bending under compression,"

$$\bar{A}_e = \frac{d}{d\sigma}(A_e\sigma) = A_e + \sigma\left(\frac{dA_e}{d\sigma}\right) \quad (46)$$

the equivalent moment of inertia, from Eq. (45), is:

$$\bar{I} = \left[\sum z^2\bar{A}_e - \frac{(\sum z\bar{A}_e)^2}{\sum\bar{A}_e}\right] \quad (47)$$

which is parallel to the expression for the ordinary moment of inertia, except that each element area is replaced by the value $\bar{A}_e$ of Eq. (46).

The value of $\bar{A}_e$ may also be affected by shear lag in the skin which will reduce the effective area in cases where L_e, the equivalent pin-ended column length, is not large in comparison to b, the width of buckling skin. This shear lag reduction has been observed in panels in which the skin was unbuckled or was placed in tension.[13, 14] In reference 14 it was found that, when a panel was subjected to uniform lateral load as a simple beam, the active width of the skin could, for practical purposes, be approximated by $[4/\pi(3 + 2\mu - \mu^2)]L$, where L is the distance between supports and μ is Poisson's ratio for the material. It therefore seems reasonable that, when the equivalent pin-end column length, L_e, is less than $0.36b$, the value of $\bar{A}_e$ of Eq. (46) should be reduced by the ratio of $0.36L/b$. If μ is assumed to increase to a value of 0.5 in the plastic region, only a slight change occurs in the shear lag correction factor.

If there is no eccentricity of loading up to the point of failure, the value of σ may be taken equal to σ_0 in determining $\bar{A}_e$. The quantity A_e and the slope of the A_e versus σ_0 curve may be obtained from load-strain data taken during panel compression tests, or, in the absence of test data, some reasonable effective width formulation may be satisfactory.

Unfortunately there are no test data available by which the foregoing analysis may be judged. Extension of the theory to include the results of eccentricity therefore seems unjustified at the present time. The effects are probably similar to those caused by plasticity, since the value of σ in Eq. (46) may differ considerably from σ_0 if curvature is appreciable.

However, the relations developed make it evident that when curvature is such as to increase compression in the skin, the column rigidity is reduced below that of the straight panel, while for bowing in the opposite direction, the rigidity may be increased. Increased column strength may sometimes be obtained, therefore, through the proper use of eccentric loading.

The relations of Eqs. (46) and (47) indicate why the short-column curve for panel specimens occasionally has a shape inconsistent with previous theory. Often the curve departs "prematurely" from the Euler relation because of reduction in $\bar{I}$ when the skin buckles. Sometimes the short-column curve resembles neither a Johnson's parabola nor a straight line but is concave upward. At times this shape has been loosely attributed to possible torsional instability, but it is readily accountable by the variations in $\bar{A}_e$ with σ.

End-Fixity of Column Test Specimens

Inaccuracies of Current Methods

It is generally assumed that an end-fixity of $c' = 3.0$ is developed when a panel compression specimen, with ends milled flat and parallel, is tested between the flat, rigid platens of a testing machine.[15, 16, 17, 18] The uncertainty of this assumption, however, is repeatedly stated in the literature. In several instances in which some determination of test end-fixity was made, values of c' have ranged all the way from below 2.0 up to 4.0.[17]

When the end-fixity is not determined, lack of scatter in the test results is no proof of the accuracy of the data, for inconsistencies would be expected rather when the tests are made under varying conditions by different observers and with different equipment. Allowable stress data in the short-column range, therefore, when determined from test data with the assumption of $c' = 3.0$, are subject to a possible error of plus or minus 20 per cent, and the existence of better accuracy is difficult to prove.

Some methods have been proposed whereby the test end-fixity is determined for each column section and test conditions.[15, 17] These methods are based on the premise that the value of c' is invariant with the specimen length and the load. Actually, it appears that the greatest variations in c' are due to the effect of the length and the magnitude of the failure load.

The fact that full fixity is not realized in column tests may be due, first, to additional moments caused by eccentricities and end-conditions and, second, due to the existence of elastic restraint conditions at the ends. The first factor will have a negligible effect on the maximum load of a long column but will cause a reduction in the strength of short columns. The effect of a given set of end-conditions may therefore be expected to be more severe as the length of the column is decreased up to the point of local buckling or block compression effects. Consequently, if initial bowing or irregular end-conditions exist, the value of c' must vary, being smaller for the shorter columns.

If, on the other hand, the reduction in c' is due to elastic restraint, the effect is again a variable one. Since α would be defined solely by the rotation of the

testing machine head and the corresponding restoring moment, it could be considered constant for different length specimens. In this case, Figs. 5 and 6 indicate that c = constant $\times$ (L/D) and, since the critical load is a function of D/L and α, c' must decrease with larger critical loads.

The assumption of constant end-fixity for different length specimens is consequently not much better than that of $c' = 3.0$ for all specimens.

Need for Improved Technique

Experience has shown that the assumption of test end-fixity of $c' = 3.0$, coupled with that of $c' = 1.5$ in the aircraft structure, leads to conservative design. Accuracy of better than plus or minus 20 per cent in either of these assumptions, however, is questionable. While the improvement in one of these quantities without a corresponding improvement in the other cannot be justified for current design purposes, test data, if properly obtained, will have a certain permanent value. If it is possible to improve the accuracy of the test data without too great an expenditure, it should be done so that identical structures will not need to be retested at some future date.

In addition, if column data obtained in tests of different structures are to be compared with each other for the purpose of determining the effects of variations in size, shape, skin thicknesses, etc., the unknown fixity effects in test conditions provide a source of error considerably larger than the effects under investigation. In order to study these effects, therefore, and some day to reduce the amount of test work necessary to determine allowable stress values for design purposes, the end-fixity in column tests must be accurately determined.

Why Built-In Support Is Not Achieved

In the case of panel compression tests, it has been the practice at Lockheed Aircraft Corporation, as well as at several other aircraft plants, to machine the ends of the specimens flat, square, and parallel to the best tolerance possible and to test between flat, fixed platens. The statement of $c' = 4.0$ implies perfect bearing on the ends of the specimen and no rotation of the test head surfaces. Reasons why such conditions are seldom achieved have been noted as follows:

(1) *Rotation of the test heads.* Under eccentric load, the test heads of some testing machines are found to rotate with respect to each other. This rotation may occur to some extent about either horizontal axis. The source of this freedom is suspected to be in the bearing of the upper test head on the screw threads, in the deflection of the supports, or in the measuring capsule. Though the rotation may be less than a degree before "bottoming" occurs, up to this point the ends of the specimen are not fixed but are elastically restrained, and afterward the specimen contains initial curvature.

Because of these effects, variations in opposite edge stresses of as much as 40 per cent have been measured in some specimens. Failure loads varying by as much as 10 per cent between identical specimens have been observed concurrent with variation in test head rotation. The process of centering under load results in more consistent results, but the technique as applied under conditions of quasi-fixity becomes increasingly difficult with larger specimens, and the incidence of skin-buckling, with consequent shift in the centroid, sometimes makes test head rotation unavoidable.

(2) *Irregularities in end-conditions.* Perfect bearing on the ends of the specimen is seldom achieved due to machining tolerances, slight irregularities in the platens, etc. Such effects produce initial eccentricities and initial curvature which will affect short-column data and may, in some cases, affect the skin-buckling phenomena and so change the effective rigidity.

Such troubles have been noted by other observers[8,11] and are probably common to many laboratories, since $c' = 4.0$ is such a rarity. Under these conditions, neither the end-restraint (α) nor the initial eccentricities can be assumed constant. The accurate evaluation of c' requires some modifications of test procedure and equipment.

Pin-End Column Tests

The use of suitable test fixtures that will insure pin-end conditions has been proposed[11, 20] as a means of eliminating uncertainties regarding the value of c'. This method of testing has distinct advantages for specimens in which skin-buckling does not occur. It is necessary to center under load in order to eliminate possible initial eccentricities; this practice, however, is not difficult, and the test data apparently have high accuracy. But, when skin-buckling occurs before the column strength is reached, the neutral axis of the specimen shifts. This shift is ordinarily of the magnitude of 0.2 to 0.4 of the core radius of the section, and the resultant decrease in strength of a short column may be 10 or 20 per cent.

To avoid such errors, it is the practice in some laboratories to repeat the tests with the loading centroid in different positions until a peak value of the test load can be defined. Such a test procedure is likely to lead to further errors of an unconservative nature, since the plane of loading for maximum test load of buckling skin specimens is not in general coincident with the neutral axis. As previously mentioned, the effective rigidity decreases when the panel bows in the direction of the stiffener but increases with bowing in the opposite direction. Consequently, initial eccentricity sufficient to predetermine bowing in the direction of the skin will result in the test load corresponding to the greater value of $\bar{I}$.

For these reasons the pin-end method of test must be rejected as unsatisfactory for the testing of panel structure.

Three-Bay Column Specimens

In the three-bay column test method, the specimen is made considerably longer than the actual test length, and pin-end support is furnished at two intermediate points. The lengths are symmetrically disposed, and the central bay is considered to be the test length.

Considering only the effects of variations in end-restraint, the equivalent fixity for the central bay of a three-bay specimen is determined, as indicated previously, by the adjacent spans and the extreme end-conditions. The values of α_2' and α_3' may be determined by Eqs. (29) and (30), and then c can be found from Fig. 5. In the case where all bays are identical, the intermediate supports are pin-ended, and the end-fixity coefficient is assumed to apply to a single span, the correspondence between test end-fixity at the extreme supports and the equivalent end-fixity for the central bay is found to be as follows:

Test End-Fixity	Equivalent Fixity for Strength of Central Bay
$c_1 = c_4 = 4.0$	$c = 1.51$
$c_1 = c_4 = 3.0$	$c = 1.41$
$c_1 = c_4 = 2.0$	$c = 1.26$
$c_1 = c_4 = 1.0$	$c = 1.0$

A certain percentage error in the assumption of test end-restraint will therefore cause one-fourth as great a percentage error in the calculated fixity effects on the test specimen.

The effect of errors due to initial eccentricities and uneven bearing conditions which produce a superimposed moment on the specimen are also somewhat reduced at the central bay. It is probable that, unless skin-buckling occurs, a reduction of about 50 per cent of possible test error may be obtained.

When skin buckling occurs, however, adjacent bays of the multiple-bay specimen have at times been observed to bow in the same direction instead of alternately in and out.[21] This higher-order wave form indicates much larger values of c than noted above and may be caused by the shift in neutral axis due to skin buckling which predisposes all bays to fail in the same direction. Until it can be proved that such conditions also prevail in the airplane structure, the multiple-bay method of test should be treated with caution.

Testing with Known End-Restraint

In reference 5, column tests were made by means of an apparatus that applied known end-restraint to the specimen. This method might be adapted to standard test work by using an auxiliary set of loading platens, supported as simple beams on calibrated springs. The determination of the equivalent end-fixity could then be made through the relations of Fig. 5 and Eqs. (36) and (42).

Analysis shows that this test arrangement is practically as sensitive to the effects of eccentricities and a moving neutral axis as is the pin-end apparatus described above and, consequently, does not offer a simple solution to the column test problem. Nevertheless, it would be possible, by making the proper measurements of end-rotation and lateral deflection, to determine the actual end-moments on the specimen and the true rigidity, D_x, of the specimen at all values of load. The variation of D_x with load and with curvature is far more significant in column analysis than the variation of ultimate stress with slenderness ratio.

While such intensive study is not practical for routine panel tests, it appears necessary at the present time to do some work along this line in order to extend the knowledge of the column phenomena. Simplification of test procedure may later become obvious.

Column Strength of Aircraft Panel Structure

It is current practice in the design of aircraft wing structure and fuselage structure to assume that the skin and stiffener combination acts as a simple column between rib or bulkhead supports and that sufficient end-restraint is furnished at these supports to result in an effective end-fixity coefficient of $c' = 1.5$.[15, 16] Experimental determinations of c' by the method of Howland[5] have indicated that a value of 1.8 is not uncommon. In view of the precision with which margins of safety of 2 and 3 per cent are computed in present-day stress analyses, it appears that the accuracy of the basic assumption of $c' = 1.5$ is entirely inadequate and that more logical strength determinations may be made from a consideration of each individual structure.

Possible Sources of Effective End-Fixity

Contrary to what some authorities have implied,[16] the source of the effective end-fixity in an aircraft panel does not lie in the rib structure. Experimental determinations of the coefficient of end-restraint due to the rib alone have shown that the ribs or bulkheads commonly used are usually incapable of providing as much as 1 per cent of the restraint necessary to develop $c' = 1.5$.

The difference between the strength of stiffened-skin panel structure and the pin-end column load may be attributed to several factors. The effect of side-fixity, the effect of lateral curvature (i.e., in a plane normal to the column load), and the increase in stability that occurs in skin-buckling panels continuous over several supports are quantities that can to some extent be treated analytically and are discussed in detail below. Other effects, such as the stabilizing or destabilizing influence of a distributed load acting normal to the skin surface and the effect of longitudinal curvature, appear too irresolute to be handled at present. More test data

and better correlation with analyses are necessary. There are undoubtedly other contributory effects as yet undetermined. Since the effective end-fixity of the structure can be determined only by reference to panel test data which, as previously mentioned, may be subject to considerable conservative error, a large part of the apparent end-fixity observed up to this time may be purely fictitious.

Side-Fixity of Panel

Timoshenko, on page 381 of reference 1, presents the solution for a compressed rectangular plate which is reinforced in the direction of the compressive load, simply supported on all four edges. The nonisotropic properties of the panel are handled by considering the flexural rigidities in the two dimensions:

$D_x = \bar{E}I_x$ = average spanwise flexural rigidity per unit width, corresponding to the moment M_x

$D_y = \bar{E}I_y$ = average chordwise flexural rigidity per unit width corresponding to the moment M_y

$D_{xy} = 2GI_{xy}$ = average torsional rigidity per unit width

The differential equation for the deflection surface of the plate is presented as:

$$D_x \frac{\partial^4 w}{\partial x^4} + 2D_{xy} \frac{\partial^4 w}{\partial x^2 \partial y^2} + D_y \frac{\partial^4 w}{\partial y^4} + P \frac{\partial^2 w}{\partial x^2} = 0 \quad (48)$$

where w is the deflection and x and y are the spanwise and chordwise coordinates. Assuming the deflection surface to be represented by:

$$w = A \sin (\pi x/L) \sin (\pi y/W) \quad (49)$$

where W equals chordwise width of the panel and A equals maximum deflection, substitution into Eq. (48) gives the maximum load for all edges simply supported as:

$$P_{max.} = \frac{\pi^2}{L^2} D_x + \left[2 \frac{\pi^2}{W^2} D_{xy} + \frac{L^2\pi^2}{W^4} D_y \right] \quad (50)$$

The first term of Eq. (50) is recognized as the pin-end column strength; the second term represents an additional strength due to side-fixity.

Solutions of this type for the more general case in which consideration is given to the chordwise shearing deformation and to several different edge conditions have been presented by Heilbron, of Lockheed Aircraft Corporation. Further refinement, however, is believed beyond the scope of the present paper.

The expression for D_x of a skin-buckling panel is given in Eq. (45). The value of D_y for panels stiffened with open sections is that of the skin alone; for corrugation panels, tests indicate D_y to be roughly double that of the skin and corrugation material considered separately. It has been found that D_{xy} may be conservatively taken equal to D_y. An experimental determination is, of course, the most satisfactory method of obtaining D_y and D_{xy}. Calculations made on representative structure indicate that the increase in strength due to edge-fixity may be of the order of 5 or 10 per cent.

Effect of Lateral Curvature

The critical stress for instability of a curved panel with longitudinal stiffeners is treated by Timoshenko on page 474 of reference 1. It is stated that the critical stress may be taken as

$$\sigma_{cr} = \sigma_e + (\sigma_{cr})_0 \quad (51)$$

where σ_e is the direct column strength of the structure neglecting curvature and $(\sigma_{cr})_0$ is critical stress of a long cylinder in which only the curvature effect is considered. This summation is also indicated by Ebner[22] and others.

For the case of a single wave between ribs, the value of $(\sigma_{cr})_0$ is:[1]

$$(\sigma_{cr})_0 = (2\bar{E}/R) \sqrt{I_y/h_x} \quad (52)$$

where R is the radius of curvature, I_y is the chordwise moment of inertia of the skin-stiffener construction per unit width (corresponding to D_y of Eq. (50)), and h_x is the equivalent thickness of the panel in the longitudinal direction. Since Eq. (52) leads to the classic value of the critical stress, which is about 0.6/0.3 times as large as experimental data and more complete analyses[23] have indicated to be true, a corresponding reduction appears to be in order. Noting that h_x is identical with the term A_e discussed in connection with Eq. (46), the relation for the increase in load due to curvature becomes, in terms of load per unit width,

$$P_{curv.} = (\bar{E}/R) \sqrt{A_{ze}I_y} \quad (53)$$

Increase in Strength Due to Skin Buckling

It has been noted repeatedly, in the testing of stiffened skin panels, that failure usually occurs in the direction of the stiffeners. The difference in effective longitudinal rigidity according to the direction of curvature was noted previously in connection with Eq. (45); the same effects may provide in some cases an increase in the strength of a skin-buckling panel that is continuous over several supports.

If pin-end supports are provided and if successive spans of the column are approximately the same in length and structure, column failure may be expected to occur by alternate spans bowing in opposite directions. Because of the curvature, the effective moment of inertia of the span which bows in the direction of the stiffener is less than the value computed by Eq. (47), while in the adjacent span the rigidity is increased. The resultant column structure may be approximately represented as in Fig. 7. The rigidity D_1 of the inward bowing panel is considered applicable over the equivalent pin-end length L_{e1}—i.e., between points of inflec-

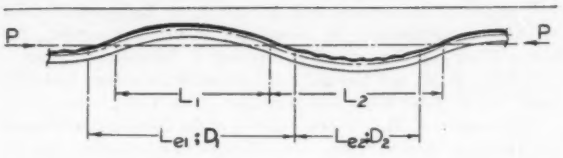

FIG. 7. Equivalent lengths and rigidities of adjacent spans of continuous panel structure.

tion—and, correspondingly, D_2 for the outward bowing panel applies to L_{e2}. It is evident that under the conditions of nonlinearity, by which D_1 and D_2 are related to the curvature, the instability load of the structure of Fig. 7 may be greater than that expected of the single-span, pin-ended column.

While the mode of failure described above is feasible and probably represents a minimum load condition, it is uncertain whether such a mode actually pertains to a given structure. If the reduction in effective skin area because of buckling is sufficient and if successive bays of the structure are practically identical, it is possible for all bays to bow in the direction of the stiffeners.[21] As previously noted, the structure may be stable under these conditions, and the failure will be that of a fixed-ended column subjected to eccentric load. It appears that the column strength under these loading conditions would be considerably greater than that predicted by the assumption of $c' = 1.5$, and it is possible that in the majority of cases no other type of failure need be considered.

Further progress may be expected in this study when information regarding the variation of D_x with curvature becomes available. It does not appear profitable at this time to extend analytical reasoning further without investigation and substantiation by means of tests.

CONCLUSIONS

No one will deny the value of a generalized approach in the treatment of a problem no matter what the problem or how specific it may be. The application of such tactical methods, however, is often difficult or obscured. In fact, in questions concerning aircraft column structure quite the opposite method of attack has repeatedly been used, and conclusions pertaining to problems somewhat general in nature have been drawn from special case solutions. While such short-cut methods are often justifiable, investigation indicates that the consequent inaccuracies have been considerably more severe than was generally suspected.

The first portion of this report is concerned with the presentation of mathematical methods sufficiently general for handling most of the possible problems concerning continuous columns elastically restrained at the supports. The practical value of this information is probably greatly exceeded by that of Figs. 5 and 6, by means of which the failure load of any particular bay may be readily computed.

Column problems are complicated by the variation of rigidity with the load which occurs due to plasticity effects and, in stiffened skin construction, due to skin buckling. When these variations exist, the slight initial eccentricities and initial bowing present in the practical column suddenly become important factors in determining the failure load. A satisfactory treatment of these several effects, including substantiating test data, is not available.

Because of initial eccentricities, as well as end-restraint conditions, the accuracy of column test data may be severely questioned. Actual test conditions are seldom if ever determined, it being current practice to assume a conservative value for c', the effective test end-fixity coefficient, or to assume that c' varies only with the cross section of the specimen. Neither of these assumptions can be justified; nor do they result in data of satisfactory accuracy. Further investigation appears to be necessary before a practical test procedure can be developed.

In the analysis of monocoque structure in aircraft, considerable possibility of improvement in accuracy exists in the determination of column strength from characteristics of the design in place of the assumption of effective end-fixity of $c' = 1.5$. Success in this method probably depends to a large extent on the accurate determination of the column properties from static tests. At present, the source of effective end-fixity is not much better than conjecture. Considerable investigation and tests are necessary before the accuracy of stress analyses can be placed on a par with the preciseness of the arithmetical work such analyses usually contain.

REFERENCES

[1] Timoshenko, S., *Theory of Elastic Stability*, 1st Edition; McGraw-Hill Book Company, Inc., New York, 1936.

[2] Way, Stewart, *Stability of Bars with Lateral and Axial Loading*, Journal of the Aeronautical Sciences, Vol. 2, No. 1, p. 46, November, 1935.

[3] Osgood, Wm. R., *Column Strength of Tubes Elastically Restrained Against Rotation at the Ends*, N.A.C.A. T.R. No. 615, 1938.

[4] Wozniak, F. B., *Beam Column End Moments for Known Fixity*, Aviation, Vol. 40, No. 1, p. 52, January, 1941.

[5] Howland, W. L., *A Method of Determining End-Fixity*, Journal of the Aeronautical Sciences, Vol. 6, No. 7, pp. 284–288, May, 1939.

[6] von Kármán, Th., *Untersuchung über Knickfestigkeit*, Mitteilungen über *Forschungsarbeiten* auf dem Gebiete des Ingenieurswesens, No. 81, p. 45, Berlin, 1910.

[7] Osgood, Wm. R., *The Double Modulus Theory of Column Action*, Civil Engineering, Vol. 5, No. 3, pp. 173–175, March, 1935.

[8] Templin, R. L., Sturm, R. G., Hartmann, E. C., and Holt, M., *Column Strength of Various Aluminum Alloys*, Aluminum Research Laboratories Technical Paper No. 1, Aluminum Company of America, New Kensington, Pa., 1938.

[9] Lundquist, E. E., *Local Instability of Symmetrical Rectangular Tubes under Axial Compression*, N.A.C.A. T.N. No. 686, 1939.

[10] Westergaard, H. M., and Osgood, Wm. R., *Strength of Steel Columns*, Transactions A.S.M.E., Vol. 50, 1938.

[11] Osgood, Wm. R., and Holt, M., *The Column Strength of Two Extruded Aluminum Alloy H-Sections*, N.A.C.A. T.R. No. 656, 1939.

[12] Cox, H. L., *Stress Analysis of Thin Metal Construction*, Journal of The Royal Aeronautical Society, Vol. 44, pp. 231–282, March, 1940.

[13] Hoff, N. J., *Instability of Monocoque Structures in Pure Bending*, Journal of The Royal Aeronautical Society, Vol. 42, pp. 291–346, April, 1938.

[14] Hartmann, E. C., and Moore, R. L., *Bending Tests on Panels of Stiffened Flat Sheet*, Aluminum Research Laboratories Technical Paper No. 4, Aluminum Company of America, New Kensington, Pa., 1941.

[15] Army-Navy-Civil Committee on Aircraft Requirements, *Strength of Aircraft Elements* (ANC-5), pp. 1–29, U.S. Government Printing Office, Washington, D.C., October, 1940.

[16] *Handbook of Instructions for Airplane Designers*, Matériel Division, U.S. Army Air Corps, Vol. I, Section II, Part IV, p. 509, Revision 4, September 1, 1940.

[17] Sechler, E. E., and Newell, J. S., *Progress Report on Methods of Analysis Applicable to Monocoque Aircraft Structures*, Air Corps Technical Report 4313, Revision I, January 15, 1942.

[18] Niles, A. S., and Newell, J. S., *Airplane Structures*, 2nd Edition, Vol. I; John Wiley and Sons, Inc., New York, 1938.

[19] Schwartz, E. H., *An Investigation of the Compressive Strength Properties of Stainless Steel Sheet Stringer Combinations, Part II*, Air Corps Technical Report, Serial No. 4096, U.S. Government Printing Office, Washington, D.C., 1937.

[20] Barlow, H. W., *A Fixture for Obtaining Pin-End Conditions in Column Testing*, Journal of the Aeronautical Sciences, Vol. 7, No. 2, p. 72, December, 1939.

[21] Holt, M., *The Effect of Methods of Testing on the Ultimate Loads Supported by Stiffened Flat Sheet Panels under Edge Compression*, N.A.C.A. T.N. No. 811, 1941.

[22] Ebner, H., *Strength of Shell Bodies—Theory and Practice*, N.A.C.A. T.M. No. 838, 1937.

[23] von Kármán, Th., Dunn, L. G., and Tsien, Hsue-Shen, *The Influence of Curvature on the Buckling Characteristics of Structures*, Journal of the Aeronautical Sciences, Vol. 7, No. 7, pp. 276–289 May, 1940.

[24] Langhaar, Henry L., *Buckling of Aluminum-Alloy Columns and Plates*, Journal of the Aeronautical Sciences, Vol. 10, No. 7, pp. 218–222, July, 1943.

Study of Exhaust-Valve Design from Gas Flow Standpoint*

SENG-CHIU HU†
China Aircraft Corporation

ABSTRACT

The object of the research described in this paper is to investigate the flow characteristics during the exhaust blowdown and to develop a rational background for designing and improving the present poppet-type exhaust valves of aircraft and automotive engines. The research was carried out in three main steps: (1) theoretic study of gas flow through exhaust valves; (2) experimental study of gas flow coefficient during exhaust blowdown; (3) correlation and discussion of the data obtained.

It is found that by means of a simple modification on a conventional valve, such as the valve from a C.F.R. engine, the maximum mass rate within the most useful range of the valve lift can be increased by at least 25 per cent. Such a gain could be obtained with no additional cost, since neither the diameter of the valve nor the size of the port need be changed.

In the course of the work a series of modifications of the profiles of valves and seats were investigated. The topics are: (1) stem fillet, (2) inner rounds, (3) outer rounds, (4) head enlargement, (5) seat angle, and (6) profile of port approach. The records of their effects on valve performance are grouped, compared, and explained both graphically and theoretically in order to give a sound basis for exhaust-valve design.

The pressure range investigated extends from critical pressure (atmospheric pressure/0.53) up to 80 lbs. per sq.in. It covers the actual operating conditions of modern unsupercharged and moderately supercharged aircraft, as well as automotive engines. Experiments agreeing with the theory indicate that the flow coefficient is almost independent of, and increases slightly with, the initial pressure. The results of this research, therefore, can be successfully applied on the safe side, to prospective highly supercharged engines with an exhaust pressure higher than 80 lbs. per sq.in.

INTRODUCTION

IT HAS LONG BEEN RECOGNIZED by designers and manufacturers of internal combustion engines that the energy lost through the exhaust valve is even greater than the remainder available to run the engine. A typical analysis of fuel energy distribution[2] clearly illustrates this fact. Is it possible to reduce such a serious loss by any considerable amount?

On the basis of a pressure-volume diagram, the exhaust loss can be graphically represented as in Fig. 1 and may be subdivided into three major parts: (a) exhaust blowdown loss, (b) exhaust stroke loss, (c) energy carried out by the exhaust gas. Both practical experience and theoretic investigation have shown the impracticability of reducing the (c) loss. However, with respect to (a) and (b) some work can be done. The exhaust valve is the first thing to be dealt with in order to reduce the energy loss of these two parts.

The exhaust valve, as well as the carburetor, the inlet valve, and the spark plug or supercharger, forms an essential part of the complete fuel system. It is the last tool by which the engine converts the fuel energy into mechanical power. A poor exhaust-valve design produces many difficulties, such as high back pressure, lower volumetric efficiency, greater frictional or throttling loss, a higher percentage of residual gas, and higher cylinder head and valve temperatures. As a result, the power is greatly reduced and the life of the engine is shortened. The superficial way to treat these troubles is to increase the size of valves and ports. Such an arrangement not only increases the weight, the cost, the vibration, and the strength problem of the engine but also produces an overheated valve that in turn decreases the volumetric efficiency and cuts down the power output of the engine.

During the last 30 years, numerous experiments and analyses in the field of the poppet-type valves have been carried out throughout the whole world,[5, 6, 7, 8, 9] but none of them has ever touched on supersonic exhaust gas flow. It is therefore the primary object of this paper to study the performance of such a supersonic flow during the exhaust blowdown period and to

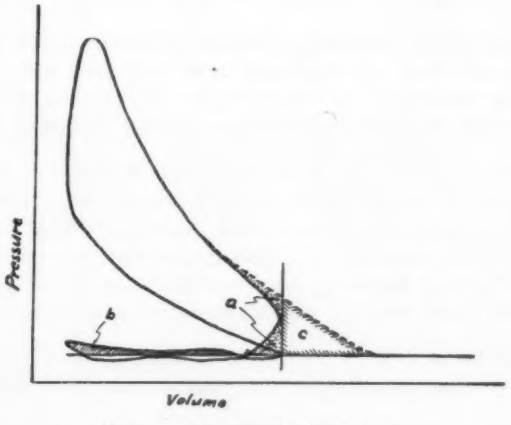

FIG. 1. Diagram of exhaust loss.

Presented at the Power Plants and Propellers Session, Eleventh Annual Meeting, I.A.S., New York, January 25–29, 1943.

* This research was conducted in the Sloan Aircraft and Automotive Engine Laboratory of the Massachusetts Institute of Technology. The author gratefully acknowledges the guidance and advice of Profs. C. F. Taylor and E. S. Taylor.

† Formerly Engineer, Chance Vought Aircraft Division, United Aircraft Corporation.

develop a rational way of designing an exhaust valve to cut down the exhaust loss without increasing the size of the valve.

Theoretic Analysis

General

Gas flow through an exhaust valve is nothing but a free blowing of some highly compressed gas through a hole from the cylinder. It is quite reasonable to consider that the frictionless adiabatic free expansion is an ideal case or the limiting case of the gas flow through an exhaust valve.

Referring to Bernoulli's equation

$$\int [(dp/\rho) + (U^2/2)]_1^2 = 0 \qquad (1)$$

$$\frac{U_2^2 - U_1^2}{2g} = \int_2^1 v\, dp \text{ or } - \frac{U_t^2 - U_t^2}{2g} = \int_t^1 v\, dp \qquad (2)$$

where U is the velocity; p, the pressure; ρ, the mass density; v, the specific volume; g, the gravitational acceleration; "1," the station inside the cylinder; "2," the station outside the cylinder; and t, the throat of the valve or the narrowest passage of the exhaust flow.

During the adiabatic process $p_1v_1^n = p_2v_2^n = p_tv_t^n$ and neglecting the velocity inside the cylinder U_1 (in comparison with the high velocity of the gas flow (U_t through the valve throat), the mass rate is

$$G = a_tU_t\rho_tg_t = \frac{a_tU_t}{v_t} = \frac{a_t}{v_t}\sqrt{2g\frac{p_1v_1n}{n-1}\left[1 - \left(\frac{p_t}{p_1}\right)^{\frac{n-1}{n}}\right]} \qquad (3)$$

where a is the cross-sectional area of the flow and n is the adiabatic exponential constant.

The condition for maximum gas flow, therefore, is

$$\frac{dG}{dp_t} = 0 \quad \text{or} \quad p_t = p_1\left(\frac{2}{n+1}\right)^{\frac{n}{n-1}} \qquad (4)$$

This is the well-known critical pressure at which the gas flows at maximum mass rate and with a sonic velocity.[4] In other words, the gas flow rate through the valve will increase until p_2 decreases to $[2/(n+1)]^{\frac{n}{n-1}}p_1$. If p_2 drops still further, the gas flow or G/a cannot decrease as indicated by Eq. (3) but will maintain a constant value corresponding to the maximum value of G/a. This implies that the velocity at the cross section a_t cannot exceed a certain critical value (sonic velocity) which corresponds to the pressure ratio $[2/(n+1)]^{\frac{n}{n-1}}$. For if the velocity at a_t could exceed this critical value, the pressure at a_t would have to be less than $[2/(n+1)]^{\frac{n}{n-1}}p_1$. This would mean that at some cross section a'', reached before a_t and larger or at least equal to a_t, the pressure $[2/(n+1)]^{\frac{n}{n-1}}p_1$ itself would be established. Since for this critical pressure G/a'' is a maximum, this would imply that more fluid passes through section a'' than through a_t, which is impossible.

Flow During Exhaust Blowdown

During the blowdown period—i.e., the period directly following the sudden opening of the exhaust valve—the pressure inside the cylinder is high in comparison with the pressure outside. In other words, the pressure inside the cylinder p_1 isf ar above the critical pressure, and the pressure at the throat p_t is $[2/(n+1)]^{\frac{n}{n-1}}p_1$. Taking the gas constant $R = 53.3$ and the adiabatic exponential constant $n = 1.4$ (or $p_t = 0.53p_1$) and substituting Eq. (4) into Eq. (3), the flow equation becomes

$$G = a_tU_t\rho_tg = a_t\sqrt{\frac{2gn}{n-1}\left(\frac{p_1}{v_1}\right)\left[\left(\frac{p_t}{p_1}\right)^{\frac{2}{n}} - \left(\frac{p_t}{p_1}\right)^{\frac{n+1}{n}}\right]} = 0.53a_t\frac{p_1}{\sqrt{T_1}} \qquad (5)$$

where a_t, the cross-sectional area of flow, is measured in square inches; p_1, the pressure inside the cylinder, in pounds per square inch absolute; T_1, the temperature inside the cylinder, in degree Rankine; and G, the flow rate, in pounds per second.

Flow at the End of Exhaust Blowdown

At the very end of the exhaust blowdown, the pressure inside the cylinder drops almost to the outside atmospheric pressure, i.e., below the critical limit. The exhaust gas flows out with a subsonic velocity. Such a flow can be directly handled by Eq. (3) but not by Eq. (10). In this paper, however, attention has been paid only to the sonic flow part of the exhaust blowdown because of the limitation of equipment. As a matter of fact, the sonic flow occupies the major part of the whole blowdown, while the subsonic flow occurs only at the very end of the exhaust process. Anything favorable to such a sonic flow would definitely improve the whole exhaust performance.

Flow Coefficient and Actual Discharge

The flow coefficient here is defined as the ratio of actual flow to that calculated by Eq. (3) (or Eq. (5) for sonic flow). The experiments described in the latter part of this paper indicate that the value of this coefficient is always less than one. This could be explained by the following possible factors: (a) presence of mechanical obstacles. The theoretic development was based on an ideal orifice, but the actual valve always has a stem and valve head that cause additional dis-

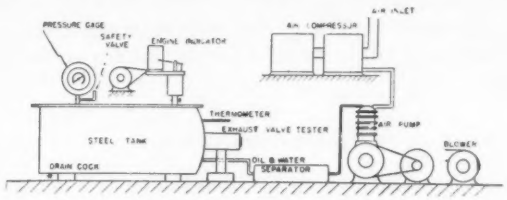

FIG. 2. Diagram of experimental setup.

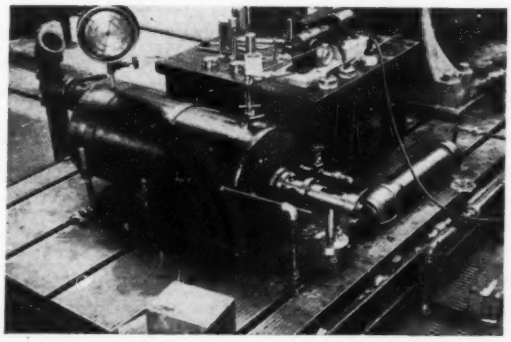

FIG. 3. Photographic view of experimental setup.

turbance of flow and loss of energy. (b) Imperfect upstream flow. In order to have a proper seating, it is impractical to use a perfectly round-shaped orifice as a valve port. A contraction of flow due to poor entrance, as illustrated by Guttermuth's experiments,[3] would always exist even at high valve lift. (c) Imperfect downstream flow. For sonic flow and supersonic flow, a De Laval nozzle can produce a "compression-shock" less flow only at its particularly designed pressure drop, while during free expansion a converging orifice always has a series of standing waves at its downstream end. The functioning of an exhaust valve is between that of a converging orifice and a nozzle; therefore, it must suffer the energy loss of such waves and shocks at its downstream end. (d) Fast expansion. In this experiment, as well as in the actual exhaust blowdown, the pressure drops rapidly. Because of the unevenness of temperature, such a rapid expansion has a complicated characteristic. Strictly speaking, it could be handled only by Gillespie's semirational formula derived from Beattie-Bridgeman's equation and in terms of apparatus constants.[10] In case of perfect gas, however, the effect is negligible, as Gillespie and Coe wrote in their report. (e) Unsteady flow. The theoretic treatment was developed on the assumption of steady flow, while the gas flow during the blowdown changes with time. This is also a reason why the theoretic equation must be used together with an experimental coefficient for practical application.

Summary of Theoretic Analysis

The theoretic analysis may be summarized as follows:

(1) The fluid will expand to the critical pressure in the throat and any further pressure drop must take place beyond this section, but the velocity and density at the throat determine the weight of flow that is possible for a given initial pressure to produce.

(2) When the pressure drop is above the critical limit, the velocity at the throat is the velocity of sound, and the velocity after the throat may be increased by further drop of pressure. For a true adiabatic expansion, no disturbance can therefore pass up a valve beyond the throat, and the weight of gas flow, as well as the pressure and the specific volume at the

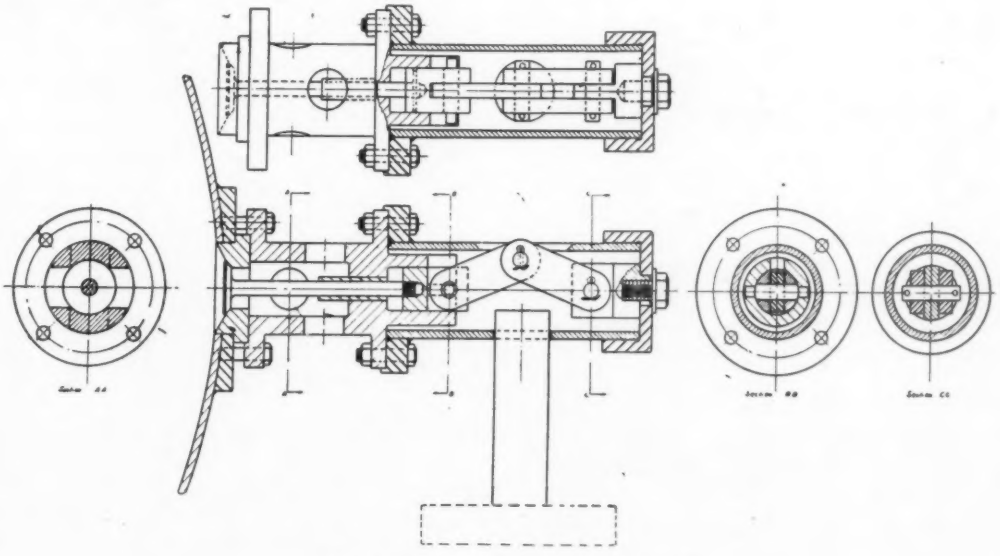

FIG. 4. Diagram of exhaust-valve tester.

throat, will not be affected by anything that happens downstream from the valve passage.

(3) The gas flow varies as the area of the restricted opening (the throat of the valve), as the pressure inside the cylinder, and inversely as the velocity of sound (which varies with temperature) (if T is constant, "$\left(\frac{G}{a}\right)_i = \left(\frac{G}{a}\right)_{max.}$" $\sim p_1$, "$p_{crit.} = p_1$" $\sim p_1$, $v_{crit.} = v_s = v_{sound}$, and $p_i \sim p_1$). Anything decreasing the friction and disturbance will help the process to approach the ideal case—that is, will improve the gas flow.

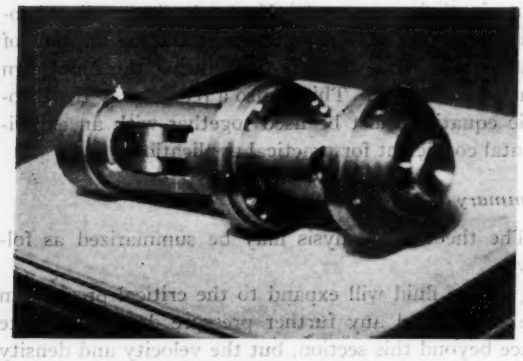

FIG. 5. Photographic view of exhaust valve tester.

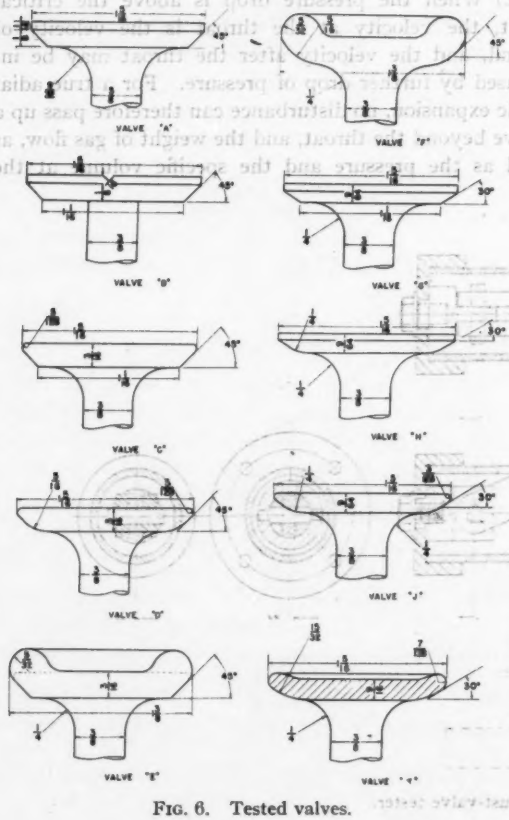

FIG. 6. Tested valves.

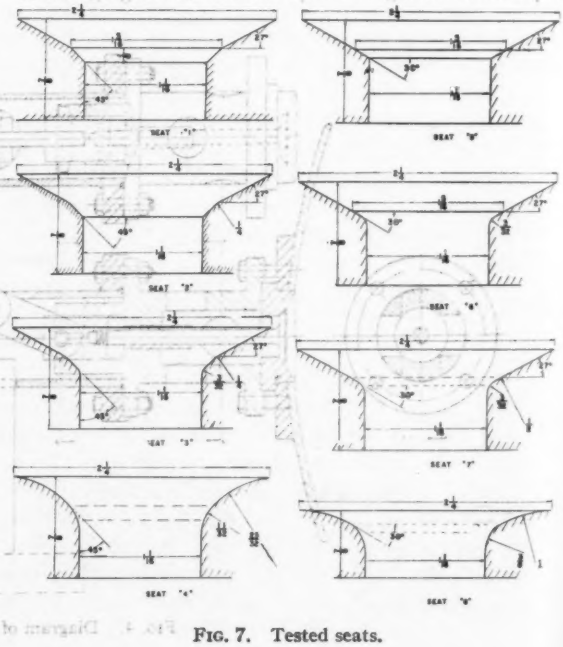

FIG. 7. Tested seats.

(4) The theoretic gas flow will differ from the actual case by certain coefficients that were determined experimentally and will be described in the latter part of this paper.

LABORATORY WORK

Figs. 2 and 3 represent the essential part of the laboratory setup. Briefly, the experiment consisted of pumping air into a steel tank to a pressure of 100 lbs. per sq.in. and suddenly releasing it through a specially designed exhaust-valve testing mechanism (Figs. 4 and 5). The pressure-time diagram was recorded by an engine indicator. In order to make a careful study of the effects of valve and seat profiles on flow performance, differently shaped valves and seats were constructed (Figs. 6 and 7) and tested in various combinations (Table 1). For each combination 27 indicator diagrams were taken at nine different valve lifts. Fig. 8 represents a sample set of such indicator cards at two different valve lifts as indicated. The final results in terms of flow rate were obtained by measuring the slope of these pressure-time curves with a milling-machine-telescope setup.

RESULTS

The preliminary results were assembled in the form of plots of flow coefficient versus pressure ratio. It is found that the value of the coefficient is almost independent of, and increases slightly with, the initial pressure. (This slight increase is probably due to the facts that a high pressure drop favors the vena contracta and that the air inside the tank absorbs the heat

TABLE 1

Various Combinations of Valves and Seats Tested (Refer to Figs. 6 and 7)

Series A1—Valve A, Seat 1—basic 45° valve (C.F.R. valve) and basic 45° seat.
Series B1—Valve B, Seat 1–45° valve and seat but without stem-to-head fillet.
Series D3—Valve D, Seat 3–45° valve and seat with inner and outer corner rounds (Fig. 10).
Series E2—Valve E, Seat 2–45° valve and seat with head enlargement.
Series F3—Valve F, Seat 3–45° valve and seat with head enlargement and inner and outer corner rounds.
Series F4—Valve F, Seat 4–45° valve and seat with head enlargement, corner rounds and converging port approach (Fig. 10).
Series G5—Valve G, Seat 5—basic 30° valve and seat (with sharp corners).
Series H6—Valve H, Seat 6–30° valve and seat with inner corner rounds.
Series J7—Valve J, Seat 7–30° valve and seat with both inner and outer corner rounds.
Series K8—Valve K, Seat 8—(optimum valve and seat) 30° valve and seat with inner corner rounds, outer corner rounds, slight head enlargement, and converging port approach.

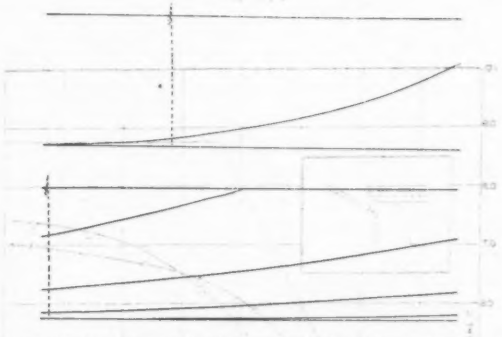

FIG. 8a (*top*). Sample indicator card at L/D = 0.424. FIG. 8b (*bottom*). Sample indicator card at L/D = 0.094.

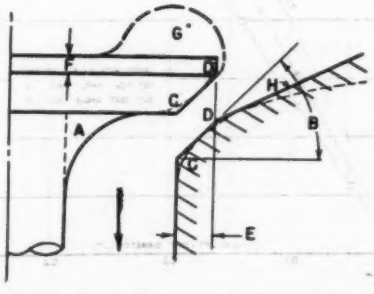

FIG. 9. Modifications of valve and seat profiles. A: stem fillet; B: seat angle; C: inner rounds (or inner corner rounds); D: outer rounds (or outer corner rounds); E: seat overlap; F: head thickness; G: head enlargement; H: port approach.

from the tank wall at the later part of the blowdown period.)

The final results are presented in Figs. 9 to 17. They are plotted in the nondimensional form of average flow coefficient (through the tested pressure range) against L/D, ratio of valve lift to port diameter.

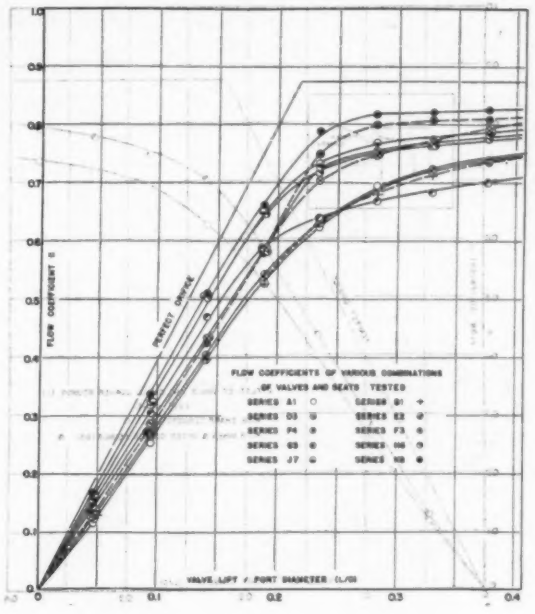
FLOW COEFFICIENT
PERFECT ORIFICE
FLOW COEFFICIENTS OF VARIOUS COMBINATIONS OF VALVES AND SEATS TESTED
VALVE LIFT / PORT DIAMETER

FIG. 10.

Calculation of Gas Flow Rate

With the experimental flow coefficients as plotted, all the theoretic equations discussed before could be used immediately to predict the characteristics of gas flow during the exhaust blowdown. However, instead of the adiabatic exponential constant of air 1.4, the actual value of that of the exhaust gas (slightly less than 1.4) should be used.

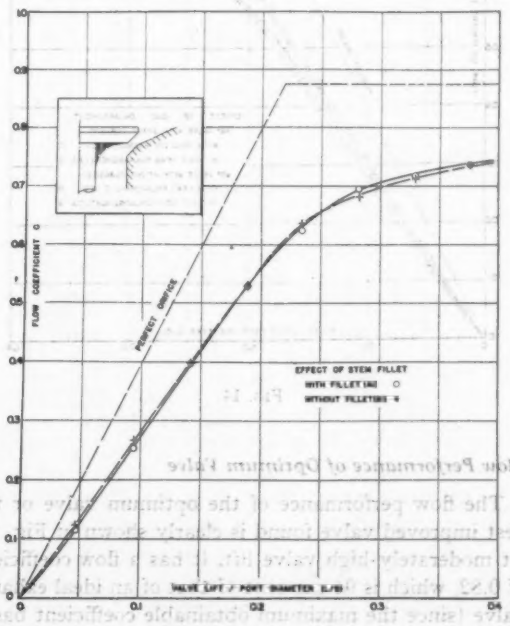

FIG. 11.

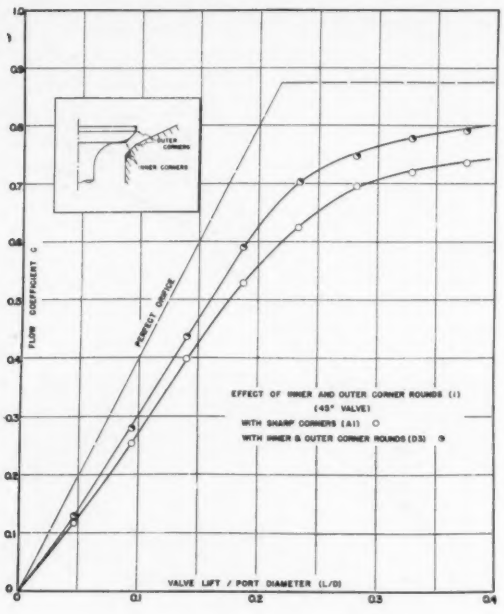
FLOW COEFFICIENT C
PERFECT ORIFICE
EFFECT OF INNER AND OUTER CORNER ROUNDS (I)
(45° VALVE)
WITH SHARP CORNERS (A1)
WITH INNER & OUTER CORNER ROUNDS (D3)
VALVE LIFT / PORT DIAMETER (L/D)

FIG. 12.

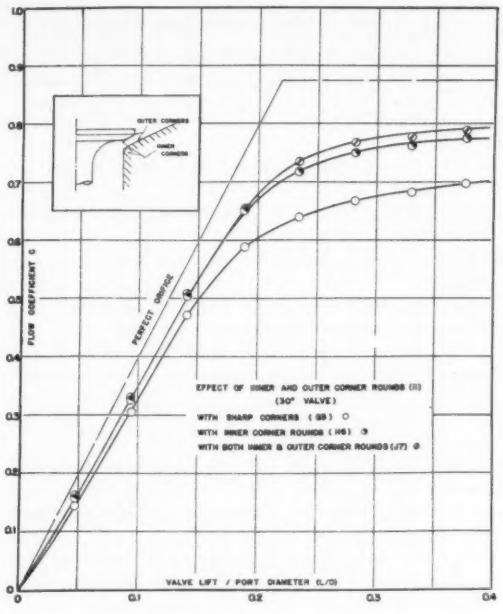
FLOW COEFFICIENT C
PERFECT ORIFICE
EFFECT OF INNER AND OUTER CORNER ROUNDS (II)
(30° VALVE)
WITH SHARP CORNERS (B3)
WITH INNER CORNER ROUNDS (H5)
WITH BOTH INNER & OUTER CORNER ROUNDS (J7)
VALVE LIFT / PORT DIAMETER (L/D)

FIG. 13.

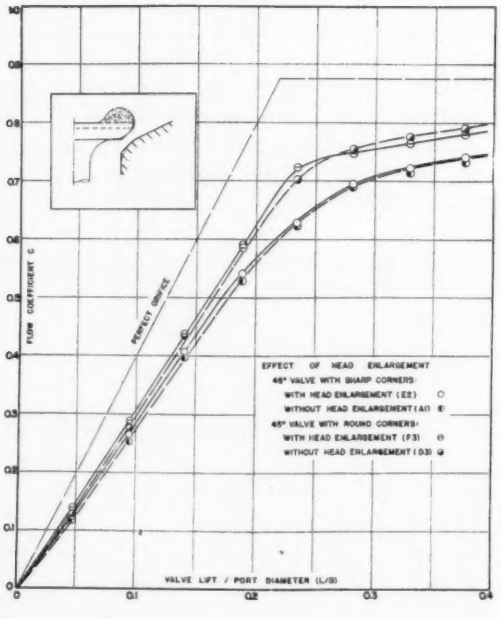
FLOW COEFFICIENT C
PERFECT ORIFICE
EFFECT OF HEAD ENLARGEMENT
45° VALVE WITH SHARP CORNERS:
WITH HEAD ENLARGEMENT (E2)
WITHOUT HEAD ENLARGEMENT (A1)
45° VALVE WITH ROUND CORNERS:
WITH HEAD ENLARGEMENT (F3)
WITHOUT HEAD ENLARGEMENT (D3)
VALVE LIFT / PORT DIAMETER (L/D)

FIG. 14.

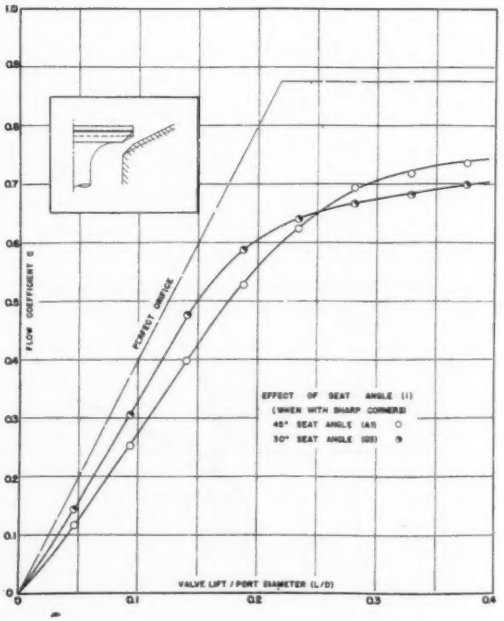
FLOW COEFFICIENT C
PERFECT ORIFICE
EFFECT OF SEAT ANGLE (I)
(WHEN WITH SHARP CORNERS)
45° SEAT ANGLE (A1)
30° SEAT ANGLE (B3)
VALVE LIFT / PORT DIAMETER (L/D)

FIG. 15.

Flow Performance of Optimum Valve

The flow performance of the optimum valve or the best improved valve found is clearly shown in Fig. 18. At moderately-high valve lift, it has a flow coefficient of 0.82, which is 94 per cent of that of an ideal exhaust valve (since the maximum obtainable coefficient based on port area is [(port diameter)^2 − (stem diameter)^2]/(Port diameter)^2 or 0.875 for C.F.R. valve and 0.82/0.875 = 94 per cent).

In comparison with C.F.R. valve at medium lift, say $L/D = 0.235$, the gain in flow capacity is (0.790 − 0.624)/0.624 = 26.6 per cent. While at low lift, say $L/D = 0.141$, the gain is (0.510 − 0.398)/0.398 = 28 per cent.

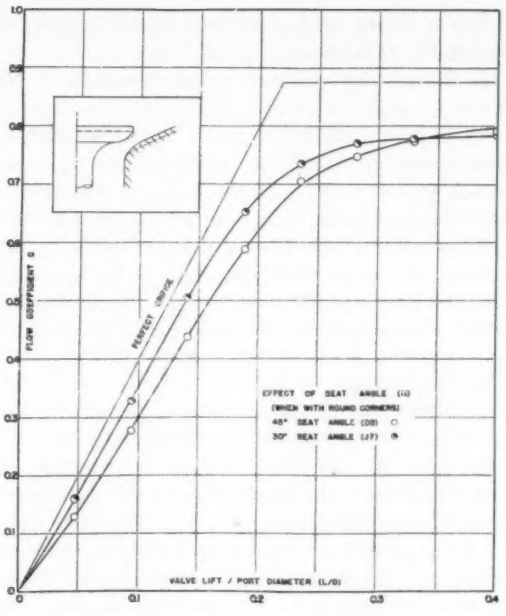
FLOW COEFFICIENT C
PERFECT ORIFICE
EFFECT OF SEAT ANGLE (I1)
(WHEN WITH ROUND CORNERS)
45° SEAT ANGLE (I09)
30° SEAT ANGLE (I17)
VALVE LIFT / PORT DIAMETER (L/D)

FIG. 16.

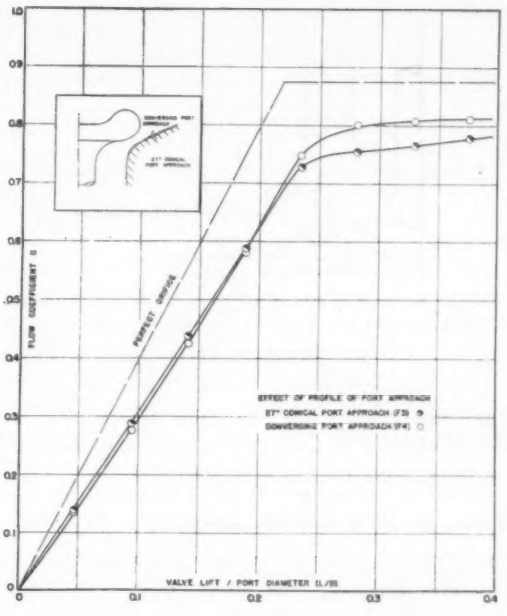
FLOW COEFFICIENT C
PERFECT ORIFICE
EFFECT OF PROFILE OF PORT APPROACH
37° CONICAL PORT APPROACH (F3)
CONVERGING PORT APPROACH (F4)
VALVE LIFT / PORT DIAMETER (L/D)

FIG. 17.

Effect of Profile Modifications

By keeping both the port diameter and valve head diameter constant, the valves and seats were tested with various modifications (Fig. 9), the effects of which are as follows: (a) Stem to Head Fillet—As shown in Fig. 11, the effect of the stem fillet is negligible. This agrees with the theoretic statement that the changes at the downstream of the throat have no effect on flow rate (for a true adiabatic expansion above critical limit). (b) Inner and Outer Corner Rounds—Valve performance can be appreciably improved by rounding the sharp corners. This can be seen from the point of separation and contraction. As represented in Figs. 12 and 13, the fact that the inner rounds are more effective than the outer rounds is probably due to the conical shape of the flow passage. As indicated in Fig. 19, air flows through the valve aperture from "O" to "I," i.e., from the larger sectional area to the smaller one. To discharge at "I" the same amount of air as at "O," the flow is choked at the narrow aperture "I" rather than at "O." The flow characteristics therefore are far more influenced by the inner rounds at "I" than by the outer rounds at "O." (c) Head Enlargement—The flow rate at low lift can be slightly increased by the enlargement of the valve head. This may be due, in part, to the formation of a better entrance. Such an increase is upset, however, at high lift by the increased volume of the obstacle (Fig. 14). (d) Seat Angle—The 30° seat angle is better than 45° seat angle at low lift. This is due to the difference in the net cross-sectional area of the passage (as in Fig. 19: $d_{30°} = L \cos 30°$, $d_{45°} = L \cos 45°$, therefore $d_{30°} > d_{45°}$). However, at high lift the narrowest passage for the flow is the area of the valve port rather than the conical seat aperture. The 45° seat angle is therefore better than the 30° seat angle because of the less acute turn of the flow at inner corner "I." Fig. 15 is the experimental proof of this statement. (e) Profile of Approach—As shown in Fig. 17, to shape the profile of the port approach as a converging orifice improves the flow only at high valve lift. The reason is that the port opening functions as a

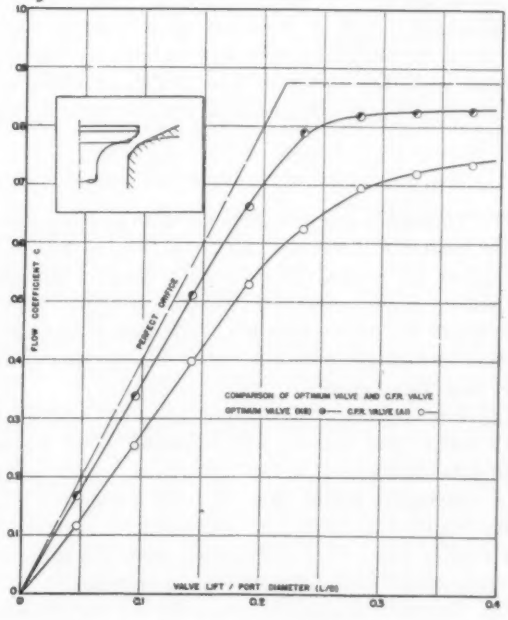
FLOW COEFFICIENT C
PERFECT ORIFICE
COMPARISON OF OPTIMUM VALVE AND C.F.R. VALVE
OPTIMUM VALVE (I08)
C.F.R. VALVE (A3)
VALVE LIFT / PORT DIAMETER (L/D)

FIG. 18.

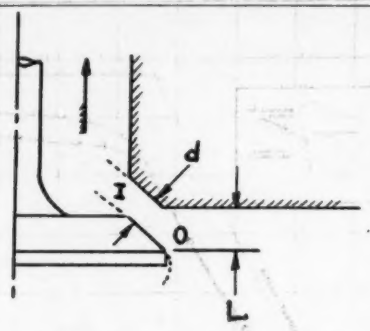

FIG. 19. Flow passing valve throat.

throat only when the valve lift is greater than one-fourth of the port diameter. At low lift, therefore, the effect of port approach is negligible.

Comparison with Previous Research

The results of this paper do not agree exactly with the knowledge obtained from inlet valve experiments. This is evidently due to the difference of flow direction and the presence of acoustic velocity. Nevertheless, the effect of seat angle and round corners on flow performance agrees very well with Tanaka's exhaust valve experiments, in spite of the existence of supersonic flow. There are no suitable data available, however, for comparison with the other results of this paper because of the absence of previous studies on such acoustic exhaust flow.

CONCLUSIONS

(1) Through a simple modification on a conventional valve, such as a valve from the C.F.R. engine, the maximum flow rate within the most useful range of the valve lift can be increased at least by 25 per cent. Such a gain could be obtained with no additional cost, since neither the diameter of the valve nor the size of the port need be changed.

(2) The optimum valve found has a 30° seat angle, with slight head enlargement, rounded at all corners with moderate radiuses and seated on a port shaped as a converging orifice (Fig. 9). At moderately high valve lift its flow coefficient is about 0.82, which is 94 per cent of that of an ideal orifice with the same net opening area (= area of port − area of stem).

(3) The maximum useful valve lift for the optimum valve found is about 28 per cent of its port diameter. However, for a conventionally shaped valve the lift should be designed as high as feasible, since the flow coefficient increases steadily with the valve lift, even when the L/D ratio is as high as 0.45.

(4) Within the pressure range investigated (from critical pressure to 80 lbs. per sq.in.), the flow coefficient is practically independent of the pressure drop across the valve. Therefore, if the exhaust valve of an aircraft engine is designed for sea-level condition and shows efficient performance during its ground test, it would so remain regardless of flying altitude, manifold pressure, or degree of supercharging. From the same point of view, it would seem that all the results of this paper could be successfully applied even to prospective highly supercharged engines with an exhaust pressure higher than 80 lbs. per sq.in.

(5) With regard to profile modifications (Fig. 9), the results may be summarized as follows: (a) Stem Fillet —The effect of a stem-to-head fillet of an exhaust valve is negligible from gas flow standpoint. (b) Inner and Outer Corner Rounds—Flow performance can be greatly improved by rounding the inner and outer corners of the valve, the former being more effective. (c) Head Enlargement—By enlarging the valve head, the flow coefficient can be slightly raised at low valve lifts. (d) Seat Angle—A 30° seat angle is favorable at low valve lift; a 45° seat angle, at high valve lift. (e) Profile of Port Approach—To shape the profile of the port approach as a converging orifice increases the flow capacity appreciably at high valve lift.

REFERENCES

[1] Taylor, C. F., and Taylor, E. S., *The Internal Combustion Engine;* International Text Book Company, Scranton, Pa., 1938.

[2] Pye, D. R., *Internal Combustion Engine;* Oxford University Press, New York, 1934.

[3] Stodola, A., and Loewenstein, L. C., *Steam and Gas Turbine;* The McGraw-Hill Book Company., Inc., New York, 1927.

[4] Tietjens, O. G., *Flow of Gases at Rate Exceeding the Acoustic Velocity,* A.S.M.E. Transactions, Vol. 53, No. 3, pp. 49–58, January–April, 1931.

[5] Lewis, G. W., and Nutting, E. M., *Air Flow Through Poppet Valves,* N.A.C.A. T.R. No. 24, 1918.

[6] Eck, Bruno, *Potential Flow in Engine Valves,* N.A.C.A. T.M. No. 343, 1925.

[7] Tanaka, K., *Air Flow Through Exhaust Valve of Conical Seat,* Report of Aero. Research Institute, Tokyo Imperial University, No. 67, January, 1931.

[8] Dennison, E. S., Kuchler, T. C., and Smith, D. W., *Experiments on Flow of Air Through Engine Valves,* A.S.M.E. Transactions, Vol. 53, No. 17, pp. 79–97, September–December, 1931.

[9] Wood, Hunter, Taylor, and Taylor, *Air Flow Through Inlet Valves,* M.I.T. Sloane Automotive Laboratory Report (unpublished), 1941.

[10] Gillespie, L. J., and Coe, J. R., *The Heat of Expansion of a Gas of Varying Mass,* Journal of Chemical Physics, Vol. 1, 1933.

Medical Activities in Military Aviation

OTIS O. BENSON, JR.,* DAVID B. DILL,† AND W. RANDOLPH LOVELACE, II‡

Aero Medical Laboratory, Engineering Division, Army Air Forces Materiel Command, Wright Field

Introduction

IT IS OBVIOUS that an air force, as a military machine, can have only three purposes for its existence: (1) destruction of the enemy or enemy matériel; (2) counter aviation; (3) transport. The last purpose more or less resolves itself into transporting fighting men to a battleground so that they can destroy the enemy or his matériel. All other functions performed by an air force are secondary to the main objectives.

It immediately becomes apparent that, to accomplish the goals mentioned, multitudinous and complicated tasks are to be performed and, first, the planes must be built. Here, then, is where efforts immediately separate into almost every conceivable form of activity: obtaining of raw materials, processing of these materials, and final fabrication of aircraft and accessories. In this gigantic task, which is written off here in a few sentences, are the efforts of untold numbers of laborers and craftsmen and the genius and skill of the engineering professions. The medical profession also has contributed in a quiet way throughout this process of fabrication, but when men fly these airplanes, aviation medicine plays a more intense and dramatic role. We must have military aircraft of all types to accomplish the purposes set forth, but, up to this date at least, men must fly them. The interest of the medical officer centers in these fliers, and it is his purpose to protect and enhance the health, morale, and tactical efficiency of these men. He, too, is not unmindful of the ground crews and supporting personnel.

The Medical Task

It is, perhaps, fitting to survey the problems that confront the medical officer and to indicate the lines along which efforts are directed. The major problems are: (1) selection of personnel of all flying categories and of technical groups; (2) training and indoctrination of personnel directly and indirectly concerned with flying; (3) maintenance of personnel of the air forces; (4) medical problems of flight; and (5) special problems occasioned by this global war.

Presented at the Physiologic Problems Session, Eleventh Annual Meeting, I.A.S., New York, January 25–29, 1943.

* Colonel, Medical Corps, U.S. Army.

† Lieutenant Colonel, Air Corps, Army of the United States.

‡ Lieutenant Colonel, Medical Corps, Army of the United States.

Selection of Personnel of All Flying Categories

It is axiomatic that if the selection of fliers is accomplished in a sound and highly successful manner, the training and maintenance of these men will be much easier and subsequent problems of personnel fewer. The statement has been made that almost any sound person can be taught the mechanics of flying, and we believe this statement might be accepted. However, the ability to fly an airplane does not denote acceptability or ability successfully to participate in military aviation—far from it! The situation requires large numbers of young men who must be able to grasp instruction rapidly, who are physically sound, and who are emotionally stable. No longer is the sole concern with selection of pilots, but navigators, bombardiers, radio engineers, flight engineers and aerial gunners are selected with equal care. The numbers involved are of such magnitude that not only must the best be selected but it is necessary to use methods of selection which will insure that all with proper aptitude are accepted for training. Stress is placed on physical, mental, and emotional soundness and on aptitude for the job.

The Air Surgeon inaugurated a special program of selection of fliers slightly more than two years ago. This program received its impetus by calling in experts in the psychologic field of vocational selection. These experts instituted various psychologic (mental) screening tests, vocational aptitude tests, and psychomotor assessments. The psychologic program has grown into a large, well-integrated, and scientifically based activity. The methods of selection have been validated against performance in training, but refinements are continually in progress. The operational success in theaters of combat of the personnel selected and trained will be the final validation of the program of selection, as well as of the program of training.

It always has been the complaint of the older flight surgeons that in selection of applicants for training in flying, they had to outguess the flying instructors. In the hands of the latter lay the final decision of whether a man would succeed or fail. This may still be a weakness in the program of selection, but it is assured that flying instructors are as carefully selected as previously and are much better schooled in their duties. Thus, a fairly uniform instructional program is assured and criteria of progress are rendered more valid than before. It is predicted that assessment of aptitude for flying during actual flight instruction will remain "instructor

opinion" and will not be reduced to a mathematical score in this war.

In summation, selection is a medical problem and has occasioned the cooperative efforts of the physician, psychologist, and Air Forces officer. The standards for selection are set by the Medical Corps and are revised at their suggestion.

Training and Indoctrination

The training of personnel of the Air Forces is principally one for specialized Air Corps men. However, the interest of the medical officer cannot be denied even at this stage of the genesis of a flier. If transition from one type of aircraft to another gives rise to a high incidence of accident, it is fitting that medical personnel request that means be taken to reduce the morbidity rate. In the instance cited, the request would be for a more gradual transition from one type of aircraft to another or for more hours of training prior to transition. Again, the medical officer might properly insist that night flying of novices in mountainous regions be prohibited.

The greatest contribution of the medical corps to the Flying Training Command has been institution of the low-pressure chamber indoctrination program. This program was initiated in November, 1940, so that it could be in complete operation by March 1, 1943. The purpose of this training is to teach fliers the character and significance of bodily changes induced by barometric pressure; to show them the need for, and proper use of, oxygen equipment; and to furnish experiences for proper understanding of the effects of altitude and of the characteristics of the atmosphere. Each man experiences the effect of oxygen want; this impresses on him the need of supplemental oxygen during flight at the proper levels and acquaints him with the symptoms, so that he may be cognizant of malfunction of his oxygen system in flight. Training is given in equalizing the pressure in the middle ear during rapid descent, and men usually are acquainted with aeroembolism. Lectures, demonstrations, and experiences in the low-pressure chamber are intermingled in this program, and those in charge of it have yet to encounter the flier, regardless of experience, who feels that he has not profited greatly by his participation. Perhaps the greatest benefit of this program is derived from the training the men receive in the proper use and care of oxygen equipment.

The selection of men for operation at extremely high altitudes, especially for flight at high altitudes for long periods of time, is included in the program. In addition, men who clear the ears with difficulty, for functional or pathologic reasons, can be eliminated or classified for operation of transports. Finally, then, all fliers will pass through the low-pressure chamber and, in addition to the valuable instruction and experience they thus will receive, their anoxia tolerance, their resistance to the ill effects of low barometric pressure, and their ability to tolerate rapid changes in barometric pressure will be entered on their records.

Lectures and demonstrations are given by medical officers on sanitation, health, and hygiene, and additional instruction on use of the eyes at night is to be instituted. Instruction of this character probably has contributed much to the excellent health of the Army Air Forces throughout the world.

Perhaps the training function of the medical personnel of the Army Air Forces should not be dismissed without mention of the important activities of the School of Aviation Medicine at Randolph Field. This institution gives instruction to medical officers which qualifies them as aviation medical examiners and, eventually, after a proper period of experience, as flight surgeons. In addition, a school is maintained there to train physiologists for their role in conducting the low-pressure chamber program. They are recognized by the Army Air Forces as constituting a new and important group and are awarded the title "Aviation Physiologist" on completion of the course of instruction. Still another important function is being carried out at Randolph Field in the training of Air Force officers to become oxygen officers of squadrons and groups. These men, on completion of a short course, return to their respective units and become the officers responsible for training of the crews in the use of oxygen, the servicing of the aircraft with oxygen, and the installation and functioning of the oxygen equipment in the airplanes of their units.

Maintenance of Personnel of the Air Forces

The expression "maintenance of personnel" has a cold and mechanical sound, but, in reality, the work entails rather intimate relationship of medical and Air Forces personnel. A multitude of important conditions come under consideration: (1) housing; (2) nutrition; (3) clothing and other personal equipment; (4) general medical care; (5) hospitalization; (6) sanitation; (7) recreation and physical fitness; (8) hours of duty; (9) frequency and length of leaves; (10) time absent from home on foreign duty; (11) type, frequency, and length of combat missions; (12) total length of combat service; and (13) status of family affairs.

Many of these problems are basically the responsibility of the commanding officers of units, of the quartermaster, or of the medical officer. Their proper solution usually requires the effective teamwork of all. In most instances the problems must be dealt with in a practical manner at the station. However, if all of the problems arising in operational flying are left to so-called common-sense solutions, great handicaps will be imposed on the tactical organizations. Should not aircraft of the United States forces be as operationally effective as possible; their crew positions as comfortable and well arranged as possible; illumination within the

aircraft as effective as technologic skill can make it; the oxygen equipment as safe and economical as can be produced; technical and professional information as factual, complete, and advanced as scientific knowledge in 1943 will permit? It seems clearly the duty of those in charge to anticipate, study, experiment, gather data, and fabricate and to supply their colleagues in combat operations with both matériel and information. This is being done to a great extent, but more remains to be done.

The health of the Army Air Forces, both at home and in every theater of operations abroad, has been surprisingly good. It is interesting that most of fliers returning from the Southwest Pacific say that dengue fever was their worst pathologic enemy. The disease was of relatively short duration and did not cause death. Under certain circumstances, the food has not been up to Army standards, but there has been no suffering or loss of morale on this account. Experts on nutrition have been included on the staffs of some U.S. expeditionary Air Forces and, in at least one instance, have rendered outstanding service. Undoubtedly some of the good fortune of the Air Forces has had its origin in the inclusion on important staffs of many categories of scientific experts, such as nutritionists, physiologists, psychiatrists, and various medical specialists. It is obvious that every field of the basic medical sciences and even the physical sciences must be drawn from in attacking the problems of wartime aviation. It is known that the problem of flier maintenance is lessened if selection is highly effective. It is known, too, that even the strongest will falter and break if the task is too arduous or is endured for unduly long periods. "Pilot fatigue," "flyer fatigue," "flying stress," and "staleness" are some of the terms applied to the fatigue observed in members of air crews. This condition does not lend itself to precise quantitative measurement but is a clinical syndrome or symptom complex. An intelligent, well-trained flight surgeon can recognize this condition in fliers with whom he intimately associates, and he is best able to cope with it if he has the full cooperation of the unit commander. Unquestionably, prevention is better than cure, and the fight against flier fatigue can best be won by adoption of the following measures: (1) employment as air crew of young men who are in excellent health and physically fit; (2) assurance that success on flying missions be readily attainable; (3) provision of aircraft and accessories that are equal to, or better than, the enemy's; (4) furnishing of facilities for adequate rest, recreation, and sports between missions; (5) proper spacing of missions, rest periods, and leaves; (6) securing of best possible living and working conditions; (7) furnishing of an opportunity to return home as a hero after a reasonable number of combat missions; (8) assurance of good medical care and evacuation home if wounded or injured; and (9) provision of freedom from family worries.

Medical Problems of Flight

The medical problems of flight are numerous, varied, and often difficult. The elements of flight that impose on man stresses that are not normally encountered can be divided into those that are encountered at low altitudes and those that are encountered at high altitudes.

Elements encountered at low altitudes comprise: (1) constant danger or threat to life itself; (2) noise, vibrations, and "foreign" odors; (3) an unstable platform (often distinctly unsteady); (4) changing spatial orientation; (5) centrifugal forces; (6) linear accelerations and decelerations; (7) the necessity of navigation and orientation; (8) rigorous visual requirements; (9) confinement; (10) change in barometric pressure, with its effect on nasal accessory sinuses, the middle ear, and the gut; (11) the special skills and constant attention required; (12) lowered oxygen tension; (13) extremes of temperature (including great cold) and rapid changes in temperature; (14) high air movement and often air blasts; and (15) crash incidents due to mishaps in taking off and landing.

Elements encountered at high altitudes comprise, besides most of those encountered at low altitudes: (1) mechanical difficulties; (2) the necessity of giving increased attention to all mechanisms; (3) extreme cold; (4) low barometric pressure, with the attendant likelihood of aeroembolism, the gaseous distention of the gut, and low partial pressure of oxygen (welfare of the flier depending on function of the oxygen equipment and its intelligent use); (5) extreme confinement; (6) the fact that, if escape from aircraft is necessary, it presents a more forbidding aspect than at low altitudes.

The problems inherent in flight in military aircraft demand special study to ameliorate or eliminate the adverse factors. Perhaps among the most important considerations are safety devices: (1) multiple engines; (2) high stress factors built into the aircraft; (3) explosion and leakproof gasoline tanks; (4) adequate armor located to give maximal protection to the crew; (5) safety belts; (6) good communication systems; (7) adequate flight control and indicating instruments; (8) parachutes; (9) life rafts; (10) large, well-placed escape hatches; and (11) good visibility. Good visibility in the cockpit cannot be overemphasized; this implies proper lighting for operation at night, elimination of light distortion, defrosting, and oil and water clearance from the wind screen during flight. To these ends the optical physicist, ophthalmologist, and aeronautical engineer join efforts.

Much consideration has been given to accelerational and centrifugal forces. Numerous groups in the allied nations are working on this problem to determine the basic physiologic disturbances engendered and means of their alleviation. It is reasonable to report considerable progress in these studies.

Crew Comfort

A significant effort has been, and is being, made to increase the comfort of the crew. It is well known that increase in comfort is reflected in higher tactical efficiency, particularly when a mission requires long-range flight. At the Aero Medical Laboratory, and with the aid of the Department of Anthropology of Harvard University, the flying population has been studied to determine the physical characteristics of the men. The important physical measurements of the gunner, the pilot, and the other members of the crew have now been established, and what their clothing and battle gear add to their significant measurements has been learned. These data have been correlated with dimensions of turret and cockpit, and some redesign of compartments of aircraft, as well as some alteration of the physical standards of selection will result. There was no significant information on this continent by which dimensions of oxygen masks could be established until anthropologists studied and measured the fliers.

Respiration

Much has been learned in the general field of respiration. Projects under this heading include the determination of oxygen requirements as a function of altitude, cold, mission, and job; evaluation of oxygen equipment in the laboratory and in flight; and development of improved oxygen equipment, whether for routine or emergency use. The closely allied field of circulation deserves close attention. What are the circulatory responses to anoxia, cold, aeroembolism, and high acceleration? Having determined these, what can be done toward preventing circulatory failure in conditions of extreme stress? The physician and physiologist must be able to answer these questions.

Airsickness

Airsickness received scant attention in peacetime when full crews seldom were carried in military aircraft and washouts at flying school for this disorder were in line with a high rate of failure. Man power was then unlimited to fill the few vacancies in the Air Corps. Airsickness now has become a rather important consideration because infantry may be air-borne, paratroops have been developed, and air crews are large. Progress is being made on studies of this disorder of flying, and there is promise of advances both in selection of personnel and in some alleviation of the condition.

Oxygen, Cold, and Aeroembolism

Oxygen, cold, and aeroembolism cause the major worries and impose the greatest problems in unrestricted operational flying. These subjects undoubtedly are receiving the principal effort. The German air force after more than 8 years of intensive study and development, and with 3½ years of combat experience, is still modifying its oxygen equipment. It seems that if manufacturers in this country could build all of the intricate and powerful mechanisms involved in aircraft they can develop a perfect oxygen system. There is hope now of obtaining a nearly perfect system and completely adequate emergency oxygen gear. It has been a long, hard process of study, laboratory, and flight test, and just now equipment is abreast of the requirements established by combat flying.

The extreme cold at high altitude should, and can, be effectively countered by heaters and insulation of crew compartments. Have adequate thought and study been given to this problem? If so, the results to date fall short of a satisfactory installation. Lacking adequate heat for compartments or turrets, it has become necessary to spend much time and energy on protective clothing. In no case has this resolved itself into a completely adequate solution for all crew members operating at high altitude on long missions. The application of electrical heat energy has been a palliative measure.

Aeroembolism, characterized by joint pain (bends), substernal oppression and respiratory difficulty (chokes), cutaneous disturbances and vasomotor malfunction, has not been of great significance to date in military aviation in this country. However, this trend cannot be projected into future operations for higher altitudes and longer periods of flight are being attained. Intensive studies by numerous research groups are in progress to determine the fundamental mechanism of aeroembolism, the precise provocative factors, and methods of prevention and alleviation. Selection of resistant personnel may well be a partial solution to this problem and adequate pressurization of the individual at high altitude a sure preventive.

It has been determined that combustion, such as that of a gasoline fire, can well be supported at 35,000 ft. and even somewhat higher, so that fire, as well as structural failure at high altitude, can occasion the necessity for escape from the aircraft. The question was raised whether or not a man could escape from an airplane at 40,000 ft. and survive the descent. It has been clearly established that an aircraft could be abandoned at that altitude and, with proper instruction, a man can reach safety without supplemental oxygen after leaving the plane.

Special Problems Occasioned by War

The war has changed many ideas concerning requirements in the way of personnel, equipment, and aircraft operation. Night fighting, extensive night bombing, airdrome activities during black-outs, and round-the-clock aerial activity were not clearly foreseen. Certainly fighting in almost every latitude and quadrant of the earth was not entirely anticipated, at least not as

(*Continued on page 66*)

Strain Energy Analysis of Incomplete Tension Field Web-Stiffener Combinations

PAUL H. DENKE*

Douglas Aircraft Company, Inc.

ABSTRACT

The paper presents a minimum potential energy analysis of thin web beams subjected to shear loads above critical. The wave form of the buckled surface is approximated by a function that contains the wave length, wave angle, and wave depth as parameters. Four more parameters—namely, the stiffener compressive strain, the cap compressive strain, the cap bending deflection, and the panel shearing strain—are introduced, and the distribution of the mid-plane tensile, compressive, and shear stresses is worked out. The energy of the entire panel-load system is then computed and the resulting expression differentiated with respect to the strain parameters. The seven resulting equations define the equilibrium configuration of the panel. Expressions are obtained for the critical condition, principal mid-plane stresses, maximum web bending stresses, stiffener and cap compressive stresses, web wave length, wave angle, and wave depth. In particular, a formula is given for the bending loads on the stiffeners produced by the wrinkling of the web. The equations are shown to reduce to those of Wagner for an infinitely thin web. A comparison is presented which shows good agreement between theoretic and experimental values of the following: principal web stresses, stiffener compressive stresses, wave depth, and wave length.

INTRODUCTION

CONSIDERABLE INTEREST attaches to the class of structural members, usually referred to as "Tension Field" or "Wagner" beams. Such members are characterized by comparatively thin webs, which are designed to buckle within their working range. For small shears the web remains flat and the laws of plane stress apply. But if the load is continuously increased, a critical condition is reached, at which time the sheet buckles into a series of diagonal wrinkles. For shear loads above critical, the stresses existing in the member can no longer be predicted by the theory of plane stress. The problem, therefore, is to find an analysis method whereby the actual stress distribution in a thin web beam, operating in the region above critical, can be computed.

It is the purpose of this paper to present a theory of shear webs which is based upon analytical rather than empirical methods. All phases of the shear web problem are considered. In particular, account is taken of the web compressive strength in reducing stiffener compressive loads and the effect of web wrinkles in producing stiffener bending loads. The effects of cap bending between stiffeners and of cap and stiffener axial deformation are also considered.

Presented at the Structures Session, Eleventh Annual Meeting, I.A.S., New York, January 25-29, 1943.

* Stress Analyst.

METHOD OF APPROACH

The following analysis is based upon the principle that the potential energy of a loaded elastic structure is minimum when equilibrium is reached. In applying this principle, one takes the standpoint that the load is applied suddenly. For example, consider the present instance, in which a constant force is applied to a shear panel. Immediately following application of the load, the panel goes through various phases of deformation. If the load is greater than critical, wrinkles form in the web, and, as distortion proceeds, their wave length, depth, and angle change. Meanwhile, stiffeners and caps undergo their own special types of distortion. After a brief period of oscillation, the structure settles into its equilibrium configuration.

During the period in which the structure seeks its lowest energy level, the load loses an amount of energy equal to its magnitude times the net distance traveled. Part of this energy is converted into strain energy of the structure, while the rest is dissipated in the form of heat. It is important to notice that the load loses energy in proportion to the deflection, while the strain energy of the structure increases slowly at first and then more rapidly as deformation proceeds. There is, therefore, a configuration in which the energy of the load diminishes as fast as that of the structure increases. This is the position of minimum energy and also of equilibrium.

In applying the principle of minimum potential energy to structural analysis, a procedure is followed which is simply a mathematical counterpart of the process just described. The first step is to make a deformation assumption—that is, to write a formula giving the deflection of each part of the structure as a function of certain variables called deformation parameters. The wave length, wave angle, and wave depth used in the present analysis will serve as examples of such parameters. These quantities vary within the mathematical framework in the same manner as the corresponding actual quantities vary during the period when the structure is seeking equilibrium. The second step is to compute the potential energy of the load and the structure as functions of the deformation parameters. The third step is to de-

termine by differentiation the magnitudes of the parameters for minimum energy. All that then remains is to put the results into a form suitable for analysis and design.

The type and number of deformation parameters are dependent upon the choice of the analyst. The solution becomes more accurate as the number and suitability of the parameters increase. However, the amount of computation increases rapidly as more parameters are added, and therefore it is desirable to place reliance on suitability rather than number. Thus the method pays a premium for good judgment.

Assumptions

The present theory applies to a thin web beam having the following characteristics:

(1) Zero bending and compression.
(2) Uniform shear.
(3) Identical panels.
(4) Parallel caps of identical cross sections.
(5) Vertical stiffeners.
(6) Complete damping of wrinkles at stiffeners and caps.
(7) Infinite length.

With slight changes, the theory may also be applied to the following cases.

(1) A single shear panel bounded on four sides by stiffeners having infinite bending rigidity.
(2) A checkerboard of panels.

These two cases are subject to restrictions similar to those given for the beam.

The above assumptions may appear to be excessively restrictive, but there are various ways by which some of the effects neglected can be taken into account. For example, the effects of bending and compression might be separately computed, and subsequently combined with the effect of shear. Where shear is nonuniform, a particular panel can be checked as though the entire beam were subjected to some multiple of the shear at that panel. If caps are not identical, a beam having caps identical to the weakest might be considered or an average might be taken.

Notation

E = modulus of elasticity
ν = Poisson's ratio
P = shear load carried by web,
In Fig. 1,
Z = stiffener section modulus about axis SS (see Sec. B-B, Fig. 1)
z = eccentricity of SS with respect to mid-plane of web
ρ_s = radius of gyration of stiffener about axis SS
r = $(b/a) + (a/b)$
A = $4ab$
μ = $[\pi^2/6(1-\nu^2)](h^2/A)$
A_h = cap area (see Sec. A-A)
I_h = cap moment of inertia about HH
A_v = total stiffener area (see Sec. B-B)
A_s = $2bh$
I_s = $\frac{2}{3}ha^3$
A_y = $2ah$
F = $(P/Ax)/E$

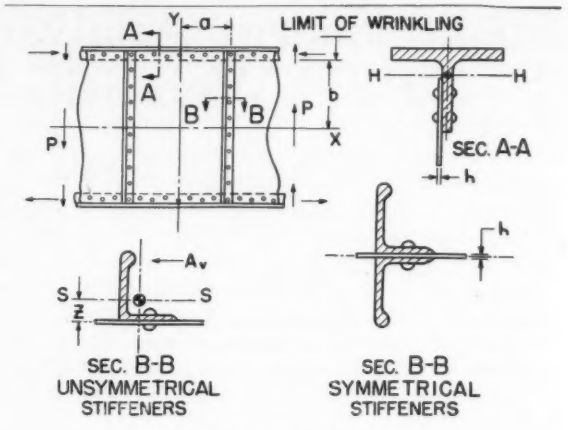

Fig. 1. Notation.

Behavior of a Beam Panel in Shear

In a thin web beam the three principal elements are the web, the stiffeners, and the caps. Fig. 2 shows the behavior of these elments under load. As the figure indicates, the stiffeners are compressed, the caps are compressed and bent, and the web forms a series of diagonal wrinkles. The stiffeners have little tendency to bend in the plane of the web because of the balancing tensions supplied by the webs of the adjacent panels.

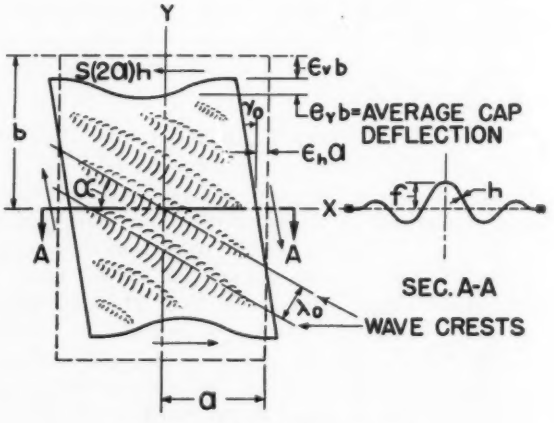

Fig. 2. Deformation parameters.

Table 1
Deformation Parameters

Part	Parameter	Symbol
Stiffener	Average compressive strain	ϵ_v
Caps	Average compressive strain	ϵ_h
	Average deflection per unit depth of web	e_y
Web	Wave length	λ_0
	Wave angle	α
	Wave amplitude (maximum)	f
Web and load	Average shearing strain	γ_0

In actual differentiation, certain functions of the above are used for convenience; however, these are the basic parameters.

Deformation Parameters

Table 1 and Fig. 2 give the deformation parameters employed in the analysis.

Web Deformation Assumption

Fig. 3a shows the coordinate system for the web. If a point $P(x, y)$ moves to P', the components of the displacement are u, v, and w. X' and Y' shown in Fig. 3b, are additional axes oriented so as to be parallel and perpendicular, respectively, to the direction of the waves.

The assumed expression for the displacement w is

$$w = f \cos \frac{\pi}{2}\frac{x}{a} \cos \frac{\pi}{2}\frac{y}{b} \cos 2\pi \frac{y'}{\lambda_0}$$

This function consists of the amplitude f, the fundamental component $\cos 2\pi(y'/\lambda_0)$, and the two damping components $\cos (\pi/2)(x/a)$ and $\cos (\pi/2)(y/b)$

$$y' = x \sin \alpha + y \cos \alpha$$

Therefore

$$\cos 2\pi(y'/\lambda_0) = \cos 2\pi((x/\lambda_0) \sin \alpha + (y/\lambda_0) \cos \alpha)$$

Figs. 3b and 4 show graphically the three components. Therefore

$$w = f \cos px \cos qy \cos (mx + ny)$$

where $p = (\pi/2a)$, $m = (\pi/\lambda) \sin \alpha$, $\lambda = \lambda_0/2$, $q = \pi/2b$, and $n = (\pi/\lambda) \cos \alpha$.

Calculation of Mean Web Stresses

One additional assumption is here made regarding the distribution of the mid-plane stress, the notation for which is shown in Fig. 5a. The rectangle is an element taken from the mid-plane, oriented as shown in Fig. 3a. It is assumed that σ_x does not vary with x, σ_y does not vary with y, and τ is constant. The assumptions for σ_x and σ_y are shown in Fig. 5b. Notice that these assumptions satisfy the equations of equilibrium,

$$\frac{\partial \sigma_x}{\partial x} = \frac{\partial \tau}{\partial y'} \qquad \frac{\partial \sigma_y}{\partial y} = \frac{\partial \tau}{\partial x}$$

The mean stresses and the stress distribution are determined for the case of a single panel in which the vertical stiffeners are free to deflect because little additional calculation is required to obtain the additional generality.

The X stress is given in terms of the X and Y strains through the well-known relation,

$$\sigma_x = [E/(1 - \nu^2)](\epsilon_x + \nu\epsilon_y)$$

where ν is Poisson's ratio. But ϵ_x and ϵ_y are given in terms of the displacements u, v, and w by

$$\epsilon_x = u_x + {}^1/_2 w_x^2$$

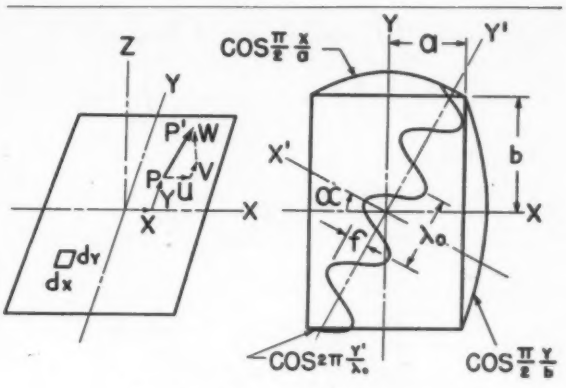

Fig. 3a (*left*). Coordinate system.
Fig. 3b (*right*). Web deformation assumptions.

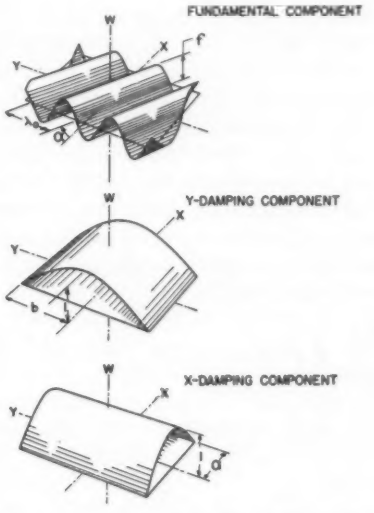

Fig. 4. Components of web deformation.

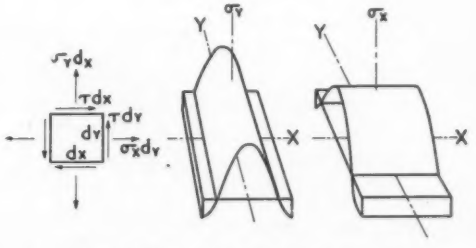

Fig. 5a (*left*). Mid-plane stress notation.
Fig. 5b (*right*). Mid-plane stress distribution assumptions.

in which the brief notation u_x and w_x replaces the usual notation $\partial u/\partial x$, $\partial w/\partial x$; therefore

$$\sigma_x = \frac{E}{1 - \nu^2}\left[(u_x + \nu v_y) + \frac{1}{2}(w_x^2 + \nu w_y^2)\right]$$

$$A\bar{\sigma}_x = \int\int_A \sigma_x \, dx \, dy$$

where A = panel area = $4ab$ and $\bar{\sigma}_x$ = average σ_x.

$$\frac{1-\nu^2}{E}A\bar{\sigma}_x = \iint_A u_x\,dx\,dy + \nu\iint_A v_y\,dx\,dy + \frac{1}{2}\iint_A w_x^2\,dx\,dy + \frac{\nu}{2}\iint_A w_y^2\,dx\,dy$$

From Fig. 2,

$$\int_{-b}^{b} v_y dy = [v]_{-b}^{b} = -2(\delta_y + \epsilon_y b)$$

Where δ_y is the vertical deflection of the cap

$$\int_{-b}^{b}\int_{-a}^{a} v_y\,dx\,dy = -2\int_{-a}^{a}\delta_y\,dx - 2\epsilon_y b\int_{-a}^{a}dx = -(2\bar{\delta}_y)2a - 2\epsilon_y b(2a) = -A(e_y + \epsilon_y)$$

Similarly,

$$\int_{-b}^{b}\int_{-a}^{a} u_x\,dx\,dy = -A(e_x + \epsilon_h)$$

The evaluation of integrals such as $\int\int w_x^2\,dx\,dy$ are omitted, since only routine procedures are involved. However, some of the integrals are found to contain certain trigonometric terms. These terms have, in all cases, been neglected because they are small for loads around the critical, and they rapidly become smaller and are periodically zero as the load increases. Neglect of these terms, therefore, corresponds to smoothing small irregularities out of the energy function. Lack of space unfortunately prohibits a complete discussion of this point.

$$\frac{1}{f^2}\iint_A w_x^2\,dx\,dy = \frac{1}{2}m^2ab + \frac{\pi^2}{8}\frac{b}{a}$$

$$\frac{1}{f^2}\iint_A w_y^2\,dx\,dy = \frac{1}{2}n^2ab + \frac{\pi^2}{8}\frac{a}{b}$$

Therefore

$$\frac{1-\nu^2}{E}\bar{\sigma}_x = \frac{1}{4}\frac{f^2}{A}\left[ab(m^2+\nu n^2) + \frac{\pi^2}{4}\left(\frac{b}{a}+\nu\frac{a}{b}\right)\right] - \left[(e_x+\epsilon_h)+\nu(e_y+\epsilon_v)\right]$$

$$\frac{1-\nu^2}{E}\bar{\sigma}_y = \frac{1}{4}\frac{f^2}{A}\left[ab(n^2+\nu m^2) + \frac{\pi^2}{4}\left(\frac{a}{b}+\nu\frac{b}{a}\right)\right] - \left[(e_y+\epsilon_v)+\nu(e_x+\epsilon_h)\right]$$

The average shear stress is given by

$$A\bar{\tau} = \iint \tau\,dx\,dy = \frac{E}{2(1+\nu)}\iint \gamma\,dx\,dy$$

$$= \frac{E}{2(1+\nu)}\iint (v_x + u_y + w_x w_y)\,dx\,dy$$

$$\int_{-b}^{b}\int_{-a}^{a} v_x\,dx\,dy = 0$$

$$\int_{-a}^{a}\int_{-b}^{b} u_y\,dx\,dy = -A\gamma_0$$

$$\frac{1}{f^2}\int_{-a}^{a}\int_{-b}^{b} w_x w_y\,dx\,dy = \frac{1}{2}mnab$$

Therefore

$$\bar{\tau} = \frac{E}{2(1+\nu)}\left(-\gamma_0 + \frac{1}{2}\frac{f^2}{A}mnab\right)$$

It is now convenient to make a change of variables and use the following dimensionless ratios:

$$\phi = \frac{A}{\lambda^2} \qquad \mu = \frac{\pi^2}{6(1-\nu^2)}\frac{h^2}{A} \qquad \theta = \left(\frac{f}{h}\right)^2$$

$$\xi = \frac{\pi^2 h^2}{16\,A}\theta \qquad \eta = \phi\sin^2\alpha \qquad \chi = \eta + \frac{b}{a} \qquad \epsilon_h = e_x + \epsilon_h \qquad (1)$$

$$r = \frac{b}{a} + \frac{a}{b} \qquad \zeta = \phi\cos^2\alpha \qquad \psi = \zeta + \frac{a}{b} \qquad e_v = e_y + \epsilon_v$$

Then,

$$\eta + \zeta = \phi \qquad \eta/\zeta = \tan^2\alpha$$

$$m^2 = \frac{\pi^2}{\lambda^2}\sin^2\alpha = \frac{\pi^2}{A}\phi\sin^2\alpha = \frac{\pi^2}{A}\eta$$

$$n^2 = \frac{\pi^2}{\lambda^2}\cos^2\alpha = \frac{\pi^2}{A}\phi\cos^2\alpha = \frac{\pi^2}{A}\zeta$$

$$p^2 = \frac{\pi^2}{A}\frac{b}{a} \qquad q^2 = \frac{\pi^2}{A}\frac{a}{b}$$

Therefore

$$(1-\nu^2)\frac{\bar{\sigma}_x}{E} = \xi(\chi + \nu\psi) - (e_h + \nu e_v)$$

$$(1-\nu^2)\frac{\bar{\sigma}_y}{E} = \xi(\psi + \nu\chi) - (e_v + \nu e_h) \qquad (2)$$

$$(1+\nu)\frac{\bar{\tau}}{E} = \xi\sqrt{\eta\zeta} - \frac{1}{2}\gamma_0$$

Thus, the average stresses have been obtained as functions of the panel parameters.

Stress Distribution

The stress distribution is obtained from continuity.

$$-2(\epsilon_y b + \delta_y) = \int_{-b}^{b} v_y\,dy = \int_{-b}^{b}(\epsilon_y - \tfrac{1}{2}w_y^2)\,dy$$

$$= \frac{1}{E}\int_{-b}^{b}(\sigma_y - \nu\sigma_x)\,dy - \frac{1}{2}\int_{-b}^{b} w_y^2\,dy \qquad (3)$$

But

$$\int_{-b}^{b}\sigma_y\,dy = 2b\sigma_y$$

since σ_y does not vary with y. Also

$$\int_{-b}^{b}\sigma_x\,dy = 2b\bar{\sigma}_x$$

since σ_x varies only with y. Also

$$\frac{1}{f^2}\int_{-b}^{b} w_y^2\,dy = \frac{1}{2}\left(n^2b + \frac{\pi^2}{4b}\right)\cos^2 px$$

For the cap deflection δ_y it is assumed that

$$\delta_y = \delta_{y0} \cos^2 px$$

This assumption is sufficiently accurate for its intended use in calculating strain energy.

$$\bar{\delta}_y = \delta_{y0}/2$$

Therefore

$$\delta_{y0} = 2\bar{\delta}_y = 2e_y b$$

Substituting the above expressions into Eq. (3)

$$-2\epsilon_y b - 4be_y \cos^2 px = 2b\,\frac{\sigma_y}{E} - 2b\nu\,\frac{\bar{\sigma}_x}{E} - \frac{f}{4}\left(n^2 b + \frac{\pi^2}{4b}\right)\cos^2 px$$

$$\frac{\sigma_y}{E} = (\xi\psi - e_y)2\cos^2\frac{\pi}{2}\frac{x}{a} + \left(\nu\frac{\bar{\sigma}_x}{E} - \epsilon_y\right)$$

Similarly,

$$\frac{\sigma_x}{E} = (\xi\chi - e_x)2\cos^2\frac{\pi}{2}\frac{y}{b} + \left(\nu\frac{\bar{\sigma}_y}{E} - \epsilon_h\right)$$

Thus, the tension stresses have been found as functions of the panel parameters.

$$\epsilon_y = \bar{\sigma}_y/E \qquad \epsilon_h = \bar{\sigma}_h/E$$

where σ_y and σ_h are the average compressive stresses in the stiffener and cap, respectively.

From Eq. (2)

$$\frac{1-\nu^2}{E}(\bar{\sigma}_x - \nu\bar{\sigma}_y) = \xi(1-\nu^2)\chi - (1-\nu^2)\epsilon_h$$

$$\xi\psi - e_x = \frac{1}{E}(\bar{\sigma}_x - \nu\bar{\sigma}_y + \bar{\sigma}_h)$$

Also

$$\xi\chi - e_y = \frac{1}{E}(\bar{\sigma}_y - \nu\bar{\sigma}_x + \bar{\sigma}_y)$$

Substituting these expressions in the equations for σ_x and σ_y

$$\frac{\sigma_x}{E} = \frac{2}{E}(\bar{\sigma}_x - \nu\bar{\sigma}_y + \bar{\sigma}_h)\cos^2\frac{\pi}{2}\frac{y}{b} - \frac{1}{E}(\bar{\sigma}_h - \nu\bar{\sigma}_y)$$

$$\frac{\sigma_y}{E} = \frac{2}{E}(\bar{\sigma}_y - \nu\bar{\sigma}_x + \bar{\sigma}_y)\cos^2\frac{\pi}{2}\frac{x}{a} - \frac{1}{E}(\bar{\sigma}_y - \nu\bar{\sigma}_x)$$

let

$$2(\bar{\sigma}_x - \nu\bar{\sigma}_y + \bar{\sigma}_h) = \sigma_{x0} - \sigma_{x1}, \quad \bar{\sigma}_h - \nu\bar{\sigma}_y = -\sigma_{x1}$$

$$2(\bar{\sigma}_y - \nu\bar{\sigma}_x + \bar{\sigma}_y) = \sigma_{y0} - \sigma_{y1}, \quad \bar{\sigma}_y - \nu\bar{\sigma}_x = -\sigma_{y1}$$

$$\begin{cases} \sigma_x = (\sigma_{x0} - \sigma_{x1})\cos^2\dfrac{\pi}{2}\dfrac{y}{b} + \sigma_{x1} \\ \sigma_y = (\sigma_{y0} - \sigma_{y1})\cos^2\dfrac{\pi}{2}\dfrac{x}{a} + \sigma_{y1} \end{cases}$$

σ_{x0}, σ_{x1}, σ_{y0}, σ_{y1} are constant for all points of the web. Thus, the tensile stresses are found to follow a $\cos^2$ distribution (see Fig. 6). This result necessarily follows from the assumption made for the lateral deflection.

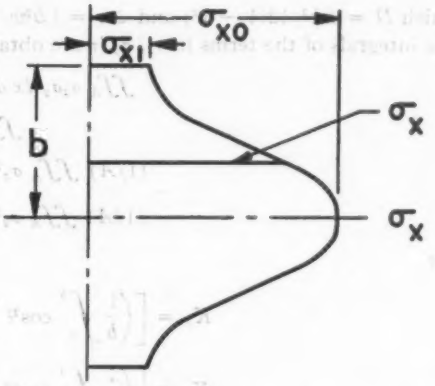

FIG. 6. Mid-plane tensile stress distribution

For the case of a very thin web, the tension field theory is generally accepted. According to this theory the shear stress is uniformly distributed, and the tensile stresses are equal to the shear stresses, thus, $\sigma_x = \sigma_y = \tau$. Therefore, the tensile stresses must be uniform. But in the above expressions for σ_x and σ_y the coefficients of the $\cos^2$ terms are not necessarily zero and, therefore, in the case of the thin web, σ_x and σ_y are not uniformly distributed. It follows that the assumed expression for w does not describe the actual wrinkled surface for all cases.

Nevertheless, test results make it appear that for all practical cases the $\cos^2$ distribution leads to satisfactory results. In order to secure a reduction to the Wagner case, however, a constant factor of $^1/_2$ is replaced in the following by the factors K_x and K_y. Thus, a check is secured on that portion of the analysis which does not involve the mid-plane stress distribution. But the theoretic values $K_x = K_y = {}^1/_2$ were used in checking the experimental data (Figs. 12 through 16) which cover a wide range of web thicknesses, including some webs that are perhaps thinner than are likely to occur in practice.

In order to secure the factors K_x and K_y, replace the above distribution by

$$\sigma_x = (\sigma_{x0} - \sigma_{x1})\cos^j\frac{\pi}{2}\frac{y}{b} + \sigma_{x1}$$

$$\sigma_y = (\sigma_{y0} - \sigma_{y1})\cos^k\frac{\pi}{2}\frac{x}{a} + \sigma_{y1}$$

Here $j = k = 0$ gives a uniform distribution.

Strain Energy of Web

The strain energy of a buckled flat plate is given as a function of the mid-plane stresses and the lateral displacement by

$$V_w = \frac{h}{2E}\iint_A [(\sigma_x + \sigma_y)^2 - 2(1+\nu)(\sigma_x\sigma_y - \tau^2)]\,dx\,dy + \frac{D}{2}\iint_A [(\Delta w)^2 - 2(1-\nu)(w_{xx}w_{yy} - w_{xy}^2)]\,dx\,dy$$

in which $D = Eh^3/12(1-\nu^2)$ and $\Delta w = (\partial^2 w/\partial x^2) + (\partial^2 w/\partial y^2)$.

The integrals of the terms in σ_x, σ_y, τ are obtained as follows:

$$\iint_A \sigma_x\sigma_y\,dx\,dy = 2a\bar{\sigma}_y \int_{-b}^{b} \sigma_x\,dy = A\bar{\sigma}_x\bar{\sigma}_y$$

$$\iint_A \tau^2\,dx\,dy = A\bar{\tau}^2$$

$$(1/A)\iint_A \sigma_x^2\,dx\,dy = \bar{\sigma}_x^2 + K_x(\bar{\sigma}_x - \sigma_{x1})^2$$

$$(1/A)\iint_A \sigma_y^2\,dx\,dy = \bar{\sigma}_y^2 + K_y(\bar{\sigma}_y - \sigma_{y1})^2$$

where

$$K_x = \left[\left(\frac{1}{b}\int_0^b \cos^{2j}\frac{\pi}{2}\frac{y}{b}\,dy\right)\Big/\left(\frac{1}{b}\int_0^b \cos^{j}\frac{\pi}{2}\frac{y}{b}\,dy\right)^2\right] - 1$$

$$K_y = \left[\left(\frac{1}{a}\int_0^a \cos^{2K}\frac{\pi}{2}\frac{x}{a}\,dx\right)\Big/\left(\frac{1}{a}\int_0^a \cos^{K}\frac{\pi}{2}\frac{x}{a}\,dx\right)^2\right] - 1$$

Thus, the integral of σ_x^2 has been separated into a part that depends only on the average tensile stress and a part that depends on the stress distribution. The K's are the distribution factors. They are functions of j and k only. For an infinitely thin web, $j = k = 0$ and, therefore, $K_x = K_y = 0$. For $j = k = 2$, $K_x = K_y = 1/2$.

The marginal stress σ_{y1} can be written in terms of the stiffener strain ϵ_v and the average x stress, thus:

$$-\epsilon_v = (1/E)(\sigma_{y1} - \nu\bar{\sigma}_x)$$

Therefore

$$\sigma_{y1} = -\bar{\sigma}_v + \nu\bar{\sigma}_x$$

$$\sigma_{x1} = -\bar{\sigma}_h + \nu\bar{\sigma}_y$$

and

$$(1/E^2A)\iint \sigma_x^2\,dx\,dy = \left(\frac{\bar{\sigma}_x}{E}\right)^2 + \frac{K_x}{E^2}(\bar{\sigma}_x - \nu\bar{\sigma}_y + \bar{\sigma}_h)^2$$

$$(1/E^2A)\iint \sigma_y^2\,dx\,dy = \left(\frac{\bar{\sigma}_y}{E}\right)^2 + \frac{K_y}{E^2}(\bar{\sigma}_y - \nu\bar{\sigma}_x + \bar{\sigma}_v)^2$$

Let

$$\left.\begin{aligned} C_x &= \frac{\bar{\sigma}_x}{E} \quad F = -\frac{\bar{\tau}}{E} \quad P_x = \frac{1}{E}(\bar{\sigma}_x - \nu\bar{\sigma}_y + \bar{\sigma}_h) \\ C_y &= \frac{\bar{\sigma}_y}{E} \qquad\qquad P_y = \frac{1}{E}(\bar{\sigma}_y - \nu\bar{\sigma}_x + \bar{\sigma}_v) \end{aligned}\right\} \tag{4}$$

Substituting into these expressions the values of $\bar{\sigma}_x$, $\bar{\sigma}_y$, and $\bar{\sigma}$,

$$\left.\begin{aligned} C_x &= \frac{1}{1-\nu^2}[\xi(\chi + \nu\psi) - (e_h + \nu e_v)] \qquad P_x = \xi\chi - e_x \qquad F = \frac{1}{1+\nu}\left(\frac{\gamma}{2} - \xi\sqrt{\eta\zeta}\right) \\ C_y &= \frac{1}{1-\nu^2}[\xi(\psi + \nu\chi) - (e_v + \nu e_h)] \qquad P_y = \xi\psi - e_y \end{aligned}\right\} \tag{5}$$

$$\iint \sigma_x^2\,dx\,dy = E^2A(C_x^2 + K_xP_x^2) \qquad \iint \sigma_x\sigma_y\,dx\,dy = E^2AC_xC_y$$

$$\iint \sigma_y^2\,dx\,dy = E^2A(C_y^2 + K_yP_y^2) \qquad \iint \tau^2\,dx\,dy = E^2AF^2$$

The value of the above integrals as well as those for w can now be substituted into the web strain energy equation, giving

$$V_w = \frac{vE}{2}\left[(C_x + C_y)^2 + (K_xP_x^2 + K_yP_y^2) - 2(1+\nu)(C_xC_y - F^2)\right] + \frac{vE}{2}\mu\xi\left[(\eta+\zeta)^2 + 2\left(3\frac{b}{a}+\frac{a}{b}\right)\eta + 2\left(3\frac{a}{b}+\frac{b}{a}\right)\zeta + r^2\right] \quad (6)$$

where $v = Ah$ = web volume.

Stiffener and Cap Axial Strain Energy

For the axial strain energy of the stiffener and cap, the expressions

$$V_A = (1/2)A_vE_v(2b)\epsilon_v^2 = (vE/2)R_v^1\epsilon_v^2 \text{ where } R_v^1 = A_v/(2a)h$$

$$V_{hA} = (1/2)A_hE_h(2a)\epsilon_h^2 = (vE/2)R_h^1\epsilon_h^2 \text{ where } R_h^1 = A_v/(2b)h$$

Cap Bending Strain Energy

For the bending strain energy of the cap, the expression

$$V_{hB}/vE = (1/4)Q'e_y^2 \quad (7)$$

will be used. This formula is exact for a uniformly distributed bending load on the cap and is nearly correct for the $\cos^2$ distribution.

Minimum Energy Equations

From Fig. 2 the energy of the shear load is

$$V_L/vE = -(s/E)\gamma_0 \quad (8)$$

The total energy is $V = V_w + 2(V_{hA} + V_{hB}) + V_L$ per panel.

The independent variables are ξ, η, ζ, γ_0, ϵ_v, ϵ_h, e_y. For minimum energy $dV = 0$; therefore $\partial V/\partial\xi = 0$, and

$$2C_x\chi + 2C_y\psi + 2K_xP_x\chi + 2K_yP_y\psi + \mu\left[(\eta+\zeta)^2 + 2\left(3\frac{b}{a}+\frac{a}{b}\right)\eta + 2\left(3\frac{a}{b}+\frac{b}{a}\right)\zeta + r^2\right] = 4F\sqrt{\eta\zeta} \quad (9)$$

$\partial V/\partial\eta = 0$; therefore

$$2C_x + 2K_xP_x + \mu\left[2(\eta+\zeta) + 2\left(3\frac{b}{a}+\frac{a}{b}\right)\right] = 2F\sqrt{\frac{\zeta}{\eta}} \quad (10)$$

Similarly,

$$2C_y + 2K_yP_y + \mu\left[2(\eta+\zeta) + 2\left(3\frac{a}{b}+\frac{b}{a}\right)\right] = 2F\sqrt{\frac{\eta}{\zeta}} \quad (11)$$

$\partial V/\partial\gamma_0 = 0$; therefore

$$F = s/E \quad (D)$$

$$\bar{\tau} = -s \quad \text{(see Eq. 4)}$$

(Eq. 10)η + (Eq. 11)ζ − (Eq. 9) → (Eq. 12)

$$\mu[(\eta+\zeta)^2 - r^2] = 2C_x\frac{b}{a} + 2C_y\frac{a}{b} + 2K_xP_x\frac{b}{a} + 2K_yP_y\frac{a}{b} \quad (12)$$

(Eq. 12) + (Eq. 10)$\frac{b}{a}$ + (Eq. 11)$\frac{a}{b}$ → (A)

$$\mu\left[(\eta+\zeta)^2 - r^2 + 2(\eta+\zeta)r + 2\frac{b}{a}\left(3\frac{b}{a}+\frac{a}{b}\right) + 2\frac{a}{b}\left(3\frac{a}{b}+\frac{b}{a}\right)\right] = 2F\left(\frac{b}{a}\sqrt{\frac{\zeta}{\eta}} + \frac{a}{b}\sqrt{\frac{\eta}{\zeta}}\right)$$

$$2\frac{F}{\mu}\left(\frac{b}{a}\sqrt{\frac{\zeta}{\eta}} + \frac{a}{b}\sqrt{\frac{\eta}{\zeta}}\right) = [(\eta+\zeta)+r]^2 + 4\left[\left(\frac{b}{a}\right)^2 + \left(\frac{a}{b}\right)^2\right] \quad (A)$$

$$\frac{\partial V}{\partial e_y} = \frac{\partial V}{\partial\epsilon_h} = \frac{\partial V}{\partial\epsilon_v} = 0$$

Therefore

$$\begin{cases} [1 + U(K_y + Q')]e_y + \nu\epsilon_h + \epsilon_v = \nu\epsilon_1 + (1 + UK_y)\epsilon_2 & (13) \\ \nu e_y + (1 + 2UR_h')\epsilon_h + \nu\epsilon_v = \epsilon_1 + \nu\epsilon_2 & (14) \\ e_y + \nu\epsilon_h + (1 + UR_v')\epsilon_v = \nu\epsilon_1 + \epsilon_2 & (15) \end{cases}$$

where $U = 1 - \nu^2$, $\epsilon_1 = \xi\chi$, $\epsilon_2 = \xi\psi$.

Eqs. (13), (14), and (15) are now solved for ϵ_h, ϵ_v, and e_y and the results substituted into Eqs. (10) and (11).

Eqs. (10), (11), and (A) will then contain the three unknowns ξ, η, and ζ; then

$$\epsilon_h = \xi(D_h\chi + O_h\psi) = e_h \quad (E)$$

$$e_y = \xi(D_y\chi + O_y\psi) \quad (F)$$

$$\epsilon_v = \xi(D_v\chi + O_v\psi) \quad (G)$$

$$e_v = \xi(D_v\chi + O_v\psi)$$

Where $R_h = 1/2R_h'$, $R_v = 1/R_v'$, and $R_Q = 1/Q'$,

$$\left.\begin{aligned} E_y &= \nu R_Q \qquad P_y = R_QK_y[(R_h+1)\times(R_v+1) - \nu^2] + R_Q(R_h+1) \\ E_h &= R_h[(R_v+1)(K_yR_Q+1) + R_Q] \qquad P_h = \nu R_h \\ E_v &= \nu R_v(K_yR_Q+1) \qquad P_v = R_v(R_h+1) \\ D &= (K_yR_Q+1)[(R_h+1)(R_v+1) - \nu^2] + R_Q(R_h+1) \end{aligned}\right\} \quad (16)$$

$$D_y = \frac{E_y}{D} \qquad O_y = \frac{P_y}{D} \qquad D_s = \frac{E_s}{D} \qquad O_s = \frac{P_s}{D}$$

$$D_h = \frac{E_h}{D} \qquad O_h = \frac{P_h}{D} \qquad D_v = \frac{E_v}{D} \qquad O_v = \frac{P_v}{D}$$

The above expressions are now substituted into Eqs. (5).

$$C_x = \frac{\xi}{1-\nu^2}\{\chi[1-(D_h+\nu D_v)]+\psi[\nu-(O_h+\nu O_v)]\}$$

$$C_y = \frac{\xi}{1-\nu^2}\{\chi[\nu-(D_v+\nu D_h)]+\psi[1-(O_v+\nu O_h)]\}$$

$$P_x = \xi\chi$$

$$P_y = \xi[-D_y\chi+(1-O_y)\psi]$$

Let

$$M_x = \frac{1-(D_h+\nu D_v)}{1-\nu^2} \qquad N_x = \frac{\nu-(O_h+\nu O_v)}{1-\nu^2}$$

$$M_y = \frac{\nu-(D_v+\nu D_h)}{1-\nu^2} \qquad N_y = \frac{1-(O_v+\nu O_h)}{1-\nu^2}$$

$$S_y = -D_y \qquad T_y = (1-O_y)$$

Therefore

$$\left.\begin{aligned} C_x &= \xi(M_x\chi+N_x\psi) & P_x &= \xi\chi \\ C_y &= \xi(M_y\chi+N_y\psi) & P_y &= \xi(S_y\chi+T_y\psi) \end{aligned}\right\} \quad (17)$$

The expressions for the M's and N's can be simplified, thus

$$\left\{M_x = \frac{D_h}{R_h} \qquad N_x = \frac{O_h}{R_h} \qquad M_y = \frac{D_s}{R_v} \qquad N_y = \frac{O_s}{R_v}\right\} \quad (18)$$

Substituting the expressions for C_x, C_y, P_x, P_y (Eqs. (17)) into Eqs. (10) and (11).

$$\frac{\xi}{\mu}(M_x\chi+N_x\psi+K_x\chi) = \frac{F}{\mu}\sqrt{\frac{\zeta}{\eta}} - \left(\chi+\psi+2\frac{b}{a}\right) \quad (10)$$

$$\frac{\xi}{\mu}[M_y\chi+N_y\psi+K_y(S_y\chi+T_y\psi)] = \frac{F}{\mu}\sqrt{\frac{\eta}{\zeta}} - \left(\chi+\psi+2\frac{a}{b}\right) \quad (11)$$

Let

$$G_x = M_x + K_x \qquad J_x = N_x$$

$$G_y = M_y + K_yS_y \qquad J_y = N_y + K_yT_y$$

Therefore

$$\frac{\xi}{\mu}(G_x\chi+J_x\psi) = \frac{F}{\mu}\sqrt{\frac{\zeta}{\eta}} - \left(\chi+\psi+2\frac{b}{a}\right) \quad (10)$$

$$\frac{\xi}{\mu}(G_y\chi+J_y\psi) = \frac{F}{\mu}\sqrt{\frac{\eta}{\zeta}} - \left(\chi+\psi+2\frac{a}{b}\right) \quad (11)$$

Eq. (6)/Eq. (7) → II $\qquad \dfrac{G_x\beta+J_x}{G_y\beta+J_y} = \rho \qquad$ (B)

Where

$$\beta = \chi/\psi \quad (19)$$

$$\rho = \frac{[\chi+\psi+2(b/a)]-(F/\mu)\sqrt{\zeta/\eta}}{[\chi+\psi+2(a/b)]-(F/\mu)\sqrt{\eta/\zeta}} \quad (20)$$

From Eq. (A)

$$\phi = \sqrt{2}\sqrt{\frac{F}{\mu}\left(\frac{b}{a}\cot\alpha+\frac{a}{b}\tan\alpha\right) - 2\left[\left(\frac{b}{a}\right)^2+\left(\frac{a}{b}\right)^2\right]} - r \quad \text{(A)}$$

$$\eta = \frac{\phi}{1+\cot^2\alpha} \qquad \zeta = \frac{\phi}{1+\tan^2\alpha} \quad (21)$$

Eqs. (A), (19), (20), and (21) give ρ as a function of β, F/μ, and b/a through the parameters α, ϕ, η, and ζ. The equation

$$\rho = \rho(\beta, F/\mu, b/a)$$

which has been plotted on Fig. 17 is especially important since it involves neither the stiffener properties nor the stress distribution factors K_x and K_y. This equation, which is equivalent to Eq. (1), gives, in effect, the wave length λ_0 in terms of the wave angle α, the thickness ratio A/h^2, the panel ratio b/a, and the load ratio $\bar{\tau}/E$.

Substituting the values of C_x, C_y, P_x, and P_y (Eqs. (17)) into Eq. (12)

$$\xi = [(\mu/2)(\phi^2-r^2)]/(F_x\chi+F_y\psi) \quad \text{(C)}$$

where

$$F_x = (b/a)G_x + (a/b)G_y$$

$$F_y = (b/a)J_x + (a/b)J_y$$

Critical Condition

The web is in the critical condition when the wave amplitude f is zero. Therefore $\xi_c = 0$ (Eqs. (1) and (2)).

From Eq. (C)

$$\phi_c = r \quad (32)$$

From Eqs. (6) and (7)

$$(F_c/\mu)\sqrt{\zeta_c/\eta_c} = \chi_c + \psi_c + 2(b/a)$$

$$F_c/\mu\sqrt{\eta_c/\zeta_c} = \chi_c + \psi_c + 2(a/b)$$

$$\frac{\eta_c}{\zeta_c} = \tan^2\alpha_c = \frac{\chi_c+\psi_c+2(a/b)}{\chi_c+\psi_c+2(b/a)}$$

$$\chi_c + \psi_c = \phi_c + r = 2r = 2[(a/b)+(b/a)]$$

$$\tan\alpha_c = \sqrt{\frac{2(a/b)+(b/a)}{2(b/a)+(a/b)}} \quad (33)$$

$$(F_c/\mu)\tan\alpha = \phi_c + r + 2(a/b)$$

Therefore

$$F_c/\mu = 2\sqrt{[2(a/b)+(b/a)][2(b/a)+(a/b)]} \quad (34)$$

Principal Average Web Stresses

From Eqs. (17) and (4)

$$\frac{\bar{\sigma}_x}{E} = \xi(M_x\chi + N_x\psi) \qquad \frac{\bar{\sigma}_y}{E} = \xi(M_y\chi + N_y\psi)$$

The principal stresses are given by

$$\frac{\sigma_{1,2}}{E} = \left(\frac{\sigma_x}{E} + \frac{\sigma_y}{E}\right)\Big/2 \pm \sqrt{\left(\frac{\tau}{E}\right)^2 + \left[\left(\frac{\sigma_x}{E} - \frac{\sigma_y}{E}\right)\Big/2\right]^2}$$

The angle of principal stress is given by

$$\tan 2\theta_p = 2\tau/(\sigma_x - \sigma_y)$$

Therefore

$$\frac{\bar{\sigma}_{1,2}}{E} = \frac{\xi}{2}(V_x'\chi + V_y'\psi) \pm \left[F \mp \frac{\xi}{2}(W_x'\chi + W_y'\psi)\right] \quad (22)$$

$$\tan 2\theta_p = \frac{-F}{(\xi/2)(W_x'\chi + W_y'\psi)} \quad (23)$$

where $V_x' = M_x + M_y$, $W_x' = M_x - M_y$, $V_y' = N_x + N_y$, and $W_y' = N_x - N_y$.

Web Bending Stresses

In a distorted flat plate the principal bending moments are

$$M_1 = D(\beta_1 + \nu\beta_2) \qquad M_2 = D(\beta_2 + \nu\beta_1)$$

The principal curvatures β_1 and β_2 are

$$\beta_{1,2} = \frac{1}{2}\left[(w_{xx} + w_{yy}) \pm \sqrt{(w_{xx} - w_{yy})^2 + 4w_{xy}^2}\right]$$

At the center of the web, $x = 0$, $y = 0$. Then

$$\frac{w_{xx}}{f} = -\frac{\pi^2}{A}\chi \qquad \frac{w_{yy}}{f} = -\frac{\pi^2}{A}\psi \qquad \frac{w_{xy}}{f} = -\frac{\pi^2}{A}\sqrt{\eta\zeta}$$

Also

$$M_{1,2} = \frac{D}{2}\left[(1+\nu)(w_{xx} + w_{yy}) \pm (1-\nu)\sqrt{(w_{xx} - w_{yy})^2 + 4w_{xy}^2}\right]$$

$$= -\frac{\pi^2}{2}\frac{fD}{A}\left[(1+\nu)(\chi + \psi) \mp (1-\nu)\sqrt{(\chi - \psi)^2 + 4\eta\zeta}\right]$$

The bending stress is given by

$$\sigma_{b1,2} = \pm[hE/2(1-\nu^2)D]M_{1,2}$$

$$\frac{\sigma_{b1,2}}{E} = \pm\pi\sqrt{\frac{h^2}{A}}\xi\left\{\frac{\chi + \psi}{1-\nu} \pm \frac{1}{1+\nu}\left[(\chi - \psi) \mp 2\sqrt{\eta\zeta}\right]\right\} \quad (24)$$

The angle of principal curvature is

$$\tan 2\theta_b = \frac{2w_{xy}}{w_{xx} - w_{yy}} \qquad \tan 2\theta_b = \frac{2\sqrt{\eta\zeta}}{\chi - \psi} \quad (25)$$

In the equation for $\sigma_{b1,2}/E$, use of the plus sign within the braces gives the maximum bending stress (σ_{b1}), while use of the minus sign gives the minimum bending stress.

Stiffener Bending Stresses

The shear per inch along an edge parallel to the YZ plane, Fig. 7, denoted Q_x, is

$$Q_x = \frac{\partial M_{yx}}{\partial y} + \frac{\partial M_x^*}{\partial x}$$

where

$$M_{yx} = -D(1-\nu)\frac{\partial^2 w}{\partial x\,\partial y} \qquad M_x = -D\left(\frac{\partial^2 w}{\partial x^2} + \nu\frac{\partial^2 w}{\partial y^2}\right)$$

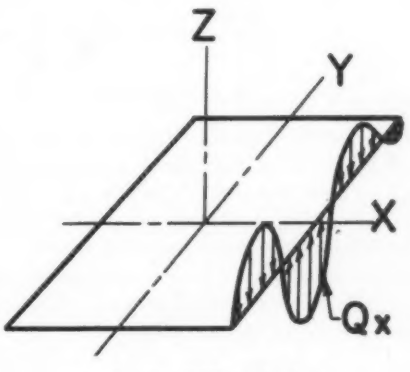

Fig. 7. Stiffener loads.

M_{yx} is the torque per inch on a plane parallel to the XZ plane, while M_x is the moment per inch on a plane parallel to the YZ plane. Then

$$-\frac{Q_x}{D} = \frac{\partial}{\partial x}(\Delta w)$$

$$\Delta w = 2fpm \sin px \cos qy \sin(mx + ny) + 2fqn \cos px \sin qy \sin(mx + ny) - f(p^2 + q^2 + m^2 + n^2)\cos px \cos qy \cos(mx + ny)$$

$$-Q_x/D = 2fp^2m \cos px \cos qy \sin(mx + ny) + 2fpm^2 \sin px \cos qy \cos(mx + ny) - 2fpqn \times \sin px \sin qy \sin(mx + ny) + 2fqmn \cos px \times \sin qy \cos(mx + ny) - f(p^2 + q^2 + m^2 + n^2) \times [-p \sin px \cos qy \cos(mx + ny) - m \cos px \cos qy \sin(mx + ny)]$$

For the right- and left-hand edges

$$x = \pm\pi/2p$$

* This M_x bears no relation to the M_x used elsewhere.

Therefore

$$-\frac{Q_x}{fpD} = \pm(p^2 + q^2 + 3m^2 + n^2)\cos qy \times \cos(\pm am + ny) \mp 2qn \sin qy \sin(\pm am + ny)$$

Use the top sign for the right-hand edge of the web and the bottom sign for the left-hand edge.

Substituting the dimensionless ratios (Eqs. (1) and (2))

$$-\frac{4}{\pi}\frac{\omega_1}{\sqrt{\theta}}\frac{Q_{xR}/h}{E} = \left[(3\chi + \psi) - 2\frac{b}{a}\right]\cos\frac{\pi}{2}\frac{y}{b}\cos\frac{\pi}{2} \times \left(\sqrt{\frac{b}{a}}\zeta\frac{y}{b} + \sqrt{\frac{a}{b}}\eta\right) - 2\sqrt{\frac{a}{b}}\zeta\sin\frac{\pi}{2}\frac{y}{b}\sin\frac{\pi}{2} \times \left(\sqrt{\frac{b}{a}}\zeta\frac{y}{b} + \sqrt{\frac{a}{b}}\eta\right)$$

$$-\frac{4}{\pi}\frac{\omega_1}{\sqrt{\theta}}\frac{Q_{xL}/h}{E} = -\left[(3\chi + \psi) - 2\frac{b}{a}\right]\cos\frac{\pi}{2}\frac{y}{b}\cos\frac{\pi}{2} \times \left(\sqrt{\frac{b}{a}}\zeta - \sqrt{\frac{a}{b}}\eta\right) + 2\sqrt{\frac{a}{b}}\zeta\sin\frac{\pi}{2}\frac{y}{b}\sin\frac{\pi}{2} \times \left(\sqrt{\frac{b}{a}}\zeta\frac{y}{b} - \sqrt{\frac{a}{b}}\eta\right)$$

where $\omega_1 = 3/\pi^2\,(1 - \nu^2)\,2\,(a/h)(A/h^2)$.

If the two panels adjacent to a stiffener are the same and are subject to the same shear load, then the total bending load upon the stiffener will be $Q_x = Q_{xR} + Q_{xL}$ or $Q_x = Q_{xR} - Q_{xL}$ depending upon whether the two panels buckle in the same or opposite modes.

A consideration of the above expressions suggests that the following simplified formula will be useful in designing stiffeners for bending:

$$\frac{Q_x/h}{E} = 4\mu\sqrt{\frac{b}{a}}\xi\,(a_1 +\!\!\rightarrow a_2)\sin\frac{\pi}{2}\sqrt{\frac{b}{a}}\zeta\frac{y}{b} \qquad (26)$$

where $a_1 = \phi + r + 2\eta$ and $a_2 = 2\sqrt{(a/b)}\zeta$.

For design purposes the stiffener is considered as a beam column as shown in Fig. 8. z is the eccentricity of the axis of the stiffeners with respect to the mid-plane of the web.

$$Q_{xm}/hE = 4\mu\sqrt{(b/a)}\xi\,(a_1 +\!\!\rightarrow a_2)$$

$$\lambda_f = 4b\sqrt{(a/b)(1/\zeta)}$$

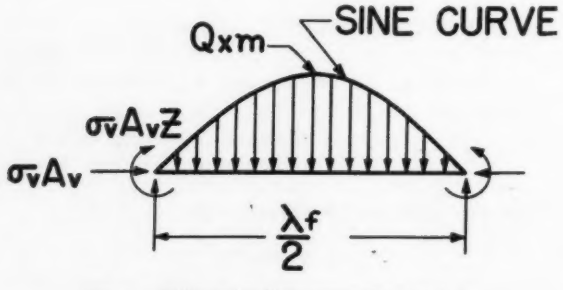

FIG. 8. Stiffener loading assumed for design.

For a beam-column subject to a sinusoidal loading the maximum bending moment is found to be

$$M_m = \frac{L^2Q_{xm}}{\pi^2 - (L^2/j^2)} + \frac{M_0}{\cos(1/2)(L/j)}$$

where

L = length
M_0 = bending moment applied at ends
I = moment of inertia of beam-column
P = column load
j = $\sqrt{EI/P}$
Q_{xm} = maximum load/in. of sinusoidal distribution

Then $M_m = Z\sigma_{vb}$, $M_0 = \sigma_v A_v z$, and $L/j = \sqrt{(L/\rho_s)^2(\sigma_v/E)}$, where

Z = section modulus
σ_{vb} = maximum beam-column stress
ρ_s = radius of gyration = $\sqrt{I/A}$

Therefore

$$Z\sigma_{vb} = \frac{L^2Q_{xm}}{\pi^2 - (L/j)^2} + \frac{M_0}{\cos(1/2)(L/j)}$$

$$L = 2b\sqrt{(a/b)(1/\zeta)}$$

$$\frac{\sigma_{vb}}{E} = \frac{\dfrac{hL^2}{Z}\dfrac{Q_{xm}/h}{E}}{\pi^2 - \left(\dfrac{L}{\rho_s}\right)^2\dfrac{\sigma_v}{E}} + \frac{\dfrac{A_v z}{Z}\dfrac{\sigma_v}{E}}{\cos\dfrac{1}{2}\sqrt{\left(\dfrac{L}{\rho_s}\right)^2\dfrac{\sigma_v}{E}}}$$

For symmetric stiffeners, $z = 0$ and

$$\frac{\sigma_{vb}}{E} = \frac{\dfrac{hL^2}{Z}\dfrac{Q_{xm}/h}{E}}{\pi^2 - (L/\rho_s)^2(\sigma_v/E)} \qquad (27)$$

TORSIONAL STIFFENER LOADS

Torsional loads are produced upon the stiffener through the action of the shears Q_{xL} and Q_{xR}, Fig. 9. From the equilibrium of moments,

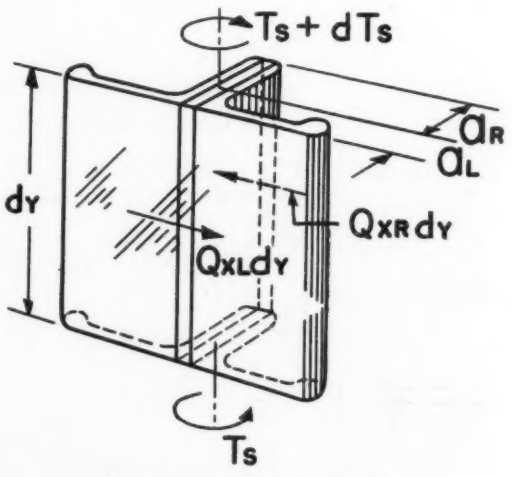

FIG. 9. Torsional stiffener loads.

$$dTs/dy = Q_{xR} \pm Q_{xL}a_L \tag{28}$$

Thus Q_x produces both torsion and bending stresses. Since these two stresses act together in making their contribution to the failure of the stiffener, design charts will be computed on the basis of bending and compression only. Torsion will be taken into account by choosing a sufficiently low allowable stress.

Tension Fields

It is of interest to examine the case where $(h^2/A) \to 0$, F, and A remain finite. From Eqs. (1) and (2),

$$\mu = [\pi^2/6(1 - \nu^2)](h^2/A)$$

Therefore $\mu \to 0$ and $F/\mu \to \infty$.

In Eq. (A)

$$(b/a) \cot \alpha + (a/b) \tan \alpha > 0$$

a and b are bounded, therefore $\phi \to \infty$. $\lambda = \sqrt{A/\phi}$, therefore $\lambda \to 0$. Therefore

$$\eta \to \infty \qquad \chi \to \eta \to \infty \qquad \chi + \psi = \phi + r$$
$$\zeta \to \infty \qquad \psi \to \zeta \to \alpha \qquad \therefore \chi + \psi \to \phi$$

From Eq. (A)

$$2(F/\mu)[(b/a) \cot \alpha + (a/b) \tan \alpha] \to \phi^2$$

$$\frac{F}{\mu} \to \frac{\phi^2}{2[(b/a) \cot \alpha + (a/b) \tan \alpha]}$$

From Eq. (B),

$$\rho \to \frac{\phi - (F/\mu) \cot \alpha}{\phi - (F/\mu) \tan \alpha}$$

$$\to \frac{1 - \dfrac{\phi}{2} \dfrac{\cot \alpha}{(b/a) \cot \alpha + (a/b) \tan \alpha}}{1 - \dfrac{\phi}{2} \dfrac{\tan \alpha}{(b/a) \cot \alpha + (a/b) \tan \alpha}}$$

$$\to \cot^2 \alpha$$

$$\beta \to (\eta/\zeta) \to \tan^2 \alpha$$

Therefore

$$\rho \to 1/\beta$$

Eq. (B):

$$(G_x\beta + J_x)/(G_y\beta + J_y) \to (1/\beta)$$
$$G_x\beta^2 + (J_x - G_y)\beta - J_y \to 0$$

Refer to Eqs. (16) and (18). Since $K_x = K_y = 0$

$$DG_x = R_v + R_Q + 1 \qquad DJ_x = \nu$$
$$DG_y = \nu \qquad DJ_y = R_h + 1$$

Therefore

$$(R_v + R_Q + 1)\beta^2 - (R_h + 1) = 0$$
$$\beta^2 = (R_h + 1)/(R_v + R_Q + 1)$$

$$\tan^2 \alpha = \sqrt{(R_h + 1)/(R_v + R_Q + 1)} \tag{29}$$

If the cap has infinite bending rigidity, $R_Q = 0$ and

$$\tan^2 \alpha = \sqrt{(R_h + 1)/(R_v + 1)} \tag{30}$$

In reference 5, p. 29, Wagner gives

$$\sin^2 \alpha = \sqrt{a^2 + a} - a$$

where

$$a = \frac{1 + (hS/2F_H)}{(ts/F_v) - (hs/2F_H)}$$

and where

h = girder height
s = web thickness
F_H = cross-sectional area of one cap
F_v = cross-sectional area of one upright
t = spacing of two uprights

In the present notation $hs/2F_H = R_h$ and $ts/F_v = R_v$; therefore

$$a = \frac{1 + R_h}{R_v - R_h}$$

Also

$$\tan^2 \alpha = \frac{\sqrt{a^2 + a} - a}{1 - \sqrt{a^2 + a} + a}$$

$$\tan^2 \alpha = \sqrt{\frac{a}{1 + a}} = \sqrt{\frac{\dfrac{1 + R_h}{R_v - R_h}}{1 + \dfrac{1 + R_h}{R_v - R_h}}} = \sqrt{\frac{R_h + 1}{R_v + 1}}$$

which is the same as Eq. (30)

From Eq. (A)

$$\frac{\mu}{2}\phi^2 \to F\left(\frac{b}{a} \cot \alpha + \frac{a}{b} \tan \alpha\right)$$

From Eq. (C)

$$\xi \to \frac{F\left(\dfrac{b}{a} \cot \alpha + \dfrac{a}{b} \tan \alpha\right)}{\phi(F_x \sin^2 \alpha + F_y \cos^2 \alpha)} \tag{31}$$

Therefore $\xi \to 0$ since $\phi \to \infty$. From Eq. (24)

$$\frac{\sigma_{b1,2}}{E} = \pm \pi \sqrt{\frac{h^2}{A}\xi\phi^2} \left\{ \frac{1}{1 - \nu} \pm \frac{1}{1 + \nu}\left[(\sin^2 \alpha - \cos^2 \alpha) + 2 \sin \alpha \cos \alpha\right] \right\}$$

The quantity in the braces is finite.

$$\frac{h^2}{A}\phi^2 = \frac{12}{\pi^2}(1 - \nu^2)\frac{\mu}{2}\phi^2 =$$
$$\frac{12}{\pi^2}(1 - \nu^2)F\left(\frac{b}{a} \cot \alpha + \frac{a}{b} \tan \alpha\right)$$

which is finite. Therefore, $(\sigma_{b1,2}/E) \to 0$ since $\xi \to 0$. From Eq. (22)

$$\frac{\bar{\sigma}_{1,2}}{E} \to \frac{1}{2}\xi\phi(V_x' \sin^2\alpha + V_y' \cos^2\alpha) \pm \left[F + \frac{\xi\phi}{2}(W_x' \sin^2\alpha + W_y' \cos^2\alpha\right]$$

Therefore

$$\frac{\bar{\sigma}_{1,2}/E}{\bar{\tau}/E} \to \frac{1}{2}\frac{\xi\phi}{F}(V_x' \sin^2\alpha + V_y' \cos^2\alpha) \pm \left[1 + \frac{1}{2}\frac{\xi\phi}{F}(W_x' \sin^2\alpha + W_y' \cos^2\alpha)\right]$$

From Eqs. (15), letting $H' = R_h + 1$ and $V' = R_v + R_Q + 1$,

$$D = H'V' - \nu^2 \qquad \tan^2\alpha = \sqrt{H'/V'}$$

$$DF_x = \frac{b}{a}V' + \frac{a}{b}\nu \qquad \sin^2\alpha = \frac{\sqrt{H'}}{\sqrt{V'} + \sqrt{H'}}$$

$$DF_y = \frac{b}{a}\nu + \frac{a}{b}H' \qquad \cos^2\alpha = \frac{\sqrt{V'}}{\sqrt{V'} + \sqrt{H'}}$$

$$\frac{b}{a}\cot\alpha + \frac{a}{b}\tan\alpha = \frac{b}{a}\sqrt[4]{\frac{V'}{H'}} + \frac{a}{b}\sqrt[4]{\frac{H'}{V'}}$$

$$F_x \sin^2\alpha + F_y \cos^2\alpha = \frac{\frac{b}{a}V' + \frac{a}{b}\nu}{H'V' - \nu^2}\frac{\sqrt{H'}}{\sqrt{V'} + \sqrt{H'}} + \frac{\frac{b}{a}\nu + \frac{a}{b}H'}{H'V' - \nu^2}\frac{\sqrt{V'}}{\sqrt{V'} + \sqrt{H'}}$$

$$= \frac{\sqrt[4]{H'V'}}{(\sqrt{H'V'} - \nu)(\sqrt{V'} + \sqrt{H'})} \times \left(\frac{b}{a}\sqrt[4]{\frac{V'}{H'}} + \frac{a}{b}\sqrt[4]{\frac{H'}{V'}}\right)$$

Therefore

$$\frac{\frac{b}{a}\cot\alpha + \frac{a}{b}\tan\alpha}{F_x \sin^2\alpha + F_y \cos^2\alpha} = \frac{(\sqrt{H'V'} - \nu)(\sqrt{V'} + \sqrt{H'})}{\sqrt[4]{H'V'}}$$

From Eq. 31

$$\frac{\xi\phi}{F} = \frac{(\sqrt{H'V'} - \nu)(\sqrt{V'} + \sqrt{H'})}{\sqrt[4]{H'V'}}$$

$$V_x' \sin^2\alpha + V_y' \cos^2\alpha = \frac{1}{\sqrt{H'V'} - \nu}$$

$$W_x' \sin^2\alpha + W_y' \cos^2\alpha = \frac{\sqrt{V'} - \sqrt{H'}}{\sqrt{V'} + \sqrt{H'}}\frac{1}{\sqrt{H'V'} - \nu}$$

$$\frac{1}{2}\frac{\xi\phi}{F}(V_x' \sin^2\alpha + V_y' \cos^2\alpha) = \frac{1}{2}\left(\sqrt[4]{\frac{V'}{H'}} + \sqrt[4]{\frac{H'}{V'}}\right)$$

$$\frac{1}{2}\frac{\xi\phi}{2}(W_x' \sin^2\alpha + W_y' \cos^2\alpha) = \frac{1}{2}\left(\sqrt[4]{\frac{V'}{H'}} - \sqrt[4]{\frac{H'}{V'}}\right)$$

Therefore

$$\frac{\bar{\sigma}_{1,2}}{\tau} = \frac{1}{2}\left(\sqrt[4]{\frac{V'}{H'}} + \sqrt[4]{\frac{H'}{V'}}\right) \pm \frac{1}{2}\left(\sqrt[4]{\frac{V'}{H'}} + \sqrt[4]{\frac{H'}{V'}}\right)$$

$$\bar{\sigma}_1/\bar{\tau} = \tan\alpha + \cot\alpha$$

$$\bar{\sigma}_2/\bar{\tau} = 0$$

Computation Procedure

When all the dimensions and the shear load are known, the panel constants can be found by simple substitution into the following formulas in the order given. After G_x, G_y, J_x, and J_y have been found, Eq. (B) can be plotted on the graph of Eq. (A) for the proper value of b/a. Using the proper value of F/μ, the values of β and ϕ can be determined. These are substituted into Eq. (C) to find ξ. The remaining quantities can be evaluated by substitution.

Single Panel

The formulas apply to the case of a single shear panel bounded on four sides by stiffeners having infinite bending rigidity, except that

$$R_v = \frac{1}{2}\frac{A_y}{A_v} \qquad R_Q = 0$$

Set of Panels

The formulas also apply to a checkerboard of panels except that

$$R_h = \frac{A_x}{A_h} \qquad R_Q = 0$$

Nonhomogeneous Construction

The formulas have been set up for the case where all portions of the beam are of the same material. However, if the caps and stiffeners are of different material from the web, multiply R_h and R_Q by E_w/E_c and R_v by E_w/E_v, where E_w, E_c, and E_v are the moduli of elasticity for the web, caps, and stiffeners, respectively.

Panel Constants

$$R_h = A_x/2A_h \qquad H = R_h + 1 \qquad K_x = K_y = 1/2$$

$$R_Q = \frac{1}{30}\frac{a}{b}\frac{I_x}{I_h} \qquad Q = K_y R_Q + 1$$

$$R_v = A_y/A_v \qquad V = R_v + 1$$

$$E_h = R_h(VQ + R_Q) \qquad P_h = \nu R_h$$

$$E = \nu R_Q \qquad P_y = R_Q[K_y(HV - \nu^2) + H]$$

$$E_s = \nu R_s Q \qquad P_s = R_s H \qquad D = Q(HV - \nu^2) + R_Q H$$

$$D_y = \frac{E_y}{D} \qquad D_h = \frac{E_h}{D} \qquad D_s = \frac{E_s}{D} \qquad O_y = \frac{P_y}{D} \qquad O_h = \frac{P_h}{D} \qquad O_s = \frac{P_s}{D}$$

$$M_x = \frac{D_h}{R_h} \qquad M_y = \frac{D_s}{R_s} \qquad S_y = -D_y \qquad G_x = M_x + K_x \qquad J_x = N_x$$

$$N_x = \frac{O_h}{R_h} \qquad N_y = \frac{O_s}{R_s} \qquad T_y = 1 - O_y \qquad G_y = M_y + K_y S_y \qquad J_y = N_y + K_y T_y$$

$$F_x = \frac{b}{a} G_x + \frac{a}{b} G_y \qquad V_x' = M_x + M_y \qquad W_x' = M_x - M_y$$

$$F_y = \frac{b}{a} J_x + \frac{a}{b} J_y \qquad V_y' = N_x + N_y \qquad W_y' = N_x - N_y$$

If $R_h \to 0$ or $R_s \to 0$, the following must be used:

$$D_s = \frac{E_y + E_s}{D} \qquad M_x = \frac{1 - (D_h + \nu D_s)}{1 - \nu^2} \qquad N_x = \frac{\nu - (O_h + \nu O_s)}{1 - \nu^2}$$

$$O_s = \frac{P_y + P_s}{D} \qquad M_y = \frac{\nu - (D_s + \nu D_h)}{1 - \nu^2} \qquad N_y = \frac{1 - (O_s + \nu O_h)}{1 - \nu^2}$$

Web Parameters

$$2\frac{F}{\mu}\left(\frac{b}{a}\cot\alpha + \frac{a}{b}\tan\chi\right) = (\phi + r)^2 + 4\left[\left(\frac{b}{a}\right)^2 + \left(\frac{a}{b}\right)^2\right] \qquad \text{(A)}$$

$$\rho = \frac{G_x\beta + J_x}{G_y\beta + J_y} \qquad \text{(B)} \qquad \chi = \frac{\phi + r}{1 + 1/\beta} \qquad \psi = \frac{\phi + r}{1 + \beta}$$

$$\xi = \frac{\mu/2(\phi^2 - r^2)}{F_x\chi + F_y\psi} \qquad \text{(C)} \qquad \eta = \chi - \frac{b}{a} \qquad \zeta = \psi - \frac{a}{b}$$

$$\gamma_0 = 2[(1 + \nu)F + \xi\sqrt{\eta\zeta}] \quad \text{(D) average shearing strain}$$

Stiffener Parameters

$$\epsilon_h = \xi(D_h\chi + O_h\psi) \quad \text{(E) cap axial strain}$$

$$\epsilon_y = \xi(D_y\chi + O_y\psi) \quad \text{(F) cap bending strain}$$

$$\epsilon_s = \xi(D_s\chi + O_s\psi) \quad \text{(G) stiffener axial strain}$$

Principal Average Mid-Plane Stresses

$$\frac{\bar\sigma_{1,2}}{E} = \frac{\xi}{2}(V_x'\chi + V_y'\psi) \mp \left[F \mp \frac{\xi}{2}(W_x'\chi + W_y'\psi)\right] \qquad (22)$$

$$\tan 2\theta_p = -F/[(\xi/2)(W_x'\chi + W_y'\psi)] \qquad (23)$$

Center Bending Stresses

$$\frac{\sigma_{b1,2}}{E} = \mp\pi\sqrt{\frac{h^2}{A}}\xi\left\{\frac{\chi + \psi}{1 - \nu} \mp \frac{1}{1 + \nu}[(\chi - \psi) \mp 2\sqrt{\eta\zeta}]\right\}$$

$$\tan 2\theta_b = 2\sqrt{\eta\zeta}/(\chi - \psi)$$

Stiffener Bending

$$\frac{Q_{xm}/h}{E} = 4\mu\sqrt{\frac{b}{a}}\xi\,(a_1 \mp a_2) \qquad a_1 = \phi + r + 2\eta$$

$$\frac{\sigma_{sb}}{E} = \frac{\dfrac{hL^2}{Z}\dfrac{Q_{xm}/h}{E}}{\pi^2 - \left(\dfrac{L}{\rho_s}\right)^2\dfrac{\sigma_s}{E}} + \frac{\dfrac{A_s e}{Z}\dfrac{\sigma_s}{E}}{\cos\dfrac{1}{2}\sqrt{\left(\dfrac{L}{\rho_s}\right)^2\dfrac{\sigma_s}{E}}} \qquad a_2 = 2\sqrt{\frac{a}{b}\zeta}$$

$$L = 2b\sqrt{\frac{a}{b}\frac{1}{\zeta}}$$

Half Wave Length	λ	$= \sqrt{A/\phi}$
Wave Angle	$\tan \alpha$	$= \sqrt{\eta/\zeta}$
Wave Amplitude	f	$= (4/\pi)h\sqrt{(A/h^2)\xi}$
Cap Axial Stress	σ_h	$= E\epsilon_h$
Stiffener Axial Stress	σ_v	$= E\epsilon_v$

The following relations also hold, although they are not ordinarily required:

$$\eta = \phi \sin^2 \alpha \qquad \phi = \eta + \zeta \qquad \beta = \chi/\psi$$

$$\zeta = \phi \cos^2 \alpha \qquad \rho = \frac{(\chi + \psi) + 2(b/a) - (F/\mu)\cot \alpha}{(\alpha + \psi) + 2(a/b) - (F/\mu)\tan \alpha}$$

Critical Conditions

$$\lambda_c = A/d \tag{32}$$

where d = length of panel diagonal and λ_c = critical half wave length.

$$\tan \alpha_c = \sqrt{\frac{2(a/b) + (b/a)}{2(b/a) + (a/b)}} \tag{33}$$

$$\frac{F_c}{\mu} = 2\sqrt{[2(a/b) + (b/a)][2(b/a) + (a/b)]} \tag{34}$$

Additional Applications

With only slight modification the theory can be made to apply to a number of additional aspects of the shear web problem. For example, the loads tending to produce tension in the web-to-stiffener rivets can be calculated from the stiffener bending load formulas. Loads on web-to-cap rivets can be obtained from the web stress formulas.

Dimensionless Ratios

A number of dimensionless factors relating to shear webs have come to light in the course of the analysis. Of particular importance is the thickness ratio, h^2/A. This quantity is the primary measure of the ability of the web to resist a shear strain by diagonal compression, although the other ratios (b/a, R_v, R_h, R_Q, F) also have an influence.

It is noteworthy that the degree to which a web is shear resistant depends not simply on its thickness but on the ratio of the square of its thickness to its unstiffened area. Thus, a thick web with a large unstiffened area may actually be closer to the Wagner case than a thin web having a small unstiffened area.

Test Results

In the following applications of the theory, the only experimental constants used are Young's modulus and Poisson's ratio.

Figs. 10, 12, and 13 relate to a shear panel test conducted at the Douglas Aircraft Company.[3] Fig. 10 is a photograph of the test setup. The specimen was a 19 by 28½ sheet of 0.064 24ST aluminum alloy. Strain measurements were made with electrical strain gauges, while wave lengths and depths were roughly measured with a straight edge and scale.

Load was transmitted into the sheet through a system of levers such that the horizontal web shear was 0.912 times the jack load. Note that the specimen shown in the photograph is not the one referred to here. The actual panel was unstiffened except for the support provided by the jig members which are considered infinitely rigid.

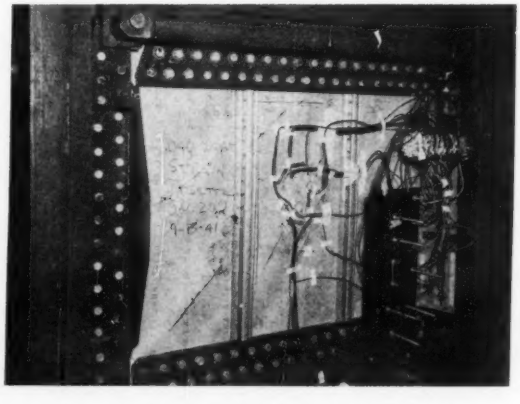

Fig. 10. Photograph of Douglas shear panel.

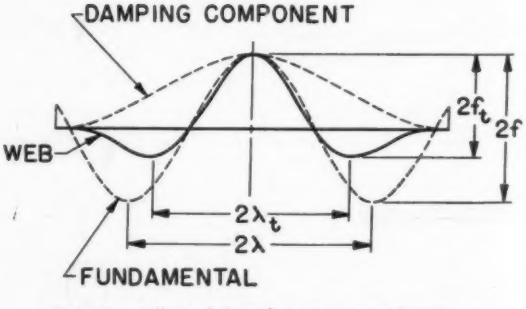

Fig. 11. Effect of damping upon wave length.

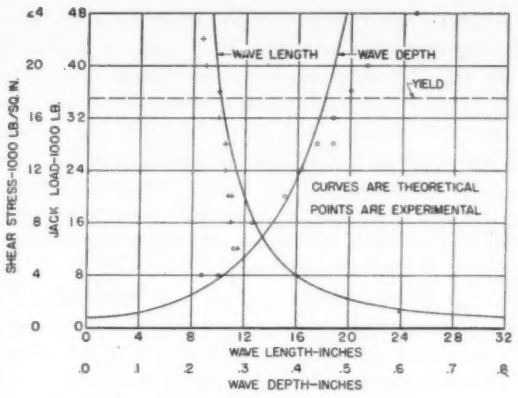

FIG. 12. Wave lengths and amplitudes.

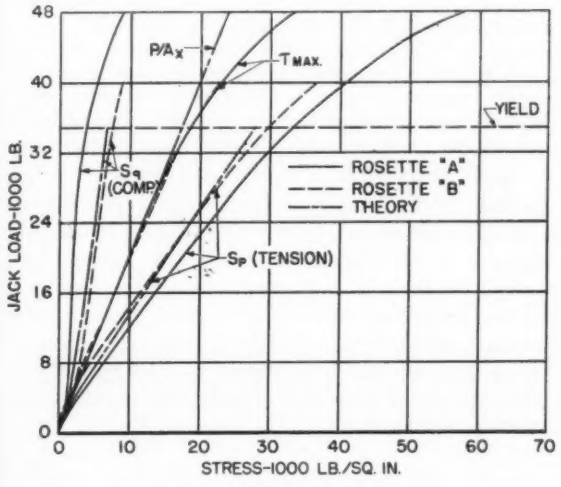

FIG. 13. Principal average stresses.

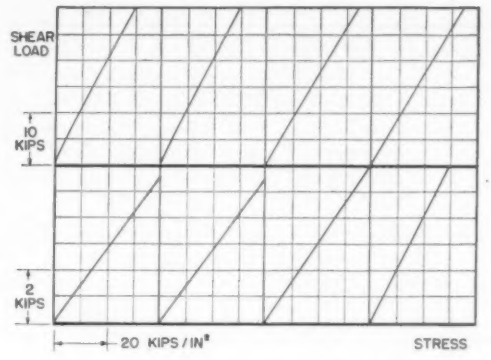

FIG. 14. Beam web strains on a 45° gauge line approximately parallel to the direction of principal tension.

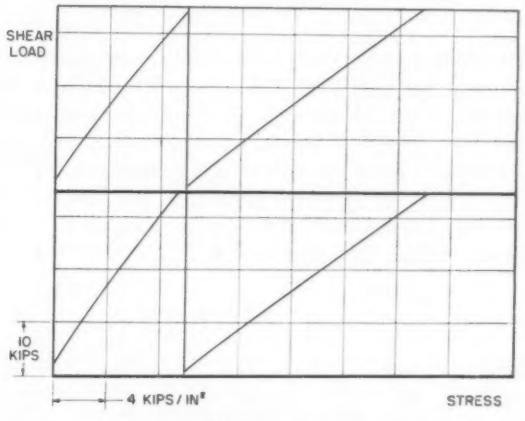

FIG. 15. Stiffener axial stresses.

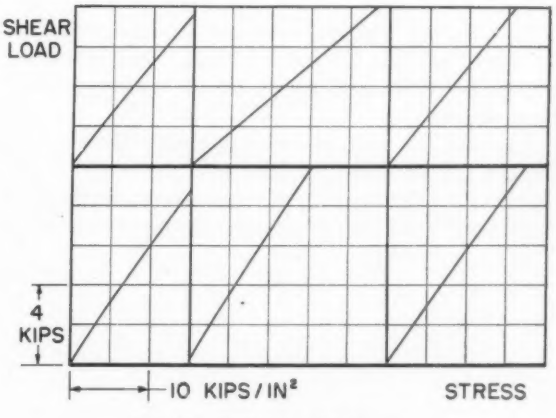

FIG. 16. Stiffener axial stresses.

Fig. 12 is a comparison of wave lengths and depths as determined by calculation and from test. Actually, the quantities measured in test were different from those that were calculated because of the effect of damping; consequently, the test values should be, and are, smaller than theoretic. Thus, Fig. 11 is a cross section of the web taken through its midpoint and perpendicular to the wave direction. It shows a possible configuration of the buckled surface. The theory gives λ and f, while λ_t and f_t, which are smaller, were measured in test. It would be possible to obtain λ and f theoretically, but it would be necessary to draw a contour map of the entire buckled surface. Note that this effect becomes negligible at higher loads because λ decreases.

Fig. 13 is a comparison of principal stresses determined theoretically and experimentally. Rosette A was located at the center of the panel, while Rosette B was located in the corner 6 in. from either edge. Because of its position, Rosette B gave stresses that were probably about average for the panel. The theoretic stresses are average. The curve marked P/A_x is the shear stress computed from the dimensions of the panel. Notice that the shear stresses given by both Rosettes A and B are approximately the same, in agreement with the theoretic assumptions.

The lines marked "yield" in Figs. 12 and 13 give the shear load at which both the load-deflection diagram and the strain gauges began to depart from linearity.

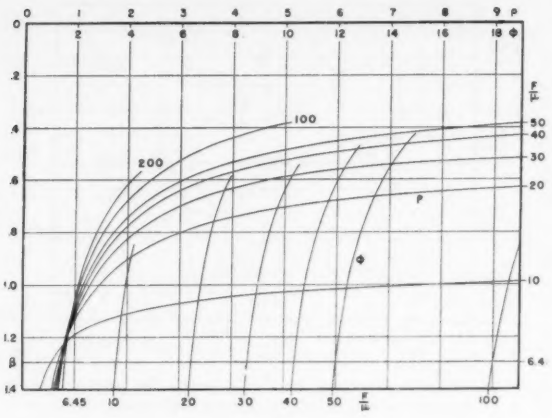

FIG. 17. Graph of Eq. (1) for $b/a = 1^1/_2$.

In addition to the Douglas company data, the results of certain tests on thin web beams are available for analysis. Figs. 14 through 16 relate to these tests. Thus Figs. 15 and 16 give calculated stiffener stresses, while Fig. 14 gives the web strains computed on a 45° gauge line (approximately parallel to the direction of principal tension) at the panel midpoints. The formula used in the latter case is

$$\frac{\epsilon_{45}}{1+\nu} = \frac{1}{2}\frac{1-\nu}{1+\nu}\xi(\chi A_1 + \psi B_1) + F$$

where

$$A_1 = (2-\nu)V_x' + (D_h + D_s)$$

$$B_1 = (2-\nu)V_y' + (O_h + O_s)$$

Since this formula is of no direct practical significance, its derivation has not been included, but it follows readily from the expressions already given for mid-plane stresses.

Figs. 14, 15, and 16 were originally intended to present a comparison between test and theory. Unfortunately, the test data have been classified as "restricted" and are, therefore, though available to the industry, unavailable for publication here. However, the agreement obtained was, in nearly all cases, within the experimental error for loads below the yield. Above the yield, the test points deviated from the theoretic curves, but this is an expected result since the analysis is based on the assumption that the structure is elastic. It is thought that for design purposes this effect can be taken into account by using a modified value of Young's modulus or by choosing suitably low allowable stresses.

The agreement obtained for the very thin webs and for the heavier webs was equally good. Consequently, it appears that the analysis is valid for as wide a range of web thicknesses as is likely to occur in practice.

In making the computations for the beams, all of the applied shear load was assumed to be carried by the web. No deductions were made from cap and stiffener areas to allow for rivet holes.

CONCLUSIONS

The foregoing comparison between theory and test indicates that wave lengths, wave amplitudes, web principal stresses, and stiffener axial stresses can be computed for loads below the proportional limit with a degree of accuracy satisfactory for design and analysis purposes. No experimental constants, other than Young's modulus and Poisson's ratio, are required. The remaining features of the analysis await further experimentation.

It is expected that the theory will be readily applicable to the construction of charts for the design of stiffened shear webs.

REFERENCES

[1] Timoshenko, S., *Theory of Elastic Stability*, 1st Edition, pp. 307 and 391; McGraw-Hill Book Company, Inc., New York, 1936.

[2] Wagner, H., *Flat Sheet Metal Girder with Very Thin Web*, N.A.C.A. T.N. No. 604, p. 29, 1931.

[3] Neuls, G. S., and Comp, L. A., *The Use of Electrical Strain Gauges on Thin Metal*, Douglas Aircraft Company Report No. SM3516, p. 8, January 30, 1942.

Loss in Aileron Effectiveness Because of Wing Twist and Considerations Regarding the Internal-Pressure Balanced Aileron

REINHARDT ROSENBERG*

Bell Aircraft Corporation

SUMMARY

The treatment of internal-pressure balanced ailerons in flutter analysis is indicated, and the conclusion is reached that, in contradistinction to Frise-type aileron balance, this type of aerodynamic balance does not affect the expressions for oscillatory wing lift and wing moment.

From a variation of conditions of aileron reversal, expressions for loss in aileron effectiveness at lesser speeds have been derived. It is shown, and substantiated by flight-test data, that deviations from two-dimensional flow are considerable and that past methods of computing aileron reversal speeds are highly conservative. Improvements on present methods are given and comparisons with flight test results are illustrated.

In many respects this paper was suggested by Shornick's paper,[8] but the solution for loss in maneuverability below the aileron reversal speed and the deviations from the "flutter equations" are new.

INTRODUCTION

BECAUSE OF present-day high flying speed and the resulting requirement of good maneuverability at these speeds, as well as the development of new and more effective ailerons, it is desirable to:

(1) Submit past methods for calculating aileron reversal speeds to a critical review.

(2) Develop methods for calculating loss in aileron effectiveness below the reversal speed.

(3) Develop methods for the treatment of new types of ailerons in flutter analysis and the analysis of associated phenomena.

THE INTERNAL-PRESSURE BALANCED AILERON

Although the internal-pressure balanced aileron is aerodynamically balanced, it cannot be directly treated by the methods developed by Küssner[1] as the following reasoning will show.

The conventional aileron with aerodynamic balance and the skeleton line by which it is replaced in Küssner's analysis are shown in Figs. 1a and 1b. It is clear from flutter theory, as well as from Fig. 1, that the forces acting on the entire wing, defined by Theodorsen[2] as P and M_a, are influenced by the fact that the aileron hinge is aft of the leading edge and that, thus, the aileron leading edge is in the air stream. This is also true for the aerodynamically balanced aileron with sealed gap, shown with the skeleton line replacing it in Figs. 2a and 2b.

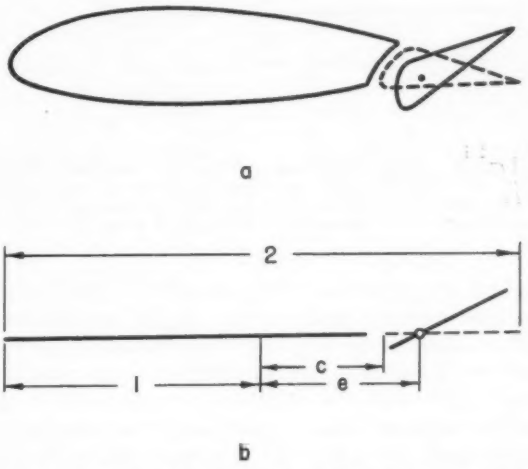

FIG. 1a. Wing with conventional aileron and aerodynamic balance. FIG. 1b. Skeleton line replacing wing-aileron combination shown above in flutter analysis.

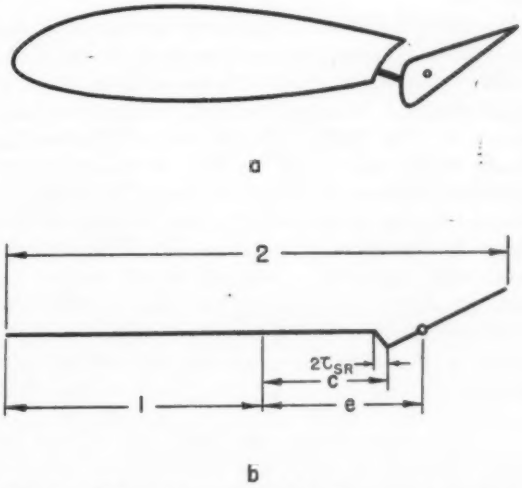

FIG. 2a. Wing with conventional aileron and aerodynamic balance, but gap is sealed. FIG. 2b. Skeleton line replacing wing-aileron combination shown above in flutter analysis.

The internal-pressure balanced aileron and the skeleton line replacing it for the determination of P and M_a,

Received May 28, 1943.

* Flutter Engineer.

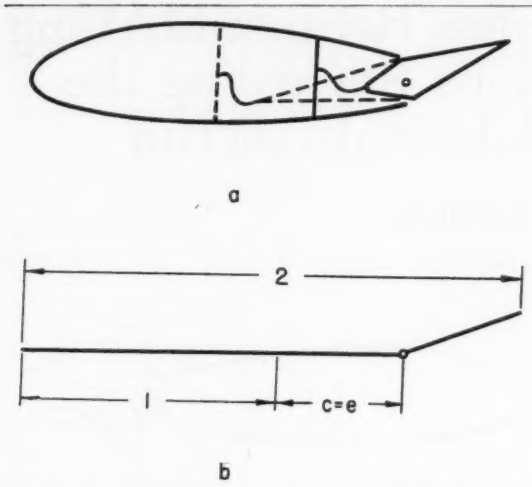

FIG. 3a. Wing with internal pressure balanced aileron. FIG. 3b. Skeleton line replacing wing-aileron combination shown above in flutter analysis for the determination of oscillatory aerodynamic lift and moment acting on wing.

but not M_β, are shown in Figs. 3a and 3b. It is obvious without rigorous analysis that the lift and moment forces acting on the wing are not influenced in any way by the aileron structure hidden within the wing and that these forces would remain unchanged if the aileron foreward structure were altered as indicated by the dotted lines in Fig. 3a. It is thus evident that, for determining the oscillatory wing lift and wing moment, this type of aileron acts as if it had no aerodynamic balance—i.e., as if its leading edge were located at the hinge line.

It is clear, on the other hand, that this reasoning does not hold for the computation of moments on the aileron about the hinge, M_β, since it is the purpose of the internal-pressure balanced aileron to reduce hinge moments. The theory of this type of aileron as it affects flutter theory has not been developed as yet. Therefore, the best procedure available for computing M_β seems to be to determine (1) the distance between aileron leading edge and hinge and (2) the distance between wing mid-chord point and aileron leading edge from an equivalent, conventional aileron which, for small deflections from neutral, has similar hinge moments as the internal-pressure balance aileron it replaces.

AILERON REVERSAL

The phenomenon of aileron reversal may be explained as follows.

Deflecting an aileron down (for instance) will increase the lift and, therefore, the angle of attack of a wing. The deflected aileron will also cause or increase an aerodynamic torque on the wing about a spanwise axis. This torque is in such a direction as to produce, in a wing of finite stiffness, twist decreasing the angle of attack. The force resisting this torque is caused by the torsional stiffness of the wing and is thus independent of the forward speed. Since the aerodynamic torque is approximately proportional to the square of the forward speed of the airplane, it is clear that at some speed the change in angle of attack due to aileron deflection is equal in magnitude and opposite in sign to the change in angle of attack caused by twist. This speed, at which no change in lift will occur when the ailerons are deflected, is defined as the aileron reversal speed.

NOMENCLATURE

The nomenclature used in this paper follows closely that used in references 2, 4, 5, and 6. (Standard aerodynamic symbols will not be defined here.)

P	= total lift acting on the wing in pounds
M_α	= total aerodynamic torque about the wing elastic axis in pound-feet
a	= distance of wing elastic axis from mid-chord point in terms of the wing half chord (positive when aft of the mid-chord point)
b	= wing half chord in feet
b_T	= wing half chord in feet at theoretic tip
b_R	= wing half chord in feet at root
c	= distance of aileron leading edge from wing mid-chord point in terms of the wing half chord (positive when aft of the mid-chord point)
e	= distance of aileron hinge line from wing mid-chord point in terms of the wing half chord (positive when aft of the mid-chord point)
α	= torsional angular displacement of wing in radians
α_a	= absolute angle of attack of wing in radians
α_T	= torsional angular displacement at tip in radians
$\alpha_T[f_2(y)]$	= torsional angular displacement at y in radians
$\beta = \delta$	= rotation of aileron with respect to wing chord in radians
ω	= flutter frequency in radians per second
L_0	= distance from the centerline of the ship to the wing root in feet
L_1	= distance from the centerline of the ship to the inboard end of the aileron in feet
L_2	= distance from the centerline of the ship to the outboard end of the aileron in feet
L_3	= distance from the centerline of the ship to the wing tip in feet
L	= wing semispan in feet
V	= air speed in feet per second
V_R	= aileron reversal speed in feet per second
m_{V_R}	= the value of m at V_R feet per second
m_{nV_R}	= the value of m at nV_R feet per second
(I.C.)	= inertia couple
(D.M.)	= damping moment
(R.M.)	= rolling moment
I	= moment of inertia in slugs-(feet)^2 of the entire airplane about the axis of roll
ρ	= density of air in slugs per (foot)^3
k	= $d\alpha/d\beta$ = rate of change of angle of attack with change in aileron angle
θ	= roll in radians
t	= time in seconds

T's are defined in reference 2

ϕ's are defined in reference 1

Forces and Moments Acting on the Wing

Theodorsen[2] derived the forces acting on an oscillating airfoil which Loring[3] presented in the following form (slightly rearranged here):

$$\frac{dP}{dy} = -\pi\rho b^3[\omega^2 A_{ch}\left(\frac{h}{b}\right) + \omega^2 A_{c\alpha}\alpha(\alpha) + \omega^2 A_{c\beta}(\beta)] \quad (1)$$

$$\frac{dM_\alpha}{dy} = -\pi\rho b^4[\omega^2 A_{ah}\left(\frac{h}{b}\right) + \omega^2 A_{a\alpha}(\alpha) + \omega^2 A_{a\beta}(\beta)] \quad (2)$$

These expressions can be reduced to nonoscillatory conditions by letting ω approach zero.

$$\left.\begin{aligned} \lim_{\omega\to 0}(\omega^2 A_{ch}) &= \lim_{\omega\to 0}(\omega^2 R_{ch} + \omega^2 I_{ch}) = 0 \\ \lim_{\omega\to 0}(\omega^2 A_{c\alpha}) &= \lim_{\omega\to 0}(\omega^2 R_{c\alpha} + \omega^2 I_{c\alpha}) = 2V^2/b^2 \\ \lim_{\omega\to 0}(\omega^2 A_{c\beta}) &= \lim_{\omega\to 0}(\omega^2 R_{c\beta} + \omega^2 I_{c\beta}) = (2V^2/b^2)(T_{10}/\pi) \end{aligned}\right\} \quad (3)$$

Substituting Eqs. (3) in Eq. (1),

$$\lim_{\omega\to 0}\frac{dP}{dy} = -2\pi\rho V^2\left(b\alpha + b\frac{T_{10}}{\pi}\beta\right) \quad (4a)$$

When appropriate values for c are substituted in T_{10} as defined in reference 2, Eq. (4a) holds for (1) Frise-type ailerons with open gap and (2) internal-pressure balanced ailerons. These two instances will be referred to as Case I.

An equivalent expression for aerodynamically balanced ailerons with sealed gap, referred to as Case II, is obtained (by making use of Küssner's[1] expression for $k\bar{d}$ in place of $k\dot{d}$):

$$\lim_{\omega\to 0}\frac{dP}{dy} = -2\pi\rho V^2\left\{b\alpha + b\left[\frac{T_{10}}{\pi} - \frac{\phi_{13}}{\pi}(e-c)\right]\beta\right\} \quad (4b)$$

(e and c correspond to Küssner's $-\cos\chi_R$ and $-\cos\phi$. $(e-c)$ is the distance between aileron leading edge and hinge, divided by the wing half-chord.)

The rolling moment for the entire airplane can now be written by integrating Eqs. (4) over the half-span, by multiplying them by a factor of 2 to account for both wings, and by including the moment arm y. Thus, for Case I, the rolling moment

$$(\text{R.M.}) = -4\pi\rho V^2\int_{L_0}^{L_3}\left\{by\alpha_T[f_2(y)] + \frac{T_{10}}{\pi}by\beta\right\}dy \quad (5a)$$

and for Case II,

$$(\text{R.M.}) = -4\pi\rho V^2\int_{L_0}^{L_3}\left\{by\alpha_T[f_2(y)] + \left[\frac{T_{10}}{\pi} - \frac{\phi_{13}}{\pi}(e-c)\right]by\beta\right\}dy \quad (5b)$$

An instructive check on the equations for rolling moment can be had by neglecting the wing twist term and writing the expression for the rolling moment due to an aileron deflection β.

$$(\text{R.M.})_{aileron} = -4\pi\rho V^2\beta\left[\frac{T_{10}}{\pi} - \frac{\phi_{13}}{\pi}(e-c)\right]\int_{L_1}^{L_3} by\,dy \quad (6a)$$

Pearson and Jones[5] give the rolling moment due to an aileron deflection δ as

$$L_{aileron} = C_{l_\delta}\delta qSb \quad (6b)$$

In the terminology of this paper Eq. (6b) becomes

$$(\text{R.M.})_{aileron} = -8\frac{C_{l_\delta}}{\left[\frac{T_{10}}{\pi} - \frac{\phi_{13}}{\pi}(e-c)\right]}\times \left[\frac{T_{10}}{\pi} - \frac{\phi_{13}}{\pi}(e-c)\right]\beta q\int_{L_0}^{L_3} b\,dy\int_{L_2}^{L_3} dy \quad (7)$$

and Eq. (6a) becomes

$$(\text{R.M.})_{aileron} = -8\pi q\beta\left[\frac{T_{10}}{\pi} - \frac{\phi_{13}}{\pi}(e-c)\right]\int_{L_1}^{L_3} by\,dy \quad (8)$$

Combining Eqs. (7) and (8)

$$\pi\int_{L_1}^{L_3} by\,dy = \frac{1}{\left[\frac{T_{10}}{\pi} - \frac{\phi_{13}}{\pi}(e-c)\right]}\times \int_{L_1}^{L_3} f(y)\,dy\int_{L_0}^{L_3} b\,dy\int_{L_2}^{L_3} dy \quad (9)$$

where

$$\int_{L_1}^{L_3} f(y)\,dy = \frac{C_{l_\beta}}{\left[\frac{T_{10}}{\pi} - \frac{\phi_{13}}{\pi}(e-c)\right]}$$

But (for a wing of uniform taper and square tips),

$$b = b_T + [(b_R - b_T)/L]y \quad (10)$$

Substituting Eq. (10) in Eq. (9) and integrating, the following relationships are obtained:

$$\frac{[C_{l_\beta}]_{y_1}^{y_2}}{\left[\frac{T_{10}}{\pi} - \frac{\phi_{13}}{\pi}(e-c)\right]} = \frac{\pi}{L^2 b_R}\int_{y_1}^{y_2}(b_T y + \frac{b_R - b_T}{L}y^2)\,dy \quad (11)$$

$$\frac{f(y)}{\left[\frac{T_{10}}{\pi} - \frac{\phi_{13}}{\pi}(e-c)\right]} = \frac{\pi}{L^2 b_R}(b_T y + \frac{b_R - b_T}{L}y^2) \quad (12)$$

$$C_{l_\beta} = \frac{[T_{10} - \phi_{13}(e-c)]}{L^2 b_R}\times \left[\frac{b_T}{2}(L_2^2 - L_1^2) + \frac{b_R - b_T}{3L}(L_2^3 - L_1^3)\right] \quad (13)$$

C_{l_β} was calculated from Eq. (13) for a wing with parameters as follows—$AR = 6$; $b_T = 0.5$, $b_R = 1.0$; $L = 4.5$; $c = .54$—and is shown graphically by the solid curve in Fig. 4. The dotted line in Fig. 4 shows values of C_{l_β} for a similar wing, obtained from Pearson and

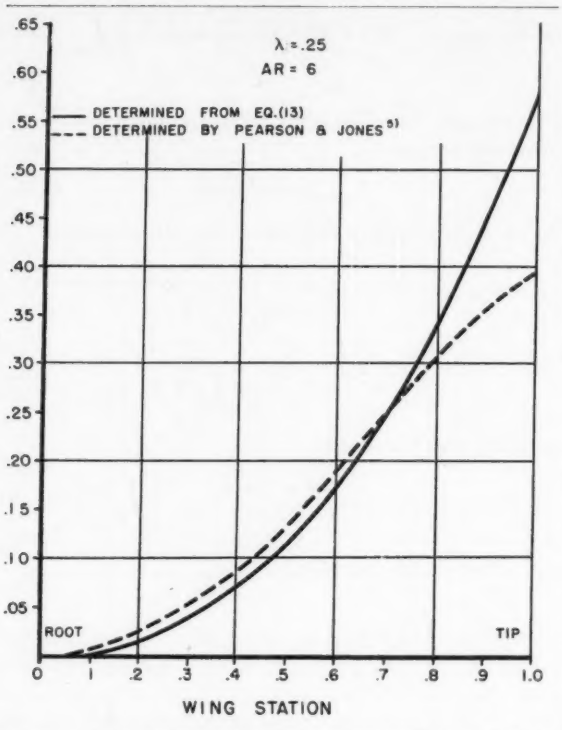

FIG. 4. Rate of change of rolling moment coefficient C_l with aileron angle. (Dotted line gives exact values; solid line is based on two-dimensional flow, straight taper, and square wing tips.)

Jones'[5] paper. Over the inboard 70 per cent of the span, the two curves show fair agreement. Actually, rolling moments due to aileron deflection, computed from the two curves in Fig. 4, show large discrepancies. Assuming the aileron to extend over the entire wing half-span, rolling moments calculated from Eq. (13) are 46 per cent larger than those based on Pearson and Jones' values. Assuming a case more nearly representative of present-day airplanes—namely, an aileron span equal to 50 per cent of the wing half-span—Eq. (13) yields a rolling moment 78 per cent larger than the value based on Pearson and Jones' work.

In determining the stability derivatives, Pearson and Jones took into account nearly all factors known to influence the results. It will, therefore, be assumed that their values are correct and that reference 5 is useful to check the "flutter equations" as applied to computing rolling moments. On the basis of reference 5 it is concluded that rolling moments, calculated on the basis of equations fundamental to flutter theory, are far too large. The straight tapered wing plan form and the square wing tips will account for some of this discrepancy. Of these, the latter has, undoubtedly, the greater effect. However, Hanson[11] has shown that the extreme error in aileron reversal speed, when an elliptical wing is replaced by one with uniform taper and square tips, does not exceed 9 per cent. The fundamental cause for the excessive values obtained from Eq. (13) will be more fully discussed later.

Loss in aileron effectiveness is calculated from a variation of conditions maintaining at the aileron reversal speed. It is, thus, necessary to calculate the aileron reversal speed. Since aileron reversal is caused by aerodynamic torque about the wing elastic axis, given in Eq. (2), this equation will be written for non-oscillatory conditions.

$$\left.\begin{aligned}
&\lim_{\omega\to 0}(\omega^2 A_{ah}) = \lim_{\omega\to 0}(\omega^2 R_{ah} + \omega^2 I_{ah}) = 0 \\
&\lim_{\omega\to 0}(\omega^2 A_{a\alpha}) = \lim_{\omega\to 0}(\omega^2 R_{a\alpha} + \omega^2 I_{a\alpha}) = \\
&\qquad -\frac{2V^2}{b^2}(1/2 + a) \\
&\lim_{\omega\to 0}(\omega^2 A_{a\beta}) = \lim_{\omega\to 0}(\omega^2 R_{a\beta} + \omega^2 I_{a\beta}) = \\
&\qquad 1/2 A_{\beta 3}\frac{2V^2}{b^2} - \frac{T_{10}}{\pi}(1/2 + a) = \\
&\qquad \frac{2V^2}{b^2}\left[\frac{T_4 + T_{10}}{2\pi} - \frac{T_{10}}{\pi}(1/2 + a)\right]
\end{aligned}\right\} \quad (14)$$

Substituting Eqs. (14) in Eq. (2), for Case I,

$$\lim_{\omega\to 0}\frac{dM_a}{dy} = -2\pi\rho V^2 b^2\left\{(1/2 + a)\alpha + \left[\frac{T_4 + T_{10}}{2\pi} - \frac{T_{10}}{\pi}(1/2 + a)\right]\beta\right\}$$

Integrating and proceeding to the limits from L_0 to y,

$$\lim_{\omega\to 0} M_\alpha = -2\pi\rho V^2\int_{L_0}^{y} b^2\left\{(1/2 + a)\alpha_T[f_2(y)] + \left[\frac{T_4 + T_{10}}{2\pi} - \frac{T_{10}}{\pi}(1/2 + a)\right]\beta\right\} dy \quad (15a)$$

By using Küssner's[1] terms $k_{\dot{\alpha}}$ and $m_{\dot{\alpha}}$ for $k_{\dot{\alpha}}^{\circ}$ and $m_{\dot{\alpha}}^{\circ}$ the aerodynamic torque for Case II becomes:

$$\lim_{\omega\to 0} M_\alpha = -2\pi\rho V^2\int_{L_0}^{y} b^2\left\{(1/2 + a)\alpha_T[f_2(y)] + \left[\frac{T_4 + T_{10}}{2\pi} - \frac{T_{10}}{\pi}(1/2 + a) + \frac{\phi_{15}}{2\pi}(e - c) - \frac{\phi_{13}}{\pi}(e - c)(1/2 + a)\right]\beta\right\} dy \quad (15b)$$

As pointed out earlier the twist caused by the aerodynamic torque is resisted by the elastic properties of the wing. Using the coefficient of torsional rigidity C_{TR} as defined in reference 6, the angle of twist at the wing tip

$$\alpha_T = \int_{L_0}^{L_4}(M_a/C_{TR})\,dy \quad (16)$$

and at a distance y from L_0 the angle of twist

$$\alpha_T[f_2(y)] = \int_{L_0}^{y}(M_a/C_{TR})\,dy \quad (17)$$

A method of successive approximations of obtaining $\alpha_T[f_2(y)]$ has been given by Pugsley and Brooke.[7] A much simpler method has been published recently by Shornick of the Matériel Center.[8] These methods are important for an accurate determination of aileron reversal speeds. They will not be discussed here, however, since this paper is primarily concerned with an extension of the case of complete aileron reversal to that of diminution of aileron effectiveness at speeds below the aileron reversal speed.

The angle β for complete aileron reversal is found from the condition that at the aileron reversal speed the rolling moment is equal to zero. The aileron angle β is obtained by solving Eqs. (5) for the rolling moment equal to zero. Expressed in terms of the angle of twist at the tip, the aileron angle is, for Case I,

$$\beta = -1/(T_{10}/\pi)\left\{\int_{L_0}^{L_3} by[f_2(y)]\,dy\right\}\Big/\int_{L_1}^{L_2} by\,dy \quad (18a)$$

(The limits L_1 and L_2 are introduced here since β and, therefore, the aileron term in Eq. (5a) are equal to zero for all values of y except $L_1 \leq y \leq L_2$). For Case II, the aileron angle

$$\beta = -\left[\frac{1}{\dfrac{T_{10} - \phi_{13}(e-c)}{\pi}}\right]\left[\frac{\displaystyle\int_{L_0}^{L_3} by[f_2(y)]dy}{\displaystyle\int_{L_1}^{L_2} by\,dy}\right] \quad (18b)$$

When the appropriate values are inserted into the integral of Eqs. (15) and the upper limit is taken as $y = L_3$, then $V = V_R$ in Eqs. (15a) and (15b) for Case I and Case II, respectively.

Loss in Aileron Effectiveness

On the basis of the previous development the loss in aileron effectiveness due to wing twist can be determined for an air speed nV_R where $0 < n < 1$. (Actually, the following development holds for all positive values of n. However, the above limitation has been placed on n to emphasize the physical aspects of the problem.)

If secondary effects—i.e., side slip and yaw—are neglected, the equation of motion of an airplane in roll can be written as

$$\text{(I.C.)} + \text{(D.M.)} - \text{(R.M.)} = 0 \quad (19a)$$

The inertia couple is given by

$$\text{(I.C.)} = I(d^2\theta/dt^2) \quad (19b)$$

Pearson and Jones[5] give the damping moment as

$$L_{\text{rolling}} = C_{l_p}(pb/2V)qSb \quad (19c)$$

In the terminology of this paper the damping moment

$$\text{(D.M.)} = \text{(d.m.)}(d\theta/dt) \quad (19d)$$

where

$$\text{(d.m.)} = 4C_{l_p}L^2nV_R\rho\int_{L_0}^{L_3} b\,dy$$

C_{l_p} = rate of change of rolling moment coefficient C_l with helix angle (numerical values for C_{l_p} are given in reference 5, page 9)

The aerodynamic torque at the aileron reversal speed is given by Eqs. (15).

If it is assumed that the air speed influences the magnitude of the aerodynamic torque but not the spanwise distribution, then for any value of y

$$\lim_{\omega\to 0}\frac{M_{\alpha_{nV_R}}}{M_{\alpha_{V_R}}} \approx \frac{n^2V_R^2}{V_R^2} = \frac{n^2}{1} \quad (19e)$$

and

$$[f_2(y)]_{nV_R} \approx n^2[f_2(y)]_{V_R} \quad (19f)$$

It can be shown that the exact value of Eq. (19e)—i.e., exact within the limits of Eqs. (15)—is

$$\lim_{\omega\to 0}\frac{M_{\alpha_{nV_R}}}{M_{\alpha_{V_R}}} = \frac{(1/2+a)\left\{\displaystyle\int_{L_0}^{L_3}\frac{b^2W}{\int_{L_0}^{L_3} b\,dy}dy + 2\pi\rho n^4V_R^2\Delta\alpha_T\int_{L_0}^{L_3}[f_2(y)]\,dy\right\} + n^2C}{(1/2+a)\left\{\displaystyle\int_{L_0}^{L_3}\frac{b^2W}{\int_{L_0}^{L_3} b\,dy}dy + 2\pi\rho\, V_R^2\Delta\alpha_T\int_{L_0}^{L_3}[f_2(y)]\,dy\right\} + C} \quad (19g)$$

where for Case I

$$C = \int_{L_1}^{L_3} b^2\left[(1/2+a)\frac{T_{10}}{\pi} - \frac{T_4+T_{10}}{2\pi}\right]\beta\,dy$$

for Case II

$$C = \int_{L_1}^{L_2} b^2\left[(1/2+a)\frac{T_{10}}{\pi} - \frac{T_4+T_{10}}{2\pi} - \frac{\phi_{15}}{2\pi}(e-c) + \frac{\phi_{13}}{\pi}(e-c)(1/2+a)\right]\beta\,dy$$

$\Delta\alpha_T[f_2(y)]$ = aerodynamic twist + structural twist at y

W = weight of airplane

It will be shown later that, when the entire airplane is considered, Eqs. (19e) and (19f) become exact.

From Eqs. (5), (19e), and (19f) it follows that for Case I the rolling moment at an air speed equal to nV_R

$$\text{(R.M.)} = -4\pi\rho n^2V_R^2\left\{n^2\int_{L_0}^{L_3} by[f_2(y)]\,dy + \frac{T_{10}}{\pi}\beta\int_{L_1}^{L_3} by\,dy\right\} \quad (19h)$$

and for Case II

$$(\text{R.M.}) = -4\pi\rho n^2 V_R^2 \left\{ n^2 \int_{L_0}^{L_1} by[f_2(y)]\, dy + \left[\frac{T_{10}}{\pi} - \frac{\phi_{13}}{\pi}(e-c)\right]\beta \int_{L_1}^{L_2} by\, dy \right\} \quad (19i)$$

The three couples, indicated in Eq. (19a), have now been defined, and the differential equation of motion can be written as

$$I\frac{d^2\theta}{dt^2} + (\text{d.m.})\frac{d\theta}{dt} - (\text{R.M.}) = 0 \quad (20)$$

The particular solution for this equation for $\theta = 0$ when $t = 0$ is

$$\theta = \frac{I(\text{R.M.})}{(\text{d.m.})^2}\left[e^{-\frac{(\text{d.m.})}{\text{I}}t} - 1\right] + \frac{(\text{R.M.})}{(\text{d.m.})}t \quad (21)$$

The amount of roll accomplished during the first second in degrees (or radians) per degree (or radian) aileron deflection at nV_R ft. per sec. is

$$\frac{\theta}{\beta} = \frac{IK_1}{\rho n V_R K_2}\left(e^{-(\rho n V_R K_2/I)} - 1\right) + K_1 \quad (22)$$

where

$$K_1 = \frac{(\text{R.M.})}{(\text{d.m.})} = \frac{1}{K_2}4\pi n V_R(n^2K_3 + K_4)$$

$$K_2 = 4C_{l_p}L^2 \int_{L_0}^{L_2} b\, dy$$

$$K_3 = \int_{L_0}^{L_2} by[f_2(y)]\, dy$$

For Case I

$$K_4 = \beta V_R \frac{T_{10}}{\pi}\int_{L_1}^{L_2} by\, dy$$

For Case II

$$K_4 = \beta V_R\left[\frac{T_{10}}{\pi} - \frac{\phi_{13}}{\pi}(e-c)\right]\int_{L_1}^{L_2} by\, dy$$

And βV_R is determined in magnitude and sign from Eqs. (18a) or (18b).

Correction of Rolling Moments

As pointed out earlier, Eq. (22) is expected to give computed rolls that are too large because of excessive rolling moments calculated from Eqs. (5). It will be remembered that the equations for rolling moment were derived from Eqs. (4). Of these latter the equation for Case I will be repeated here.

$$\lim_{\omega\to 0}\frac{dP}{dy} = -2\pi\rho V^2\left(b\alpha + b\frac{T_{10}}{\pi}\beta\right) \quad (4a)$$

Eq. (4a) is obviously the same as (in terms more familiar to the aerodynamicist)

$$\frac{dL}{dy} = \frac{dC_L}{d\alpha}q(c\alpha_a + kc\delta) \quad (23)$$

where $k = d\alpha/d\delta$. The differences in Eqs. (4a) and (23) are:

(1) $dC_L/d\alpha$ in Eq. (23) is replaced by 2π in Eq. (4a).

(2) k in Eq. (23) is replaced by T_{10}/π in Eq. (4a).

(3) The absolute angle of attack α_a in Eq. (23) is replaced by the torsional angular displacement α in Eq. (4a).

The first of these differences amounts to assuming an infinite aspect ratio or two-dimensional flow. The success that flutter theory has enjoyed in predicting critical speeds has demonstrated that in the oscillatory case deviations from two-dimensional flow are not important. An explanation for this fact has been given on the basis that in the oscillatory case the induced velocities from successive free and trailing vortices tend to cancel each other because of opposite signs of successive shed vortices.[10] It seems obvious that this explanation or similar ones cannot be applied to non-oscillatory conditions such as the case on hand and that for the determination of aileron performance the assumption of two-dimensional flow introduces serious errors (although calculated aileron reversal speeds are conservative).

The second one of the differences between Eqs. (4a) and (23) is that Eq. (4a) gives, for $d\alpha/d\delta$, an analytical expression developed for thin wings. Pearson and Jones[5] state that it is better to determine $d\alpha/d\delta$ from an analysis of experimental data than to rely on the theoretic value.

The third difference between Eqs. (4a) and (23) states that in the oscillatory case total lift is replaced by spanwise variation in lift. This is equally true for the present case as the following reasoning will show: (a) Since roll is produced by a spanwise variation in lift, only the spanwise variation in angle of attack can influence roll. (b) The aerodynamic torque is a function of the absolute angle of attack. However, the aerodynamic torque due to the angle of attack is of the same magnitude and in the same direction for both wings. It will, thus, increase the contribution of one aileron and reduce that of the other. Therefore, the net effect of the angle of attack on the aerodynamic torque is seen to be zero. This renders Eqs. (19e) and (19f) entirely correct when integrations are carried out over both wings.

On the basis of the foregoing it is suggested that more nearly true values for computing the loss in aileron effectiveness can be obtained if the following substitutions are made:

(1) In Eqs. (5), (15), (18), and (22), replace 2π by $dC_L/d\alpha$.

(2) In Eqs. (5), (15), (18), and (22), replace T_{10}/π for Case I and $[(T_{10}/\pi) - (\phi_{13}/\pi)(e-c)]$ for Case II by a numerical value of k as computed from wind-tunnel tests.

(3) In Eqs. (15), replace $[(T_4 + T_{10})/2\pi]$ by $[(T_4/2\pi) + (k/2)]$.

It is not expected that the revisions enumerated above will permit accurate calculations of aileron performance because many factors have not been considered. The more important ones are enumerated below:

(1) Yaw and side slip. Rolls in which yaw is not controlled by rudder action will be faster than pure rolls for the following reasons: For the wing with down-aileron, lift, and therefore drag are increased; whereas, for the wing with up-aileron, drag is decreased. The resulting yawing moment is overcome by application of the rudder. Since the center of pressure of the rudder is above the axis of roll, a moment about the axis of roll will be set up which opposes the rolling moment. Thus, theoretic results are expected to show smaller rolling moments than flight test data from maneuvers in which only the ailerons were operated.

(2) Loss in forward speed due to the maneuver. Flight tests are likely to be conducted in that range of air speed in which the rolling velocity increases with speed. Since there is a loss of speed during the maneuver, theoretic values for rolling velocity tend to be high.

(3) Torsional deflection in the aileron. The aileron angle β has been assumed constant over the aileron span. This is an approximation resting on the assumption that either the torque on the aileron about the hinge per unit span does not vary over the aileron span or that the aileron is, torsionally, infinitely stiff. The first of these assumptions is, in general, incorrect and the second is never correct. The assumption of constant aileron angle over the aileron span tends to make calculated values somewhat high when compared with flight tests.

(4) Although the suggested aspect ratio correction is considered better than the assumption of two-dimensional flow, it is not strictly correct. As pointed out earlier, the added lift increment due to a change in angle of attack produces roll. Since this added increment is zero at the centerline of the airplane, as well as at the wing tips, the "dynamic" aspect ratio is expected to be smaller than the geometric aspect ratio. Thus, the applied correction might appear to be too small. On the other hand, it is known that the slope of the lift curve increases with Mach number. This latter phenomenon has not been taken into consideration because (1) beyond the critical speed the slope of the lift curve decreases again and (2) even at its maximum the slope of the lift curve does, probably, not attain a value of 2π.

Conclusions

It is concluded that, in spite of the approximations enumerated above, Eq. (22) as revised in the previous section gives a good account of the facts. This is illustrated in Fig. 5 where the solid line represents a constant times the theoretic values of degrees of roll accomplished during the first second per degree aileron deflection versus true air speed. The values presented by this curve were obtained from Eq. (22), but wind-tunnel data were used for the computation of $dC_L/d\alpha$ and k. The dotted line in Fig. 5 was also obtained from Eq. (22). However, the slope of the lift curve was assumed equal to 2π and theoretic values for $d\alpha/d\beta$ were used. The circles in Fig. 5 indicate flight-test data. These experimental values are the results of rolls combined with sideslip and yaw and were reduced to their present form from values of the helix angle $pb/2V$. All calculated and test values contain a constant of proportionality making the maximum calculated rolling velocity equal to unity.

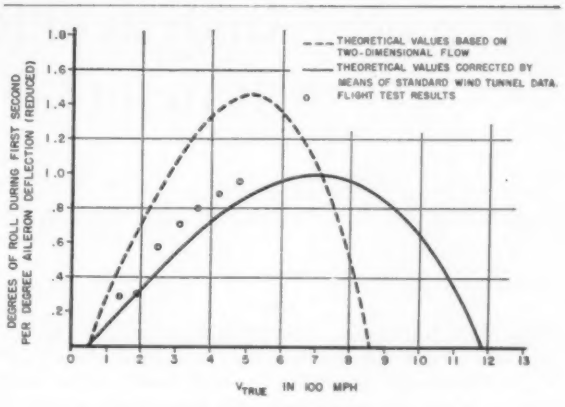

Fig. 5. Aileron effectiveness versus air speed.

It is inherent in the theory of aileron reversal that an aileron that produces, on a given wing, lower rolling velocities than another aileron has the greater aileron reversal speed of the two. Since rolling velocities are related to the speed of aileron reversal, it is felt that low computed reversal speeds should not cause too much concern to the designer unless rolling velocities, computed by the methods outlined in this paper either agree reasonably well with expected rolling velocities or are appreciably lower.

References

[1] Küssner, H. G., and Schwarz, L., *Der schwingende Flügel mit aerodynamisch ausgeglichenem Ruder*, Luftfahrtforschung, Vol. 17, No. 11/12, pp. 337–354, December, 1940.

[2] Theodorsen, T., *General Theory of Aerodynamic Instability and the Mechanism of Flutter*, N.A.C.A. T.R. No. 496, 1935.

[3] Loring, S. J., *General Approach to the Flutter Problem*, S.A.E. Journal, Vol. 49, No. 2, pp. 345–356, August, 1941.

[4] Theodorsen, T., and Garrick, I. E., *Nonstationary Flow About a Wing-Aileron-Tab Combination Including Aerodynamic Balance*, N.A.C.A. Advance Restricted Report, March, 1942.

[5] Pearson, H. A., and Jones, R. T., *Theoretical Stability and Control Characteristics of Wings with Various Amounts of Taper and Twist*, N.A.C.A. T.R. No. 635, 1938.

(*Continued on page 62*)

Graphical Analysis of Response Characteristics of Rate-of-Climb Indicators

KALMAN J. DEJUHASZ*†
The Pennsylvania State College

SUMMARY

The static and dynamic response characteristics of the leak type rate-of-climb indicator have been determined with the aid of graphic analysis, the method has been applied to an actual instrument, and the results have been compared with those of mathematical analysis. Influence of altitude on the calibration coefficient is determined and the effects of compensating means discussed.

INTRODUCTION

THE LEAK-TYPE RATE-OF-CLIMB INDICATOR, schematically shown in Fig. 1, and first proposed in 1910 by Bestelmeier, comprises a thermally insulated chamber communicating with the atmosphere through a small leak opening and fitted with a sensitive pressure gauge on which the difference between the pressure inside the chamber and the atmospheric pressure can be read. When the airplane is in a sustained level flight, then the pressures inside and outside the chamber equalize and the pressure gauge indicates a zero pressure difference. When the airplane is in a sustained climb or dive, then, because of the resistance of the leak opening and the changing atmospheric pressure, equalization does not take place, and the pressure gauge will indicate a pressure difference that is a measure of, and approximately proportional to, the rate of change of altitude. Hence, the pressure gauge can be calibrated in terms of rate-of-climb units.

This simple relationship, however, is complicated by two influences: (a) The factor of proportionality, termed the "calibration coefficient," is not constant but varies with the altitude; (b) when the rate of climb changes from a previous value to a new value, then the new value is not indicated instantaneously but is approached gradually in an asymptotic fashion, which is characterized by the "characteristic time."

The calibration coefficient characterizes the static behavior of the instrument under various conditions of pressure and temperature; the characteristic time characterizes its dynamic behavior under various maneuvering conditions; together these two factors define the response characteristics of the instrument.

Received April 16, 1943.

* Professor of Engineering Research, School of Engineering.

† The author expresses his appreciation to Drs. C. S. Draper, W. G. Brombacher, and D. P. Johnson for their comments and suggestions and to Mr. Alexander Yorgiadis for his care in executing the figures and checking the calculations and for his numerous constructive suggestions.

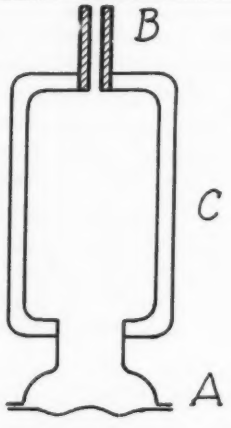

FIG. 1. Schema of rate-of-climb indicator with capillary leak. *A*, diaphragm-type pressure gauge; *B*, capillary leak; *C*, chamber.

The determination of response characteristics of rate-of-climb indicators has been the subject of numerous investigations, both theoretic and experimental.[1, 3, 4, 5] The purpose of the present treatment is to complement and clarify existing knowledge and procedures with the aid of graphic analysis, which has the merits of clarity of visualization of the phenomena and of possibility of application to phenomena not accessible to mathematical analysis.

SYMBOLS, DEFINITIONS, AND UNITS

V_0 = volume of chamber at $\Delta p = 0$, m.³
V = $V_0 + A\,\Delta p$ = volume of chamber + pressure gauge at $\Delta p \neq 0$, m.³
D = area of diaphragm of pressure gauge, m.²
k/D = elastic constant of diaphragm, kg./m.²
A = $D^2/k = dV/d(\Delta p)$ = rate of change of volume per unit change of differential pressure, due to the displacement of diaphragm, kg. m.⁵
C_0 = $V_0/\kappa p_i$ = capacity of chamber at $\Delta p = 0$, m.⁵/kg.
C = $C_0 + A$ = capacity of chamber + pressure gauge, m.⁵/kg.
L = length of capillary leak tube, m.
d = diameter of capillary leak tube, m.
α = $128L/d^4\pi$ = leak coefficient, 1/m.²
η = viscosity of air, kg. sec./m.² (see Fig. 3)
R = $\alpha\eta$ = resistance to flow of capillary leak tube, kg. sec./m.⁵
q = $(p_i - p_a)/R$ = rate of volume flow through capillary leak tube, m.³/sec.
p_i = pressure inside chamber, kg./m.²

p_a = atmospheric pressure outside chamber, kg./m.²
$\Delta p = p_i - p_a$ = differential pressure, kg./m.²
ρ_i = density of air inside chamber, kg. sec.²/m.⁴
ρ_a = density of air outside chamber, kg. sec.²/m.⁴
g = acceleration of gravity = 9.81 m./sec.² = 32.2 ft./sec.²
T_a = absolute temperature of atmosphere, F.
h = altitude, m. or ft.
$v_p = dp_a/dt$ = rate of change of atmospheric pressure, kg./(m.²sec.)
$v_h = dh/dt$ = rate of change of altitude, m./sec. or ft./sec.
K_p = calibration coefficient with respect to v_p
K_h = calibration coefficient with respect to v_h
t = time, sec.
τ = characteristic time, sec.

Assumptions

(a) The treatment is restricted to the pneumatic system alone; inertia and damping effects of the moving mechanical parts, which have only secondary importance, will not be considered.

(b) The change of state of air within the chamber is assumed to be adiabatic. The relation between density change and pressure change is expressed by $d\rho_i/\rho_i = dp_i/(\kappa p_i)$; $\kappa = 1.4$.

(c) The change of state of air outside the chamber, as a function of altitude, is assumed to follow the relations of the U.S. Standard atmosphere as defined by Fig. 3.

(d) The differences between the pressures, densities, and temperatures in the chamber, in the leak, and in the atmosphere are small compared to their absolute values. Hence, quantities such as ρ_i/ρ_a, p_i/p_a, and T_i/T_a are considered as equal to unity, and the error involved is regarded as negligible.

(e) The instrument is sensitive not to the rate of altitude change $dh/dt = v_h$ as such but to the rate of pressure change, $dp_a/dt = v_p$. The two quantities are related by the equation: $v_p = -\rho_a g v_h$.

(f) Two cases will be treated: one with a capillary leak tube characterized by laminar flow according to the relation $q = (1/R)\Delta p$, and the other with a leak orifice characterized by turbulent flow according to the relation $q = \sqrt{2/\rho}\sqrt{\Delta p}$.

Mathematical Analysis

Derivation of the General Equation

The equation of the rate-of-climb indicator is based on the equality of the mass flowing through the leak in dt time with the change of mass inside the chamber, which can be expressed in mathematical form by the equation:

$$q\rho_a dt = d(V\rho_i) = Vd\rho_i + \rho_i dV$$

where flow q into the chamber is considered positive.

Considering that $V = V_0 + A\,\Delta p$, then for a constant rate of change of atmospheric pressure:

$$\Delta p = p_i - p_a = p_i - (p_{a0} + v_p t)$$

and substituting:

$$d\rho_i/\rho_i = dp_i/(\kappa p_i);\quad \rho_i \approx \rho_a\ \ p_i; \approx p_a;\ C_0 = V_0/\kappa p_a;\quad C = C_0 + A$$

the rate of flow can be expressed by

$$q = C(dp_i/dt) - Av_p$$

whence the differential equation of the phenomenon can be written:

$$dp_i/(g + Av_p) = dt/C \qquad (1)$$

According to the relationship $q = f(p_i)$, the solution of the differential equation can take various forms, of which two cases—that of laminar and of turbulent flow—will be treated.

Laminar Flow Through Leak

Assuming a leak in the form of a capillary tube characterized by laminar flow it can be written:

$$-q = (1/R)\Delta p = (1/R)(p_i - p_a) \qquad (2)$$

where $1/R$ can be interpreted as the rate of flow for unit pressure difference. Differentiating according to time:

$$dq/dt = -(1/R)[(dp_i/dt) - v_p]$$

whence

$$(dp_i/dt) = -R(dq/dt) + v_p$$

and substituting this expression and also $C_0 = C - A$ into Eq. (1) the differential equation for laminar flow

$$dq/(C_0 v_p - q) = dt/CR$$

is obtained, the solution of which is

$$q = C_0 v_p(1 - e^{-t/CR})$$

Hence, combining with Eq. (2), the function

$$\Delta p = -C_0 R v_p(1 - e^{-t/CR}) \qquad (3)$$

is obtained, which can be written also in the form

$$\Delta p = -K_p v_p(1 - e^{-(t/\tau)})$$

In this, $K_p = C_0 R = (v_0/\kappa p_a)R$ = calibration coefficient and $\tau = CR = (C_0 + A)R = K_p + AR$ = characteristic time.

It is seen that the value of Δp—i.e., the indication of the instrument—approaches the limiting value $K_p v_p$ as time increases according to an exponential function, while the transient term $K_p v_p e^{-(t/\tau)}$ approaches zero.

For sensitivity of indication the instrument should have a large calibration coefficient K_p, and for rapidity of response it should have a small characteristic time τ. It is seen that the two desiderata are conflicting because both K_p and τ are changed in the same sense by changing C_0, C and R. Therefore in the design of rate-of-climb indicators a compromise is unavoidable in this respect. The elasticity of the diaphragm,

expressed by A, does not contribute to the sensitivity as expressed by K_p but increases the characteristic time τ—i.e., it reduces the rapidity of response.

Particular Case

In the particular case when the change of chamber volume due to the displacement of the diaphragm is considered negligible—i.e., when $A = 0$—the calibration coefficient is equal to the characteristic time

$$K_p = \tau = C_0 R$$

It is of interest to note that this case is analogous with the charging or discharging of an electrical condenser having the capacity C, through an ohmic resistance R, from or against a linearly changing terminal voltage E. Referring to Fig. 2, it can be written:

$$E_c - E = Ri; \quad idt = -CdE_c$$

whence

$$E_c - E = -CR(dE_c/dt)$$

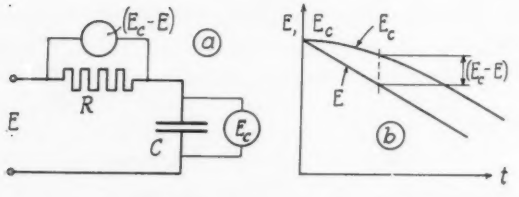

FIG. 2. Electrical analogy. (a) Schema of electric circuit, involving capacity C, ohmic resistance R, and variable terminal voltage E. (b) Diagram of variation of terminal voltage E, and voltage across resistance $(E_c - E)$ as a function of time t.

For $E = E_0 + (dE/dt)t = E_0 + E't$ the solution is:

$$E_c - E = CRE'(1 - e^{-t/RC}) = \tau E'(1 - e^{-t/\tau})$$

Rate of Change of Altitude

Considering that $v_p = -g\rho v_h$, the calibration coefficient relative to the rate of climb can be written:

$$K_h = K_p \rho g = C_0 R \rho g = \frac{V_0 \alpha}{\kappa g} \frac{\rho}{p} \eta$$

For the standard atmosphere $\rho/p^{0.81} = \text{const.}$, and as the viscosity decreases slowly with decreasing temperature T_a (i.e., with increasing altitude, see Fig. 3), the expression

$$\frac{\rho\eta}{p} = \left(\frac{\rho}{p^{0.81}}\right)\left(\frac{\eta}{p^{0.19}}\right) = \text{Const.} \frac{\eta}{p^{0.19}}$$

holds good. As the viscosity change due to decreasing temperature is nearly proportional to the change of $p^{0.19}$, the calibration coefficient K_h is nearly independent of, but slightly increases with, the altitude. This is illustrated in Fig. 4, which refers to an instrument assumed in later examples with data given there.

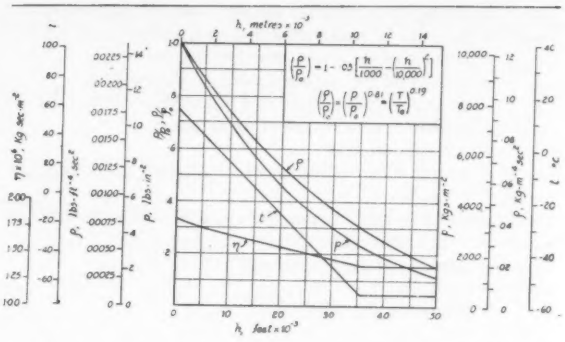

FIG. 3. Data of U.S. Standard atmosphere (N.A.C.A.), based on tables of Warner and Johnson (*Aviation Handbook*, 1st Ed., pp. 181–182, 1931) showing the variation of pressure p, density ρ, temperature t, and air viscosity η, as functions of altitude. Both English and metric scales are given (cf. reference 6).

It is possible to compensate for the increasing tendency of the calibration coefficient by means responsive to pressure or to temperature or both. In the Kollsman instrument[1] this effect is attained by shortening the capillary tube with the aid of a sealed diaphragm cell containing a constant amount of air, which expands when the atmospheric pressure decreases and thus brings about a shortening of the capillary tube, reducing its resistance to flow.

Turbulent Flow Through Leak

Assuming an orifice leak characterized by turbulent flow, the rate of flow as a function of pressure difference can be expressed by the equation

$$q = F\sqrt{2/\rho}\sqrt{-\Delta p} = Q\sqrt{-\Delta p}$$

$Q = F\sqrt{2/\rho}$ can be interpreted as the volume flow at unit pressure difference, and thus it is analogous with

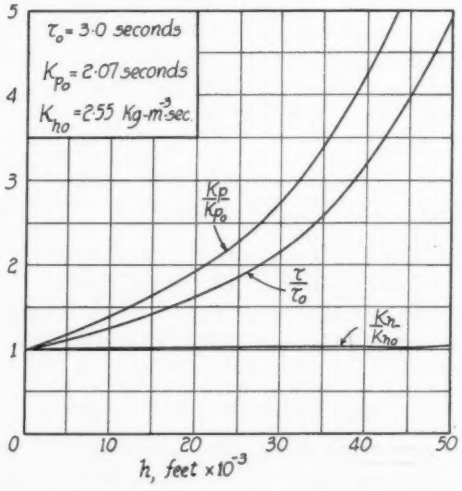

FIG. 4. Effect of altitude on calibration coefficient and characteristic time for rate-of-climb indicator assumed in the paper.

the $1/R$ in the case of laminar flow. Squaring this equation and differentiating:

$$q^2 = -Q^2 \Delta p$$

$$2q(dq/dt) = -Q^2 \left(\frac{dp_i}{dt} - \frac{dp_a}{dt} \right)$$

Combining with Eq. 1, $2q(dq/dt) = (Q^2/C)(C_0 v_p - q)$ and simplifying, the differential equation for turbulent flow is obtained:

$$[q/(C_0 v_p - q)]/dq = (Q^2/2C)dt$$

or

$$\frac{q}{C_0 v_p} + \log \left(1 - \frac{q}{C_0 v_p} \right) = - \frac{Q^2}{2CC_0 v_p} t$$

This is an implicit exponential function which yields for q, as time increases, the limiting value of $\lim q = C_0 v_p$. At $\tau = 2CC_0 v_p / eQ^2$: $q_1 = C_0 v_p [1 - (1/e)]$. The pressure difference corresponding to the limiting value of flow is:

$$\lim \Delta p = \frac{(\lim q)^2}{Q^2} = \frac{C_0^2}{Q^2} v_p^2 = \frac{V_0^2}{2\kappa^2 F^2} \frac{\rho_a}{p^2} v_p^2 = K_p v_p^2 = K_h v_h^2$$

where

$$K_p = (V_0^2/2\kappa^2 F^2)(\rho_a/p^2)$$

and

$$K_h = K_p \rho_a^2 g^2 = \frac{g^2}{2\kappa^2} \frac{V_0^2}{F^2} \frac{\rho_a^3}{p^2}$$

Considering that in the standard atmosphere $\rho_a/p^{0.81} = \text{const.}$ and $\rho_a^3/p^{2.43} = \text{const.}$, therefore with increasing altitude K_p increases proportionally with $p^{-1.19}$ (rapidly), and K_h decreases proportionally with $p^{0.43}$ (slowly).

It is seen that with an orifice leak the indication (Δp) is proportional not with the rate of pressure change (and with the rate of altitude change), as is the case with capillary leak, but with the second power of these quantities. Furthermore, the calibration coefficient K_h decreases with increasing altitude, i.e., exhibits an opposite trend of variation compared with the K_h for the capillary type leak.

These considerations establish the advantage of the capillary leak over the orifice type leak for purposes of rate-of-climb indicators. Nevertheless, the properties of the orifice-type leak are utilized as a means of compensation for variations of altitude, at least in one make of rate-of-climb indicators, in which a leak is used having a flow relationship that is between the laminar and turbulent (porous material), whereby a practical altitude compensation within a wide range of altitude variation is claimed to have been achieved.

Graphic Analysis

For the complete explanation of the graphic method attention is directed to reference 2 dealing with airspeed indicators and to the references listed therein. Briefly stated, it is considered that the phenomenon takes place in successive small time intervals dt, during each of which the state of flow—i.e., volume rate of flow and pressure—are assumed to be interrelated by linear functions—i.e., their changes are proportional. The data valid for a certain time element serve for the determination of the data of the next following time element, and so on, until the whole duration of interest of the phenomenon is covered. The graphic analysis operates with charts involving the pressure p, rate of flow q, time t and location x, in which the states of flow are determined and defined by intersecting straight lines in a manner analogous to the methods of graphic statics.

For the purposes of graphic analysis, the basic differential equation Eq. (1) is rewritten in the following form:

$$dp_i/(q + Av_p) = dt/C = \tan \beta$$

Choosing an arbitrary small time interval dt (which must be small and preferably a fraction such as $^1/_4$ to $^1/_{10}$ of the characteristic time τ), this equation expresses the relation that the change of p_i in the chamber during this interval is proportional to the value of $(q + Av_p)$.

Furthermore, for the capillary leak it can be written:

$$(p_i - p_a)/q = R = \tan \rho$$

which expresses the relation that the differential pressure $(p_i - p_a)$ is proportional to the rate of flow q.

The procedure will be illustrated and explained by an example.

Example

The data of one rate-of-climb indicator previously examined are as follows:

$V_0 = 216.0 \times 10^{-6}\text{m.}^3$, volume of chamber
$A = D^2/k = dV/d(\Delta p) = 66.7 \times 10^{-10}\text{m.}^5/\text{kg.}$, elasticity of pressure gauge
$\alpha = 10^{15}/12.8 = 78.0 \times 10^{12}/\text{m.}^3$, leak coefficient

It is assumed that the airplane is flying at a 5,000-ft. altitude, at which altitude $p_a = 8{,}620$ kg./m.^{2}, and $T = 7°$ C. (see Fig. 3). The viscosity of air is: $\eta = (1.75 \times 10^{-6}/\text{m.}^2)\text{kg. sec.}$ With these values:

$C_0 = V_0/(1.4)(8620) = 179.0 \times 10^{-10}\text{m.}^5/\text{kg.}$
$C = C_0 + A = 245.7 \times 10^{-10}\text{m.}^5/\text{kg.}$
$R = 136.0 \times 10^6$ kg. sec./m.^{5}

It is assumed, furthermore, that after a steady level flight, during which $p_i = p_a$, the airplane instantaneously starts a climb at the rate of 2,000 ft. per min., which corresponds to $v_p = 10.90$ kg./(m.^{2}sec.).

In the q-p chart for the graphic analysis enter the following relations for the leak: $\tan \rho = (136.0 \times 10^6/\text{m.}^5)\text{kg. sec.}$ = directrix for leak. For the chamber, choosing $dt = 1.0$ sec. as the time element:

$$\tan \beta = 10^{10}/245.7 = (40.7 \times 10^6/\text{m.}^5)\text{kg. sec.} = \text{directrix for chamber}$$

$$Av_p = 727.0 \times 10\text{m.}^3/\text{sec.}$$

$$v_p dt = (10.9 \times 1.0/\text{m.}^2)\text{kg.}$$

It is assumed that the total change of altitude is not very great, so that the same values of $\tan \rho$, $\tan \beta$, and v_p are valid for the total phenomenon. The procedure is as follows (see Fig. 5c).

The successive values of p_a valid at the end of the first, third, fifth, and so on, intervals, are marked on the p-axis and from each of these points a flow-directrix $\tan \rho$ is drawn. The value Av_p is marked to the left of the p-axis and a parallel line drawn therewith. The angle β is determined, denoting the slope $\tan \beta$ of the chamber-directrix. The chamber pressure valid at the end of the first interval is found by intersecting the $\tan \rho$ directrix drawn from point $2'$ with the $\tan \beta$ directrix drawn from point 1 on the Av_p = Const. line. The chamber pressure increment at the end of the second interval will be twice (approximately) the previous value as denoted by point 2. The construction is continued to obtain point 3, denoting the flow condition and chamber pressure at the end of the third interval, and point 4, denoting the chamber pressure at the end of the fourth interval. In this manner the successive points 5, 6, 7, ... are found. Entering the p_i values as ordinates on the base of time as abscissa, the history of the chamber pressure $p_i = f(t)$ can be drawn (Fig. 5a). In this also the mathematically determined exponential curve is entered showing a close agreement with the graphically obtained diagram. The approximation can be made closer by choosing a smaller dt time as the basis of construction, though at the cost of an increased amount of labor. Plotting the $\Delta p = (p_i - p_a)$ values over the time base the history of the indication of the rate of climb indicator is obtained (Fig. 5b), upon which also is superimposed the mathematically obtained expression.

When the limiting value $\Delta p = (p_i - p_a)_{max.}$ is attained then $\Delta p = \text{const.}$—i.e., for a given time interval dt it can be written: $dp_i = dp_a$. On this basis the differential pressure corresponding to a given rate of pressure change can be constructed, as shown in Fig. 6, from which:

$$\lim \Delta p = \left(\frac{dp_i}{\tan \beta} - Av_p\right) \tan \rho = \left(\frac{dp_i}{dt} C - Av_p\right) R = C_0 R v_p$$

which is the same value as obtained mathematically.

Fig. 6 shows similar constructions for the Δp corresponding to different altitudes, according to the U.S. Standard atmosphere, showing that Δp (and, hence,

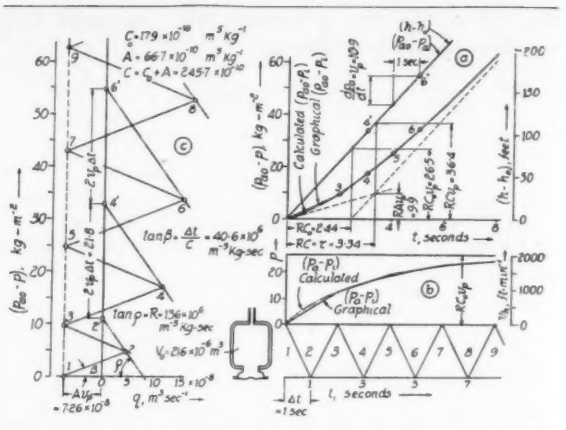

FIG. 5. Graphic analysis of rate-of-climb indicator having capillary leak, assuming a constant rate of change of pressure. (a) History of atmospheric pressure and chamber pressure; (b) history of pressure difference; (c) q-p diagram.

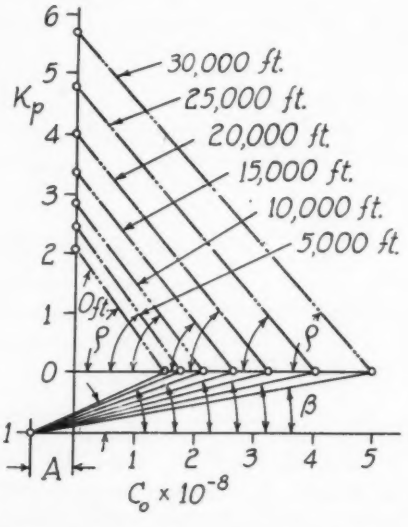

FIG. 6. Effect of altitude on calibration coefficient K_p, for rate-of-climb indicator with capillary leak, assumed in the paper. Note that both $\tan \rho$ and $\tan \beta$ change with altitude.

K_p) increases with increasing altitude. These values are in agreement with mathematically obtained Fig. 4, which in turn is in agreement with the results of Schliestett.[4]

Fig. 7 represents the graphic analysis of the response of the same instrument to a maneuver consisting of a sinusoidal rate of climb, after which the maneuver is stopped and the airplane continues its level flight at a new level (see Fig. 6 of reference 3). This is a comparatively slow maneuver, lasting 16.4 sec., which is about five times the characteristic time of the instrument. The procedure is similar to that described in the previous example. The altitude changes according to a cosine function as shown by the $p_a = f(t)$ line. Choosing an arbitrary dt = 1-sec.

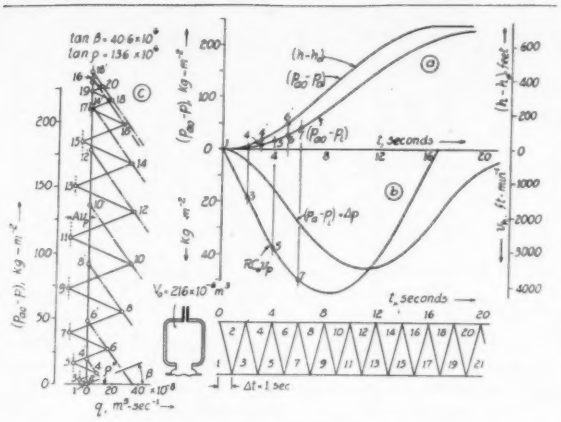

FIG. 7. Graphic analysis of rate-of-climb indicator having capillary leak, assuming a maneuver of slow sinusoidal change of altitude. (a) History of atmospheric pressure and chamber pressure; (b) history of rate of change of atmospheric pressure and of differential pressure; (c) q-p diagram.

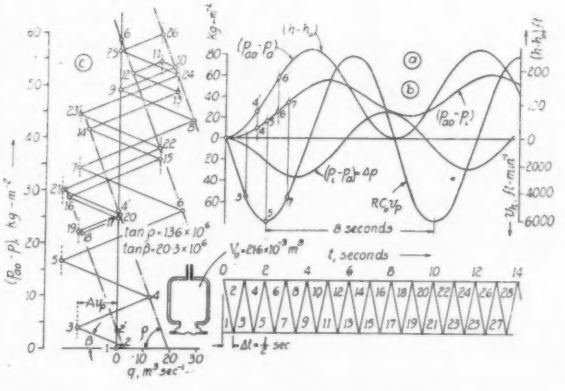

FIG. 8. Graphic analysis of rate-of-climb indicator having capillary leak, assuming a maneuver of rapid sinusoidal change of atmospheric pressure. (a) and (b) History of atmospheric pressure, rate of change of atmospheric pressure, and of pressure difference; (c) q-p diagram.

time interval, the p_a and v_p values are measured off from the time diagram for the successive dt intervals and the p_a and Av_p values are transferred to the q-p diagram. Determining the tan β directrix the points 1, 2, 3, 4, ... are found by intersecting with the tan β directrices the R-lines and Av_p-lines valid for successive dt intervals. The ordinates of the points 1, 2, 3, 4, ... are then transferred to the time diagram whereby the $p_i = f(t)$ function is found. Forming the difference: $p_a - p_i = \Delta p$ the rate of climb, as indicated by the instrument, is obtained.

It is seen that there is a certain error in the indication, both as to magnitude and to phase, as compared with the actual rate of climb. Nevertheless, the sense of indication is correct—i.e., the indications show a climb while the maneuver is in progress. The numerical values found by this graphic analysis are in agreement with those found by Draper and Schliestett mathematically and experimentally.

Fig. 8 is the graphic analysis of another maneuver consisting of rapid changes of rate of climb to descent according to a sinusoidal function (see Fig. 9 of reference 3). The procedure is similar to that used in the previous example, except that a $dt = 0.5$ sec. is chosen in view of the rapidity of the maneuver (duration of change from maximum climb to maximum descent = 4 sec.). In this case the error is considerable, both in magnitude and in phase, and even the sense of the indication is incorrect, the maximum rate of climb being indicated when the airplane is already in descent. The graphically obtained results show a substantial agreement with those found by Draper and Schliestett both mathematically and experimentally.

These examples were chosen deliberately from previous literature with the purpose of comparison of the different methods. The graphic method can be applied to any other type of assumed maneuver, which need not be defined by a mathematical expression but only by a graphic $p_a = f(t)$ curve.

Orifice Leak

The graphic analysis of a rate-of-climb indicator having an orifice leak is performed identically with that having a capillary leak, except that a parabolic flow characteristic $q = F\sqrt{2/\rho_a}\sqrt{\Delta p}$ is used instead of the straight line characteristic in the latter case. The procedure is illustrated in Fig. 9, in which the data are identical to those used in Fig. 5 except that an orifice having $F = 0.008$ mm.^{2} effective area is assumed. It is assumed that the maneuver involves an altitude change not too great, so that the parabolas have been constructed on the basis of constant air density ρ_a. But this is not a necessary limitation, and, if the altitude change is great, then the parabolas can be constructed on the basis of the true, variable, air density, corresponding to the varying altitudes.

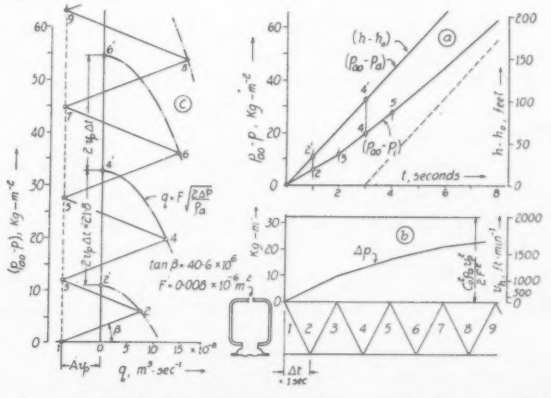

FIG. 9. Graphic analysis of rate-of-climb indicator having orifice leak, assuming a constant rate of change of atmospheric pressure. (a) History of atmospheric pressure and chamber pressure; (b) history of pressure difference; (c) q-p diagram.

The construction is not restricted even to a parabolic interrelationship between the rate of flow q and the differential pressure Δp, but any other experimentally determined relationship can be used which can be expressed by a $q = f(\Delta p)$ curve.

The calibration coefficient K_p as a function of altitude is illustrated on Fig. 10 for the orifice leak (to be compared with Fig. 6 for the capillary leak). It is seen that the orifice leak involves far greater dependency on the altitude than does the capillary leak, which has been shown also by the previous mathematical analysis.

Conclusions

Wherever both the mathematical and graphic analyses are applicable, these yield results in agreement with each other. This should be expected, since both methods are based on the same physical relationships and differential equations. The two methods usefully complement each other: the mathematical analysis yields more general answers to broad questions such as the dependence of the calibration coefficient and characteristic time on the altitude, but it is applicable only to such specific cases which are expressible by mathematical functions; the graphic analysis is applicable to any specific problem provided the conditions and interrelationships can be expressed in graphically stated functions.

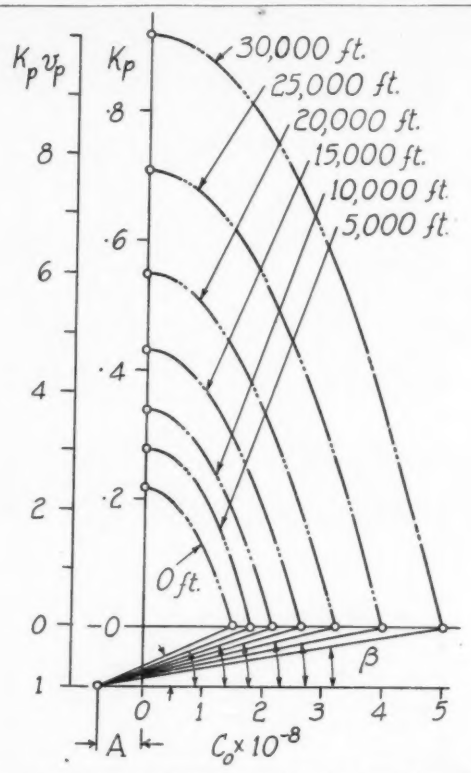

Fig. 10. Effect of altitude on calibration coefficient K_p for rate-of-climb indicator having orifice leak, assumed in paper. Note that both the parabolas and the tan β change with altitude.

References

[1] Johnson, Daniel P., *Aircraft Rate-of-Climb Indicators*, N.A.C.A. Report No. 666, 1939. Bibliography contains references to previous work, including that of the originator, A. Bestelmeyer (1910), A. H. Mears, W. S. Diehl, W. G. Brombacher, W. Oppelt and F. Wenk, and others.

[2] DeJuhasz, K. J., *Graphical Analysis of Delay of Response in Air-Speed Indicators*, Journal of the Aeronautical Sciences, Vol. 10, No. 3, pp. 91–97, March, 1943.

[3] Draper, C. S., and Schliestett, G. V., *Dynamic Errors of the Rate-of-Climb Meter*, Journal of the Aeronautical Sciences, Vol. 5, No. 11, pp. 426–430, September, 1938.

[4] Schliestett, G. V., *Altitude Effects on an Uncompensated Rate-of-Climb Meter*, Journal of the Aeronautical Sciences, Vol. 6, No. 8, pp. 323–328, June, 1939.

[5] Brombacher, W. G., *Measurement of Altitude in Blind Flying*, N.A.C.A. T.N. No. 503, August, 1934.

[6] Pankhurst, A. C., and Conn, J. F. C., *Physical Properties of the Standard Atmosphere*, N.A.C.A. T.M. No. 1891, November, 1942.

Take-Off Distance of a Glider Train

WIESLAW Z. STEPNIEWSKI*
De Havilland Aircraft of Canada

SUMMARY

The take-off distance of a glider train is one of the most important factors in the consideration of the practical use of this kind of transport for military and perhaps future civil uses.

Some simple formulas are given in this paper, for the approximate value of the take-off distance necessary to clear an obstacle of a given altitude (50 ft.). However, when preliminary considerations are being made, there are often no complete data regarding the engine-propeller group. For this case a rough but simple method is established allowing the reader to estimate all the necessary characteristics. The primary considerations are for a glider train, in general, but the final formulas are established rather for the large transport gliders towed by planes equipped with constant-speed propellers.

It is sometimes important to know whether it is better to overload an existing plane to some possible limit or to put this additional load into a glider towed by the airplane. For this reason an example is presented which gives the ratio of the take-off distance of an overloaded plane of the DC-3 class to the take-off distance when the plane has its normal weight. A similar comparison is made for the glider train, supposing that the additional load is put into a glider towed by this plane having its normal weight. The comparison assumes that the empty weight of a transport glider plus the weight of its crew will be approximately 40 to 45 per cent of its total weight. In other words, it is understood that about 60 to 55 per cent of the gross weight of such a glider may be considered as pay load.

INTRODUCTION

THE COMPLETE TAKE-OFF of a glider train may be divided into several periods analogous, to some extent, to take-off periods usually considered for an airplane:

Period "a." This is the ground run, when the masses of both the towing plane and glider are accelerated up to a speed sufficient for the glider† to take off.

Period "a_1." This is a period corresponding to a further acceleration of the train as a whole at the instant the glider becomes air-borne (transition period for the glider).

Period "b." This is from the moment when the glider starts to fly at some constant level up to the time when the train attains a speed sufficient to take off the airplane.

Period "b_1." This is a transition period of the towing plane.

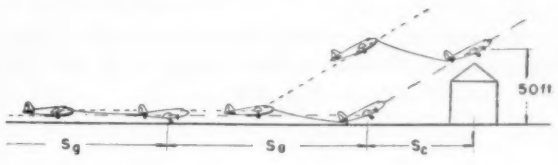

FIG. 1.

Period "c." This corresponds to the steady climb of the whole train, up to an altitude sufficient to clear an obstacle of a given height.

From the periods listed above, the run on the ground (period "a") and the steady climb (period "c") present no special difficulty for an analytical investigation. A more complicated stage is the so-called "transition period." In the case of airplanes this problem attracted the attention of many investigators, and there exist a number of papers dealing with it.[1,2,3] But in the case of the take-off of a glider train, it seems allowable to simplify the problem by omitting consideration of the transition phase of the glider and the towing plane.

Such simplification may be justified by the following: Since the train attains a speed sufficient to take off the glider, the proper maneuver of the take-off itself is usually executed gently; hence, the vertical acceleration is small and may be neglected. In other words, in this phase the lift may be considered as equal to the gross weight of the glider and the take-off speed may be considered as exceeding by some small percentage the stalling speed of glider with flaps in the take-off position.

After a climb up to some feet from the ground, the pilot keeps the glider at the same level, which may be considered as practically identical with the level of the towing machine‡ (Fig. 1).

The take-off of the towing machine is also performed gently, and the so-called "zoom take-off" has no place here. It seems quite reasonable to assume that at the end of period "b," when the whole train attains a speed exceeding by some percentage the stalling speed of the plane with flaps in the take-off position, the towing machine starts a steady climb at this speed. By such

Received February 11, 1943.

* Design Engineer in charge of Structures Division.

† Strictly stated it should be: "up to a speed sufficient to take off that component of the train which has a lower take-off velocity." But in most practical cases, the glider usually has a lower take-off speed, and in the analysis only such a case will be considered.

‡ Theoretically, there may be considered also another type of take-off: Immediately the glider leaves the ground, it climbs very steeply, and while doing so exerts some lift to the towing plane through the towing cable. But in the case of transports and even sport gliders, such a procedure seems to be not advisable.

an assumption, the height gained because of the higher speed of flight than actually needed for the take-off, as well as the energy accumulated in the deflected undercarriage, etc., may be neglected. In assuming this, in subsequent analytical considerations no attention will be paid to "the transition phase" of the towing airplane. We will therefore consider only periods "a" and "b" up to the beginning of steady climb of the whole train.

In period "c," the towing plane is assumed to climb together with the towed glider, which is at the same level as the towing machine (Fig. 1).

NOTATIONS

C_L	= lift coefficient
C_D	= drag coefficient
A.R.	= aspect ratio
W	= weight (lbs.); *without subscript*—of the whole train; *with subscript*—of the glider or plane
S	= wing area (sq.ft.)
P	= engine power (b.hp.) of one engine
P_t	= engine power (b.hp.) of the whole airplane
V	= air speed (ft. per sec.)
D	= propeller diameter (ft.)
n	= propeller speed (r.p.s.)
$J = V/nD$	= advance ratio
η	= propeller efficiency
T	= thrust (lbs.)
T_e	= effective thrust (lbs.)
φ	= angle of climb
μ	= ground friction coefficient
s	= take-off distance (ft.)
ρ	= air density (slugs)
g	= acceleration of gravity (32.17 ft. per sec.^{2})
p	= wing loading (lbs. per sq.ft.)
t	= time (sec.)
g	= glider (subscript)
a	= airplane (subscript)
t	= take-off (subscript)
e	= climb (subscript)

BASIC FORMULAS

In order to facilitate the discussion of the particular phases of take-off, the relation between C_D and C_L should be expressed by the most simple analytical expression. For this purpose the polar diagrams of the towing plane and glider are replaced by the parabolas of the induced drag displaced to the right by the quantity $C_{D_{min.}}$ (Fig. 2).

The equation of this parabola will therefore be:

$$C_D = C_{D_{min.}} + (C_L^2/\pi A) \tag{1}$$

The parabola expressed by Eq. (1) constitutes the first approximation, but even for the take-off consideration, when for higher values of C_L the difference between the real polar diagram and its substitute is greater, the relations resulting from Eq. (1) will be sufficiently accurate.

Period "a"

The general equation of motion of a glider train during the run on the ground will be as follows:

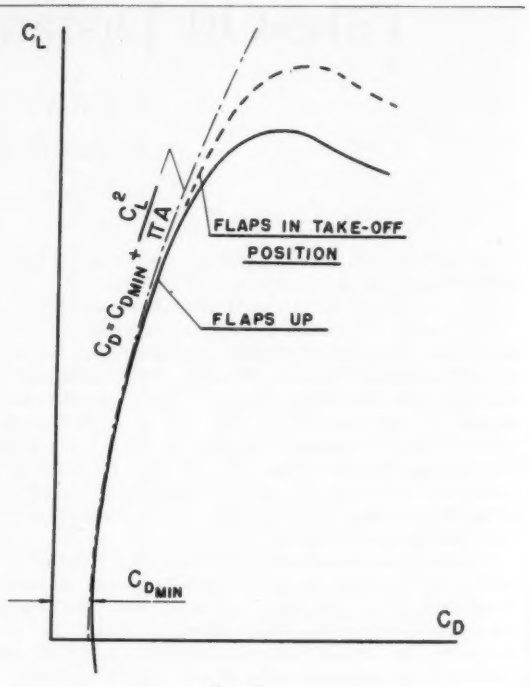

FIG. 2.

$$\frac{W}{g}\frac{dV}{dt} = T - \left[C_{Da}S_a\frac{\rho}{2}V^2 + \left(W_a - C_{Lta}S_a\frac{\rho}{2}V^2\right)\mu + C_{Dg}S_g\frac{\rho}{2}V^2 + \left(W_g - C_{Ltg}S_g\frac{\rho}{2}V^2\right)\mu\right] \tag{2}$$

As the greatest possible acceleration is desired at this stage of the take-off, the bracketed expression should be kept as small as possible. By finding the minimum of this quantity, it is easy to find C_{Lta} and C_{Ltg} corresponding to the shortest run on the ground.

Considering C_D according to Eq. (1) and taking $\partial/\partial C_{Lg} = 0$ and $\partial/\partial C_{La} = 0$ of the bracketed expression, the optimum value of C_L for the glider will be:

$$C_{Ltg} = (1/2)\pi\mu A_g \tag{3a}$$

and for the towing airplane:

$$C_{Lta} = (1/2)\pi\mu A_a \tag{3b}$$

If the wing aspect ratio and the friction coefficient are increased, C_L at the take-off should also be increased.*

Assuming that both glider and airplane are kept, during period "a," in a position providing an angle of incidence corresponding to C_{Lt} given by Eqs. (3a) and

* There may arise some doubt whether the higher values of C_{Lt} found from Eqs. (3a) and (3b) will lie within the limits of good conformity of the substituted parabola to Eq. (1) with the real polar diagram of a plane or glider. But in considering that the friction coefficient will practically not be higher than $\mu = 0.08$ (soft turf[4]) and the aspect ratio of today's transport glider and airplane is seldom greater than 10, C_{Lt} should be not higher than 1.25 which is within the mentioned limits.

(3b), then the effective force T_e accelerating the train in each instance of period "a" will be as follows:

$$T_e = T - [(B_a S_a + B_g S_g)_2 V^2 + W\mu] \quad (4)$$

where the symbols B denote:

$$B_a = C_{Dmin.a} - (1/4)A_a\mu^2 \quad (5a)$$

$$B_g = C_{Dmin.g} - (1/4)A_g\mu^2 \quad (5b)$$

Considering next that $dt = ds/V$, Eq. (2) may be written as

$$ds = (WV/gT_e)dV$$

The distance run on the ground up to the moment when the train will attain a speed, V_g, practically sufficient to take off the glider will be:

$$s_g = \int_{V=0}^{V=V_g} (WV/gT_e)dV \quad (6)$$

Period "b"

During period "b" when the glider is already in the air flying horizontally a few feet off the ground and the towing plane is still running on the ground, the force acting in the towing rope may be considered as equal to the horizontal thrust necessary to keep the glider in a level flight. This force may be expressed as:

$$H_g = W_g(C_{Dg}/C_{Lg})$$

In substituting Eq. (1) for C_{Dg} and considering that in horizontal flight $C_L = (W/S)(2/\rho)(1/V^2)$, the last equation will be expressed as:

$$H_g = \left[C_{Dmin.g} + \frac{1}{\pi A_g}\left(\frac{W_g}{S_g}\frac{2}{\rho}\frac{1}{V^2}\right)^2\right]\frac{S_g\rho V^2}{2}$$

The effective accelerating force T_e for the whole train in each instance of period "b" will be as follows:

$$T_{eb} = T - \left\{B_a S_a + \left[C_{Dmin.g} + \frac{1}{\pi A_g}\left(\frac{W_g}{S_g}\frac{2}{\rho}\frac{1}{V^2}\right)^2\right]S_g\right\}\times \frac{\rho}{2}V^2 - W_a\mu \quad (7)$$

hence,

$$ds = (WV/gT_{eb})dV$$

The distance run on the ground in period "b" during an increase of the train velocity from take-off speed of the glider, V_g, to take-off speed of the airplane, V_a, will be:

$$s_a = \int_{V=V_g}^{V=V_a} (WV/gT_{eb})dV \quad (8)$$

Period "c"

According to the simplified scheme previously established for the take-off of the train when it has reached a speed, V_a, practically sufficient to get the plane into the air, the whole train begins a steady climb up to an altitude sufficient to clear an obstacle of given height. The length of the horizontal projection s_c of the path to be followed until this altitude will be reached may be found in the following way:

The condition of equilibrium of the forces acting on the glider may be expressed as follows (Fig. 3):

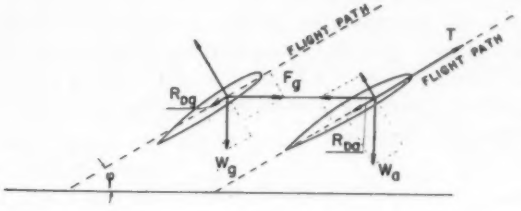

FIG. 3.

$$F_g \cos\varphi = R_{Dg} + W_g \sin\varphi \quad (9a)$$

and for the towing airplane:

$$T = R_{Da} + F\cos\varphi + W_a \sin\varphi \quad (9b)$$

Finding F_g from Eq. (9a), introducing it into Eq. (9b), and remembering, in addition, that $R_{Da} = W_a(C_{Da}/C_{La})$ and $R_{Dg} = W_g(C_{Dg}/C_{Lg})$, it is easy to express sin φ as follows:

$$\sin\varphi = \left[T - \left(W_g\frac{C_{Dgc}}{C_{Lgc}} + W_a\frac{C_{Dac}}{C_{Lac}}\right)\right]\Big/ W \quad (10)$$

where the new symbols C_{Dgc}, C_{Dga}, C_{Lgc}, and C_{Lga} denote drag and lift coefficients during climb.

For most practical cases the values of φ will be rather small; hence, it may be assumed that tan φ = sin φ.* The horizontal projection s_c of the flying path to be flown before an altitude h will be reached will therefore be:

$$s_c = h\left\{W/\left[T - \left(W_g\frac{C_{Dgc}}{C_{Lgc}} + W_a\frac{C_{Dac}}{C_{Lac}}\right)\right]\right\} \quad (11a)$$

when the aerodynamic characteristics of the towing plane and glider are known, it is not difficult to find for both elements of the train C_D/C_L corresponding to a given flight speed. But, in preliminary considerations when it is sometimes necessary to operate with some known or only estimated parameters as $C_{Dmin.}$, A, etc., another formula for s_c may be more useful:

$$s_c = h\left(\frac{W}{T - \left\{\left[C_{Dmin.a} + \frac{1}{\pi A_a}\left(\frac{W_a}{S_a}\frac{2}{\rho}\frac{1}{V_a^2}\right)^2\right]S_a + \left[C_{Dmin.g} + \frac{1}{\pi A_g}\left(\frac{W_g}{S_g}\frac{2}{\rho}\frac{1}{V_a^2}\right)^2\right]S_g\right\}\frac{\rho V_a^2}{2}}\right) \quad (11b)$$

* For $\varphi = 12°$ (slope about 1:4.7) the difference between tan and sin is only about 2.2 per cent.

The total distance for a take-off to clear an obstacle h feet high is

$$s = s_g + s_a + s_c$$

When all the necessary characteristics of the propeller and engine are known, as well as the aerodynamic data of the glider and airplane, it is possible in each instant of the run on the ground to calculate the effective accelerating force according to Eqs. (4) and (7), and next find the distances s_g and s_a by a graphic integration[11] of Eqs. (6) and (8), or by using other methods established for airplanes as given on page 738 of reference 5. For practical use it seems advisable to have some approximate formulas for finding s_g and s_a by simple calculations. For the above purposes some analytical relations giving $\eta = f(V)$ or $T = f(V)$ should first be established, and all possible simplifications should be thoroughly discussed.

Approximate Formulas

Propeller Diameter

To calculate propeller thrust it is necessary to know, in addition to other factors, such values as propeller diameter, D; its efficiency, η, r.p.m., N, or r.p.s., n; and b.hp. of the engine, P. It is easy to find the last two items in any technical description of the engine. But it may sometimes be difficult to find exact data regarding the propeller diameter, and it will be necessary to make an approximate estimation. For this purpose the diagram given on Fig. 4 should be useful. This diagram, based on the N.A.C.A. data[6, 7] for several two-, three-, and four-blade variable-pitch propellers, gives the average values of the best advance ratio V/nD plotted against the coefficient

$$c_s = [0.638 \text{ m.p.h. } (\rho/\rho_0)^{1/5}/[(\text{b.hp.})^{1/5}(\text{r.p.m.})^{2/5}]$$

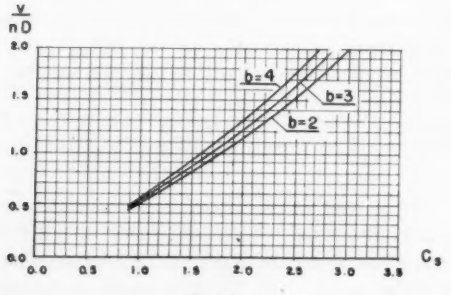

FIG. 4.

The procedure for finding the propeller diameter with the help of Fig. 4 is simple: Knowing the maximum or cruising speed of an airplane at some definite altitude and having the maximum or cruising power of the engine, as well as r.p.m. of the propeller, it is easy to calculate c_s. Knowing the number of propeller blades, one finds from Fig. 4 the optimum value $(V/nD)_{opt.}$ from which the propeller diameter may be found:

$$D = \text{m.p.h. } 88/\text{r.p.m.}(V/nD)_{opt.}$$

where m.p.h. denotes the same speed that was used to calculate c_s.

Since Fig. 4 represents an average of the modern multiposition or constant-speed propellers, the diameter found with its help and on the basis of a normal technical description of the airplane (performance) and engine (b.hp., r.p.m.) will probably not differ to any considerable extent from the diameter of the propeller actually used on the airplane.*

Thrust

Thrust T, in pounds, of any propeller can be expressed as:

$$T = 550\eta P/V \tag{12}$$

where V is in ft. per sec. and P is in b.hp. The propeller efficiency η is usually found from wind-tunnel tests and is presented as a function of the advance ratio V/nD, which will be denoted by the symbol J. There is no general relation between η and J which could be easily expressed by an equation based on the physical relations existing between those two quantities. Nevertheless, for the take-off condition it seems to be possible to substitute for $\eta = f(J)$ one of the following general equations:

$$\eta = J(a - bJ) \tag{13a}$$

or

$$\eta = J(a - b_1J^2) \tag{13b}$$

In both of these equations, the coefficient a should be equal to $d\eta/dJ$ when $J = 0$. In other words, a is a value of the slope of the tangent to the curve $\eta = f(J)$ at the origin of the coordinates. The coefficients b and b_1 may be expressed by $b = a^2/4\eta_{max.}$ and $b_1 = 0.148\ (a^3/\eta_{max.}^2)$; but sometimes some small deviations may be needed from the above values of a, b, and b_1 in order to approximate more closely a real curve $\eta = f(J)$.

In general, Eq. (13a) will probably give a better approximation of the whole curve $\eta = f(J)$, but it leads to more complicated formulas for s_g and s_a. Eq. (13b) gives simpler final formulas but does not approximate as well as Eq. (13a), a real value $\eta = f(J)$, especially for the higher J values. Nevertheless, in a case where at the end of the take-off (climb) J does not exceed the limits of a good approximation for a real $\eta = f(J)$ by Eq. (13b), it seems to be advisable to use this equation.

For constant-speed propellers, where throughout the whole take-off both P and n are constant, it is not difficult to express thrust T as a function of air speed V when $\eta = f(J)$ is known. Introducing Eqs. (13a) or (13b) into Eq. (12) and remembering that $J = V/nD$,

* Propeller diameter may also be evaluated by using empirical formulas that are sometimes given in official publications or in textbooks (see page 478, reference 8).

the total thrust of the towing plane will be expressed as:

$$T = T_0 - 550[bP_t/(nD)^2]V \qquad (14a)$$

or

$$T = T_0 - 550[b_1P_t/(nD)^2]V^2 \qquad (14b)$$

where in the both equations P_t denotes the total power of all airplane engines and T_0 is the total static thrust (sum of the static thrusts of the particular airplane engines) which may be expressed as:

$$T_0 = 550(aP_t/nD) \qquad (15)$$

$\eta = f(J)$ is shown as a continuous line on Fig. 5. This may be considered as quite typical for constant-speed propellers installed on modern transport planes such as the Douglas DC-3 or the Curtiss Commando. The graph mentioned above is drawn as an average of propeller efficiency for two-, three-, and even four-blade propellers, representing groups of modern propellers tested by the N.A.C.A.[6, 7] The values of the power coefficient C_p for which the curve $\eta = f(J)$ was established were chosen as an average for the modern transport machines. On Fig. 5 are also drawn two approximating curves: one based on $\eta = J(2.05 - 1.3J)$, corresponding to Eq. (13a); another based on $\eta = J(1.95 - 2.2J^2)$, corresponding to Eq. (13b). Fig. 5 will show that for $0 \leqslant J \leqslant 0.54$ both equations approximate quite well the function $\eta = f(J)$, which is assumed to be a real one. Within the mentioned limits of J, the difference in values of η given by the approximating functions from the real $\eta = f(J)$ does not exceed 4 per cent. For $J > 0.54$, approximation by formula (13b) is not accurate, and only formulas based on Eq. (13a) should be considered.

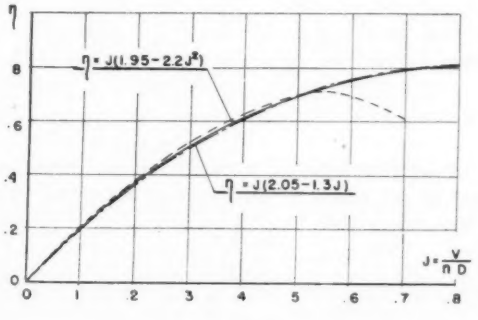

FIG. 5.

Run on the Ground

To calculate the distance run on the ground during the period "a," the formulas based on Eq. (13b) may be used. The thrust will then be found from Eqs. (12) and (13b) and the values given in Fig. 5

$$T = T_0 - 1{,}210[P_t/(nD)^2]V^2$$

where $T_0 = 1{,}072.5(P_t/nD)$.

Integration of Eq. (6) will result in finding the distance of the run on the ground up to the moment of the take-off of the glider. This distance s_g (in feet) will be:

$$s_g = 0.0358(W/c)\log_{10}[T_{c0}/(T_{c0} - cV_g^2)] \qquad (16a)$$

where the symbols c and T_{c0} denote:

$$c = (B_aS_a + B_gS_g)(\rho/2) + 1{,}210[P_t/(nD)^2]$$

and

$$T_{c0} = T_0 - W\mu$$

In Eq. (16a) V_g is expressed in ft. per sec. and should be taken about 5 to 7 per cent higher than the stalling speed of the glider with its flaps in the take-off position.

For the average values of μ ($\mu = 0.05$–0.06), a reasonable $C_{Dmin.}$, and aspect ratio for today's transport gliders and planes ($C_{Dmin.} = 0.022$–0.028; $A = 9$–12), B_a and B_g may be considered as equal or almost equal to 0. Hence, $B_aS_a(\rho/2)$ and $B_gS_g(\rho/2)$ may be considered as negligibly small, and they may be omitted in the formula for s_g. Under such assumptions Eq. (16a) is simplified to the following form:

$$s_g = 0.0358\frac{W(nD)^2}{1{,}210P_t} \times \log_{10}\frac{T_{c0}}{T_{c0} - 1{,}210[(P_t/(nD)^2]V_g^2} \qquad (16b)$$

During the period "b" when the glider is already in the air, its drag offered is equal to $W_g(C_{Dg}/C_{Lg})_b$. But in considering the substitution of a parabola (Eq. (1)) for the relationship between C_D and C_L the drag may be represented in a form dependent on the flight speed:

$$W_g\left(\frac{C_{Dg}}{C_{Lg}}\right)_b = W_g\left[C_{Dmin.g}\left(\frac{\rho}{2}\right)\left(\frac{V^2}{p_g}\right) + p_g\left(\frac{2}{\pi A_g\rho V^2}\right)\right] \qquad (17)$$

In order to simplify the final formulas for s_a, it is permissible to assume $(C_{Dg}/C_{Lg})_b = \text{Const.}$ during the whole of period "b." Such a simplification is justified in the first place by the fact that for the average transport gliders, the difference between $(C_{Dg}/C_{Lg})_b$ at V_g and at V_a will not exceed some 15 to 20 per cent,* even considering the take-off speed of the towing plane V_a to be 50 per cent higher than that of the glider. Second, since the drag offered by the glider in flight is only one of the forces tending to decrease the effective thrust, the above assumption of $(C_{Dg}/C_{Lg})_b = \text{Const.}$ during period "b" will result in a possible inaccuracy not exceeding a small percentage.

* For a glider with the following characteristics: $C_{Dmin.g} = 0.024$, $A_g = 10$, $p_g = 13$ lbs. per sq.ft., and practical take-off speed $V_g = 50$ m.p.h., C_{Dg}/C_{Lg} at this speed will be about 0.067. At a speed 50 per cent higher it will be equal to about 0.055.

In practice, it seems to be more advisable to take a higher value of $(C_{Dg}/C_{Lg})_b$—i.e., that corresponding to the lower speed (V_g).

When the preliminary calculations are being made (and no exact values of C_{Dg} and C_{Lg} are available), $W(C_{Dg}/C_{Lg})_b$ may be calculated on the basis of the general construction parameters as $C_{Dmin\cdot g}$, A_g, and p_g.

If even at the end of period "b" the value of advance ratio J does not exceed $J = 0.54$ (the limit value for the substitution of so-called real $\eta = f(J)$ by Eq. (13b) then the distance (in feet) corresponding to this phase of the take-off will be expressed (after integration of Eq. (8) and in considering all the simplification) as:

$$s_a = 0.0358 \frac{W}{c_b} \log_{10} \frac{T_{0b} - c_b V_g^2}{T_{0b} - c_b V_a^2} \tag{18}$$

where

$$c_b = \left[\frac{1{,}210 P_t}{(nD)^3} + B_a S_a \frac{\rho}{2} \right]$$

and

$$T_{0b} = T_0 - W_g \left(\frac{C_{Dg}}{C_{Lg}} \right)_b - \mu W_a$$

For preliminary calculations it may be assumed that $W_g(C_{Dg}/C_{Lg}) = \mu W_g$. Assuming next, analogous to previous considerations, that $B_a = 0$, it is easy to obtain an approximate formula (similar to Eq. (16b)) which gives roughly the total distance from the beginning of the take-off up to the moment when the towing plane becomes air-borne:

$$s_{g,\,a} = 0.0358 \frac{W(nD)^3}{1{,}210 P_t} \log_{10} \frac{T_{e0}}{T_{e0} - 1{,}210 \dfrac{P_t}{(nD)^3} V_a^2} \tag{19}$$

V_a in this last formula, as well as in Eq. (18), should be taken to be 5 to 7 per cent higher than the stalling speed of the towing plane with flaps in the take-off position.

In rather exceptional cases, when at the end of the period "b" $J > 0.54$, integration of Eq. (8), with the simplification that $W_g(C_{Dg}/C_{Lg}) = \text{Const.}$, leads to the following formula:

$$s_a = 0.031 W \times$$
$$\left[\frac{1.15}{\alpha} \log_{10} \frac{\delta - \beta V_g - \alpha V_g^2}{\delta - \beta V_a - \alpha V_g^2} + \frac{1.15\beta}{\alpha \sqrt{\beta^2 + 4\alpha\delta}} \log_{10} \frac{(-2\alpha V_g - \beta - \sqrt{\beta^2 + 4\alpha\delta})(-2\alpha V_a - \beta + \sqrt{\beta^2 + 4\alpha\delta})}{(-2\alpha V_g - \beta + \sqrt{\beta^2 + 4\alpha\delta})(-2\alpha V_a - \beta - \sqrt{\beta^2 + 4\alpha\delta})} \right] \tag{20a}$$

where α, β, and δ denote, respectively:

$$\alpha = B_a S_a (\rho/2); \quad \beta = 715 P_t/(nD)^2; \quad \delta = T_0 - (C_{Dg}/C_{Lg}) W_g - \mu W_a$$

When it is possible to assume that $B_a = 0$, then Eq. (20a) takes a much simpler form:

$$s_a = 0.031 W \left[2.3 \frac{\delta}{\beta^2} \log_{10} \frac{\delta - \beta V_g}{\delta - \beta V_a} - \frac{1}{\beta}(V_a - V_g) \right] \tag{20b}$$

For the preliminary calculations it seems to be possible to assume $C_{Dg}/C_{Lg} = \mu$ and then, Eq. (20b) may be expressed as:

$$s_a = 0.031 W \left[2.3 \frac{T_{e0}}{\beta^2} \log_{10} \frac{T_{e0} - \beta V_g}{T_{e0} - \beta V_a} - \frac{1}{\beta}(V_a - V_g) \right] \tag{20c}$$

The take-off distance corresponding to period "c" is easy to calculate and needs no special explanation. It may be noted, however, that in a case when no definite aerodynamic characteristics of the airplane and glider are known the values of C_{Dg}/C_{Lg} and C_{Da}/C_{La} needed for Eq. (21) may be evaluated for the glider by Eq. (17) and for the towing plane by a formula completely analogic to Eq. (17). The value of air speed should, of course, be taken as equal to V_a.

If at the end of period "b" and also during the period "c" the advance ratio does not exceed a value of $J = 0.54$, then the expression for thrust may be based on Eqs. (14b) and (11a) giving the take-off distance in period "c" (to attain a height of 50 ft.) will take the form:

$$s_c = \frac{50W}{T_0 - 1{,}210 \dfrac{P_t}{(nD)_3} V_a^2 - W_g \left(\dfrac{C_{Dg}}{C_{Lg}} \right)_c - W_a \left(\dfrac{C_{Da}}{C_{La}} \right)_c} \tag{21a}$$

If in the period "c" $J > 0.54$, then the thrust value should be evaluated on the basis of Eq. (14a) and s_c will be expressed as:

$$s_c = \frac{50W}{T_0 - 715 \dfrac{P_t}{(nD)^2} V_a - W_g \left(\dfrac{C_{Dg}}{C_{Lg}} \right)_c - W_a \left(\dfrac{C_{Da}}{C_{La}} \right)_c} \tag{21b}$$

Numerical Example

Consider a towing airplane with the following known characteristics: normal gross weight, $W_a = 22{,}000$ lbs.; wing area, $S_a = 1{,}000$ sq.ft.; aspect ratio, $A_a = 9$; maximum flying speed, $V_{max.} = 220$ m.p.h. at 6,000 ft. $(\rho/\rho_0 = 0.801)$; stalling speed at sea level (flaps partially deflected), $V_{min.} = 70$ m.p.h. Let this plane

be powered with two engines each developing 1,000 hp. at both 6,000 ft. and at the take-off: Revolutions per minute of the engine are 2,300; of three-bladed propeller, 1,530. $C_{Dmin.}$ at the take-off: $C_{Dmin._a} = 0.028$.

This airplane tows a transport glider with the following characteristics: $W_g = 16{,}000$ lbs., $S_g = 1{,}000$ sq.ft., $A_g = 10$, $C_{Dmin._g}$ is known to be equal (at the take-off) to 0.025; stalling speed with flaps in the take-off position, $V_{min.} = 55$ m.p.h.

Find, for the train composed of this plane and glider, the total take-off distance needed to clear a 50-ft. obstacle.

At first, in order to establish the propeller diameter, the coefficient c_s is calculated. As $c_s = 1.8$, from Fig. 4, $(V/nD)_{opt.} = 1.1$; hence the propeller diameter $D = 11.5$ ft. The static thrust for the whole airplane will be $T_0 = 7{,}300$ lbs. In assuming that $\mu = 0.05$ the effective static thrust will be $T_{\mu 0} = 5{,}400$ lbs. Consider the take-off speed for glider to be 7 per cent higher than 55 m.p.h.: $V_g = 59$ m.p.h. or 72 ft. per sec. The take-off distance for glider, calculated according to Eq. (16a), will be $s_g = 615$ ft. Using approximate formula (16b) this distance will be found to be equal to $s_g = 590$ ft. The take-off speed of the plane is to be $70 + 0.07 \times 70 = 75$ m.p.h. or 110 ft. per sec., and the advance ratio corresponding to this speed will be $J = 0.375$; hence, to calculate s_a Eq. (18) may be used. But first, $W_g(C_{Dg}/C_{Lg})_b$ should be found. This will be $W_g(C_{Dg}/C_{Lg})_b = 930$ lbs. The next values needed for Eq. (18) are: $c_b = 0.123$ and $T_{0b} = 5{,}270$ lbs. Finally, the take-off distance corresponding to period "b" will be $s_a = 985$ ft. Hence, $s_g + s_a = 1{,}600$ ft. This total distance calculated by the approximate formula (19) will be $s_{g,a} = 1{,}500$ ft.—i.e., a difference of 6.25 per cent. The take-off distance in period "b," calculated by the approximate formula (20c)* based on Eq. (13a), will give $s_a = 980$ ft. To calculate s_c, the $W_a(C_{Da}/C_{La})_c$ value is needed. According to Eq. (17) it will be 1,580 lbs., and s_c according to Eq. (21a) will be $s_c = 530$ ft. The total take-off distance is finally determined as $s = s_g + s_a + s_c = 2{,}130$ ft.

Comparison of Overloaded Plane with Glider Train

In order to give some idea as to whether it is practical or not to carry cargo in a towed glider instead of in an overloaded plane, the following comparison has been made: A transport plane of the DC-3 class was assumed, with the characteristics given in the numerical example. Some additional load was then assumed to be put into this plane, overloading it to some extent. The ratio of the total take-off distance (to clear 50 ft.) to that of the plane having its normal weight (s_a/s_{an}) was plotted against this additional load (Fig. 6).

A similar calculation has been made in assuming that this transport plane, having its normal weight, tows a glider (or gliders) in which this additional load is carried. The ratio of the take-off distance of the train to that of the towing plane (having its normal weight) (s_t/s_{an}) is plotted on Fig. 6 against the additional load. The aerodynamic characteristics of the glider were assumed to be as in the numerical example. The total weight of the glider was assumed to be 1.8 to 1.7 times greater than the weight of the load to be transported. In other words the pay load is assumed to be equal to 55 to 60 per cent of the total weight.

A glance at Fig. 6 will show that under the above assumptions the take-off distance of a glider train carrying some additional load, with a normally loaded towing plane, is smaller than the take-off distance of the overloaded plane.

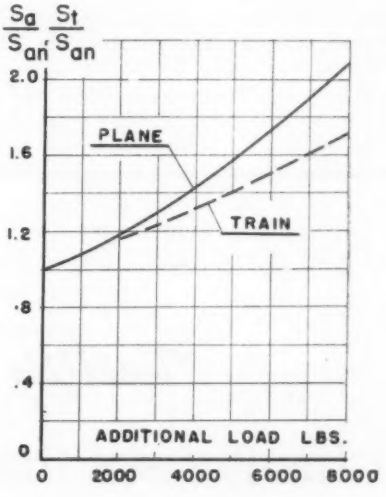

Fig. 6.

As the above comparison was made for a train representing an average transport plane and an average transport glider, it seems possible to arrive at the following general conclusion: that in considering take-off qualities and dividing of the load to be transported, the glider will probably give better results than overloading of the transport plane.†

References

[1] Welling, Omer, *An Approximate Method to Predict the Transition or "Flare" Flight Path in the Take Off or Landing of an Airplane*, Journal of the Aeronautical Sciences, Vol. 9, No. 1, pp. 17–23, November 1941.

* In Eq. (20c) the T_0 will, of course, be slightly different than previously found, $T_0 = 7{,}300$ lbs. It will be so, because in Eq. (15), when it is based on Eq. (14a), $a = 2.05$ is used instead of $a = 1.95$, as it is for the formula based on Eq. (14b).

† The analysis of the take-off made in this paper gives only one of many aspects of the transport problems by glider trains. More information regarding these problems can be found in previously published articles.[9, 10]

[2] Wetmore, J. W., *The Transition Phase in the Take-Off of an Airplane*, N.A.C.A. T.R. No. 626, 1938.

[3] Rolinson, D., *Take-Off and Landing of Aircraft*, R. & M. 1406, 1931.

[4] Wetmore, J. W., *The Rolling Friction of Several Airplane Wheels and Tires*, N.A.C.A. T.R. No. 583, 1937.

[5] Bairstow, L., *Applied Aerodynamics;* Longmans, Green and Company, London, 1939.

[6] Hartman, E. P., and Biermann, D., *The Aerodynamic Characteristics of Full-Scale Propellers Having 2, 3, and 4 Blades*, N.A.C.A. T.R. No. 640, 1938.

[7] Biermann, D., and Hartman, E. P., *Tests of Five Full-Scale Propellers in the Presence of a Radial and a Liquid-Cooled Engine Nacelle*, N.A.C.A. T.R. No. 642, 1938.

[8] Warner, E. P., *Airplane Design, Performance;* McGraw-Hill Book Company, New York, 1936.

[9] Stepniewski, W., *Air Transport by Gliders (Some Technical Observations)*, The Aeroplane, Vol. 50, No. 1561, pp. 476–477, April 25, 1941.

[10] Stepniewski, W., *The Prediction of Performance*, Aircraft Engineering, Vol. 12, Nos. 141 and 142, pp. 329–331, 338, 361–365, November and December, 1940.

[11] Mokrzycki, G. A., *Graphic Determination of Distance in Accelerated Airplane Motion*, Journal of the Aeronautical Sciences, Vol. 10, No. 1, pp. 36–37, January, 1943.

(*Continued from page 47*)

[6] Brown, C. G., *Torsional Characteristics of Cantilever Wings*, A.A.F. T.R. No. 3412, February 20, 1931.

[7] Pugsley, A. G., and Brooke, G. R., *The Calculation by Successive Approximation of the Critical Reversal Speed for an Elastic Wing*, R. & M. 1508, 1933.

[8] Shornick, L. H., *The Computation of the Critical Speeds of Aileron Reversal, Wing Torsional Divergence and Wing-Aileron Divergence*, Army Air Forces Memorandum Report Serial No. ENG-M-51/VF 18, Add. 1.

[9] Theodorsen, T., and Garrick, I., *Mechanism of Flutter*, N.A.C.A. T.R. No. 685, 1940.

[10] Lyon, H. M., *A Review of Theoretical Investigation of the Aerodynamic Forces on a Wing in Non-Uniform Motion*, R. & M. 1786, 1937.

[11] Hanson, J., *Critical Speed of Monoplanes*, Journal of The Royal Aeronautical Society, Vol. 41, pp. 703–726, August, 1937.

Twelfth Annual Meeting

Institute of the Aeronautical Sciences

The Twelfth Annual Meeting of the Institute will be held January 25, 26, and 27, 1944, in the Pupin Physics Laboratories of Columbia University. To facilitate attendance at technical sessions, meetings will be held only during the afternoon and evening of each day.

The technical sessions will be preceded by the Honors Night Dinner of the Institute at the Hotel Waldorf-Astoria, New York, Monday evening, January 24, 1944.

Medical Activities in Naval Aviation

J. C. ADAMS,* B. GROESBECK, JR.,* AND E. F. DuBOIS†

U.S. Navy Bureau of Medicine and Surgery

Physiologic Limits as Vital Factors in Aeronautical Design

It has long been obvious that aeronautical engineers have been able to produce planes that exceed the present physiologic and psychologic limits of the pilot. These advancements have been a frank challenge to the flight surgeon, the physiologist, and the psychologist. The answer has been an active program in aviation medical research in which the efforts in this country have been pooled with those of Canada and England. It is becoming increasingly clear, however, that the physiology of man is not subject to change at will. Therefore, if this gap between man's physical limitations and further advancement in aircraft performance is to be bridged, it will be necessary to modify future aircraft design and auxiliary flying equipment to effect these physical adjustments.

Pilot Selection

Physical Requirements

The Navy program calls for the procurement of large groups of young men who must show a good expectancy for success under flight instruction. These young men will come largely from the civilian population and must meet the physical and psychologic standards prescribed. So long as there remains a sufficient reservoir of personnel, the physical requirements will be held at a high level. True, there are instances of distinguished fliers who have lost one leg or one eye. However, this is not sufficient reason for lowering physical standards. Availability of personnel will govern the level of physical requirements in time of war and, commensurate with this fact, the physical requirements will be maintained at the highest practical level.

Psychologic Fitness

In addition to strict physical requirements, there must be psychologic fitness with a high degree of vocational aptitude. Methods have been devised to evaluate this gift and eliminate before training starts many of the inept who waste instructors' time.

The Navy has, through psychologic research, established selection methods with high validity for the appraisal of aptitude for flying. This research was in process of development well in advance of the outbreak of war, and immediately upon the declaration of hostilities these selective methods were ready to be instituted as a part of the expanded training program.

In order to maintain rigid and uniform standards the Navy limited the selection of flying personnel to only fifteen boards located strategically throughout the country. The procedure at all boards is standardized, so that the results can be used for statistical analysis. The special psychologic tests identify personnel according to their respective probability for success or failure under training as naval aviators. The tests are mass administered on prescribed forms. Scoring is accomplished ingeniously by electrically operated machines in the Navy Department. The scoring keys of course, are confidential. By these methods it is possible to process large numbers of personnel quickly and accurately. The personal equation of the examiner is entirely eliminated. Of equal or greater importance, it is possible from these records to raise or lower the qualifying score at will, thereby regulating the flow of any class of expectancies for flight training as may be indicated to meet the needs of the training program at any time.

Preflight Schooling

Once selected, the cadet is sent to one of the preflight schools for a three-month period of physical training and hardening. This is in no sense abusive, but it is vigorous and tough and it eliminates those few who do not possess the physical and psychologic fortitude to stand the exposure and loss of rest that are encountered in the type of war that is now being waged without quarter.

Qualifications of Flight Instructors

To further perfect our training program the Navy has given consideration to the qualifications of its flight instructors. A special flight instructor's school has been established. Prospective instructors receive indoctrination in training methods. Special attention is being given to their voice recording, which is played back to them and criticized and appraised by speech experts for the improvement of diction. Intercommunication between instructor and student is being improved. Standard patter guides for instructors are now available. Most of these improvements have been accomplished through the conjoined efforts of the flight surgeon and psychologist and assistance from the Command.

Presented at the Physiologic Problems Session, Eleventh Annual Meeting, I.A.S., New York, January 25–29, 1943.

* Captains, Medical Corps, U.S. Navy.

† Captain, Medical Corps, U.S.N.R.

The largest task for the psychologic section still lies ahead. All of the existing predictors have been validated against performance in training. This is important in its own right. But training is of little value unless the pilots prove effective in combat. Only when a job analysis has been validated against combat performance or other flight performance can it be certain that good fighters and not merely good pilots are being selected and trained. This study is being intensely pursued.

Altitude Problems

Flight performance at extreme altitudes imposes special stress on the pilot. Formerly this was thought of in terms of anoxia. Later the symptoms of decompression illness—namely, aeroembolism or bends were recognized. Now the total effects of high-altitude stress have been recognized, not only in terms of anoxia and bends but also of the debilitating effects of cold and other physiologic changes induced in the body as a result of such exposure. Certain individuals are more susceptible than others to the effects of anoxia, bends, and to the total effects of high altitude. Age and physical condition have bearing in this regard.

The Low-Pressure Chamber

Important military flights have been forcibly terminated because certain crew members have proved incapable of completing the mission at high altitudes. This is of practical military significance. To meet this situation it has become necessary to select and indoctrinate pilots for high-altitude flying. This is accomplished by means of the low-pressure chamber. There are low-pressure chambers in several training stations, and soon there will be at least one at every large station.

As indicated, these chambers are used for classification and indoctrination of pilots and crew for high-altitude flying. The principal object is to acquaint the individual with the actual effects of anoxia and bends, thereby enabling him to evaluate more readily the importance of symptoms as they affect him. It is also by these means that the pilot is properly indoctrinated to the need of oxygen and the use of his oxygen appliance.

The importance attached to anoxia is of practical concern only to the extent of insuring the use of oxygen at all altitudes above 10,000 ft. and from the ground up in flights to 30,000 ft. or above. The validities of these regulations have been long established. It naturally follows that only in case of failure of oxygen supply should anoxia become a practical concern. Unfortunately, at critical altitudes the margin of safety even with the best oxygen apparatus becomes small and, for practical purposes, is terminated at approximately 40,000 ft. when used at prevailing barometric pressures.

Bend Susceptibility

Altitude runs in the low-pressure chamber will give a fair idea of a man's susceptibility to low oxygen but less specific information as to his susceptibility to bends. Susceptibility to bends not only varies with the individual but also varies from day to day within the same individual. Certain individuals, however, are proved susceptibles, and it becomes necessary to identify them and exclude them from high-altitude flying. Standardized procedures are in effect at all low-pressure chambers. Cold low-pressure chambers are being installed to provide additional means of studying personnel embodying the low temperature effects at all given altitudes.

Night Vision

The use of the eyes in the dark for night flying is a new exaction—and an important one—in the present war. This problem has involved not only a tremendous program of research relating to the subject but has also necessitated revolutionary changes in cockpit illumination. These accomplishments are now far advanced and in practical operation.

Pilot Fatigue

Pilot fatigue is of major importance, and at this time it cannot be measured accurately by any machine or laboratory test or questionnaire. As a consequence, the problem must be dealt with in a practical manner. For this purpose there is no substitute for the accomplished flight surgeon who lives and thinks with his pilots and who acts as physician, friend, and counselor. Such a flight surgeon is able to detect the early manifestations of fatigue and institute measures for relief of flying or modification in routine.

Flight Surgeon Training

Unfortunately it takes time to train a Navy flight surgeon, and great importance is attached to his training. He not only receives instruction in the technical subjects of his specialty but he is required to complete a prescribed course of indoctrinal flight training which participates in every phase of flight instruction prescribed for pilots. He shares in similar manner the ground-school training, and during this period he lives entirely with other student aviators. It is by these means that his first-hand appreciation of flying stress is gained and his approach to his special mission is made practical and realistic. The school for Navy flight surgeons is located at Pensacola, Fla. It is well staffed and is highly progressive in the accomplishment of its mission.

Instrument Flying

The factors conducive to pilot fatigue are too varied and numerous to be discussed here in detail. However,

instrument flying or blind flying is particularly strenuous and requires continuous attention and concentration. By and large, any and all conditions conducive to physical and emotional strain are contributing factors to fatigue. Environmental factors, such as extreme cold, noise, glare and rough weather, are depreciating and distracting influences. In time of war, the emotional equivalents incident to combat and other added hazards are a tremendous influence.

Fatigue

Much can be done to relieve fatigue, and here again these measures are varied and ramifying. Administrative measures regulating flights and conserving the demands made on pilots can be most helpful. Proper relief from operational assignments against the enemy and the use of recreational and recuperative centers have their importance. Careful selection and training are most essential. However, there remains much in the field of engineering which can contribute materially. There is need for greater physical comfort in military aircraft. Improvement in clothing and other items of flying equipment is needed. Better protection from cold, noise, and vibration is required. This is only part of the picture, but it can be seen that it is a problem that requires the efforts of all for its improvement.

Aviation Medical Research

A research division in naval medicine started in 1917, continued with difficulty in lean years of peace, but grew rapidly with war. Research in respiratory problems was first conducted in Washington and spread to Pensacola with the development of the Research Division in the School of Aviation Medicine. There, work broadened to include visual problems, communication systems, oxygen equipment, selection, and training, indeed all the medical and physiologic matters that affect the flier. Special work in motion sickness was started in Boston; night vision research and the training of lookouts, in New London; and other studies, in scattered places. Meanwhile, liaison officers were in constant touch with the large amount of work carried on by the U.S. Army, the Canadians, the British and the N.R.C. Committee on Aviation Medicine. Recently, there has been completed a large and well-planned research laboratory at the Naval Medical School at Bethesda. It will be equipped to study almost any problem connected with naval or aviation medicine. A similar research laboratory is in process of completion at Pensacola and will be devoted entirely to the problems of aviation medicine. While these provisions speak well for aviation medical research, they can never within themselves provide the total answer to human limitation in modern high-performance aircraft. This is readily apparent when it is realized that human physiology is not subject to marked alteration. The physical limitations of man in control of modern aircraft has already been referred to, especially at extreme altitudes. While medical research no doubt will provide means of some further adjustment of the human element to these stresses, in large measure it can only serve to reveal the nature of the human limitations.

It is clear then that if these deficiencies are incapable of solution by further adjustment within the individual, it will be necessary to effect these changes within the environment to which he is subjected—namely, the aircraft itself. Here, then, is the clear necessity for engineering and its technical ramifications to enter the picture. It is for them to develop and perfect those measures within the aircraft by which means the human element may function beyond its normal physiologic limitations.

Lack of sufficient appreciation of these basic facts has seriously retarded ultimate accomplishments in flying. It is of the greatest importance that the medical man be actively joined by the engineer and by the industry in an integrated approach to the solution of these problems. This applies also to the improvement of accessory equipment, such as oxygen supply appliances, clothing, etc., as well as to changes in aircraft per se.

Physiologic Limitation and Problems

Oxygen Requirements

What then are some of these problems of physical limitation? The first is oxygen, since man's nominal altitude limitation with oxygen supplied under the prevailing barometric pressure is roughly 40,000 ft. If this performance is to be exceeded the prevailing barometric pressure to the pilot must be modified. This involves pressurized compartments, cabins, or suits. This field is large and almost unapproached and is an outstanding challenge for the future.

Cold Protection

Further protection from cold is needed. The solution does not lie in clothing alone but involves heating of the plane. The matter has no simple solution, as indicated by the problem of meeting pilot comfort at a ground temperature that may be as high as 120°F. and, within a few minutes, the discomfort of extreme cold at 30,000 ft. altitude. Certain parts of planes are more exposed to the cold than others and personnel suffers accordingly. Extreme cold, more than any other local condition, rapidly lowers morale and efficiency.

Noise and Vibration

Then there is the matter of noise and vibration. In long flights these are conducive to fatigue and are major factors in distractibility with consequent depreciation of efficiency.

Physical Comfort

Pilots and crew are frequently cramped in certain types of aircraft. Movement is restricted; seats are hard and uncomfortable. The element of reasonable provision for physical comfort has not been adequately provided.

Crash Hazards

The present types of military aircraft have installations within the cockpits or compartments particularly conducive to injury in case of forced landing or crash. Especially is the head in danger of needless injury. There is the greatest need for engineering improvements in the modification of protruding objects, corners, and items of installation to minimize unnecessary injury to personnel in case of forced landing or crash. This goes hand in hand with the need for more effective measures of protective appliance for flying personnel. Simplification of instrument paneling is also indicated. Further improvement of cockpit illumination is most important for night operations. There is need for active measures to improve the integration of headgear, goggles, oxygen masks, and clothing. Many of these items may be individually good, but they do not fit together as a whole. The result is a leaking oxygen mask or goggle, bulky clothing, and consequent impairment of pilot comfort and efficiency.

Conclusion

These are some of the problems requiring the joined cooperation of the doctor, the engineer, and the industry. There are others that fit into this general picture. Much has been accomplished by the selection and training of air crews and flight surgeons and by the development of new equipment, but the planes have pushed the pilots to their physiologic limits. Additional adjustment must come in large measure through engineering improvements in aircraft and equipment to bridge this gap between human limitations and advance in aircraft performance.

(*Continued from page 24*)

a simultaneous venture. Aircraft in peacetime did not normally carry first-aid kits, but this small item alone has developed into a godsend and has been responsible for relief of much suffering. Its effect on morale has been great.

Numerous accessories have been developed, such as life rafts with innumerable components such as water, food, signaling devices, fishing gear, first-aid equipment, and many lesser items. Selection of the proper food for such a purpose has occasioned a great deal more thought and study than might be immediately evident. Likewise, methods for obtaining water in mid-ocean on a life raft are the focus of intensive study. Solutions for these problems are in sight, but it is regretted that so much human suffering has been endured to this point in time.

Column with Equal-Spaced Elastic Supports

SHOU-NGO TU*

Massachusetts Institute of Technology

SUMMARY

The buckling load of a column with equal-spaced elastic supports is calculated by solving a difference equation of the second order. Two types of end conditions are considered: simple supported and built-in. In each case, a column with one, two, or three intermediate supports is examined. An asymptotic expression is derived for the case when the number of supports approaches infinity.

NOTATION

m = number of spans of the column
L = length of a span of the column
C = spring constant of the elastic supports
EI = bending stiffness of the column
S = stiffness ratio, CL^3/EI
P = buckling load of the column
t = a dimensionless parameter, PL^2/EI
M = bending moment, sign according to beam convention
R = reaction of support, positive if upward
y = deflection of the column, positive if upward
x = an integer between 0 and m
λ = a parameter defined by Eq. (7)

INTRODUCTION

THE BUCKLING LOAD of a column with equal-spaced elastic supports can be obtained either by using the energy method or by solving the differential equations.[1] In both cases, when the number of spans is large, the labor required to arrive at the final result is great. But it may be shown that, if we keep the length of a single span (L) and the stiffness of the elastic supports (C) constant, the change in the buckling load of a column (P) with the change in the number of spans (m) is small when m is large. It is therefore desirable to find some asymptotic expressions for the buckling load as m approaches infinity. The present paper suggests a new method of attack by which such an asymptotic expression can be obtained. When the number of spans is finite, the labor required to find the buckling load by the present method is at most equal to that required by other methods.

FORMULATION OF THE PROBLEM

Consider a column cylindric in form and uniform in material. Between the two end rigid supports there are $(m - 1)$ equally spaced elastic supports. These supports are assumed to take tension or compression only. Their rigidity against deflection is denoted by C. If the distance between two neighboring supports is L and the bending rigidity of the column is EI, by the three-moment equation for beams under axial compression we have the following relation between the moments at three consecutive supports:[2]

$$\alpha(M_{x-1} + M_{x+1}) + 2\beta M_x = P(y_{x-1} - 2y_x + y_{x+1}) \quad (1)$$

where

$$\alpha = t \csc t - 1, \qquad \beta = 1 - \cot t, \qquad t^2 = PL^2/EI$$

Now the reaction at the xth support is R_x (Fig. 1),

$$R_x = \frac{1}{L}\left[M_{x-1} - 2M_x + M_{x+1} + P(y_{x-1} - 2y_x + y_{x+1})\right]$$

and the force exerted by the support on the column is $-Cy_x$ (the negative sign is used to make the sign convention consistent). We then have

$$-CLy_x = M_{x-1} - 2M_x + M_{x+1} + P(y_{x-1} - 2y_x + y_{x+1}) \quad (2)$$

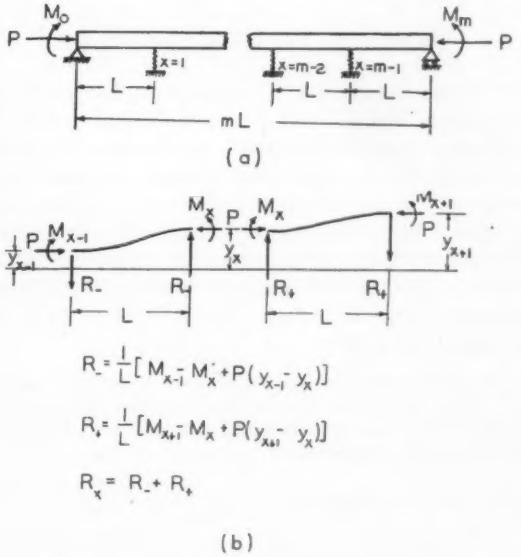

FIG. 1. A column with m intermediate supports.

Subtracting Eq. (1) from Eq. (2) and rearranging,

$$-CLy_x = (\alpha + 1)(M_{x-1} + M_{x+1}) + 2(\beta - 1)M_x \quad (3)$$

Substituting Eq. (3) in Eq. (1) to eliminate the y's,

Received March 23, 1943.

* Aeronautical Department. Now Structures Engineer, Curtiss Airplane Division, Curtiss-Wright Corporation.

$$(\alpha+1)(M_{x-2}+M_{x+2})-\left(2\alpha-2\beta+4-\frac{CL}{P}\alpha\right)\times$$
$$(M_{x-1}+M_{x+1})+2\left(\alpha-2\beta+3+\frac{CL}{P}\beta\right)M_x=0 \quad (4)$$

Let

$$S=CL^3/EI \quad (5a)$$

$$A=\frac{1}{\alpha+1}\left(2\alpha-2\beta+4-\frac{CL}{P}\alpha\right)=$$
$$2+2\cos t-\frac{S}{t^3}\left(t-\sin t\right) \quad (5b)$$

$$B=\frac{1}{\alpha+1}\left(\alpha-2\beta+3+\frac{CL}{P}\beta\right)=$$
$$1+2\cos t+\frac{S}{t^3}\left(\sin t-t\cos t\right) \quad (5c)$$

then Eq. (4) becomes

$$(M_{x-2}+M_{x+2})-A(M_{x-1}+M_{x+1})+2BM_x=0$$

The solution to this difference equation is[3]

$$M_x=a_1\cos\lambda_1 x+b_1\sin\lambda_1 x+a_2\cos\lambda_2 x+b_2\sin\lambda_2 x \quad (6)$$

where λ_1 and λ_2 are roots of the equation

$$\cos 2\lambda-A\cos\lambda+B=0 \quad (7)$$

From Eq. (3) we find the displacement at the xth support is

$$y_x=$$
$$-\frac{2t}{CL\sin t}\Big[(\cos\lambda_1-\cos t)(a_1\cos\lambda_1 x+b_1\sin\lambda_1 x)+$$
$$(\cos\lambda_2-\cos t)(a_2\cos\lambda_2 x+b_2\sin\lambda_2 x)\Big] \quad (8)$$

To determine the relative value of the four arbitrary constants in Eqs. (7) and (8), there are four conditions to satisfy: one for each end* and two for the static equilibrium of the whole column when considered as a free body. If the conditions at both ends are the same, the type of displacement at buckling is either symmetric or antisymmetric with respect to the midpoint of the column. This fact reduces the number of arbitrary constants from four to two. In case of symmetric displacement, we expect

$$M_x=M_{m-x}$$

Therefore, from Eq. (6),

$$a_1\sin(m/2)\lambda_1-b_1\cos(m/2)\lambda_1=0$$
$$a_2\sin(m/2)\lambda_2-b_2\cos(m/2)\lambda_2=0$$

Consequently, Eqs. (6) and (8) become

$$M_x=a\cos[(m/2)-x]\lambda_1+b\cos[(m/2)-x]\lambda_2 \quad (9)$$

$$y_x=\frac{2t}{CL\sin t}\Big[a(\cos\lambda_1-\cos t)\cos\left(\frac{m}{2}-x\right)\lambda_1+$$
$$b(\cos\lambda_2-\cos t)\cos\left(\frac{m}{2}-x\right)\lambda_2\Big] \quad (10)$$

In case of antisymmetric displacement, we expect

$$M_x=-M_{m-x}$$

Therefore from Eq. (6)

$$a_1\cos(m/2)\lambda_1+b_1\sin(m/2)\lambda_1=0$$
$$a_2\cos(m/2)\lambda_2+b_2\sin(m/2)\lambda_2=0$$

Consequently, Eqs. (6) and (8) become

$$M_x=c\sin\left(\frac{m}{2}-x\right)\lambda_1+d\sin\left(\frac{m}{2}-x\right)\lambda_2 \quad (11)$$

$$y_x=-\frac{2t}{CL\sin t}\Big[c(\cos\lambda_1-\cos t)\sin\left(\frac{m}{2}-x\right)\lambda_1+$$
$$d(\cos\lambda_2-\cos t)\sin\left(\frac{m}{2}-x\right)\lambda_2\Big] \quad (12)$$

Column with Simply Supported Ends

Symmetric Displacement

If the type of displacement of the column at buckling is symmetric with respect to the midpoint, the moment and displacement at the xth support are given by Eqs. (9) and (10). The boundary conditions are: The moment at the end support is zero and the resultant force acting on the column is zero. In symbols,

$$M_1=0 \text{ and } \sum_{x=1}^{m}R_x=0$$

Now

$$R_x=-Cy_x, \qquad x=1,2,\ldots(m-1) \quad (13)$$

$$R_0=\frac{1}{L}\left(-M_0+M_1+Py_1\right),$$

$$R_m=\frac{1}{L}\left(M_{m-1}-M_m+Py_{m-1}\right) \quad (14)$$

Hence the conditions are

$$a\cos(m/2)\lambda_1+b\cos(m/2)\lambda_2=0$$

$$a\left[\frac{2}{L}\cos\left(\frac{m}{2}-1\right)\lambda_1-\frac{4Pt}{CL^2\sin t}(\cos\lambda_1-\cos t)\cos\left(\frac{m}{2}-1\right)\lambda_1+\frac{2t}{L\sin t}(\cos\lambda_1-\cos t)\sum_{x=1}^{m-1}\cos\left(\frac{m}{2}-x\right)\lambda_1\right]+$$

$$b\left[\frac{2}{L}\cos\left(\frac{m}{2}-1\right)\lambda_2-\frac{4Pt}{CL^2\sin t}(\cos\lambda_2-\cos t)\cos\left(\frac{m}{2}-1\right)\lambda_2+\frac{2t}{L\sin t}(\cos\lambda_2-\cos t)\times\right.$$
$$\left.\sum_{x=1}^{m-1}\cos\left(\frac{m}{2}-x\right)\lambda_2\right]=0$$

* In fact two boundary conditions should be satisfied for each end. Here the condition that the displacement at the end is zero is not used directly. It is included, however, in computing the reactions at the end supports.

Eliminating a and b from these two equations and simplifying (making use of Eq. (7)),

$$\frac{4t^3}{SL\sin t}(\cos\lambda_1 - \cos\lambda_2)\cos\frac{m}{2}\lambda_1\cos\frac{m}{2}\lambda_2 = 0$$

Since $\cos\lambda_1$ and $\cos\lambda_2$ are in general not equal to each other, the above equation reduces to

$$\cos(m/2)\lambda = 0$$

Therefore

$$\lambda = [(2n+1)/m]\pi, \qquad n = 0, 1, 2\ldots(m-1)$$

Substituting in Eq. (7),

$$\cos\left(\frac{2n+1}{m}\right)2\pi - \left[2 + 2\cos t - \frac{S}{t^3}(t - \sin t)\right]\times \cos\left(\frac{2n+1}{m}\right)\pi + \left[1 + 2\cos t + \frac{S}{t^3}(\sin t - t\cos t)\right] = 0 \tag{15}$$

From Eq. (15) the buckling load may be obtained.

Antisymmetric Displacement

In this case the moment and displacement at the xth support are given by Eqs. (11) and (12), respectively. The boundary conditions are: The moment at the end support is zero and the moment acting on the column is in equilibrium. In symbols,

$$M_0 = 0$$

$$M_1 - M_m + mR_0L + \sum_{x=1}^{m-1} R_x(m-x)L = 0$$

Making use of Eqs. (13) and (14), they become

$$c\sin\frac{m}{2}\lambda_1 + d\sin\frac{m}{2}\lambda_2 = 0$$

$$c\left[m\sin\left(\frac{m}{2}-1\right)\lambda_1 - \frac{2Ptm}{CL\sin t}(\cos\lambda_1 - \cos t)\times \sin\left(\frac{m}{2}-1\right)\lambda_1 + \frac{2t}{\sin t}(\cos\lambda_1 - \cos t)\sum_{x=1}^{m-1}(m-x)\sin\left(\frac{m}{2}-x\right)\lambda_1\right] + d\left[m\sin\left(\frac{m}{2}-1\right)\lambda_2 - \frac{2Ptm}{CL\sin t}\times (\cos\lambda_2 - \cos t)\sin\left(\frac{m}{2}-1\right)\lambda_2 + \frac{2t}{\sin t}(\cos\lambda_2 - \cos t)\times \sum_{x=1}^{m-1}(m-x)\sin\left(\frac{m}{2}-x\right)\lambda_2\right] = 0$$

Eliminating c and d and simplifying by the use of Eq. (7),

$$(m-2)\left(\frac{t}{\sin t}\right)\left[\frac{(\cos\lambda_1 - \cos\lambda_2)(1-\cos t)}{(1-\cos\lambda_1)(1-\cos\lambda_2)}\right] - \sin\frac{m}{2}\lambda_1\sin\frac{m}{2}\lambda_2 = 0$$

With the same reasoning as before, it reduces to

$$\sin(m/2)\lambda = 0$$

Therefore

$$\lambda = 2n\pi/m, \qquad n = 1, 2, \ldots m$$

Substituting in Eq. (7),

$$\cos\frac{4n}{m}\pi - \left[2 + 2\cos t - \frac{S}{t^3}(t - \sin t)\right]\cos\frac{2n\pi}{m} + \left[1 + 2\cos t + \frac{S}{t^3}(\sin t - t\cos t)\right] = 0 \tag{16}$$

From this equation we may solve for the buckling load corresponding to antisymmetric displacement.

Buckling Load

For a given number of spans (m) and for a given stiffness ratio S, the buckling load is given by either Eqs. (15) or (16), depending upon which is smaller. In fact, these two equations can be combined into one—that is,

$$\cos\frac{2n\pi}{m} - \left[2 + 2\cos t - \frac{S}{t^3}(t - \sin t)\right]\cos\frac{n\pi}{m} + \left[1 + 2\cos t + \frac{S}{t^3}(\sin t - t\cos t)\right] = 0 \tag{17}$$

where n is any integer between 1 and m. If we plot t versus S, Eq. (17) gives a set of m curves. The lowest border thus formed is the required buckling load versus support stiffness curve.

One Intermediate Support ($m = 2$)

In this case Eq. (17) becomes

$$\cos n\pi - \left[2 + 2\cos t - \frac{S}{t^3}(t - \sin t)\right]\cos\frac{n\pi}{2} + \left[1 + 2\cos t + \frac{S}{t^3}(\sin t - t\cos t)\right] = 0$$

where n may be 1 or 2. Letting n take these values, we have the following equations:

$$2\cos t + (S/t^3)(\sin t - t\cos t) = 0$$
$$4(1+\cos t) - (S/t^3)(t - 2\sin t + t\cos t) = 0$$

The second equation may be put in the form

$$2(1+\cos t)\left[2 - \frac{S}{t^3}\left(\frac{t}{2} - \tan\frac{t}{2}\right)\right] = 0$$

For all values of S the first factor always gives the smaller buckling load. Therefore we have the following two equations that relate the buckling load with the stiffness ratio:

$$S = 2t^3/(t - 2\tan t)$$
$$t = \pi$$

These are plotted in Fig. 2. The transition takes place when S has a value $2\pi^2$.

Two Intermediate Supports ($m = 3$)

Let n take the value 1, 2, or 3, respectively. From Eq. (17) we have, after simplification and transforma-

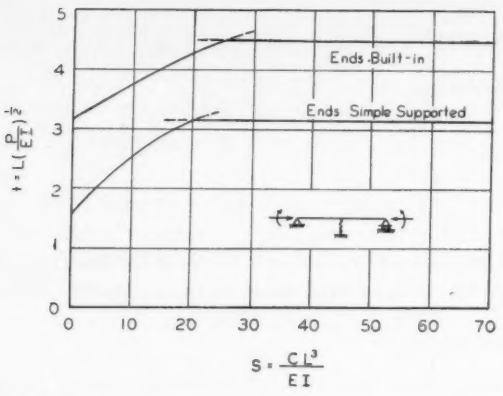

FIG. 2. Buckling load of a column with one intermediate support.

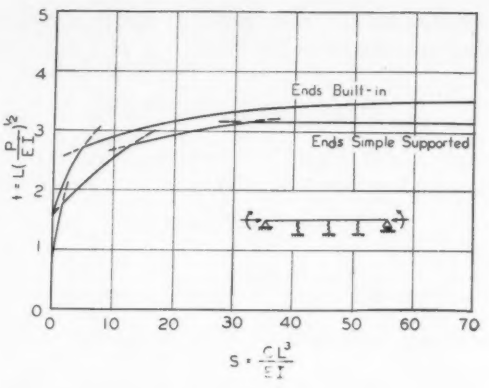

FIG. 4. Buckling load of a column with three intermediate supports.

tion, the following three equations that give the relation between the buckling load and the stiffness ratio:

$$S = t^3/\{t + [\sin t/(1 - 2\cos t)]\}$$
$$S = t^3/\{(t/3) - [\sin t/(1 + 2\cos t)]\}$$
$$t = \pi$$

These equations are plotted in Fig. 3. The transition takes place when S is equal to 4.6 and $3\pi^2$.

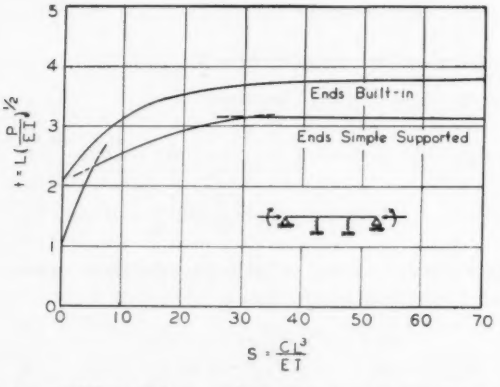

FIG. 3. Buckling load of a column with two intermediate supports

Three Intermediate Supports ($m = 4$)

Let n take the values 1, 2, 3, and 4 in each case. From Eq. (17) we have the following four equations that give the relation between t and S:

$$S = t^3/\left(\frac{t}{2 - \sqrt{2}} + \frac{\sin t}{\sqrt{2} - 2\cos t}\right)$$
$$S = 2t^3/(t - \tan t)$$
$$S = t^3/\left(\frac{t}{2 + \sqrt{2}} - \frac{\sin t}{\sqrt{2} + 2\cos t}\right)$$
$$t = \pi$$

These equations are plotted in Fig. 4. The transition takes place when S is 1.3, 13.0, or $(2 + \sqrt{2})\pi^2$.

Asymptotic Expression

For a column with $(m - 1)$ intermediate supports, the t versus S curve is given by the lowest border formed by a set of curves derived from Eq. (17). As the number of supports increases, it becomes the envelope of the curves given by Eq. (17). To find the envelope, we differentiate Eq. (17) with respect to n and equate the resulting expression to zero:

$$-\frac{\pi}{m}\left\{2\sin\frac{2n\pi}{m} - \left[2 + 2\cos t - \frac{S}{t^3}(t - \sin t)\right]\sin\frac{n\pi}{m}\right\} = 0$$

or

$$\sin\frac{n\pi}{m}\left\{4\cos\frac{n\pi}{m} - \left[2 + 2\cos t - \frac{S}{t^3}(t - \sin t)\right]\right\} = 0$$

Unless n equals m,

$$\cos\frac{n\pi}{m} = \frac{1}{4}\left[2 + 2\cos t - \frac{S}{t^3}(t - \sin t)\right]$$

Substituting in Eq. (17) and simplifying,

$$(t - \sin t)^2\left(\frac{S}{t^3}\right)^2 - 4(1 - \cos t)(t + \sin t)\left(\frac{S}{t^3}\right) + 4(1 - \cos t)^2 = 0 \quad (18)$$

This equation gives π as the maximum value for t and it occurs at S equals $4\pi^2$. When n equals m

$$\sin\pi = 0, \qquad \cos\pi = -1$$

From Eq. (17),

$$1 + \cos t = 0$$

That is

$$t = \pi \quad (19)$$

Now from Eq. (17) it is readily seen that the transition from the type of displacement corresponding to $n = (m - 1)$ to that corresponding to $n = m$ when m approaches infinity occurs at $S = 4\pi^2$. Therefore the asymptotic expression consists of two parts: For S less than $4\pi^2$ it is given by Eq. (18), and for S greater than $4\pi^2$ it is given by Eq. (19). These are plotted in Fig. 5.

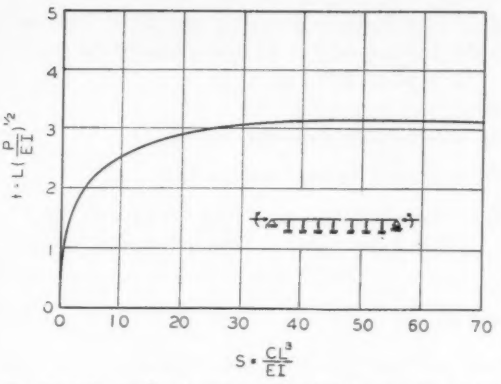

FIG. 5. Buckling load of a column with infinite number of intermediate supports.

COLUMN WITH BUILT-IN ENDS

Symmetric Displacement

In this case the moment and displacement at the xth support are given by Eqs. (9) and (10), respectively. The boundary conditions are: The slope at the end support is zero and the resultant force acting on the column is zero. In symbols,

$$\beta M_0 + \alpha M_1 = P y_1$$

$$R_0 + R_m + \sum_{x=1}^{m-1} R_x = 0$$

Using Eqs. (13) and (14) and taking into consideration Eq. (7),

$$a\left[2(\cos\lambda_1 - \cos t)\cos\frac{m}{2}\lambda_1 + (-A + 2 + 2\cos\lambda_1) \times \sin\lambda_1 \sin\frac{m}{2}\lambda_1\right] + b\left[2(\cos\lambda_2 - \cos t)\cos\frac{m}{2}\lambda_2 + (-A + 2 + 2\cos\lambda_2)\sin\lambda_2 \sin\frac{m}{2}\lambda_2\right] = 0$$

$$a\frac{1+\cos\lambda_1}{\sin\lambda_1}\sin\frac{m}{2}\lambda_1 + b\frac{1+\cos\lambda_2}{\sin\lambda_2}\sin\frac{m}{2}\lambda_2 = 0$$

Eliminating a and b, after some further simplification, we have the following expression from which the buckling load of the column corresponding to symmetric displacement may be derived.

$$\frac{(\cos\lambda_1 - \cos t)\sin\lambda_1}{1+\cos\lambda_1}\cot\frac{m}{2}\lambda_1 = \frac{(\cos\lambda_2 - \cos t)\sin\lambda_2}{1+\cos\lambda_2}\cot\frac{m}{2}\lambda_2 \quad (20)$$

Antisymmetric Displacement

In this case the moment and displacement of the xth support are given by Eqs. (11) and (12), respectively, and the boundary conditions are

$$\beta M_0 + \alpha M_1 = P y_1$$

$$M_0 - M_m + mR_0L + \sum_{x=1}^{m-1} R_x(m-x)L = 0$$

Proceeding as before, we finally arrive at the equation

$$\frac{(\cos\lambda_1 - \cos t)\sin\lambda_1}{1+\cos\lambda_1}\tan\frac{m}{2}\lambda_1 = \frac{(\cos\lambda_2 - \cos t)\sin\lambda_2}{1+\cos\lambda_2}\tan\frac{m}{2}\lambda_2 \quad (21)$$

From it we can derive the buckling load of the column corresponding to antisymmetric displacement.

Buckling Load of a Column When the Stiffness of the Intermediate Supports Becomes Infinite

This is the case corresponding to a column with equal-spaced intermediate rigid supports. From Eq. (7), as S approaches infinity

$$\cos\lambda_1 = -\infty$$

$$\cos\lambda_2 = -\frac{\sin t - t\cos t}{t - \sin t}$$

hence, λ_1 is imaginary and is equal to $\pi + (i)(\infty)$. From Eq. (20)

$$\cot(m/2)\lambda_2 = \infty$$

therefore

$$\lambda_2 = \frac{2n\pi}{m}, \qquad n = 1, 2, 3 \ldots m \quad (22)$$

From Eq. (21)

$$\tan(m/2)\lambda_2 = \infty$$

therefore

$$\lambda_2 = (2n+1)\pi/m, \qquad n = 0, 1, 2, \ldots (m-1) \quad (23)$$

Eqs. (22) and (23) can be combined into one equation

$$\lambda_2 = n\pi/m, \qquad n = 1, 2, \ldots m$$

hence,

$$\cos\lambda_2 = \cos\frac{n\pi}{m} = -\frac{\sin t - t\cos t}{t - \sin t}$$

For a column with built-in ends the smallest buckling load is obtained by setting n equal to $(m-1)$ in the above equation:

$$\frac{\sin t - t\cos t}{t - \sin t} = \cos\frac{\pi}{m} \quad (24)$$

Some solutions of Eq. (24) are given in Table 1.

TABLE 1

m	1	2	3	4	5	6	∞
t	2π	4.49	3.86	3.57	3.43	3.35	π

One Intermediate Support ($m = 2$)

In the case of symmetric displacement, we have, from Eq. (20),

$$\frac{\cos\lambda_1 - \cos t}{1+\cos\lambda_1}\cos\lambda_1 = \frac{\cos\lambda_2 - \cos t}{1+\cos\lambda_2}\cos\lambda_2$$

Simplifying by Eq. (7),

$$\frac{(A - 2\cos t)\cos\lambda_1 - (B - 1)}{1 + \cos\lambda_1} = \frac{(A - 2\cos t)\cos\lambda_2 - (B - 1)}{1 + \cos\lambda_2}$$

or

$$(A + B - 1 - 2\cos t)(\cos\lambda_1 - \cos\lambda_2) = 0$$

Since $\cos\lambda_1$ is not equal to $\cos\lambda_2$,

$$A + B - 1 - 2\cos t = 0$$

Solving for S,

$$S = \frac{t^3}{[(t/2) - \tan(t/2)]} \qquad (25)$$

In the case of antisymmetric displacement, we have, from Eq. (21),

$$\frac{\cos\lambda_1 - \cos t}{1 + \cos\lambda_1}\sin\lambda_1\tan\lambda_1 = \frac{\cos\lambda_2 - \cos t}{1 + \cos\lambda_2}\sin\lambda_2\tan\lambda_2$$

or

$$\frac{1}{\cos\lambda_1}(\cos\lambda_1 - \cos t)(1 - \cos\lambda_1) = \frac{1}{\cos\lambda_2}(\cos\lambda_2 - \cos t)(1 - \cos\lambda_2)$$

Simplifying by Eq. (7),

$$(B - 1 - 2\cos t)(\cos\lambda_1 - \cos\lambda_2) = 0$$

Since $\cos\lambda_1$ is not equal to $\cos\lambda_2$,

$$(S/t^3)(\sin t - t\cos t) = 0 \qquad (26)$$

t is then a constant.

Both Eqs. (25) and (26) are plotted in Fig. 2. There is a transition point when S is 25.5. For S less than 25.5, the displacement at buckling is symmetric with respect to the midpoint of the column; for S greater than 25.5, the displacement is antisymmetric.

Column with Two Intermediate Supports ($m = 3$)

Proceeding as in the case of one support, from Eq. (20)

$$[(t - \sin t) - (\sin t - t\cos t)][2(\sin t - t\cos t) - (t - \sin t)](S/t^3)^2 + [(5 + 6\cos t)(t - \sin t) - (9 + 10\cos t)(\sin t - t\cos t)](S/t^3) - 4(1 + \cos t) \times (1 + 2\cos t) = 0 \qquad (27)$$

From Eq. (21)

$$[2(\sin t - t\cos t)^2 - t(1 - \cos t)(t - \sin t)](S/t^3)^2 + [4(1 + \cos t)(\sin t - t\cos t) + 2(t - \sin t) + t(1 - \cos t)(1 + 2\cos t)](S/t^3) = 0 \qquad (28)$$

The numerical values calculated from Eqs. (27) and (28) show that for the whole range of S the buckling load of the column is given by Eq. (27). This means that the displacement is always symmetric at buckling. Eq. (27) is plotted in Fig. 3.

Three Intermediate Supports ($m = 4$)

Proceeding as before, from Eq. (20)

$$[(\sin t - t\cos t) - (t - \sin t)](\sin t - t\cos t)(S/t^3)^2 + [(3 + 4\cos t)(\sin t - t\cos t) - \cos t(t - \sin t)] \times (S/t^3) + 2\cos t(1 + \cos t) = 0 \qquad (29)$$

From Eq. (21)

$$[2(\sin t - t\cos t)^2 - (t - \sin t)^2](S/t^3)^2 + (\sin 2t - 2t\cos 2t)(S/t^3) = 0 \qquad (30)$$

They are plotted in Fig. 4. In this case, there is again one transition point at which the type of displacement changes.

Asymptotic Expression

To calculate the buckling load of a column with built-in ends and $(m - 1)$ intermediate supports, an equation of $\frac{1}{2}m$th or $\frac{1}{2}(m + 1)$th degree (depending on whether m is even or odd) should be solved. But if m approaches infinity, the buckling load may be found in the following manner. As m becomes large, corresponding to a given S, the buckling loads calculated from Eqs. (20) and (21) should approach each other; as m becomes infinite, they should be equal. Hence from Eqs. (20) and (21), we have, as m approaches infinity,

$$\tan^2(m/2)\lambda_1 = \tan^2(m/2)\lambda_2$$

This is satisfied if the roots of Eq. (7) are equal. Consequently,

$$A^2 - 8(B - 1) = 0$$

or

$$(t - \sin t)^2(S/t^3)^2 - 4(1 - \cos t)(t + \sin t)(S/t^3) + 4(1 - \cos t)^2 = 0 \qquad (31)$$

This equation is identical to Eq. (18). As stated before, the value of t given by this equation reaches its maximum when S is equal to $4\pi^2$. At that value of S, the deflection of all supports may be shown to be zero and the column buckles with the supports as node points. If S is larger than $4\pi^2$, by the principle of least work, it is reasonable to assume that the buckling form will not be different from that when S is $4\pi^2$.* Conse-

* In case the displacement form at buckling changes when S is larger than $4\pi^2$, the number of half waves in the new form must be larger than that in the old one. Consequently, the strain energy stored in the column is increased. At the same time, as the supports are deflected, additional strain energy is stored in them. This is contradictory to the principle of least work. Therefore the buckling form remains unchanged if S is greater than $4\pi^2$.

(*Continued on page 75*)

Design of Elbows in Potential Motion

BOLESŁAW SZCZENIOWSKI*

École Polytechnique, Montreal

ELBOWS WITH A CIRCULAR CURVATURE, in general use today, are, no doubt, causing certain losses of energy manifested by a decrease of pressure. In case of ordinary steam, water, or air pipe lines, these losses can be considered as admissible because of the simplicity of construction and low manufacturing cost obtained through the use of ordinary elbows with a circular curvature. The case is different when it comes to shaping elbows of extremely large dimensions meant for the transfer of a large quantity of fluid, as, for instance, in the case of pipe lines for large water turbines where the construction of the duct is bound to be a complicated one. In such a case the shaping of the elbows in accordance with certain theoretic considerations should not raise the manufacturing cost, yet there will be a considerable advantage in the reduction of losses of potential energy in the functioning of the turbine.

The shaping of wind tunnels is a different problem. In that case it is important to obtain, after the turn, an even stream of fluid, free from vortexes and having a velocity as uniform as possible throughout the cross section. Here the shaping of the elbows with the hydrodynamic equation of continuity of the fluid in view seems to be particularly indicated.

The purpose of this study is the solution of the problem of the shaping of elbows in such a way as to fulfill the equation of continuity of the fluid in a two-dimensional flow:

$$(\partial^2\Psi/\partial x^2) + (\partial^2\Psi/\partial y^2) = 0$$

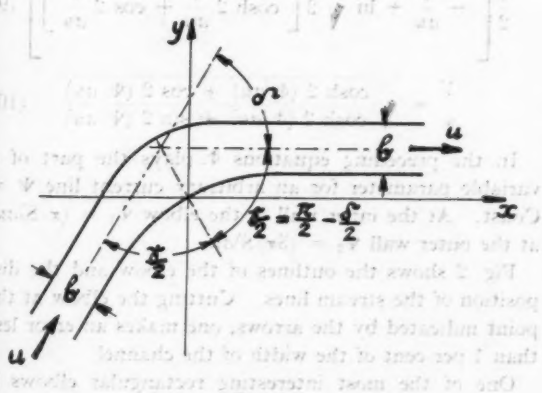

FIG. 1.

where Ψ = Const. designates the stream lines and x, y are rectangular coordinates. The elbows thus obtained may have a rectangular cross section as well as a circular one, or, for that matter, any outline representing a closed line, provided the stream velocity u remains uniform before and after the bend. In a more general case where the velocity after the bend is different (corresponding to su, where $s \neq 1$), the cross section of the elbow can be rectangular only because of the two-dimensional character of the motion. In the present study the solution for a quite arbitrary angle δ is given (Fig. 1).

BOUNDARY CONDITIONS; THE FORM OF COMPLEX POTENTIAL

We will limit ourselves to the stationary, two-dimensional motion of an ideal incompressible fluid. Suppose that a two-dimensional stream, having a width b and uniform velocity u, is deflected from its original direction at an angle δ and, after the deflection again becomes a stream having the width b and uniform velocity u. That condition is strictly fulfilled only when the stream before and after the deflection is approaching uniform and rectilinear motion asymptotically. We also assume that the elbow is symmetric with respect to the bisector of the angle $\gamma = \pi - \delta$.

The following form of complex potential takes into account all the above conditions:

$$e^{\left[\frac{ie^{-i(\delta/2)}}{\sin(\delta/2)}\right](z/a)} = e^{\left[\frac{ie^{-i(\delta/2)}}{\sin(\delta/2)}\right](W/au)} + e^{\left[\frac{ie^{i(\delta/2)}}{\sin(\delta/2)}\right](W/au)} \qquad (1)$$

where $z = x + iy$, $i = \sqrt{-1}$, $W = \Phi + i\Psi$, with Φ designating velocity potential; Ψ, stream function; a, any linear parameter; and u, any constant velocity (the velocity of a uniform stream in infinite).

VELOCITIES

In a potential motion expressed by the equation $z = F(W)$ the component velocities v_x, v_y are defined from the equation $v_x - iv_y = 1/F'$, where F' represents the derivative of F. The total velocity is $V = \sqrt{v_x^2 + v_y^2}$.

The following two conditions are imposed: (1) The total velocity V should at no point of the flow exceed the boundary value u—that is, $V \leq u$; (2) no stream line should have singular points. The latter condition

Received March 1, 1943.

* Agrégé Professor.

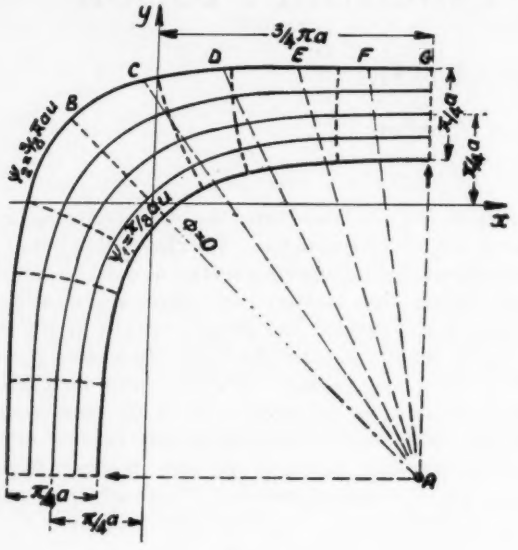

FIG. 2.

is identical with the condition that the velocity V should not reach the singular values (0 or ∞).

The extremes of V are obtained from the condition

$$\text{real part}\left|\frac{F'}{F''}\right| = 0 \tag{2}$$

If it is desired to consider the condition $V \leq u$, put:

$$(n\pi) + \frac{\pi}{2} + \frac{\delta}{4} \geq \frac{\Psi}{au} \geq \frac{\delta}{4} + (n\pi) \tag{3}$$

The third and last condition imposed is to avoid inflection points on any stream line within the elbow.

The condition of inflection of a given stream line $\Psi = \text{Const.}$ is $d^2y/dx^2 = 0$, which is identical with the condition

$$\text{imaginary part}\left|\frac{F''}{F'}\right| = 0 \tag{4}$$

Applied to potential (1), two conditions are obtained to avoid inflection points, of which the following one is more convenient since, it gives broader limits for Ψ:

$$(n\pi) + \frac{\delta}{4} - \frac{\pi}{4} \leq \frac{\Psi}{au} \leq \frac{\delta}{4} + \frac{\pi}{4} + (n\pi) \tag{5}$$

Considering at the same time condition (3) and assuming that $n = 0$:

$$\frac{\delta}{4} \leq \frac{\Psi}{au} \leq \frac{\delta}{4} + \frac{\pi}{4} \tag{6}$$

Consider the delineations of the walls of the elbows, where $\Psi_1 = (\delta/4)au$ and $\Psi_2 = [(\delta/4) + (\pi/4)]au$.

In the particular case when $\delta = 180°$ the upper limit should be slightly lower then Ψ_2 as it reaches the infinite.

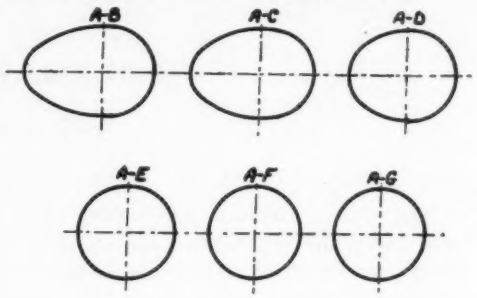

FIG. 3.

RECTANGULAR ELBOW

A case particularly interesting from the technical standpoint is $\delta = 90°$, or

$$e^{(i+1)(z/a)} = e^{(i+1)(W/au)} + e^{(i-1)(W/au)} \tag{7}$$

which will give

$$\frac{x}{a} = \frac{1}{2}\arctan\left[\frac{\cot\frac{\Psi}{au} + \cot\frac{\Phi}{au}\tanh\frac{\Phi}{au}}{\cot\frac{\Phi}{au}\cot\frac{\Psi}{au} - \tanh\frac{\Phi}{au}}\right] + \frac{1}{2}\left[-\frac{\Psi}{au} + \ln\sqrt{2\left(\cosh 2\frac{\Phi}{au} + \cos 2\frac{\Psi}{au}\right)}\right] \tag{8}$$

$$\frac{y}{a} = \frac{1}{2}\arctan\left[\frac{\cot\frac{\Psi}{au} + \cot\frac{\Phi}{au}\tanh\frac{\Phi}{au}}{\cot\frac{\Phi}{au}\cot\frac{\Psi}{au} - \tanh\frac{\Phi}{au}}\right] - \frac{1}{2}\left[-\frac{\Psi}{au} + \ln\sqrt{2\left[\cosh 2\frac{\Phi}{au} + \cos 2\frac{\Psi}{au}\right]}\right] \tag{9}$$

$$\frac{V}{u} = \sqrt{\frac{\cosh 2\,(\Phi/au) + \cos 2\,(\Psi/au)}{\cosh 2\,(\Phi/au) + \sin 2\,(\Psi/au)}} \tag{10}$$

In the preceding equations Φ plays the part of a variable parameter for an arbitrary current line $\Psi = \text{Const.}$ At the inner wall of the elbow $\Psi_1 = (\pi/8)au$; at the outer wall $\Psi_2 = (3\pi/8)au$.

Fig. 2 shows the outlines of the elbow and the disposition of the stream lines. Cutting the elbow at the point indicated by the arrows, one makes an error less than 1 per cent of the width of the channel.

One of the most interesting rectangular elbows is the one destined for a pipe line of a circular cross section. The shape of any desired cross section of such an elbow is easily determined by the condition that the stream lines that formerly were on the walls

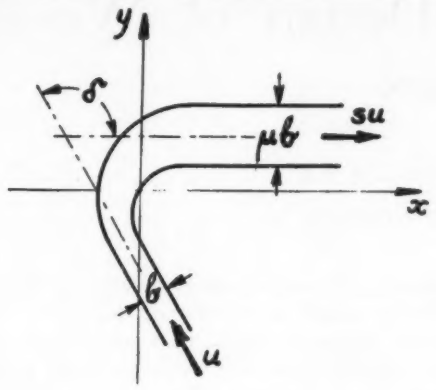

FIG. 4.

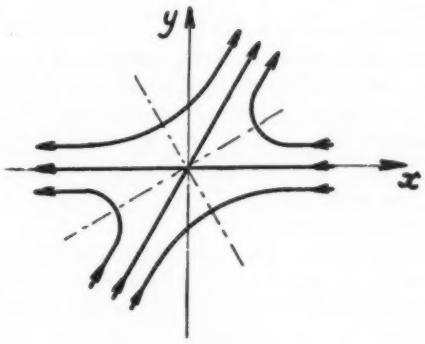

FIG. 5.

of the straight circular pipe should remain afterward on the walls of the elbow, while the motion remains flat. The cross sections thus determined ($\overline{AB}$, $\overline{AC}$, $\overline{AD}$, $\overline{AE}$, $\overline{AF}$, $\overline{AG}$) (see Fig. 2) are given on Fig. 3.

GENERALIZATION: VELOCITY RATIO $s \neq 1$

In this case the two-dimensional stream with uniform velocity u becomes, after deflection at any desired angle δ, a stream with the uniform velocity $su = u/\mu$ (Fig. 4). The complex potential here will be:

$$e^{\left[\frac{ie^{-i(\delta/2)}}{\sin(\delta/2)}\right](z/a)} = e^{\left[\mu\frac{ie^{-i(\delta/2)}}{\sin(\delta/2)}\right](W/au)} + e^{\left[\frac{ie^{i(\delta/2)}}{\sin(\delta/2)}\right](W/au)} \qquad (11)$$

ELBOWS WITH STRAIGHT OUTER WALLS

In order to obtain elbows with straight outer walls (Fig. 5), the following form of complex potential may be used:

$$\cosh\left\{\left[\frac{ie^{-i(\delta/2)}}{\sin(\delta/2)}\right]\left(\frac{z}{a}\right)\right\} = e^{i(W/au)\cot(\delta/2)}\cosh\left(\frac{W}{au}\right) \qquad (12)$$

The reader will easily find a certain analogy of this form with the solution given by Milne-Thomson.[1]

REFERENCE

[1] Milne-Thomson, L. M., *Theoretical Hydrodynamics*, p. 286; The Macmillan Company, London, 1938.

(*Continued from page 72*)

quently, t remains constant and equal to π for S larger than $4\pi^2$. Therefore the asymptotic expressions are identical to those for a column with simple supported ends. This is a logical result because the conditions at the ends of a long column with intermediate supports have negligible effects on the buckling load of the column.

REFERENCES

[1] Klemperer, W. B., and Gibbons, H. B., *Über die Knickfestigkeit eines auf elastischen Zwischenstützen gelagerten Balkens*, Z.A.M.M., Vol. 13, p. 251, 1933.

[2] Niles, A. S., and Newell, J. S., *Airplane Structure*, Vol. 2, p. 105; John Wiley & Sons, Inc., New York, 1938.

[3] von Kármán, Th., and Biot, A. B., *Mathematical Methods in Engineering*, p. 439; McGraw-Hill Book Company, Inc., New York, 1940.

Stress Problems in the Design of Wooden Airplanes

ZBIGNIEW KRZYWOBLOCKI*
Polytechnic Institute of Brooklyn

SUMMARY

Stress problems in wood design encountered in previous years are presented. Starting with the difficulties of the mutual interaction between wood and plywood, the problems of the strength/weight ratio and of brittleness and vibration are discussed. The paper concludes with an analysis of the present state and the probable future development of the construction of wood airplanes.

SYMBOLS

δ	= elongation
P_1	= load on the part of the beam made from material 1
P_2	= load on the part of the beam made from material 2
L_1	= length of the part of the beam made from material 1
L_2	= length of the part of the beam made from material 2
A_1	= cross-section area of the part of the beam made from material 1
A_2	= cross-section area of the part of the beam made from material 2
E	= modulus of elasticity
W	= total load
σ_t	= tension stress
M_1, M_2	= partial bending moments taken by one or another part of the beam
M	= total bending moment
σ_{b1}, σ_{b2}	= bending stresses
I_1, I_2	= partial moduli of inertia of a beam composed of two materials
r	= radius of curvature of a deflected beam
θ	= angle of twist per unit length
M_{t1}	= torque acting on the part of the beam consisting of material 1
M_{t2}	= torque acting on the part of the beam consisting of material 2
G_1, G_2	= moduli of rigidity
I_{p1}, I_{p2}	= polar moduli of inertia
$\tau_{max.\,1}$, $\tau_{max.\,2}$	= shearing stresses on the outside diameters
d_1, d_2	= outside diameters of solid and hollow cylinders
γ	= specific weight

INTRODUCTION

THE PURPOSE OF THIS PAPER is to present the stress problems the author met in wood aircraft design in previous years in European aircraft companies and research institutes and the resulting trend in such development. This presentation is based entirely on the experiences gained in actual wood design and research involving full-scale static tests of various wooden wings, including those of a bomber, and the analysis of various aircraft accidents. The ideas contained are an extension of opinions expressed by the author some time ago.[1, 2]

The discussion first deals with the interaction of two materials with different elastic properties in tension, bending, and torsion. It is assumed that the two materials are ideally connected together and that there is no sliding between them. The interaction of two materials having different elastic properties is considered to be best when both materials simultaneously reach their ultimate stresses.

It is shown that the stresses are distributed in accordance with the moduli of elasticity or rigidity and that greater stresses are taken by the material with the greater modulus of elasticity or rigidity if the deflections and deformations are the same for both materials. In structures of ordinary wood (hereafter referred to as wood) and plywood, there is no interaction between these materials. That is one reason why wooden structures are not lighter than metal structures. With regards to the strength/weight ratio the average value of the strength/weight ratios in tension and compression may be accepted. That is another reason why wooden structures are not lighter than metal structures.

Probably the most vital problem in wood construction is the brittleness of wood and plywood. The great internal damping of wood probably causes the "explosive" type of vibrations sometimes vividly described by pilots of wooden airplanes. To add to this picture, the proper joining of plywood sheets is not yet satisfactorily solved for commercial production.

A short review of existing types of wooden airplanes follows. Then an overall picture is presented of the various types of construction of wings and fuselages in all-wood airplanes and in mixed construction airplanes, with special emphasis on commercial and military applications.

BEAM OF TWO DIFFERENT MATERIALS IN TENSION

Assume a beam composed of two different materials. The two materials are ideally connected together and there is no sliding between them. Also assume that the

Received April 14, 1943.
* Instructor.

beam is in tension and that the elongations of both materials are the same.

$$\delta = P_1L_1/A_1E_1 = P_2L_2/A_2E_2 \quad (1)$$

$$P_1 + P_2 = W \quad (2)$$

After some transformation:

$$P_1 = \left(\frac{L_2A_1E_1}{L_1A_2E_2 + L_2A_1E_1}\right)W \quad (3)$$

$$P_2 = \left(\frac{L_1A_2E_2}{L_1A_2E_2 + L_2A_1E_1}\right)W \quad (4)$$

Assuming the length is the same for both parts of the beam, then:

$$P_1/P_2 = A_1E_1/A_2E_2 \quad (5)$$

or

$$\sigma_{t1}/\sigma_{t2} = E_1/E_2 \quad (6)$$

Therefore, in the case of the interaction of two materials, both of the same length, composing a beam in tension, the tension stresses are distributed in proportion to the moduli of elasticity.

Beam of Two Different Materials in Bending

Assume a beam in bending composed of two different materials, ideally connected together. The deflections of both materials are the same so that the beam works as one whole. There is no sliding between the materials and the radius of curvature for each point of surface of connection is the same.

$$M = M_1 + M_2 \quad (7)$$

$$M_1 = E_1I_1/r \quad (8)$$

$$M_2 = E_2I_2/r \quad (9)$$

$$M_1/M_2 = E_1I_1/E_2I_2 \quad (10)$$

Assuming that the heights of the cross sections of both materials are the same,

$$\sigma_{b1}/\sigma_{b2} = E_1/E_2 \quad (11)$$

In the case of interaction of two materials composing a beam in bending, the bending stresses are distributed again in proportion to the moduli of elasticity. For a more detailed derivation of the above equations, refer to works treating the subject of strength of materials.[3, 4]

Beam of Two Different Materials in Torsion

Assume a beam in torsion composed again of two different materials, ideally connected together. There is no sliding between the materials. The angle of twist is the same for both parts of the beam. One material composes the solid core; and other, a hollow cylinder around the solid core.

$$\theta = M_{t1}/G_1I_{p1} = M_{t2}/G_2I_{p2} \quad (12)$$

$$\tau_{max.\,1} = M_{t1}d_1/2I_{p1} \quad (13)$$

$$\tau_{max.\,2} = M_{t2}d_2/2I_{p2} \quad (14)$$

From the above,

$$(M_{t1}/I_{p1}) : (M_{t2}/I_{p2}) = G_1/G_2 \quad (15)$$

$$\tau_{max.\,1}/\tau_{max.\,2} = (M_{t1}d_1/I_{p1}) : (M_{t2}d_2/I_{p2}) \quad (16)$$

Assuming a special case of the distribution of the torque on two beams having the same circular cross section, ideally connected together and acting parallel,

$$\tau_{max.\,1}/\tau_{max.\,2} = (M_{t1}/I_{p1})(M_{t2}/I_{p2}) = G_1/G_2 \quad (17)$$

Similarly, for two beams having the same rectangular section,

$$\tau_{max.\,1}/\tau_{max.\,2} = G_1/G_2 \quad (18)$$

Therefore, in case of the interrelation of two materials, having the same cross section, composing a beam in torsion, the shear stresses are distributed in proportion to the moduli of rigidity.

Application to Wooden Structures

In the case of an airplane consisting of wood and plywood, of plastic wood and wood, or of any other combination of the above-mentioned materials, there is a condition of the interaction of two materials having various elastic properties. From the derived elementary equations, the greater stresses are taken by the material having the greater moduli of elasticity and rigidity, provided the deformations and deflections are the same for both materials. Table 1 gives the moduli of elasticity for some kinds of wood and plywood.[5]

Table 1

Kind of Wood	Modulus of Elasticity of Wood Parallel to Grain, E, Lbs. per Sq.In.	Modulus of Elasticity of Plywood (Three Plies) Parallel to Direction of the Grain of the Faces, E, Lbs. per Sq.In.
Hard Woods		
Ash, black	1,340,000	1,073,000
Ash, white	1,460,000	1,420,000
Bass wood	1,250,000	1,213,000
Beech	1,440,000	2,149,000
Birch	1,780,000	2,259,000
Hickory	1,860,000	1,704,000
Mahogany, African	1,280,000	1,261,000
Mahogany, true	1,260,000	1,252,000
Poplar, yellow	1,300,000	1,544,000
Soft Woods		
Douglas fir	1,700,000	1,566,000
Pine, northern white	1,140,000	1,274,000
Spruce	1,300,000	1,395,000

Modulus of Elasticity

These values represent, of course, the average values for various kinds of wood. Some investigators obtained different values of E in tests of wood or plywood specimens.[6] In any case, it is seen there there are sometimes considerable differences in E between wood and plywood made from the same wood. At the same time the strength of plywood (three plies or five plies) parallel to the direction of the grain of the faces is less than the strength of wood parallel to grain, sometimes about 30 to 33 per cent.[7] It is also difficult to obtain a good combination of two materials whose interaction will answer the problems met in wing design as well as in fuselage design. Still another quality must be taken into account—namely, that the value of the modulus of elasticity for plywood depends on the angle between the direction of grain of the faces and the acting load. It is possible to obtain such a curve experimentally[6, *] and theoretically.[8, 9, 11] Both the tests and the theoretic calculations showed that, on an average, the value of E for plywood varies considerably with the above-mentioned angle. In design the plywood is usually put at the angle 0° or 45° between the direction of grain of the faces of plywood and the direction of grain of wood. The opinion is usually held that the plywood has the greatest modulus of rigidity when the grain is inclined at the angle of 45°. In both cases when the angle equals 0° or 45°, there is no interaction between plywood and wood. The modulus of elasticity of plywood, when the angle between the direction of grain of faces and applied load equals 45°, is much smaller than the modulus of elasticity of wood parallel to the grain. One part of the construction takes only bending; another, only shearing. This is probably the chief reason why wooden construction is not lighter than metal construction. When one uses plywood having a higher E than wood, greater stresses are taken by the plywood, which may fail prematurely.† The problem of proper interaction between plywood and wood could be solved eventually by putting the plywood at a special angle, but this would not be economical with present plywood panels. Another approach is to make the modulus of elasticity of plywood equal to that of wood by producing a plywood having more equal values of E in all directions, although in both those cases one may have the differences between the values of moduli of rigidity for both materials. But this problem is less important because shearing is usually taken only by one material—i.e., plywood. On the contrary, bending should be taken by both materials. The Research Institutes in Germany tried some years ago to create a plywood having more uniform elastic properties by laying plies at angles of 30° and even 15° (similar to a star) to make plywood a more homogeneous material than it is now in commercial use. The results obtained were promising.

Modulus of Rigidity

Similar remarks regarding the modulus of elasticity might be applied to the modulus of rigidity, although, as mentioned above, this problem is less important in designing. For example, the modulus of rigidity for spruce wood equals 84,000 lbs. per sq.in.; spruce plywood at 45°, 420,000 lbs. per sq.in. At the same time the maximum shearing stress for spruce wood equals about 1,000 lbs. per sq.in. and for spruce plywood at 45° equals about 2,370 lbs. per sq.in. It has already been noted that the plywood has the greatest modulus of rigidity when the grain is inclined at 45°. This opinion should be revised because some tests showed that the modulus of rigidity passes through a definite maximum at about 60°.[6] Of course, this fact again complicates the whole problem. A discussion of premature failures of wings and leading edges, consisting of combinations of various wood and plywood, having different elastic properties, during static tests, is given in reference 21.

Problems of this kind, met with in the design of airplanes made from plywood and ordinary wood, probably caused the development of various processes to produce from wood a more homogeneous material. Here one may include plastic wood, molded wood and plywood, Duramold, Vidal process, Skyply, and so on. Of course, if a designer wishes to combine in a design molded wood and ordinary wood and if both materials possess various elastic properties, the problems mentioned above are always present. Some values of the elastic constants of Duramold and Skyply have already been published.[20] The elastic properties of plastic and molded wood and plywood are high, sometimes even higher than those of metal.[20, ‡] The future of wood aircraft structures using these materials is promising.

Strength/Weight Ratio

Very often the high value of strength/weight ratio in tension for wood is cited as a proof of the superiority of wood in comparison to metal from a design point of view. But at the present time the strength/weight ratio is not considered in all circles as a characteristic value of a material. In the case of wood it would be necessary to take an average value from the strength/weight ratios in tension and in compression. The comparison would tend to show that wood has no advantage over metal in the weight of aircraft structures. In Table 2 the values of ultimate tensile strength/specific gravity ratios for various materials are given.[7] Included also are values of strength/weight ratios according to the

* See German literature on the subject of wood tests in the years from 1935, especially papers of Dr. Kraemer.

† This fact was observed during a full-scale static test of a bomber's wing.

‡ Concerning the elastic constants of various kinds of wood and plywood, it must be kept in mind that, especially for wood and plywood, the results obtained from tests of small specimens cannot be transferred directly to full-scale airplanes. The results obtained from these tests are usually too conservative.

TABLE 2*

Material	Ultimate Tensile Strength, Lbs. per Sq.In.	Specific Gravity	Ultimate Tensile Strength/Specific Gravity	Strength/Weight (Author's Assumption)
Normal plywood:				
Birch or beech	13,200	0.67	19,700	15,300
Philippine mahogany	10,670	0.53	20,500	15,900
Spruce	5,600	0.43	13,000	10,100
High density plywood:				
Birch or beech	28,500	0.97	29,400	22,800
Philippine mahogany	20,000	0.95	21,100	16,400
Steel—heat-treated	100,000	7.75	12,900	....
	125,000	7.75	16,100	....
	150,000	7.75	19,300	....
	175,000	7.75	22,600	....
Aluminum—various alloys	40,000	2.81	14,200	....
	50,000	2.81	17,800	....
	60,000	2.81	21,400	....

* It is difficult to find in the literature values of ultimate compressive strength for plywood. The author assumes that the ultimate compressive strength equals 0.55 ultimate tensile strength. Also, according to these assumptions:

$$\frac{\text{Strength}}{\text{weight}} = \frac{\text{ultimate tensile strength } (1 + 0.55)}{2 \times \text{specific gravity}} = 0.775 \frac{\text{ultimate tensile strength}}{\text{specific gravity}}$$

High density plywood is not yet used in aviation. As is seen, plywood has no advantage in comparison to metals.

author's assumption. It is seen again from this that wood constructions are not lighter than metal constructions, particularly when taking into account the thin airfoils of modern airplanes. In fact, the considerations of some authors tend to prove that, at small wing thickness/chord length ratios, metal is better than wood because a lighter wing can be obtained.[3]

Some calculations treating wood and plywood as homogeneous materials show results that appear to be more favorable to wood.[22] These results, however, should be used with caution unless checked by exhaustive experiments. The structural weight of modern plywood shells may be made less to some degree, and some papers show good agreement between theoretically predicted and experimentally realized buckling load.[23] Some investigators apply different weight ratios for various conditions of stress.

BRITTLENESS

Materials are usually spoken of as ductile or brittle depending on how much permanent deformation takes place before fracture. But sometimes the opinion is held that brittle materials may, under special mechanical conditions, be brought into the plastic state. Perhaps the most widely accepted opinion is that it is more correct to speak of the brittle or plastic state of materials rather than of brittle or ductile materials.[12] If the material has a high modulus of elasticity, is stressed in tension, and does not deform permanently to any considerable extent before fracture, it is termed "brittle."†

In any case, the fact that wood, plywood and all plastics and molded woods are brittle materials which cannot compete with metals in the field of plasticity must be taken into account. If one can introduce an idea of "airplane brittleness" as a whole, it is evident that a part will be played by the climate of a country, the condition of the airfields, etc. The problem may be important, particularly in the design of the fuselage of a military airplane. Very often small cracks are observed on wooden fuselages after hard landings.

The problem of the influence of holes is closely connected with brittleness. Here the factor of stress concentration is important. The stress distribution, especially beyond the proportionality limit, depends on the ductility of the material. A ductile material can be subjected to considerable stretching beyond the yield point without great increase in stress. But in the case of a brittle material a weakening effect of any hole or notch may be observed, and points of stress concentration may have a great influence on the whole structure.[4] Concerning the possibility of the appearance of great stress concentration around holes one should take into account a case of a "hard landing." In the well-known accident to the "de Havilland Albatross," which was carefully stress-analyzed, the plane broke between the window and door because of an unexpected stress concentration. The brittleness of wood is perhaps the most vital problem in wood construction.‡

† An opinion expressed by Dr. A. Nádai in a letter to the author.

‡ There were many crashes of the French fighter "Spad" in the period after the first World War. The airplane was made entirely of wood and the fuselage was pure monocoque. The crashes took place after some years of peacetime service, and in typical cases the fuselage broke during take-off on a dry airfield during hot summer or after an unexpected flutter developed in the air, although the flutter was never before observed on this airplane. In the defense of the airplane it is necessary to mention that it was glued with casein and was in service some years.

The importance in avoiding stress concentration is also emphasized by other authors.[21] With this fact is closely connected the increase in the weight of a wood airplane because of the use of extra material required near fittings.

Vibration

The opinion is often held that wood is an excellent material in its resistance to vibration. This opinion is true to some degree. Recently, some computations of the writer showed that with respect to wing flexural oscillations and wing torsional oscillations the decisive factors, from a material standpoint, are the ratios E/γ and G/γ.[13, 14] By applying these expressions, plywood and even Duramold do not show up so well as aluminum alloys, magnesium alloys, and steel. From this point of view, wood cannot be classified an excellent material. Wood possesses a great internal damping, but again the question must be critically examined. When the vibration producing forces are not great, a wooden element will show excellent qualities. But when great exciting forces act, there can arise in a wooden element a sudden vibration in an "explosive" manner. With increase of speed the amplitude of oscillation also increases. At the critical speed the amplitude reaches the highest value. The relation between oscillation and speed can be expressed as a curve. The value of internal damping will exert an influence on the slopes of that curve and also on the value of the critical speed. The first influence will be much greater and the great internal damping of wood is believed to have such an influence on the shape of the curve that at first the slope of the curve is small and later suddenly increases, causing the "explosive" vibration. By comparison, the slope of the curve for a metal element increases progressively. The above opinion is based on observations of failure in flight of wooden and mixed construction airplanes due to flutter. It is quite understandable that the "explosive" type of vibration is more dangerous because there is no warning to the pilot.* The author has calculated, in accordance with theoretic assumptions, that great damping may cause an "explosive" type of wing vibration.

Joining of Plywood Sheets

It is common practice to join plywood sheets with a 1:12 or 1:15 scarfed joint. In preparing the plywood panels for a scarf joint, the joint surface with its bevel of 1:12 consists of strips of wood alternating with strips of the resin adhesive that is used as the bonding agent for the plywood sheets. These strips of resin adhesive do not glue well to the opposing joint surface. Therefore, we have scarf joints with weak zones, producing a joint whose strength is 80 per cent of normal[15] as compared to the strength of the plywood. These joints represent weak points in the whole wood construction and create a new stress problem, especially from the standpoint of vibration.

Design of Wooden Airplanes

Taking into consideration the total weight of an air plane and its wing loading as the most characteristic values, Tables 3, 4, and 5, based on available references,[16, 17] give a general view of wood design, particularly with respect to the construction of the fuselage and wing in relation to the total weight and wing loading. The following conclusions can be drawn:

The Airplane as a Whole

(1) All-wood airplanes are produced up to 36,000 lbs. of total weight and 35 lbs. per sq.ft. of wing loading. (In contrast, there are today metal planes of 80 tons weight.)

(2) The general application of all-wood airplanes is for commercial and cargo uses rather than military uses.

(3) Plywood and wood are applied in landplanes up to about 20,000 lbs. total weight and in seaplanes on floats up to about 36,000 lbs. These materials are suitable because in seaplanes there is no shock on the fuselage during taxiing and "watering" (landing).

(4) The biggest all-wood airplanes are produced by special construction (plastic wood, various processes, etc.).

(5) Mixed construction with wooden wings is used up to about 38,000 lbs. total weight and up to about 38 lbs. per sq.ft. wing loading.

(6) Mixed construction is applied generally to commercial, cargo, and military planes. In military airplanes with wooden wings, the tendency is to apply wooden wings to fighters and medium bombers (having a greater load factor) rather than to long-range heavy bombers having a smaller load factor.

The Wooden Fuselage

(1) Longerons and frame construction are used in small and medium airplanes up to 20,000 to 22,000 lbs. total weight. This type is used for landplanes, both commercial and military.

(2) For larger airplanes, semimonocoque and monocoque plywood construction is used. This construction is used mostly for seaplanes on floats for commercial and military purposes. This type of construction is less resistant to shocks than the longeron-frame construction.

*An interesting case in the support of the idea of the "explosive" type of flutter was the crash of the prototype of a bomber of mixed construction, caused probably by this type of vibration. Unfortunately, the entire crew was killed so there is no positive confirmation of this explanation of the crash. In another case, a sudden buffeting in diving of all-wood tail surfaces of the prototype of a military two-seater airplane of mixed construction resembled the "explosive" type of vibration. The airplane disintegrated in the air.

TABLE 3

All-Wood Airplanes and Mixed Construction Airplanes with Wooden Wings

Material	Type of Construction	Type of Airplane	Total Weight, Lbs.	Wing Loading, Lbs. per Sq.Ft.
All-wood airplanes	Plywood and ordinary wood	Gliders	....	...
		Private and commercial landplanes	10,250	19.80
		Commercial amphibians	15,950	21.45
		Commercial flying boats	16,830	20.55
		Commercial seaplanes on floats	23,100	25.42
		Transoceanic seaplanes on floats	35,200	35.00
		Bombers—landplanes	20,350	32.00
		Bombers—seaplanes on floats	27,080	28.90
	Special constructions: plastic wood, molded wood, Vidal process, Duramold, etc.	Private landplanes	2,400	15.80
		Commercial and cargo airplanes (de Havilland Albatross, Curtiss Caravan); reconnaissance bomber (Mosquito); trainers	29,500	27.40
Mixed construction	Steel tube fuselage and wooden wings	Private, commercial and cargo airplanes	37,400	29.30
		Torpedo bombers, reconnaissance airplanes, fighter-bombers, fighters	19,700	31.30
		Bombers	27,080	37.92

TABLE 4

Construction of Wooden Fuselages

Type of Construction	Type of Airplane	Total Weight, Lbs.	Wing Loading, Lbs. per Sq.Ft.
Longerons and frames	Gliders	....	...
	Private and commercial landplanes	10,250	19.80
	Commercial amphibians	15,950	21.45
	Commercial flying boats	16,830	20.55
	Bombers—landplanes	20,350	32.00
Semimonocoque and monocoque (plywood and ordinary wood)	Military landplanes	7,500	23.40
	Commercial seaplanes on floats	23,100	25.42
	Transoceanic seaplanes on floats	35,200	35.00
	Bombers—seaplanes on floats	27,080	28.90
Special construction: plastic wood, molded wood, Vidal process, Duramold, etc.	Private planes	2,400	15.80
	Commercial and cargo airplanes (de Havilland Albatross, Curtiss Caravan)	29,500	27.40
	Reconnaissance bomber (Mosquito)	....	...
	Trainer	....	...

TABLE 5

Construction of Wooden Wings

Type of Construction	Type of Airplane	Total Weight, Lbs.	Wing Loading, Lbs. per Sq.Ft.
1 Spar	Gliders	....	...
	Private airplanes	1,400	11.30
2 Spars	Private and commercial landplanes	11,400	18.05
	Torpedo bombers, reconnaissance, fighter-bombers, bombers, fighters	20,350	32.00
3 Spars	Commercial, transoceanic seaplanes	37,400	35.00
	Bombers	27,080	28.90
Special constructions: plastic wood, molded wood, Vidal process, Duramold, etc., spars and skin	Private airplanes	2,400	15.80
	Commercial and cargo airplanes (de Havilland Albatross, Curtiss Caravan)	29,500	27.40
	Reconnaissance bombers	....	...
	Trainers	....	...

(3) Geodetic construction until now has only been applied to small airplanes.

(4) The fuselages of big landplanes are made chiefly from plastic wood, molded wood, etc. It is also probable that this type of construction is more resistant to shock during landing.

The Wooden Wing

(1) As a rule it can be assumed that with the increase in the size of an airplane the quantity of spars will increase from one to three.

(2) Each type of wing construction is applied for both military and commercial uses.

Conclusions

(1) Wood is used today in all kinds of airplanes, both commercial and military, up to about 38,000 lbs. total weight, in all-wood construction or mixed construction.

(2) It appears that plywood-wood construction of fuselages is better applied to small and medium landplanes and to large seaplanes on floats. Plastic wood construction can best be used for large landplanes.

(3) The future of wood construction may depend on the development of plastic wood because of its more homogeneous composition. The elastic properties of plywood may be improved.

(4) Large all-wood airplanes may be designed for commercial, cargo, and training uses rather than for military combat purposes.

(5) It is probable that the future of all-wood airplanes lies in the designing of large seaplanes on floats.

(6) Wooden wings in mixed construction might be applied in the future to larger military airplanes, although at present they are applied to fighters and medium bombers.

(7) The chief stress problems in wood construction are: interaction of wood and plywood, high strength/weight ratio when compressive strength of wood is taken into account, brittleness and high factor of stress concentration, and the possibility of "explosive" type of vibration and the joining of plywood sheets.

(8) Wood design is more difficult than metal design, and systematic research is necessary.[19, 21] Strictly speaking, until now only two countries have done any systematic research in wood for use in aviation—namely, Germany and Russia. However, neither of these countries uses wood to a great degree in aircraft production. Germany has utilized wood construction in auxiliary aviation; Russia has used it for some fighters and possibly in small bombers.[18]

(9) In designing wood airplanes for long years of service, the brittleness of wood, the decreasing elastic properties of wood, and maintenance problems must all be taken into consideration.

References

[1] Krzywoblocki, Zbigniew, *Wooden Aircraft Wings*, Journal of the Association of Polish Aeronautical Engineers "Technika Lotnicza," Warsaw, May, 1938.

[2] Krzywoblocki, Zbigniew, *Wooden Fuselages*, Journal of the Association of Polish Aeronautical Engineers "Technika Lotnicza," Warsaw, June, 1938.

[3] Younger, John E., *Mechanics of Aircraft Structures*, 2nd Edition; McGraw-Hill Book Company, Inc., New York and London, 1942.

[4] Timoshenko, Stephen, *Strength of Materials*, 2nd Edition; D. Van Nostrand Company, Inc., New York, 1940–1941.

[5] ANC-5, *Strength of Aircraft Elements*, Revised Edition, Army-Navy-Civil Committee on Aircraft Requirements, U.S. Government Printing Office, Washington, 1940.

[6] Hearmon, R. F. S., *The Elastic Constants of Plywood*, Aircraft Engineering, Vol. XIV, No. 166, p. 336, December, 1942.

[7] Perry, Thomas D., *Modern Plywood;* Pitman Publishing Corporation, New York, Chicago, 1942.

[8] Gubrynowicz, Z., *Moduli of Elasticity of Alder Plywood;* Reports of the Instytut Techniczny Lotnictwa, December, 1937.

[9] Krzywoblocki, Zbigniew, "Plywood in Glider Construction," *Materials in Glider Construction*, Vol. 2; Published by the Aeronautical Institute attached to the Lwow Institute of Technology under the direction of Diploma Ingenieur Wiestaw Stepniewski, Lwow, Poland, 1938.

[10] Nichols, W., *Plastics and Aircraft*, Flight, Nos. 1760 and 1761, pp. 313–315, 342–344, September 17 and 24, 1942.

[11] Marhoefer, L. J., *Design Considerations for Plywood Structures—Part III*, Aviation, Vol. 42, No. 1, p. 150, January, 1943.

[12] Nádai, A., *Plasticity;* McGraw-Hill Book Company, Inc., New York and London, 1931.

[13] Krzywoblocki, Zbigniew, *Torsional and Aileron Flutter*, Journal of the Aeronautical Sciences, Vol. 10, No. 5, pp. 161–168, May, 1943.

[14] Krzywoblocki, Zbigniew, *The Problem of Wing Oscillation*, Aircraft Engineering Vol. XV, No. 174, pp. 234–237, August, 1943.

[15] Perry, Thomas E., *Progress in Aircraft Plywood, 1941–1942*, Aeronautical Engineering Review, Vol. 2, No. 2, p. 7, February, 1943.

[16] *Aerosphere—1939, 1940, 1941, 1942*, Edited by Glenn D. Angle; Aircraft Publications, New York, 1939–1942.

[17] *Wood Geodetics*, Aircraft Production, Vol. IV, No. 44, p. 412, June, 1942.

[18] Winter, William, *Wooden Airplanes—Why!* Air Progress, Vol. 2, No. 4, p. 12, April, 1943.

[19] Klemin, Alexander, *Problems in the Use of Plywood in Airplane Construction*, Mechanical Engineering, Vol. 69, pp. 105–109, February, 1943.

[20] Klemin, Alexander, *Moulded Shell Construction in Plywood*, Aero Digest, Vol. 42, p. 148, January, 1943.

[21] Peterson, Ivar C., *Problems in Wood Aircraft*, Paper presented at the National Aeronautic Meeting of the Society of Automotive Engineers held in New York City, April 8–9, 1943.

[22] Stepniewski, W., *Stressed-Skin Wooden Construction*, Aircraft Engineering, Vol. XV, No. 170, p. 110, April, 1943.

[23] Blumrich, S., *Ein Beitrag zur Ousbildung von Sperrholzschalen*, Luftfahrtforschung, Vol. 19, No. 9, pp. 331–337, September 20, 1941.

Blade Section Variation on Small-Scale Rotors

KENNETH RAZAK*
University of Kansas

ABSTRACT

A technique for small-scale rotor testing incorporating the use of a three-component balance, torque measurements, and stroboscopic speed measurement is described. Fifteen rotors using a related series of airfoil sections were tested. On the basis of maximum L/D, the optimum thickness ratio and the optimum camber were found to be 12 and 2 per cent, respectively. The small-scale rotors proved to be extremely sensitive to a change in both thickness and camber. Pointed or sharp-nosed sections are undesirable. It was determined that the position of maximum camber greatly influenced rotor characteristics. The center of pressure travel before and after the stall point is reflected in the pitching moments of rotors with the horizontal hinge at the axis of rotation.

SYMBOLS

The terminology and symbols used in this paper conform to those used by the N.A.C.A. as set forth in their Technical Report No. 552.[1]

- α = rotor angle of attack (angle between plane perpendicular to axis of rotation and relative wind)
- θ = rotor blade pitch angle, measured from zero lift chord line of blade section
- L = rotor lift, lbs.
- D = rotor drag, lbs., from N.P.L. balance
- D' = drag derived from rotor torque
- M = pitching moment of rotor, ft.lbs.
- Q = rotor torque, ft.lbs.
- n = rotor speed, r.p.s.
- ω = angular velocity, rad. per sec.
- V = wind speed, ft. per sec.
- R = rotor radius, ft.
- C_L = coefficient of lift, $L/(\rho/2)\pi R^2V^2$
- C_{D_0} = drag coefficient from N.P.L. balance drag, $D_0 = D/(\rho/2)\pi R^2V^2$
- C_D' = drag coefficient from D'
- C_D = total drag coefficient, C_{D_0} plus C_D'
- C_M = moment coefficient, $M/(\rho/2)\pi R^3V^2$
- μ = tip speed ratio, $V \cos \alpha/\omega R$

INTRODUCTION

IN AN EFFORT to extend the findings of the N.A.C.A. from their rotor tests of 1936[1] in which four different airfoil sections were used, as well as to determine the sensitivity of small-scale rotors to blade section variation, 15 rotors using a related series of airfoil sections were tested in the University of Kansas wind tunnel.[2] This related series included the following sections:

Thickness variation—N.A.C.A. 0009, 0012, 0015, 0018.

Camber variation—N.A.C.A. 0012, 2412, 4412, 6412.

Thickness and camber variation—N.A.C.A. 4409, 4412, 4415, 8318.

Thickness shape variation—N.A.C.A. 23012, 23012-33.

Camber shape variation—N.A.C.A. 0012, 2412, 23012, 2R$_3$12, 4412, 43012, 6412, 6712.

This group of sections was used by the N.A.C.A. in their investigation of the effect of Reynolds Number on the characteristics of airfoil sections.[3]

CONSTRUCTION OF BLADES

For each section a template was made from stainless steel by scribing the outline of the section on the thin steel and cutting it out with fine files. These templates were used to form the basswood blades. Since the blades were very close to final dimensions after forming, little or no thickness could be added. Therefore the blades were finished with a thin coat of shellac, which was sanded and buffed to a high polish.

ROTORS

The rotors had a diameter of 36 in. with a blade chord of 2.5 in. This produced a solidity of 0.0885. The center of gravity of the solid blades at approximately 44 per cent of the chord necessitated placement of the vertical pin at that position. The pins were offset from the axis of rotation by $1^7/_{16}$ in. The blades were carried on a horizontal hinge that passed through the axis of rotation, the flapping axis of both blades being the same.

The hub contained adjustments for pitch and also an adjustment for moving the blades forward and backward in the plane of rotation. This latter adjustment was necessary in order to secure proper balance of the rotor by placing the centers of gravity of the separate blades directly opposite to each other. Pitch adjustment was secured by rotating the blades about their span axes by means of pitch adjustment screws incorporated in the hub. The test rotor is shown in Fig. 1.

TESTING APPARATUS

The rotor was driven by a $^1/_3$-hp. electric motor which was mounted on a support of streamline tubing, offset so as not to interfere with the flapping of the blades. The plane of rotation was vertical with the center of rotation on the centerline of the tunnel, which

Received January 11, 1943.

* Assistant Professor, Aeronautical Engineering Department. Now, Associate Professor of Aeronautical Engineering, University of Wichita.

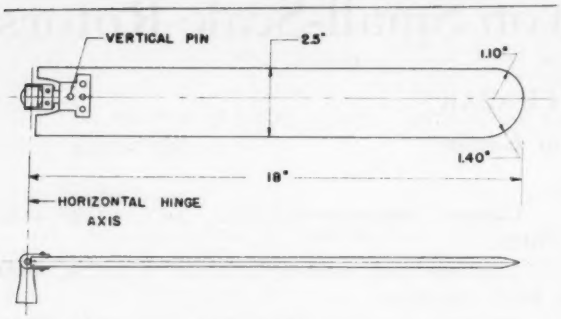

FIG. 1. Test rotor.

made all balance scales direct reading. The motor was completely enclosed in a fairing to reduce tare drag. Speed adjustment was secured by a series of rheostats which allowed the speed to be adjusted while the test was being conducted. The speed of the rotor was measured by a stroboscope. This stroboscope also allowed studying of the rotor while in motion and was instrumental in eliminating practically all of the rotor vibration.

In order to record the power requirements of the rotor, the motor was mounted in trunnions about its shaft axis and a torque arm was connected to a small beam balance on the outside of the tunnel.

The balance at the University of Kansas wind tunnel is of the N.P.L. type described in N.A.C.A. T. R. No. 72.[4] The atmospheric pressure tunnel is built to the specifications of the 5-ft. closed-throat tunnel at the Massachusetts Institute of Technology. It has a speed range from 50 to 85 m.p.h., and sphere tests have shown that it has a critical Reynolds Number of 150,000.

TESTS

Two series of tests were conducted. From one series of tests, the autorotative characteristics of the different sections were obtained, and from the other series of tests the maximum L/D values were determined. These tests served as a check against each other.

In the autorotative tests, all rotors were set at the same pitch and adjusted to 1,200 r.p.m. before the wind was turned on. The rheostats by which the motor speed was controlled were not changed during the entire run. Therefore, all changes in rotor speed were a function of the rotor and influenced by the section. The rotor was set at angles of attack at increments of one degree, and at each setting readings were taken of lift, drag, moment, revolutions per minute, torque, and dynamic pressure.

In the maximum L/D tests the same readings were taken, but, instead of permitting the rotor to find its own speed, at any attack angle, the speed was controlled in order to maintain a constant tip speed ratio. Three tests were run for each rotor during which the tip speed ratios were held at 0.340, 0.370, and 0.425, respectively. At each tip speed ratio the rotors were first run with the blades set at a low pitch angle and then rerun through the same angles of attack with the blades set at a high pitch angle. Previous experiments by Hays and Gustafson at the University of Kansas have shown that two runs for the same rotor at a different pitch will produce a continuous lift-drag curve, and at any angle of attack different values of lift coefficient may be secured by changing the pitch angle of the blade. The range of lift coefficients thus secured was large enough to produce values well beyond the maximum L/D point.

Complete tests of the tare drag of the rotor support and electric motor fairing were taken at frequent intervals, and the results checked so closely that an average tare curve was used for the entire series of tests.

CALCULATION OF DATA

Density values were used to convert the rotor data to coefficient form. Tare corrections were then applied and this left the lift and moment coefficients in their final form. The drag coefficient, however, did not take into account the drag as evidenced by the torque. At low values of lift coefficient it is necessary to drive the small-scale rotors and the power input must be charged against the rotor. Conversely, at high values of lift the small-scale rotors autorotate and the electric motor then serves as a brake and holds the rotor down to a desirable speed. At this time the torque has a negative value that should be credited to the rotor. An analysis shows that the power supplied by the motor is dissipated in skin friction and induced blade drag. It is logical that this torque value should be charged, or credited as the case may be, to the drag values of the rotor.

The horsepower as required by the torque may be equated to the horsepower that would be used by a direct drag force. Thus:

$$\text{hp.}_D = D'V/550$$

where hp._D is the horsepower consumed by an equivalent direct drag force, D', and the velocity is in feet per second.

Also

$$\text{hp.}_t = 2\pi nQ/550$$

where hp._t is the horsepower consumed by the torque, Q. Equating

$$\text{hp.}_t = \text{hp.}_D$$

Or

$$D'V/550 = 2\pi nQ/550$$

Thus

$$D' = 2\pi nQ/V$$

This force, D', may be converted to a coefficient and added to or subtracted from the drag coefficient as de-

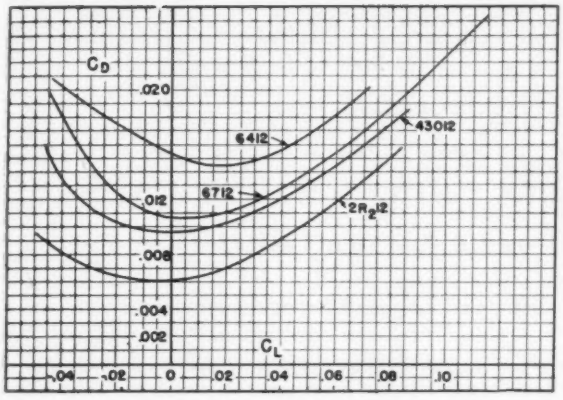

FIG. 2. Typical curve, total drag coefficient vs. lift coefficient for autorotative test.

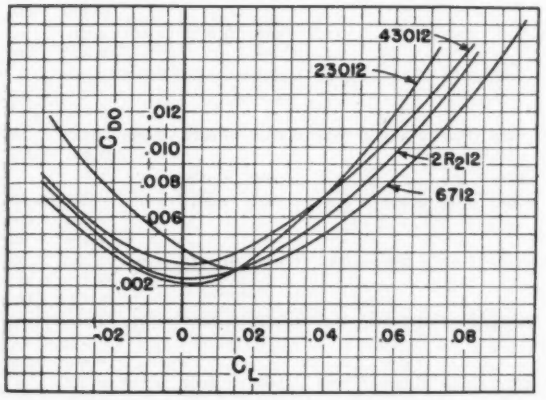

FIG. 3. Typical curve, N.P.L. drag vs. lift coefficient, autorotative test.

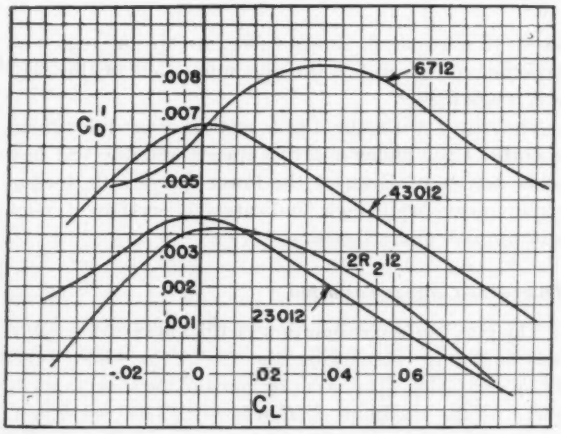

FIG. 4. Typical curve, torque drag vs. lift coefficient, autorotative test.

rived from the N.P.L. balance to give the total drag of the rotor. The drag coefficient as derived from the torque, called C_D', Fig. 4, is used as a measure of the autorotative characteristics of the section: a high value of C_D' denoting a section with poor autorotative characteristics and one that required excessive power for operation. Since the highest lift coefficient secured from these tests was that for a rotor in high-speed flight, this relationship does not hold for vertical or near vertical descent.

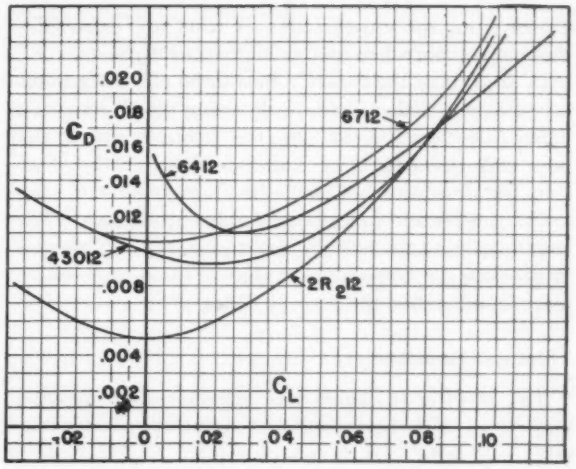

FIG. 5. Typical curve, total drag vs. lift coefficient, maximum L/D tests.

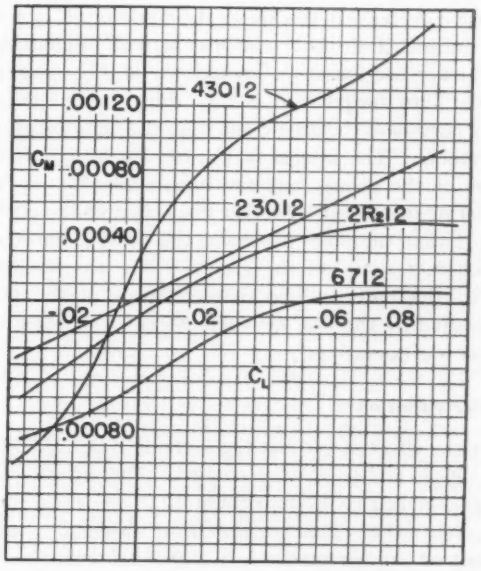

FIG. 6. Typical moment curve.

RESULTS

The sample graphs, Figs. 2, 3, 4, 5, and 6, illustrate the type of curves from which the conclusions of the investigation were drawn. Since the range of attack angles was limited by the apparatus and the difficulty of keeping the rotor down to a safe speed, the conclusions

drawn from the entire series of tests are essentially those for a rotor when used in high-speed flight.

In all tests of the rotors, a maximum efficiency point was located, with a definite dropping of efficiency on either side. On the one side, the drop was due to the poor stall characteristics of the sections; on the other side, the drop was due to the high drag characteristics of the thicker and excessively cambered sections. The combination of inefficiency due to low stall angles and inefficiency due to high drag values or other undesirable features magnified the poor qualities of the rotor.

Thickness Variation

The effect of thickness was determined by studying the rotors with blade sections N.A.C.A. 0009, 0012, 0015, and 0018. Of these sections, the N.A.C.A. 0012 produced the highest L/D and also exhibited the best autorotative tendencies. With an increase in thickness, a definite increase in minimum C_D was noted with a corresponding decrease in maximum L/D.

With a decrease in thickness, the minimum C_D for the rotor increased abruptly and was actually higher than for thicker sections. A breakdown of the drag coefficient into torque and N.P.L. drag showed that a major portion of the drag came from the high torque requirements. The minimum C_{D_0} for the 0009 was the lowest of the group, but the maximum C_D' was the highest of the group. Further inspection of the curves showed that the 0009 possessed the poorest autorotative characteristics of the group. This was probably due to the bad stalling characteristics of the 0009 aggravated by the low Reynolds Number at which the section was operating.

Camber Variation

For the effect of camber the sections N.A.C.A. 0012, 2412, 4412, and 6412 were studied. The order of this group as indicated by maximum L/D was 2412, 0012, 4412, and 6412. This suggests that although a small amount of camber produces a higher efficiency an excessive amount of camber is undesirable.

The N.A.C.A. in their tests of a 10-ft. diameter autogiro rotor have also found that cambered blades are more effective than symmetric sections and that a thickness ratio of 18 per cent is less efficient than the thickness ratio of 12 per cent. The higher efficiency of the cambered blades was attributed to an effective twist in the rotor blades as tested by the N.A.C.A. In the small-scale rotors, however, the effective twist was shown to be negligible because of the torsional rigidity of the solid blades. Therefore, the increase in efficiency was due to the camber alone.

In this group, the curves for the 0012, 2412, and 4412 were well spaced, but the curves for the 6412 were definitely isolated, indicating that a camber ratio of about 4 per cent is the upper limit for rotor sections. The differences in the drag coefficients of the 0012 and the 2412 were small, almost falling within the region of experimental error, but the maximum L/D of the 2412 was much higher.

The rotor with the 6412 section was difficult to operate at the higher rotative speeds and one test had to be omitted. Even at the lower speeds, the torque requirements were high, indicating a section of poor autorotative characteristics.

TABLE 1

Tabulation of Rotor Characteristics

	Autorotative Tests						C_L at Max. L/D Tests	
Section	L/D max.	at μ	C_D min.	C_{D_0} min.	C_D' max.	Auto-rotation	μ	L/D max.
0009	4.59	0.360	0.0067	0.0014	0.0056	0.096	0.340	5.62
							0.373	5.71
							0.426	4.90
0012	5.58	0.353	0.0049	0.0018	0.0032	0.063	0.320	5.33
							0.370	5.50
							0.426	5.18
0015	4.59	0.345	0.0061	0.0027	0.0045	0.077	0.340	5.16
							0.370	4.85
							0.425	4.75
0018	5.11	0.310	0.0073	0.0027	0.0048	0.068	0.340	4.93
							0.370	4.75
							0.425	4.19
2412	5.58	0.353	0.0054	0.0018	0.0040	0.062	0.344	6.09
							0.370	6.01
							0.426	5.84
4412	4.93	0.335	0.0065	0.0022	0.0032	0.068	0.340	5.92
							0.370	5.73
							0.426	5.09
6412	3.65	0.340	0.0143	0.0039	0.0113	0.120	0.373	5.10
							0.426	5.08
4409	5.00	?	0.0075	0.0023	0.0054	0.078	0.340	5.92
							0.370	5.73
							0.426	5.09
4415	3.50	0.350	0.0098	0.0027	0.0071	0.090	0.373	5.06
							0.426	4.63
8318	?	?	0.0120	0.0082	0.0130	?	?	?
23012	5.00	0.340	0.0061	0.0020	0.0041	0.070	0.340	6.14
							0.373	6.00
							0.426	5.40
23012-33	5.00	0.340	0.0064	0.0020	0.0041	0.062	0.340	5.78
							0.373	5.33
							0.426	5.00
2R$_3$12	5.56	0.300	0.0059	0.0022	0.0037	0.076	0.340	6.61
							0.373	5.95
							0.426	5.08
43012	4.59	0.320	0.0096	0.0032	0.0067	0.110	0.373	5.44
							0.426	4.93
6712	4.54	0.353	0.0106	0.0029	0.0084	?	0.345	4.52
							0.373	3.58
							0.426	4.55

Thickness-Camber Variation

The effect of a combination of thickness and camber was found by comparing the N.A.C.A. 4409, 4412, 4415, and 8318. The order of merit of these sections as given by the maximum L/D was 4412, 4409, 4415, and 8318. The sections 4412 and 4409 gave similar results, with the exception of the higher drag at zero lift for the latter.

The study of the thickness-camber variation revealed that a combination of excessive thickness and excessive camber provided a section that was impossible

to operate. No difficulty was encountered in operating the 0015 and the 0018 sections at the high rotative speeds, but the 8318 could be operated only at the lowest speed of 1,160 r.p.m. and the 4415 could not be operated at the high speed of 1,450 r.p.m. Thickness alone did not appear to be so detrimental as a combination of thickness and camber, particularly excessive camber.

Thickness Shape Variation

Through examination of the sections N.A.C.A. 23012 and 23012–33, the sensitivity of small-scale rotors to minor changes in blade section was determined. The only difference between these two sections is that the nose radius of the 23012–33 is one-fourth that of the 23012. Both are of the same thickness and camber, but the stall angle of the 23012–33 is 3° lower.

The autorotative tests did not reveal any great difference between the two sections, both having practically the same maximum L/D and autorotative characteristics. However, on the tests to determine maximum L/D, the 23012 was consistently better. It exhibited a higher maximum L/D in all three tests and lower minimum drag figures, indicating that sections with sharp-nose shapes are not desirable as rotor sections.

Camber Shape Variation

The camber shape series provided a group of sections with the points of maximum camber occurring at 15, 40, and 70 per cent of the chord. The maximum efficiency occurred with the maximum camber position at about 40 per cent of the chord.

Two sections, the 23012 and the 43012, with the maximum camber at 15 per cent of the chord, were tested.[5] The drag coefficients of the 43012, with 4 per cent total camber, were much higher, and the maximum L/D was about 10 per cent lower than those values for the 23012.

Three sections, the 2412, 4412, and 6412, with the maximum camber occurring at 40 per cent of the chord, were tested. Again, sections with 2 per cent camber gave the highest maximum L/D values. However, the 4412, while not so efficient as the 2412, was definitely superior to the 43012. The 6412 was less effective than the other sections, with the maximum camber at 40 per cent of the chord. It was only slightly less efficient than the 43012, indicating that about 5 per cent camber at 40 per cent of the chord would produce approximately the same results as 4 per cent camber at 15 per cent of the chord.

The 6712, with a camber of 6 per cent at 70 per cent of the chord, produced approximately the same results as the 43012. However, it produced better results than the 6412, since the latter required excessive amounts of torque.

Trailing-Edge Shape Variation

A consistent variation in trailing-edge shape was achieved by the use of the $2R_212$, the 2412, 6412, and 6712. The order of the group as indicated by maximum L/D was the same. The $2R_212$ was the most efficient section of the entire series of tests. This section was similar to the 2412 in all respects with the exception of the reflexed mean line. The positive pitching moment produced by the reflexed mean line probably accounted for the good showing of the $2R_212$, not only in maximum L/D but also in drag and autorotative characteristics.

Although the 6412 produced a higher maximum L/D than the 6712 in the maximum L/D tests, in the autorotative tests it produced a lower maximum L/D and inferior values of minimum drag. It also required a larger amount of torque at low values of lift. This indicates that a large value of camber near the trailing edge does not adversely affect rotor performance and that a trailing edge flap may be used for rotor control.

Effect of Blade Section on Rotor Moments

At the time that the tests of blade section variation were run, the rotor moments were considered as a secondary factor. Hence, the same care was not exercised in checking the moment results and the accuracy was not so great as in the case of the lift and drag measurements.

The rotor moments were converted to coefficients and plotted against the lift coefficient. From these graphs definite trends were noted. All rotors had unstable moment curves. However, movement of the camber backward produced a definite decrease in the slope of the moment curve.

The 6712, with 6 per cent camber at 70 per cent of the chord, was the most stable of the group, whereas the 43012 was very unstable. Changes in thickness and changes in camber at any one position had little or no effect upon the slope of the moment curve. The values of moment coefficient corresponded to values as determined from full-scale tests.

Conclusions

1. The sensitivity of small-scale testing was shown to be great enough to justify the exploration of other rotor problems with the use of small-scale rotors.

2. The autorotative characteristics of the various sections pointed out that some sections would be usable in high-speed flight but would not be effective for slow or hovering flight.

3. A small amount of camber for rotor blade sections is desirable, but excessive amounts of camber decrease the efficiency of the rotor.

4. The stalling characteristics of the sections are reflected in the rotor performance as shown by the drop in efficiency of the thin and sharp-nosed sections.

(Continued on page 96)

Vibration Frequencies of Continuous Beams

EDWARD SAIBEL*

Carnegie Institute of Technology

SUMMARY

A method is developed for finding the natural frequencies of vibration of a continuous beam from a knowledge of the natural frequencies and natural modes of the beam supported at the ends in the same manner as the continuous beam but not subjected to any of the constraints between the ends. The method is easily applied and can be carried out to any desired degree of approximation for any number of modes of vibration in a quick and simple manner. Calculations are given for two cases, the second of which is related to the problem of the braced cantilever wing.

INTRODUCTION

THE CUSTOMARY METHOD for finding the natural frequencies of a continuous beam is to set up the general solution of the differential equation for each span separately. This necessitates the evaluation of four constants of integration for each span. Two of these constants are disposed of at each end of the beam by means of the boundary conditions at these ends, respectively. Relating the deflections, slopes, and moments of contiguous spans at their common supports gives rise to a set of linear homogeneous equations in the constants. Setting the determinant of the coefficients of the constants equal to zero, the necessary condition, for a nontrivial solution, yields the characteristic or frequency equation. This is a long and tedious procedure. It is the object of this paper to develop a simple and readily applied method whereby the natural frequencies may be evaluated to any desired degree of approximation. The continuous beam is thought of as an ordinary beam of the same length subject to constraints at the inner points of support. The characteristic (or eigen) functions and corresponding characteristic (or eigen) values for the ordinary beam are known or can be found without difficulty, and the solution for the continuous beam is developed in terms of these known properties.

DISCUSSION

The differential equation of a beam vibrating without external exciting forces is[1]

$$\frac{\partial^2}{\partial x^2}\left[EI(x)\frac{\partial^2 y}{\partial x^2}\right] = -\,m(x)\frac{\partial^2 y}{\partial t^2} \tag{1}$$

where EI = the flexural rigidity of the beam, m = the mass per unit length, and y = the deflection. Using the customary method, we may express y in the form

$$y = Y(x)\sin(pt + e)$$

where p = the circular frequency (rad. per sec.) and e = the phase angle. Eq. (1) becomes

$$\frac{d^2}{dx^2}\left[EI(x)\frac{d^2Y}{dx^2}\right] = m(x)p^2Y \tag{2}$$

Associated with Eq. (2) and the boundary conditions at the ends of the beam—namely, simply supported, clamped, or free—there is a closed set of characteristic functions $\phi_r(x)$ and characteristic values $\lambda_r = p_r^2$ ($r = 1, 2, \ldots$), which correspond to the shape and to the square of the circular frequency in the rth mode of vibration. The ϕ_r's satisfy the following equations:[2]

$$\left.\begin{aligned}\textstyle\int_0^l m(x)\phi_r(x)\phi_s(x)\,dx &= 0;\ r \neq s\\ \textstyle\int_0^l m(x)\phi_r^2(x)\,dx &= 1\end{aligned}\right\} \tag{3}$$

An arbitrary deflection $y(x, t)$ satisfying the boundary conditions prescribed at the ends of the beam and vibrating with an arbitrarily chosen frequency $\sqrt{\lambda}$ may be represented by the generalized Fourier Series

$$y(x, t) = [a_1\phi_1(x) + a_2\phi_2(x) + \ldots.]\sin(\sqrt{\lambda}\,t + e) \tag{4}$$

since $Y(x) = a_1\phi_1(x) + a_2\phi_2(x) + \ldots..$ The deflection of the beam in its position of maximum displacement may be thought of as being produced by a steady system of continuously distributed inertia forces of intensity $\lambda m(x)Y(x)$ per unit length. The strain energy (V_1) stored in the beam in this position is given by[1]

$$\tfrac{1}{2}\textstyle\int_0^l EI(x)(d^2Y/dx^2)^2\,dx$$

Integrating by parts leads to

$$V_1 = \frac{E}{2}\left\{\left[I(x)\frac{d^2Y}{dx^2}\frac{dY}{dx}\right]_0^l - \int_0^l \frac{dY}{dx}\frac{d}{dx}\left[I(x)\frac{d^2Y}{dx^2}\right]dx\right\}$$

At a simply supported or free end, $EI(x)(d^2Y/dx^2)$ vanishes since this expression is the negative of the bending moment; at a clamped end dY/dx vanishes. Thus, V_1 reduces to

$$-\frac{E}{2}\int_0^l \frac{dY}{dx}\frac{d}{dx}\left[I(x)\frac{d^2Y}{dx^2}\right]dx$$

If this is integrated by parts, the following expression for V_1 is obtained:

Received April 26, 1943.

* Associate Professor of Mechanics.

$$V_1 = -\frac{E}{2}\left\{\left[\frac{d}{dx}\left\{I(x)\frac{d^2Y}{dx^2}\right\}Y\right]_0^l - \int_0^l Y\frac{d^2}{dx^2}\left[I(x)\frac{d^2Y}{dx^2}\right]dx\right\}$$

Now, at a simply supported end or at a clamped end, Y vanishes; at a free end $(d/dx)[I(x)(d^2Y/dx^2)]$ is zero, since it is proportional to the shear. Therefore, V_1 becomes

$$\frac{E}{2}\int_0^l Y\frac{d^2}{dx^2}\left[I(x)\frac{d^2Y}{dx^2}\right]dx$$

and upon the substitution of Eq. (2) into this expression and by the use of Eqs. (3), V_1 takes the form

$$(1/2)(a_1^2\lambda_1 + a_2^2\lambda_2 + \ldots.)$$

The potential energy (V_2) of the inertia loading is given by

$$(\lambda/2)\int_0^l m(x)\,Y^2(x)\,dx$$

and using Eqs. (3) and (4) this becomes

$$(\lambda/2)(a_1^2 + a_2^2 + \ldots.)$$

Furthermore, let the beam be subjected to a constraint such as an additional support between the ends of the beam, at $x = c$, for example. This constraint may be expressed by

$$0 = a_1\phi_1(c) + a_2\phi_2(c) + \ldots.$$

and may be introduced into the expression for the total potential energy (V) through an undetermined multiplier μ as follows:[3]

$$V = V_1 - V_2 - \mu[a_1\phi_1(c) + a_2\phi_2(c) + \ldots.] \quad (5)$$

The necessary conditions that V be a minimum are:

$$\partial V/\partial a_r = 0;\ r = 1, 2, \ldots. \quad (6)$$

and

$$\frac{\partial V}{\partial \mu} = 0 \text{ or } a_1\phi_1(c) + a_2\phi_2(c) + \ldots. = 0 \quad (7)$$

Eq. (6) leads to $a_r = \mu[\phi_r(c)/(\lambda_r - \lambda)]$. The substitution of this value into Eq. (7) gives the frequency equation of the system of restraint—namely,

$$\frac{\phi_1^2(c)}{\lambda_1 - \lambda} + \frac{\phi_2^2(c)}{\lambda_2 - \lambda} + \ldots. = 0 \quad (8)$$

In those cases where the beam is uniform and the ends are any combination of simply supported, built-in, or free, the ϕ_r's and the λ_r's are known. Let the λ_r's be ordered such that $\lambda_1 < \lambda_2 < \lambda_3 < \ldots.$ For any variety of end conditions the convergence of Eq. (8) is so rapid that it is sufficient to consider only the first two terms. This leads to a linear equation in λ, and a close approximation to the frequency of the constrained system in the first mode of vibration is obtained. If three terms are taken, a quadratic equation in λ results and a close approximation to the lowest frequency together with a good approximation to the next higher frequency is found. The approximations to the lower frequencies are so good that as more terms are taken these roots may be divided out and at each stage it is only necessary to solve a quadratic equation.

Eq. (8) has an interesting interpretation. It is shown in the theory of integral equations[4] that the periodic induction function $G(x, s; \lambda)$, which expresses the deflection at any point x of the system due to a unit load of frequency $\sqrt{\lambda}$ located at point s, may be expressed in the form $G(x, s; \lambda) = \sum_{r=1}^{\infty}\phi_r(x)\phi_r(s)/(\lambda_r - \lambda)$. Thus if a unit load vibrating with frequency $\sqrt{\lambda}$ is acting at $x = c$, frequency Eq. (8) is obtained by use of the condition that λ must be such as to produce no deflection at $x = c$.

If more than one constraint is operative—that is, if the beam is supported at more than one point between the ends, for example, at $x = b$ and $x = c$—the additional constraints may be introduced into the expression for the total potential energy, Eq. (5), as follows:

$$V = V_1 - V_2 - \mu\sum a_r\phi_r(b) - \nu\sum a_r\phi_r(c)$$

The necessary conditions for a minimum are:

$$\frac{\partial V}{\partial a_r} = 0, \frac{\partial V}{\partial \mu} = 0, \frac{\partial V}{\partial \nu} = 0$$

The results of applying these three conditions and eliminating a_r are:

$$\mu\sum\frac{\phi_r^2(b)}{\lambda_r - \lambda} + \nu\sum\frac{\phi_r(b)\phi_r(c)}{\lambda_r - \lambda} = 0$$

$$\mu\sum\frac{\phi_r(b)\phi_r(c)}{\lambda_r - \lambda} + \nu\sum\frac{\phi_r^2(c)}{\lambda_r - \lambda} = 0$$

The necessary condition for a nontrivial solution is the vanishing of the determinant of the coefficients of μ and ν in these two equations. This leads to the frequency equation

$$\sum\frac{\phi_r^2(b)}{\lambda_r - \lambda}\sum\frac{\phi_r^2(c)}{\lambda_r - \lambda} - \left[\sum\frac{\phi_r(b)\phi_r(c)}{\lambda_r - \lambda}\right]^2 = 0$$

The functions ϕ_r need not be normalized. It is sufficient to know that in the second of Eq. (3)

$$\int_0^l m(x)\phi_r^2(x)\,dx = \text{constant}$$

This is the case in both of the examples given below.

Examples

(1) A simply supported beam of length l is propped between the ends so that the ratio of spans is $l_1:l_2 = 6:4.5$.[1] In this case

$$\phi_r(x) = \sin k_r x$$

where

$$k_r^4 = \lambda_r m/EI$$

and

$$k_r l = r\pi; \; r = 1, 2, \ldots.$$

Eq. (8) becomes

$$\frac{\sin^2 \frac{\pi \times 6}{10.5}}{(\pi^4/l^4)(EI/m) - \lambda} + \frac{\sin^2 \frac{2\pi \times 6}{10.5}}{(16\pi^4/l^4)(EI/m) - \lambda} + \ldots = 0$$

Using the first three terms, there results

$$p_1 = \sqrt{\lambda_1} = (11.7/l_1^2)\sqrt{EI/m}$$
$$p_2 = \sqrt{\lambda_2} = (23.7/l_1^2)\sqrt{EI/m}$$

which agree closely with the values given in reference (1).

(2) A cantilever of length l is propped three-quarters of the way out from the built-in end. In this case[1]

$$\phi_r(x) = \left\{(\cos k_r x - \cosh k_r x) + \frac{(\sin k_r x - \sinh k_r x)(\sin k_r l - \sinh k_r l)}{(\cos k_r l + \cosh k_r l)}\right\}$$

where $k_r l = 1.875, 4.694, 7.855, \ldots.$; for $r = 1, 2, 3, \ldots.$; and again $k_r^4 = \lambda_r m/EI$. Simplifying the problem by making it nondimensional—that is, letting l and m/EI be each equal to unity—it is found that

$$\phi_1^2(0.75) = 1.729$$
$$\phi_2^2(0.75) = 0.0676$$

and Eq. (8) becomes

$$\frac{1.729}{12.36 - \lambda} + \frac{0.0676}{486 - \lambda} + \ldots = 0$$

Using these two terms only, $\sqrt{\lambda_1} = 21.6$ or $p_1 = (21.6/l^2)\sqrt{EI/m}$, which compares very well with the exact value,[5] $(21.8/l^2)\sqrt{EI/m}$.

Conclusion

The problem of finding the natural frequencies of vibration of a continuous beam has been greatly simplified in the case where the beam is uniform. The method is valid for a beam of nonuniform cross section and can be used with advantage to simplify the solution in such cases, though the finding of the characteristic functions and characteristic values for the unconstrained nonuniform beam is somewhat more difficult than for the uniform beam.

The method here developed is also helpful in the problem of the continuous beam with concentrated masses, such as a wing with attached engine nacelles. In this type of problem the procedure generally followed is that of synthesis of mass,[2] which leads to the following equation:

$$1/\omega^2 \leq (1/\omega_1^2) + (1/\omega_2^2)$$

In this expression, ω is the natural frequency, ω_1 is the frequency of the masses attached to a weightless beam having only elastic properties, and ω_2 is the frequency of the vibrating beam without attached masses. The method of the present paper is directly applicable to the calculation of this latter term and, by virtue of its simplicity, is preferable to the standard method.

References

[1] Timoshenko, S., *Vibration Problems in Engineering;* D. Van Nostrand Company, Inc., New York, 1937.

[2] Temple and Bickley, *Rayleigh's Principle;* Oxford University Press, London, 1933.

[3] Osgood, W. F., *Advanced Calculus;* The Macmillan Company, New York, 1925.

[4] Lovitt, W. V., *Linear Integral Equations;* McGraw-Hill Book Company, Inc., New York, 1924.

[5] Hohenemser, K., *Die Methoden zur Angenaherten Losung von Eigenwertproblemen in der Elastokinetik;* Julius Springer, Berlin, 1932.

(*Continued from page 87*)

5. Tests of sections with large amounts of camber near the trailing edge showed that the use of trailing-edge flaps would be an effective means of rotor control.

References

[1] Wheatley, John B., and Bioletti, Carlton, *Wind Tunnel Tests of 10-Foot Diameter Autogiro Rotors,* N.A.C.A. T.R. No. 552, 1936.

[2] Gustafson, Frederick B., *A Study of Small Scale Rotors,* University of Kansas, Lawrence, Kan., 1939.

[3] Jacobs, Eastman N., Ward, Kenneth E., and Pinkerton, Robert M., *The Characteristics of 78 Related Airfoil Sections from Tests in the Variable-Density Wind Tunnel,* N.A.C.A. T.R. No. 460, 1933.

[4] Warner, Edward P., and Norton, F. H., *Wind Tunnel Balances,* N.A.C.A. T.R. No. 72, 1919.

[5] Jacobs, Eastman N., and Pinkerton, Robert M., *Tests in the Variable-Density Wind Tunnel of Related Airfoils Having the Maximum Camber Unusually Far Forward,* N.A.C.A. T.R. No. 537, 1935.

Letters to the Editor

Dear Sir:

As in the case of Cozzone's paper[1] in the May, 1943, issue of the JOURNAL, it is again gratifying to see thought given to the plastic range in structural design. One or two comments come to mind in reading Wolford's paper.[2]

Wolford's Eq. (15) is one of those derived by von Kármán in 1910.[3] The equation applies to the idealized H-section (negligible web) or an idealized box section as Wolford has shown it in his Fig. 2. If it is to be applied to "hollow rectangular sections," the sides parallel to the plane of bending must offer negligible resistance to bending compared to the other two sides.

Wolford suggests that Eqs. (2) and (15) represent extreme conditions for the sections likely to be encountered. Eq. (15) for the idealized H-section definitely represents one extreme condition for sections symmetric in a plane perpendicular to the plane of bending. According to Gehler,[4] however, the values of the double modulus for the I-section are higher than for the rectangular section when the plane of bending is perpendicular to the web. For sections unsymmetric in a plane perpendicular to the plane of bending, the double modulus may approach the tangent modulus on the one hand or the modulus of elasticity on the other, depending on the shape and on the direction of bending.

Wolford states that "in computing effective column length, 0.6 in. was added to the specimen length to compensate for the adapter thickness." If the adapters are very stiff relative to the specimen, the effective length can be computed accurately from the formula

$$\cot (\pi L/2L_0) = \pi d/L_0$$

where L is the length of the specimen; L_0 is the effective, or free, length of the column; and d is the distance between a knife edge and the near end of the specimen—that is, the thickness of the adapter. The formula assumes that the adapters are rigid.

When the section cannot be approximated by two flanges (idealized H-section), the problem of the plastic range becomes practically much more complicated. It has been worked out for a number of assumed stress-strain curves. The most reasonable ones have not expressed the stress and the strain as continuous analytic functions of each other, however, and added complications have resulted from this lack. Moreover the forms of the expressions have not been applicable to a wide variety of materials. Some time ago I hit upon a continuous function that applies surprisingly accurately to many structural materials, at least up to a strain of 0.01. The expression is

$$e = s/E + K(s/E)^n, \qquad n > 1 \tag{1}$$

where e is the strain, s is the stress, E is the modulus of elasticity, and K and n are empirical constants. When Eq. (1) represents stress-strain data accurately, K and n may be determined by plotting s/E against $e - (s/E)$ on logarithmic paper, for

$$\log [e - (s/E)] = \log K + n \log (s/E)$$

Eq. (1) lends itself readily to the determination of column curves based on the double-modulus theory.

WM. R. OSGOOD
Materials Engineer
National Bureau of Standards

Dear Sir:

The recent paper by Max G. Scherberg on "Regions of Infinite Acceleration and Flow Realms in a Compressible Fluid" (JOURNAL OF THE AERONAUTICAL SCIENCES, Vol. 10, No. 7, pp. 223–226, 231, July, 1943) is an interesting contribution to the now much discussed subject of compressibility effects in aerodynamics. However, it contains some statements that are difficult to understand. For instance, the author said that in the paper by Theodore von Kármán (JOURNAL OF THE AERONAUTICAL SCIENCES, Vol. 8, No. 9, pp. 337–355, July, 1941) "some conditions were specified under which regions of infinite acceleration may be located. . . ."; and in his paper: "A more complete set of such conditions is developed." It is hard to see that Scherberg's set of conditions is more *complete* than von Kármán's, because one is completely equivalent to the other.

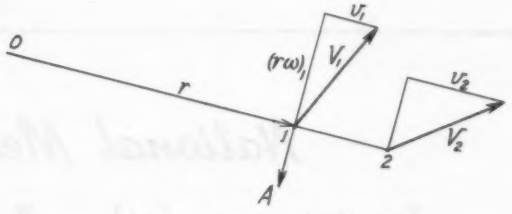

FIG. 1. Case I of minus realm of flow.

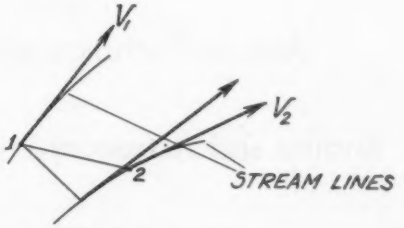

FIG. 2. Expanding stream tube—subsonic flow.

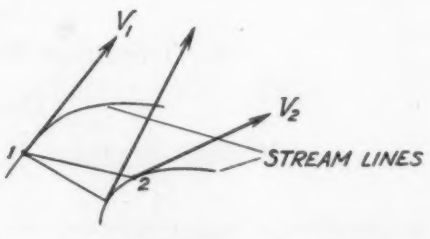

FIG. 3. Contracting stream tube—supersonic flow

---

[1] Cozzone, Frank P., *Bending Strength in the Plastic Range*, Journal of the Aeronautical Sciences, Vol. 10, No. 5, p. 137, May, 1943.

[2] Wolford, Don S., *Significance of the Secant and Tangent Moduli of Elasticity in Structural Design*, Journal of the Aeronautical Sciences, Vol. 10, No. 6, p. 169, June, 1943.

[3] von Kármán, Th., *Untersuchungen ueber Knickfestigkeit*, Verein Deutscher Ingenieure, Forschungsarbeiten, No. 81, Berlin, 1910.

[4] W. Gehler, Proceedings of the Second International Congress for Applied Mechanics, p. 366, September 12–17, 1926.

Now consider the so-called case I of the minus realm of flow, where the following conditions are satisfied (the notations are Mr. Scherberg's):

$$\partial v/\partial r > 0, \qquad r\omega > 0, \qquad A < 0$$

The situation is indicated in the accompanying Fig. 1. Because of the zero radial acceleration, the two neighboring points 1 and 2 on the radial line have the same pressure. Then, by Bernoulli's theorem, the magnitudes of the velocities V_1 and V_2 at these points are also equal. However, since $\partial V/\partial r > 0$ and $V_1 < V_2$, the two velocity vectors at point 1 and point 2 tend to separate from each other. Furthermore, because of the fact that $A < 0$, the fluid flows against the pressure. The author then concludes that the flow is physically like that of case I in his Fig. 1, which represents an outward radial subsonic flow. However, it can be easily seen that such is not necessarily the case. If s is the distance measured along a stream line in the direction of flow and Δn the distance between two neighboring stream lines, then by using Eqs. (43) and (44) on page 345 of von Kármán's paper, one has

$$\frac{1}{\Delta n}\frac{\partial \Delta n}{\partial s} = \left(\frac{V^2}{a^2} - 1\right)\frac{1}{V}\frac{\partial V}{\partial s}$$

Therefore, for subsonic flows the stream tube expands when the fluid flows against the pressure, i.e., $\partial V/\partial s < 0$. This is the physical characteristic of the subsonic flow as shown by case I of Mr. Scherberg's Fig. 1. The case I of the minus realm of flow can be physically similar to the subsonic flow only if the stream tube expands in the direction of flow. However, the stream tube for this case can either expand or contract as shown by Figs. 2 and 3. The cross section of a stream tube must be measured normal to the stream line and not at an angle to the stream line as the line 1–2. If the stream tube expands, the flow velocity must be subsonic and no infinite acceleration can occur. If the stream tube contracts, the flow velocity must be supersonic and an infinite acceleration may appear. Hence, the mystery of the claim that "even though the flow may be supersonic, the fluid particles respond to its physical surroundings as in an ordinary subsonic flow" is dispelled.

The theory of the infinite accelerations in compressible flow is interesting and is of great practical importance. Since the publication of von Kármán's paper, two German authors, F. Ringleb ("Über die Differentialgleichungen einer adiabatischen Gasströmung und den Strömungstoss," *Deutsche Mathematik*, Vol. 5, pp. 337–384, 1941) and W. Tollmien ("Grenzlienien adiabatischen Potentialströmungen," *Z. angew. Math. Mech.*, Vol. 21, pp. 140–152, 1941), have developed the details of the theory. Recently, the theory has been further generalized to include the three-dimensional flows.

HSUE-SHEN TSIEN
Guggenheim Aeronautical Laboratory
California Institute of Technology

National Meetings Schedule

Institute of the Aeronautical Sciences

January 25, 26, and 27, 1944

Annual Technical and Business Meeting, New York

April, 1944

Engine and Accessory Production Meeting, Detroit, Michigan

July, 1944

Design and Post-War Planning Meeting, Los Angeles, California

October, 1944

Air Transport Meeting, Washington, D. C.

December 17, 1944

Wright Brothers Lecture and Dinner, New York

Services of the Aeronautical Archives of the Institute of the Aeronautical Sciences

The services of the Aeronautical Archives are available to all members of the Institute, to Corporate Members, to advertisers in the Aeronautical Engineering Review and, under usual library limitations, to the public. Four specialized services are available.

The Paul Kollsman Library

This lending library service makes available, *without charge*, the latest and more important aeronautical books.

As far as the facilities permit, any person in the United States over 18 years of age who can furnish references which certify to his or her responsibility may become a member of the library.

Members may request the loan of any aeronautical or technical book they wish to borrow. Through an exchange agreement with the Engineering Societies Library, any book on general engineering may be borrowed from its great collection of over 160,000 volumes.

A photostating service is available at usual library rates.

Applications for membership in the library and further information will be sent on request.

The Burden Reference Library

This reference library contains over 14,000 aeronautical books, magazines, pamphlets, photographs, reports, and clippings gathered from world-wide sources and is one of the most complete aeronautical libraries in the world. Material from this library is not available for loan but may be used for reference purposes at the Aeronautical Archives.

The Pacific Aeronautical Library

6715 Hollywood Boulevard
Hollywood, California

Established in cooperation with the aircraft companies the library serves. The leading aircraft companies in or near Los Angeles participate in its support and operation.

This service library for aeronautical research is available to the public for reading privileges. Source material includes aerodynamic and structural research reports, as well as books on drafting, production methods, history, and allied sciences. It furnishes books, periodicals, and pamphlet material to the participating aircraft companies to supplement their engineering libraries.

The Aeronautical Archives Technical Information Service

This service has experienced personnel under the supervision of trained aeronautical engineers to compile any information desired. The services range from listing specialized reference books to the preparation of exhaustive bibliographies, digesting of reports, and general surveys of any aeronautical subject. Some of the available services are:

Bibliographies on any aeronautical subject.
Reports on any aeronautical subject.
Digests of aeronautical books, papers, periodicals, and references.
Translations.
Engineering investigations of special aeronautical subjects.
Biographies of individuals engaged in aeronautics.
Photostats of any aeronautical or general engineering material.
Microfilms made on special order.
Photographs made from the Institute's photographic collection.
Drawings and tracings made.

In addition to the services mentioned any commission which comes within the scope of the Service will be accepted. Special arrangements may be made for work requiring several weeks or months.

Translators are available for accurate transcriptions of all foreign language data. Translations are carefully edited by trained engineers.

Reproductions of any material in the Aeronautical Archives of the Institute may be ordered at standard photostat rates.

INSTITUTE OF THE AERONAUTICAL SCIENCES
1505 RCA BUILDING WEST
30 ROCKEFELLER PLAZA, NEW YORK 20, N. Y.

SUGGESTIONS FOR CONTRIBUTORS TO THE PUBLICATIONS *of the* INSTITUTE *of the* AERONAUTICAL SCIENCES

The Institute of the Aeronautical Sciences invites both members and nonmembers from any country to submit papers for publication in the JOURNAL OF THE AERONAUTICAL SCIENCES and the AERONAUTICAL ENGINEERING REVIEW. The Institute, following the practice of other societies, does not pay for contributions.

The following directions for the preparation of papers, if followed by authors, will save correspondence, avoid the return of papers for changes, minimize the work of preparation for the printer, and save the expense due to the charges made for "author's corrections."

MANUSCRIPTS: Papers must be written in English, in original typewriting on one side only of white paper sheets, consecutively numbered and be double or triple spaced with wide margins. Manuscripts should be prepared with great care so that they will be typographically accurate. Paragraphing should be given special attention. Papers should be written in the third person, reference to the writer being made as "the author." Avoid the use of the words "I," "we," and "you." Blueprint copies of papers are unacceptable as it is impossible to mark directions to the printer on them. Correcting, changing, or adding to papers after they are in type is costly. It is, therefore, imperative that papers submitted be in final form. Typographical errors may be corrected on proofs, but if authors wish to add material, they may do so at their own expense. In mailing, drawings may be rolled, but manuscripts should be sent flat. Send by first class mail (register if you wish for your own protection) to the Editorial Office, Institute of the Aeronautical Sciences, 1505 RCA Bldg. West, 30 Rockefeller Plaza, New York 20, N. Y. All manuscripts will be examined by the Editorial Committee and by the Editor. Authors will be advised as promptly as possible whether the paper is acceptable for publication.

TITLES: The title of the paper should be brief. The name and initials of the author should be written as he prefers. The use of the full name of an author is advocated because of the frequent duplication of initials and surnames which sometimes makes it difficult to establish the identity of the author. This is particularly important for large annual indexing and abstracting services. All titles and degrees or honors are omitted. The name of the organization with which the author is associated should be placed after his name on a separate line. The date on which the paper is received will be inserted by the Editor.

SUMMARIES OR ABSTRACTS: An abstract to be printed at the beginning should accompany each article. It should be adequate as an *index* and as a *summary*. It should contain a statement of major conclusions reached, since summaries in many cases constitute the only source of information used in compiling scientific reference indexes. Abstracts printed in other journals, especially foreign, in most cases, consist of summaries from printed papers. The summary should explain as adequately as possible the major conclusions to a nonspecialist in the subject. The summary should contain from 100 to 300 words, depending on the length of the paper.

SUBHEADINGS: Subheadings should be inserted by the author at frequent intervals. The work of editorial preparation will be simplified by the author providing many subheadings. Owing to the breaking of columns and the insertion of illustrations, some of the subheadings may have to be omitted.

SHORTENING OF PAPERS: Some papers, at the end, fill in only a portion of a page. This leaves much wasted blank space as succeeding articles are started at the top of a page. Authors should indicate by notation on the left-hand side of the page what matter may be omitted when "runovers" occur. This request is important as the Journal cannot afford in the future, as it has in its earlier issues, to have blank half pages or more at the end of papers.

MATTER USUALLY DELETED: Acknowledgments of assistance in preparation of paper, except by collaborators. Photographs or illustrations of little technical interest and not showing advances in general practice. Too detailed tabular matter (general results of such tables may be included in the text). Lengthy descriptions of materials or processes or of preliminary experiments or theories that preceded final results; salient features only are of interest.

REFERENCES AND FOOTNOTES: References should appear as footnotes only, numbered consecutively, grouped together at the end of the manuscript. The arrangement should be as follows: (for books)—[1] Durand, W. F., *Aerodynamic Theory*, 1st Edition, Vol. 1, p. 23; Julius Springer, Berlin, 1934. (For magazines)—

[1]Englund, C. R., Crawford, A. B., and Mumford, W. W., *Some Results of a Study of Ultra-Short-Wave Transmission Phenomenon*, Proc. I. R. E., Vol. 20, No. 12, pp. 481 and 482, March, 1933. Please give author, title, edition, volume, page, publisher and date of publication as indicated. Omission of one required fact causes much extra editorial work and possible inaccuracies. All references are grouped at the end of the article.

ILLUSTRATIONS: Illustrations should accompany manuscripts and each should always be referred to in the text, preferably by number. Drawings or graphs should not be larger than 12 × 16 inches, and must be made with jet black India Ink on white paper or tracing cloth, the latter being preferred. *Do not use typewriter for lettering.* The smallest lettering on 8 × 10 inch figures should be no less than 1/4 inch high. Cross-section paper (white with black lines) may be used, but should not have more than 4 lines per inch. If finer ruled paper is used, the major division lines should be drawn in with black ink, omitting the finer divisions. In the case of finely ruled paper, only blue-lined paper can be accepted. *Tracing paper and blueprints* are not acceptable. Lettering and all markings must be large enough to be readable after reduction. Mail rolled or flat, never fold. Drawings that cannot be reproduced (including pencil drawings) will be returned to the author for redrawing, thus delaying publication of the paper. Photographs should be very distinct and show clear black and white contrasts. They must be on glossy white paper. Avoid round and oval photographs.

CAPTIONS AND LEGENDS: Legends or captions must accompany each drawing or photograph submitted. If written on the drawing or photograph, they should be placed below and well outside the part to be reproduced. It is better to place them on separate sheets of paper pasted to the back of the drawings or photographs. Each table should have a caption such as Table 1, Table 2, Table 3, etc. Captions should be complete in themselves so as to make the data intelligible to the reader without reference to the text. A duplicate list of captions for figures should be included as the last page of the manuscript. Use "Fig. 1" (not Figure 1), Figs. 3 and 4, etc., in both the text and the numbering of illustrations. In the text, "Eq. (1)," or "Eqs. (1) and (2)" are preferable to "Equation (1)." In captions and legends, except for "Fig." and "Eq." and table headings, write all words in full; do not abbreviate. Avoid placing explanatory written matter in the drawings; it should be in the text.

MATHEMATICAL WORK: Only the simplest formulas should be typewritten; all others should be carefully written in pen and ink, the writing to be large enough so that ample room is provided to mark mathematical matter for the printer. A considerable space for marking should be allowed above and below all equations. All complicated equations should be repeated on separate sheets with plenty of space left for marking. The solidus should be used for simple fractions appearing within the text. Make all expressions clear to the typesetter. Greek letters used in formulas should be clearly designated by name on the margin of the manuscript. All symbols should be clearly written and carefully checked. The difference between capital and lower-case letters should be clearly distinguished and care taken to avoid confusion between zero (0) and the letter (o), between the numeral (one) and the letter (ell) and the prime ('), between alpha and a, kappa and k, u and mu, v and nu, n and eta. All subscripts and exponents should be clearly marked and dots and bars over letters or mathematical expressions should be avoided. Avoid complicated exponents and subscripts. When it is necessary to repeat a complicated expression, it should be represented by some convenient symbol.

NOMENCLATURE AND ABBREVIATIONS: The National Advisory Committee for Aeronautics Nomenclature should be used in preference to any others. Standard abbreviations should be used, and it should be noted that most abbreviations are lower case, such as m.p.h., b.m.e.p., i.hp., b.hp., hp., . . . etc.